Contents

Chapter 1

Introduction

1.1 The Evolution of Wireless Cellular Systems

Wireless cellular systems have evolved rapidly over the last two decades and cellular phones are now an indispensable part of modern society [1]. In many countries, cellular phone use is approaching 100% of the population and modern third generation (3G) cellular systems offer a viable alternative to fixed line broadband networks [2, 3]. In countries with limited existing fixed line infrastructure, cellular systems have enabled voice and data services to be deployed at only a fraction of the cost required to deploy a fixed line network and in a much shorter time frame [4]. When originally conceived, the goal of cellular systems was to provide a voice service similar to a fixed line network but with the added benefit of user mobility [5]. This goal has been achieved both technologically and commercially. The next phase in the evolution of cellular systems is to support multiple packet based services, such as high speed Internet, in addition to the traditional cellular voice service [6].

To effectively support packet based services consideration must be given to the different types of traffic that they generate and their associated quality of service (QoS) requirements. An understanding of how cellular systems perform with different types of traffic is essential and the question of whether existing cellular system design methodologies are sufficient for new packet based services must be addressed. These questions are the primary focus of this thesis.

Cellular systems are comprised of two main components, namely, a radio component and a core network component, as illustrated in Figure 1.1. The radio component encompasses the radio propagation channel over which user data is transmitted and the base transceiver stations (BTS's) in the system are managed with radio network controllers (RNC's). The core network component interconnects the system's radio component with the public switched telephone network (PSTN) and other external data networks to enable traffic routing. The core network component is in many ways similar to a traditional fixed line network and similar design methodologies can be used for both [7].

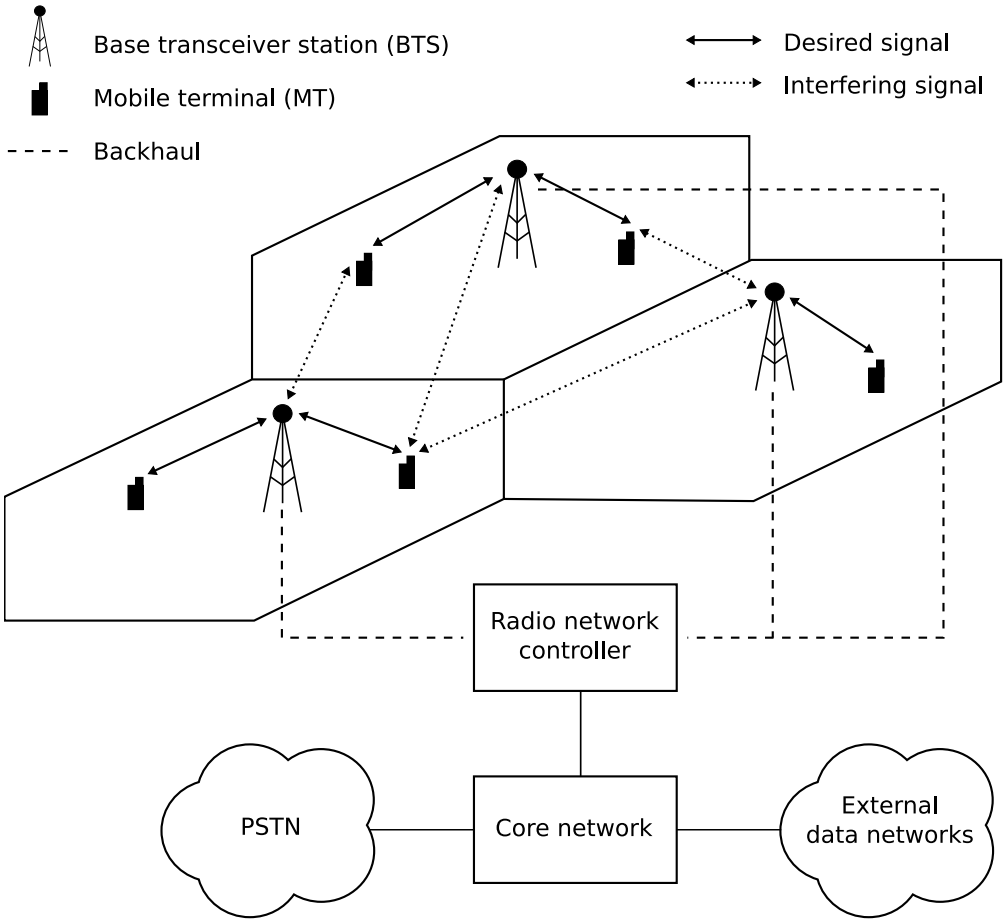

Figure 1.1: Cellular system components.

The radio propagation channel is the distinguishing feature of a cellular system and also the performance bottleneck. Only a limited amount of radio bandwidth is available to each system operator and this places a fundamental limit on the data throughput and number of users that a system can support with the available bandwidth. In order to support an arbitrarily large number of users, a cellular system divides its total geographic coverage area into a number of smaller areas, known as cells, and the system bandwidth is reused within the different cells. This concept is known as frequency reuse and is the fundamental basis of cellular systems [5]. As the number of users in the system increases, bandwidth can be reused more intensively by breaking larger cells into multiple smaller cells in order to increase system capacity. However, each new cell requires its own BTS and this adds to the system cost and careful attention must be paid to the level of co-channel interference caused by cells reusing the same bandwidth.

When designing a cellular system there are two key radio related considerations. Firstly, it must be ensured that the signal strength at the receiver is sufficiently strong at all potential mobile terminal (MT) locations, and secondly, the level of co-channel interference caused by cells reusing the same bandwidth must be controlled to ensure that an adequate

signal-to-interference-plus-noise ratio (SINR) is maintained at all receivers. Both of these considerations influence the selection of BTS locations, cell sizes, and transmitter powers, and an accurate radio propagation model is essential to estimate received power and effectively design a system. Cell sizes can vary from large outdoor macro-cells (>1km) to small indoor pico-cells (<100m) and the propagation characteristics of the environment where cells are deployed must be factored into the design process.

When dimensioning a cellular system, an estimate of the expected cell traffic loads is required and this must take into account the fact that users are mobile and cell traffic loads can vary significantly depending on factors such as the time of day (e.g. higher loads in business districts during business hours) or the occurrence of special events (e.g. higher loads in a cell hosting a music concert) [8]. Traditionally, the statistical properties of individual user traffic streams have not been taken into account during the radio related aspects of cellular system design as a constant-bit-rate (CBR) voice service was generally assumed and a fixed size radio bearer was simply allocated to a user for the duration of their service [9, 10, 11]. Instead, the mean traffic load and statistical properties of the arrival process of service requests were the primary focus. The statistical properties of the arrival process are used to ensure an acceptable level of service availability e.g. the well known Erlang traffic formulae are commonly used to estimate the probability that a service request is blocked due to a lack of available transmission capacity [12]. With packet based services, individual user traffic streams are highly variable and their statistical properties are an important dimensioning and design consideration [13].

With first generation (1G) and second generation (2G) cellular systems that use frequency division multiple access (FDMA) or time division multiple access (TDMA) techniques to share resources on the radio channel, the statistical properties of the user traffic streams do not impact the system's propagation dependent performance e.g. bit error rate (BER) [14]. This is an inherent property of these multiple access techniques as user traffic is transmitted on independent frequencies or time slots and the momentary user traffic load has no impact on the SINR of the receivers in the system. However, with modern 3G cellular systems that use the direct-sequence code division multiple access (DS-CDMA) technique, the statistical properties of the user traffic streams do impact the system's propagation dependent performance [14]. This occurs because users transmit on a common frequency at the same time and variations in the momentary user traffic load cause variations in the level of system interference which impacts the SINR of all receivers in the system. Hence, in DS-CDMA cellular systems there is a direct relationship between the statistical properties of the user traffic streams and the system's propagation dependent performance.

1.2 Packet Based Services and Variable-Bit-Rate Traffic

The prime motivation for the deployment of modern 3G DS-CDMA cellular systems is to offer new packet based services such as high speed Internet, video, and voice over IP (VoIP) just to name a few, and in doing so also compete with traditional fixed line broadband [3, 6]. Packet based services generate discrete variable sized packets and the resultant traffic streams are variable-bit-rate (VBR) in nature [13]. Figure 1.2 shows a sample traffic stream from a packet based video broadcast and the traffic stream generated has sub-second variability. In contrast, the traffic stream generated by the traditional cellular voice service is constant-bit-rate (CBR) in nature.

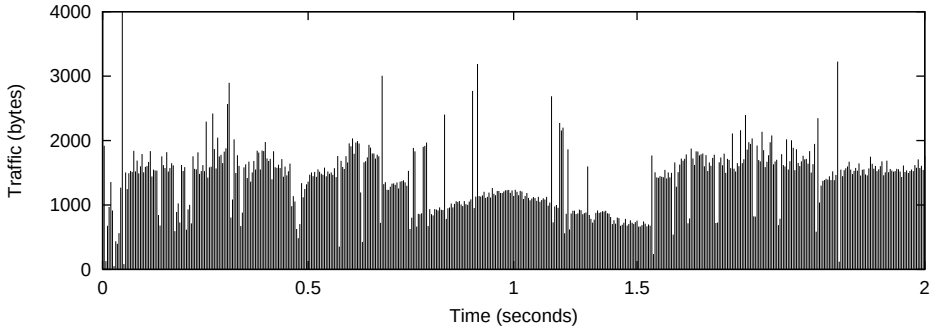

Figure 1.2: Video traffic stream generated by a TV news broadcast encoded with a mean bitrate of 64 kbps and the H.263 codec [15].

For systems that carry only CBR traffic, a fixed size radio bearer can be allocated to a user for the duration of their service and this is an efficient method for carrying this type of traffic as the bearer can be exactly matched to the traffic stream so that no capacity is wasted. However, with packet based services the allocation of a fixed size radio bearer would be inefficient as there would be periods of time when the user's allocated bearer capacity would go unused and could be better allocated to another user. Because radio bandwidth is scarce, dynamic resource allocation on the radio channel is essential in order to efficiently support VBR traffic and packet based services.

With DS-CDMA cellular systems there is a soft capacity limit on the radio channel, specifically, additional capacity can be allocated to users at the cost of increased system interference and it is up to the system to ensure that an acceptable level of system interference is maintained. With dynamic resource allocation on the radio channel, a BTS can vary a user's allocated data rate on a sub-second frame-by-frame basis and this technique is considered in this thesis and is illustrated in Figure 1.3.

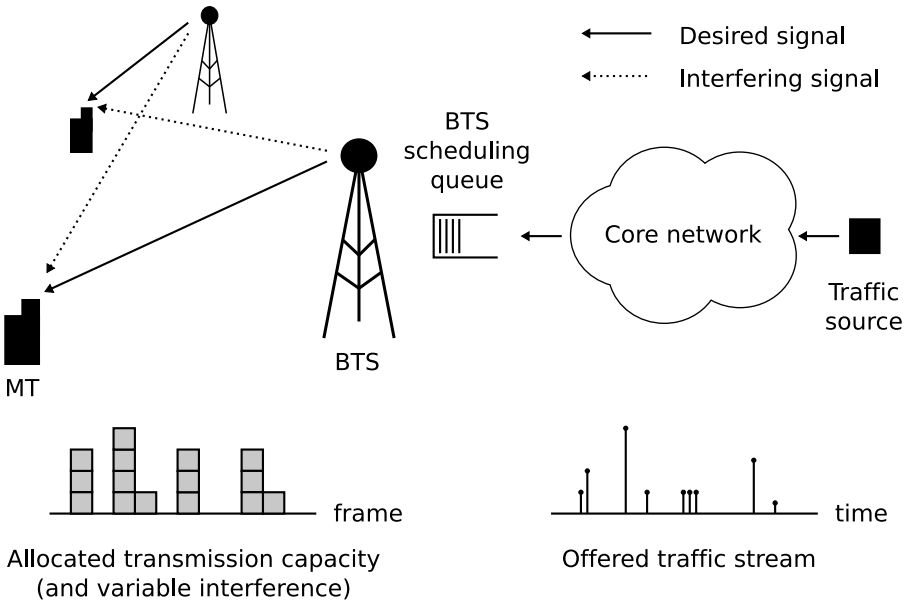

Figure 1.3: Frame-by-frame dynamic resource allocation on the radio channel.

1.3 Context and Objectives of this Thesis

The deployment of 3G DS-CDMA cellular systems is resulting in a transition from cellular systems that predominantly carry CBR voice traffic to multi-service packet based systems that predominantly carry VBR traffic. With earlier generation cellular systems based on FDMA and TDMA techniques there is no relationship between the statistical properties of the user traffic streams and the system's propagation dependent performance. With 3G DS-CDMA cellular systems there is a relationship between the two and this is the focus of this thesis.

Previous studies on the propagation dependent performance of DS-CDMA cellular systems have generally assumed only CBR traffic, often because a traditional CBR voice service was assumed [16, 17, 18, 19, 20]. This author is unaware of any studies where propagation dependent performance has been investigated with VBR traffic and frame-by-frame dynamic resource allocation on the radio channel. **The purpose of this thesis is to investigate the impact of VBR traffic on the propagation dependent performance of DS-CDMA cellular systems that utilise frame-by-frame dynamic resource allocation on the radio channel.** Only downlink (i.e. BTS to MT) performance is considered as this form of dynamic resource allocation is more suited to the downlink where the BTS has complete and immediate information about all traffic requiring transmission.

The primary objectives of this thesis are:

- to identify and model different types of VBR traffic that could potentially be present in 3G cellular systems.
- to develop a DS-CDMA cellular system model that can be used to estimate system performance with different types of traffic.
- to determine whether traffic type has a significant influence on system performance, in particular propagation dependent performance, and if so under what circumstances.
- to identify the implications of VBR traffic on DS-CDMA cellular system performance and develop a set of system design guidelines.

The findings of this thesis can be used to determine whether existing performance evaluation and design techniques are suitable for DS-CDMA cellular systems with packet based services or whether new techniques and procedures need to be implemented.

1.4 Contributions and Structure of this Thesis

To investigate the impact of VBR traffic on the performance of DS-CDMA cellular systems a system model and performance evaluation method must first be developed. Chapters 2–5 lay the foundation necessary to develop a system model and review the key components of a DS-CDMA cellular system, namely, the DS-CDMA technique, the propagation environment, user services and traffic, and traffic scheduling.

Chapter 2 provides an overview of the fundamentals of DS-CDMA cellular systems and proposes a method to estimate propagation dependent performance with a relatively small number of system parameters. It is shown that an accurate radio propagation model is essential to estimate performance and that both spreading code selection and synchronisation are important system parameters. RAKE receiver diversity and antenna space diversity techniques are outlined and these techniques are used in Chapters 6, 8, and 9 to improve system performance.

Chapter 3 discusses the main radio propagation mechanisms in a cellular system and proposes two propagation models that are used in Chapters 6–9 to estimate desired signal power and interference power at the receiver. Both outdoor and indoor propagation environments are considered.

Chapter 4 outlines packet based services that could potentially be offered by a cellular system. The characteristics of the traffic generated by these services is discussed and five

traffic models with diverse characteristics are proposed along with a BTS traffic scheduling policy. The proposed traffic models are evaluated in Chapters 6–9.

The original contributions of this thesis are presented in Chapters 5–9 and the publications related to this thesis are [21, 22, 23, 24]. The contributions presented in each chapter are detailed below.

Chapter 5 uses the information presented in Chapters 2–4 to develop a DS-CDMA cellular system model that is used in Chapters 6–9 to evaluate system performance with different traffic types. The system model consists of a user traffic model that describes the traffic offered to the BTS, a traffic scheduling policy that is used to perform frame-by-frame dynamic resource allocation on the radio channel, a propagation model that is used to estimate received signal power, and a user mobility model. The system performance metrics measured include the probability of bit error (BER), receiver SINR distribution, packet scheduling delay, and probability of packet dropping.

Chapter 6 evaluates system performance in an outdoor macro-cellular propagation environment with two statistically dissimilar traffic models and identifies scenarios where the system's propagation dependent performance is sensitive to traffic type. A number of scenarios are considered and these include: different numbers of users per cell, different DS-CDMA spreading code lengths, desirable and undesirable MT locations, non-time dispersive and time dispersive propagation environments, and different levels of propagation environment hostility.

Chapter 7 evaluates system performance in an indoor pico-cellular propagation environment with two statistically dissimilar traffic models and identifies scenarios where the propagation dependent performance is sensitive to traffic type. A number of scenarios are considered and these include: different numbers of users per cell, different DS-CDMA spreading code lengths, desirable and undesirable MT locations, different BTS deployment configurations, and different modulation schemes.

Chapter 8 expands on the results presented in Chapters 6 and 7 and in the scenarios where propagation dependent performance was identified as sensitive to traffic type, system performance is evaluated with a wider variety of traffic types. The impact of specific traffic types on system performance is evaluated.

Chapter 9 evaluates the impact of different traffic scheduling policies on system performance. Scheduling policies that deliberately alter the statistical properties of the user traffic are considered and the question of whether such scheduling policies are desirable is addressed.

Chapter 10 consolidates the results presented in Chapters 6–9 and outlines the implications of VBR traffic on DS-CDMA cellular system design. Traffic modelling requirements for system design are discussed and design recommendations are proposed.

Chapter 11 summarises the findings of this thesis.

In summary, the unique contributions of this thesis are:

- the development of a DS-CDMA cellular system model that can be used to estimate system performance with different traffic types.
- the identification of scenarios where the downlink performance of both outdoor and indoor DS-CDMA cellular systems is sensitive to the statistical properties of the user traffic streams.
- the evaluation of DS-CDMA cellular system performance with diverse traffic types.
- the evaluation of DS-CDMA cellular system performance with different traffic scheduling policies that deliberately alter the statistical properties of the user traffic.
- the development of design guidelines for DS-CDMA cellular systems with VBR traffic.

Chapter 2

Performance Estimation of DS-CDMA Cellular Systems

2.1 Introduction

This thesis investigates the performance of direct-sequence code division multiple access (DS-CDMA) cellular systems with different types of traffic. A key characteristic of DS-CDMA cellular systems is that users transmit on a common frequency at the same time and the traffic transmitted by other users acts as a source of interference that degrades system performance. It is essential that the fundamentals of DS-CDMA and the relationship between system performance and traffic type is first well understood.

DS-CDMA is based on the concept of direct-sequence spread-spectrum and an overview of this fundamental concept is given in Section 2.2 followed by a description of the code division multiple access (CDMA) technique in Section 2.3. The application of DS-CDMA to a cellular environment and the differences between downlink and uplink communication are discussed in Section 2.4. A mathematical technique to estimate the momentary signal-to-interference-plus-noise ratio (SINR) and momentary bit error rate (BER) at the receiver is presented in Section 2.5 and this technique is used throughout this thesis to estimate system performance. The assumptions related to this technique are also outlined.

RAKE receiver diversity and antenna space diversity techniques are discussed in Section 2.6 and these are used in later chapters to improve system performance.

2.2 Direct-Sequence Spread-Spectrum

Direct-sequence spread-spectrum systems deliberately spread user data over a bandwidth much larger than required in order to increase the resilience of the user data to interference

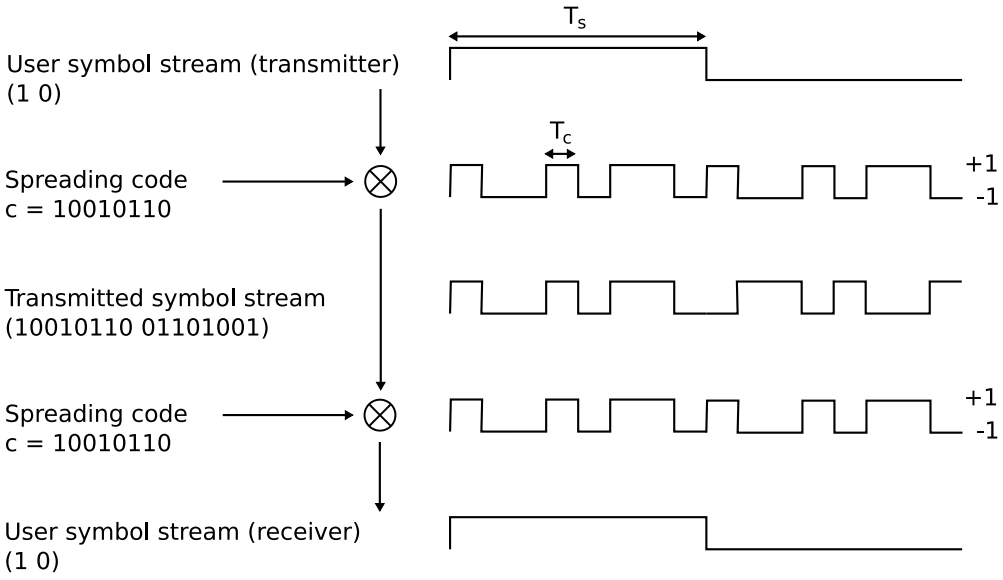

Figure 2.1: Direct-sequence spread-spectrum concept.

and noise [25]. The user data bandwidth is spread by multiplying the user data symbols with a pseudo-random sequence known as a spreading code, as illustrated in Figure 2.1. The original user symbol stream is recovered by multiplying the spread symbol stream with the original pseudo-random sequence. The pseudo-random spreading code pulses are commonly referred to as chips and the number of chips per user symbol is an integer value equal to the length of the spreading code. The factor by which the user data bandwidth is spread is called the *spreading factor* and is equal to

$$s_f = \frac{T_s}{T_c} \tag{2.1}$$

where T_S is the user symbol period and T_c is the chip period.

The advantage of spreading user data bandwidth is evident when one considers the energy per user bit to interference plus noise spectral density ratio. The received energy per user symbol is equal to

$$E_s = ST_s \tag{2.2}$$

$$= \frac{S}{R_s} \tag{2.3}$$

where S is the average received signal power, T_s is the user symbol period, and R_s is the user symbol-rate (the inverse of the user symbol period T_s). The interference plus noise spectral density is defined as

$$I_0 = \frac{I+N}{W} \tag{2.4}$$

where I is the average received interference power, N is the average received noise power, and W is the channel bandwidth. The energy per user symbol to interference plus noise spectral density ratio is therefore given by

$$\frac{E_s}{I_0} = \frac{W}{R_s}\frac{S}{I+N} \tag{2.5}$$

where $S/(I+N)$ is the SINR prior to de-spreading. If the system spectral efficiency is ε bits/s/Hz then the system chip rate (the inverse of the chip period T_c) is equal to

$$R_c = \frac{\varepsilon W}{b} \tag{2.6}$$

where b is the number of bits per symbol. The energy per user bit to interference plus noise spectral density ratio can then be expressed as

$$\frac{E_b}{I_0} = \frac{1}{\varepsilon}\frac{R_c}{R_S}\frac{S}{I+N} \tag{2.7}$$

$$= \frac{s_f}{\varepsilon}\frac{S}{I+N} \tag{2.8}$$

where $E_s = bE_b$. Hence, the energy per user bit to interference plus noise spectral density ratio is proportional to the spreading factor and the SINR after de-spreading is effectively equal to the SINR prior to de-spreading multiplied by the spreading factor[1].

2.3 Direct-Sequence Code Division Multiple Access

DS-CDMA is a multiple access technique that utilises the properties of direct-sequence spread-spectrum to enable multiple users to transmit on a common frequency at the same time [14, 26]. Individual users are each assigned their own unique spreading code with which they transmit and the composite received signal at a receiver consists of both the user's desired signal and also interfering signals from other users who have been assigned different spreading codes. A correlation receiver matched to the user's spreading code extracts the desired signal and the SINR at the receiver after de-spreading is proportional to the SINR prior to de-spreading multiplied by the user's spreading factor. Additional users act as a source of interference and this places a fundamental limit on the number of users that a

[1] Also referred to as processing gain.

system can support as a minimum acceptable SINR needs to be maintained at the receiver. A mathematical technique to estimate system performance is presented in Section 2.5.

With a limited system bandwidth and a fixed chip rate there is a trade off between the number of users a system can support and the user data rate. A larger spreading factor increases the SINR at the receiver output and allows a larger number of users to be supported but this comes at the cost of a reduced user data rate. Table 2.1 lists the accepted spreading factors and data rates specified in the 3GPP standards for 3G cellular systems. Users can be allocated different spreading factors or multiple spreading codes to vary their data rate and the system must ensure that an acceptable SINR is maintained at all receivers at all times.

Spreading factor (s_f)	Symbol rate (ks/s)	Uplink data rate (kb/s) BPSK modulation	Downlink data rate (kb/s) QPSK modulation
512	7.5	–	15
256	15	15	30
128	30	30	60
64	60	60	120
32	120	120	240
16	240	240	480
8	480	480	960
4	960	960	1920

Table 2.1: Spreading factors and data rates specified in the 3GPP standards for 3G cellular systems (chip rate of 3.84 Mcps) [27].

2.4 DS-CDMA Cellular Systems

A cellular system divides its total geographic coverage area into a number of smaller areas, known as cells, and the system bandwidth is reused within the different cells. This concept is known as frequency reuse and is the fundamental basis of cellular systems [5]. This allows an arbitrarily large number of users to be supported with only a limited bandwidth but careful attention must be paid to the level of co-channel interference caused by cells reusing the same bandwidth[2].

Figure 2.2 shows communication between a base transceiver station (BTS) and mobile terminal (MT) in a DS-CDMA cellular system that uses frequency division duplexing i.e. the downlink and uplink are independent. As discussed in the previous section, users appear as a source of interference to one another and the interference that emanates from users in

[2]DS-CDMA cellular systems typically reuse the entire system bandwidth in every cell i.e. a frequency reuse factor of 1 [14].

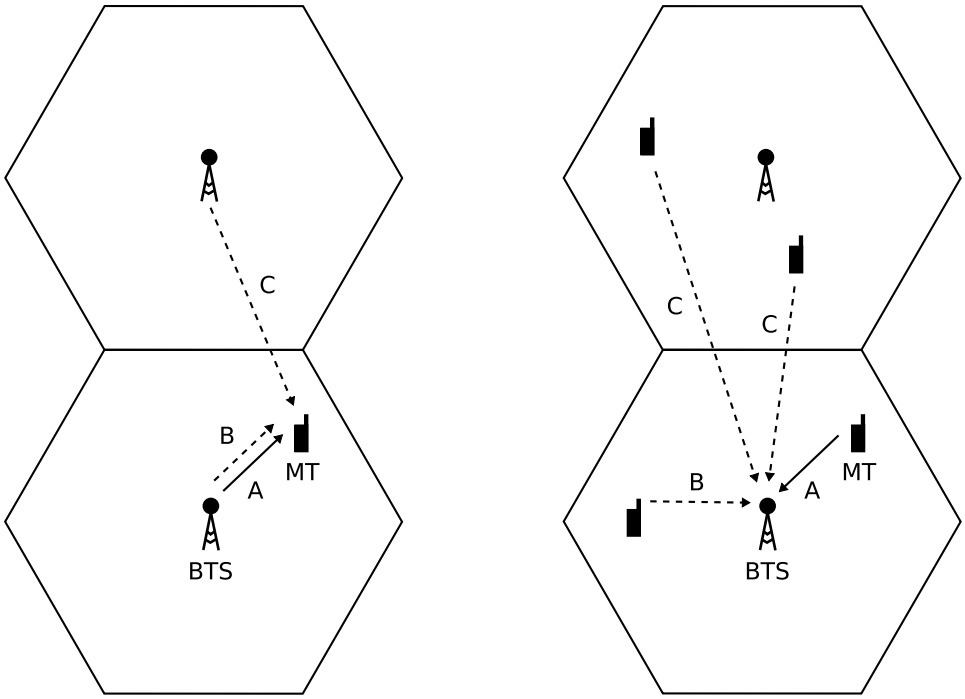

(a) downlink (b) uplink

Figure 2.2: Communication between a BTS and MT in a DS-CDMA cellular system where (A) is the desired signal, (B) is intra-cell interference, and (C) is inter-cell interference.

the same cell is referred to as intra-cell interference and the interference that emanates from users in co-channel cells is referred to as inter-cell interference.

Of particular interest is whether the desired and interfering signals are synchronous or asynchronous at the receiver as this affects how they combine during receiver processing, as will be outlined in the following section. On the downlink, the desired signal and intra-cell interference is synchronous as both are transmitted from the same BTS and transverse the same propagation path to the receiver. The desired signal and inter-cell interference is asynchronous as they are transmitted from different BTS's and transverse different propagation paths with different propagation delays to the receiver. On the uplink, the desired signal and both the intra-cell interference and inter-cell interference are asynchronous as they are transmitted from different MT's and transverse different propagation paths with different propagation delays to the receiver.

2.4.1 Power Control

Because users appear as a source of interference to one another, careful attention must be paid to transmitter power levels to ensure that users do not transmit with a too higher power that would cause excessive interference for other users [26]. Users ideally transmit with the lowest possible power to achieve their target SINR at the receiver.

Power control on the uplink is especially important as the propagation path loss between MT's and a BTS can vary by orders of magnitude depending on the MT location [28]. If MT's use the same transmitter power then the power received from MT's near the BTS will tend to be higher than the power received from MT's far away and consequently the SINR at the receiver will be good for MT's near the BTS and poor for those MT's far away[3]. Power control can be used to minimise this problem via MT's continuously adjusting their transmitter power so that their target SINR is achieved at the BTS.

Power control on the downlink is less important as intra-cell transmissions originate from the same BTS and experience the same propagation loss due to the common propagation path between the BTS and MT i.e. the ratio of the desired signal power to intra-cell interference power is identical at both the BTS and MT. Power control can of course still be used on the downlink to optimise system performance if some users have unnecessarily high SINR's at the receiver [29].

2.5 DS-CDMA Performance Estimation

This section presents a mathematical technique to estimate the SINR and BER at a receiver in a DS-CDMA cellular system and these two metrics are used throughout this thesis to measure system performance. The method presented was proposed by Pursley and a full mathematical derivation can be found in [30] and only the key results are presented below. The system considered is assumed to have K active users and the transmitted signal of the kth user is given by

$$s_k(t) = \sqrt{2P_{t,k}}d_k(t)c_k(t)\cos(w_c t + \phi_k) \tag{2.9}$$

where $P_{t,k}$, d_k, c_k, and ϕ_k are the transmitter signal power, user symbol, spreading code, and carrier phase offset of the kth user, respectively. Note that the multiplication of the user symbol and spreading code spreads the user bandwidth. The received signal is the sum of all individual user signals and is equal to

$$r(t) = \sum_{k=1}^{K} \sqrt{2P_k}d_k(t-\tau_k)c_k(t-\tau_k)\cos(w_c t + \theta_k) + n(t) \tag{2.10}$$

where P_k and τ_k are the received signal power and propagation time delay of the kth user, respectively, $\theta_k = \phi_k - w_c t$, and $n(t)$ is additive white Gaussian noise with a power spectral density of $N_o/2$. Without loss of generality it can be assumed that $\tau_i = 0$ and $\theta_i = 0$ and

[3] This is commonly referred to as the near-far problem.

the output of a coherent correlation receiver matched to the spreading code of the ith user is given by

$$z_i(t) = \int_0^{T_s} r(t)c_i(t)\cos(w_c t)dt \quad (2.11)$$

$$= D_i + I_i + \eta \quad (2.12)$$

where T_s is the user symbol period, D_i is the desired signal component, I_i is the multiple access interference from the other $K-1$ users, and η is the noise component. The SINR of the ith user at the output of the receiver (i.e. after de-spreading) is defined as

$$SINR_i = \frac{D_i^2}{\mathrm{Var}[I_i] + \mathrm{Var}[\eta]} \quad (2.13)$$

where $\mathrm{Var}[x]$ is the variance of x. The signal components in Equation 2.12 can be approximated as

$$D_i^2 = \frac{P_i T_s^2}{2} \quad (2.14)$$

$$\mathrm{Var}[\eta] = \frac{N_o T_s}{4} \quad (2.15)$$

$$\mathrm{Var}[I_i] = \frac{s_f T_c^2}{6} \sum_{k=1,k\neq i}^{K} P_k \quad (2.16)$$

and the assumptions related to these equations are detailed in [30]. The $\mathrm{Var}[I_i]$ term depends on the cross correlation properties of the desired and interfering spreading codes over the user symbol period [16, 30, 31]. Equation 2.16 assumes that pseudo-random spreading codes are used and that the desired and interfering spreading codes are asynchronous and have a random phase offset. If orthogonal spreading codes are used and the desired and interfering spreading codes are synchronous then theoretically there is no interference (i.e. $\mathrm{Var}[I_i] = 0$) and this scenario is discussed in the following section. Continuing with the assumptions made in Equations 2.14–2.16, the SINR of the ith user is equal to

$$SINR_i = \left(\frac{N_o}{2E_s} + \frac{1}{3s_f} \sum_{k=1,k\neq i}^{K} \frac{P_k}{P_i} \right)^{-1} \quad (2.17)$$

where $E_s = T_s P_i$ and is equal to the energy per user symbol and s_f is the spreading factor defined in Equation 2.1. If the sum of the interference and noise is assumed to be a Gaussian

random variable [32] then the probability of symbol error with a BPSK or QPSK modulation scheme is given by

$$P_s = Q\left(\sqrt{SINR_i}\right) \tag{2.18}$$

$$= Q\left(\sqrt{\left(\frac{N_o}{2E_S} + \frac{1}{3s_f}\sum_{k=1,k\neq i}^{K}\frac{P_k}{P_i}\right)^{-1}}\right) \tag{2.19}$$

where

$$Q(x) = \int_x^\infty \frac{1}{\sqrt{2\pi}} e^{-y^2/2} dy \tag{2.20}$$

and is the Q-function. In cellular systems the noise power is often assumed to be insignificant when compared to the interference power and if this is assumed then the probability of bit error (BER) with a BPSK or QPSK modulation scheme is given by

$$P_b = Q\left(\sqrt{\frac{3s_f}{\sum_{k=1,k\neq i}^{K}\frac{P_k}{P_i}}}\right) \tag{2.21}$$

Equations 2.17 and 2.21 show that an accurate knowledge of the desired signal power and interference power at the receiver is essential to calculate system performance. A number of propagation models are presented in the following chapter and these are used to estimate received power.

2.5.1 OVSF Spreading Codes

Orthogonal spreading codes are a set of codes that have pairwise cross correlations of zero when the phase offset between the codes is zero [33]. This property is extremely useful in DS-CDMA cellular systems as this means a correlation receiver effectively cancels out all multiple access interference if the user's code and the interfering codes are synchronised. The requirement for perfect synchronisation generally restricts the usefulness of orthogonal codes to the downlink where the BTS can ensure that codes are synchronised [33]. Non-orthogonal code sets are generally better suited to the uplink since code synchronisation cannot be guaranteed e.g. Gold codes are often used on the uplink since they have low cross correlations at non-zero phase offsets [33].

Orthogonal variable spreading factor (OVSF) codes[4] have been selected for use on the down-

[4]Also known as Walsh codes.

link in the 3GPP standards for 3G cellular systems and this code set is used throughout this thesis [34]. The set of OVSF codes with length $n = 2^k$, $k \geq 0$, consists of the n rows of an $n \times n$ matrix which is recursively defined as

$$W_1 = (0) \qquad W_{2n} = \begin{pmatrix} W_n & W_n \\ W_n & \overline{W_n} \end{pmatrix} \tag{2.22}$$

where $\overline{A}$ is the matrix A with every bit replaced by its logical NOT. For example, OVSF code sets with lengths 1, 2, and 4 are given by

$$W_1 = (0) \qquad W_2 = \begin{pmatrix} 0 & 0 \\ 0 & 1 \end{pmatrix} \qquad W_4 = \begin{pmatrix} 0 & 0 & 0 & 0 \\ 0 & 1 & 0 & 1 \\ 0 & 0 & 1 & 1 \\ 0 & 1 & 1 & 0 \end{pmatrix} \tag{2.23}$$

OVSF spreading codes have the desirable property that codes of different lengths can be assigned to users and code orthogonality is still maintained. Hence, users can be allocated different spreading factors to achieve different user data rates and the system can still retain the benefits of code orthogonality. Figure 2.3 shows an OVSF code tree and in order to maintain orthogonality between allocated OVSF codes no new code can be allocated if its position in the code tree is below that of an already allocated code. For example, if codes '00' and '0011' are already allocated then code '0110' can be allocated but codes '0000' and '0101' cannot because they are below the already allocated code '00'.

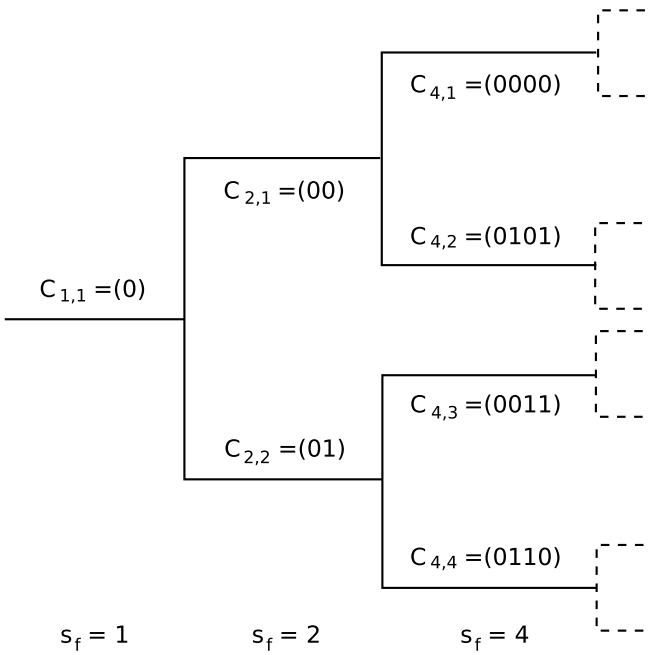

Figure 2.3: OVSF code tree with spreading factors (s_f) of 1, 2, and 4.

2.6 Receiver Diversity

Receiver diversity is a technique that improves system performance by utilising the random nature of the radio propagation channel and the multiple propagation paths that typically exist between a BTS and MT [14]. Figure 2.4 illustrates how multiple versions of a transmitted signal, separated in either time or space, can arrive at the receiver. Time separation occurs when the transmitted signal transverses multiple propagation paths to the receiver and each path has a different propagation delay. Spacial separation can be achieved with the use of multiple receiver antennas.

The multiple received signal versions ideally have uncorrelated powers so that if one version of the signal is weak another version of the signal is hopefully strong and can be captured by the receiver. The following chapter outlines common radio propagation mechanisms and shows that the received signal power can differ by orders of magnitude for signal versions that are separated by as little as a chip in time or a fraction of a wavelength in space. The two diversity techniques considered in this thesis are a RAKE receiver (temporal diversity) and antenna space diversity and these are outlined in the following sections.

There are numerous techniques that can be used to process and combine the received signal versions in order to make a best estimate of the transmitted data symbol. These techniques vary in complexity and maximal ratio combining is considered in this thesis [14]. With perfect maximal ratio combining the SINR at the receiver output is simply the sum of the individual SINR's from each diversity source.

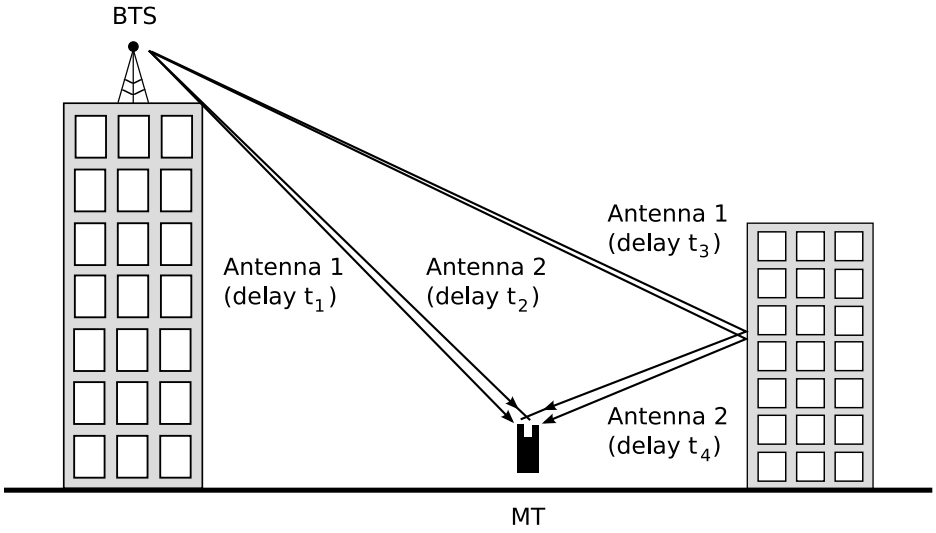

Figure 2.4: Multipath propagation and temporal and spacial receiver diversity.

2.6.1 RAKE Receiver

A RAKE receiver is a diversity receiver specifically designed for DS-CDMA [14]. It takes advantage of the fact that the system chip rate is generally much greater than the user symbol rate and that spreading codes typically have very low auto-correlation values with non-zero phase offsets. If different versions of the transmitted signal arrive at the receiver and are separated by at least a chip in time then the receiver's correlator synchronises to one version of the signal and the other signal versions appear as uncorrelated interference and experience no processing gain. A RAKE receiver has multiple correlators, often referred to as *fingers*, and each correlator synchronises with a different time shifted version of the transmitted signal, as illustrated in Figure 2.5. Each finger is a separate source of diversity and if a perfect RAKE receiver is assumed then the SINR at the receiver output is the sum of the individual SINR's on each finger.

It is shown in the following chapter that when received signal versions are separated by only chips in time the desired signal power and interference power on each finger can vary by orders of magnitude. This means that a time-dispersive propagation channel can actually be advantageous in terms of system performance due to the diversity benefits. It should be noted that signal versions not synchronised with the active correlator act as a source of self-interference.

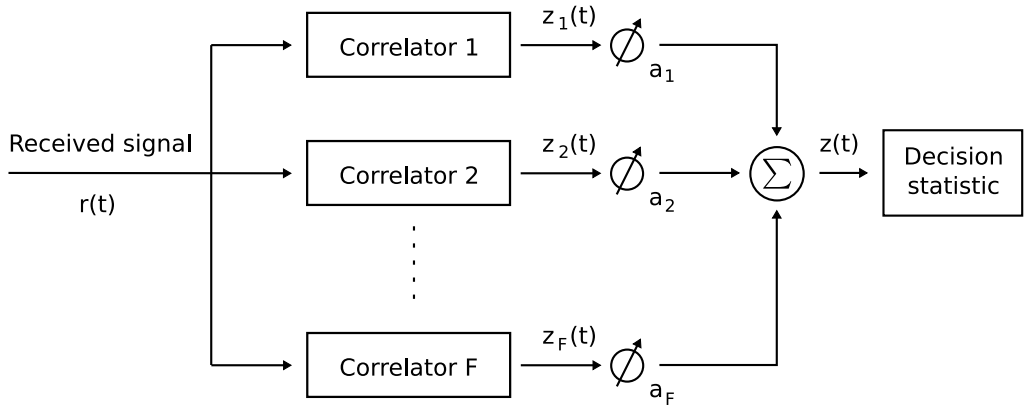

Figure 2.5: An F-finger RAKE receiver where each correlator synchronises with a different time shifted version of the transmitted signal.

2.6.2 Antenna Space Diversity

Antenna space diversity exploits the rapid and large fluctuation in received signal power that is typically observed in cellular systems when a receiver moves only small distances (in the order of wavelengths) [28]. This phenomenon is caused by multipath propagation and is discussed in the following chapter. Multiple receiver antennas separated in space can be used

to capture multiple samples of the received signal and this can be used as a source of diversity. If the physical separation between the antennas is large enough then the received power on each antenna will be relatively uncorrelated [35]. Maximal ratio combining is one technique that can be used to combine the received signal samples and this technique is assumed in this thesis i.e. the SINR at the receiver output is the sum of the individual SINR's on each receiver antenna [14].

2.7 Summary

DS-CDMA cellular systems are based on the concept of direct-sequence spread-spectrum which deliberately spreads user data over a bandwidth much larger than required in order to increase the resilience of the user data to interference and noise. This additional resilience allows multiple users to share a common frequency and transmit at the same time and also provides a multiple access mechanism. Users appear as a source of interference to one another and the number of users in the system must be carefully controlled to ensure that excessive interference does not unduly degrade system performance.

A mathematical technique to estimate the SINR and BER at a receiver in a DS-CDMA cellular system was presented and this technique is used in Chapters 6–9 to evaluate system performance. The assumptions related to this technique were outlined and it was shown that an accurate radio propagation model is essential to estimate system performance. Spreading code synchronisation and the properties of orthogonal and non-orthogonal spreading codes were discussed. RAKE receiver diversity and antenna space diversity techniques were outlined and it was explained how these techniques can improve system performance.

Chapter 3

Outdoor and Indoor Propagation Environments

3.1 Introduction

The radio propagation channel is the distinguishing feature of a cellular system and also the performance bottleneck. An accurate model of the propagation environment is essential for cellular system analysis and design as both the desired signal power and interference power at the receiver must be known to estimate system performance.

The propagation environment of a typical cellular system is very hostile as a direct line-of-sight propagation path between the BTS and MT rarely exists and short-term variations in received power in excess of 20 dB are common [28]. A propagation model captures this behaviour and is used to estimate the momentary received signal power at different MT locations.

Section 3.2 outlines the key radio propagation mechanisms in outdoor and indoor cellular propagation environments. Section 3.3 describes large-scale path loss which explains the variation in mean received power as a MT moves over large distances, while Section 3.4 describes small-scale fading which explains the rapid and large fluctuation in received power as a MT moves only short distances (in the order of wavelengths). Two specific propagation models are presented in Section 3.5 and these are used in Chapters 6–9 to estimate the performance of outdoor and indoor cellular systems.

3.2 Radio Propagation Mechanisms

The physical environments where cellular systems are deployed means that there will rarely be a direct line-of-sight propagation path between the BTS and MT e.g. buildings obstruct the

propagation path. Radio wave propagation between the BTS and MT is still however possible due to three key propagation mechanisms, namely, reflection, diffraction, and scattering [36]. These mechanisms are illustrated in Figure 3.1 and are described below:

- Reflection occurs when a radio wave propagates into an object that has dimensions much larger than the wavelength of the wave e.g. the earth's surface, buildings, and walls. Depending on the electromagnetic properties of the obstacle, the incident wave is either partially or completely reflected.
- Diffraction occurs when the propagation path between the BTS and MT is obstructed by an obstacle with a sharp irregularity e.g. the edge of a building. Diffraction leads to an apparent "bending" of the radio wave around the obstacle and this is explained by Huygens' principle [37]. As the propagation path becomes more obstructed and the wave is required to "bend" further the received signal power decreases rapidly.
- Scattering occurs when a radio wave propagates into an object that has dimensions comparable to the wavelength of the wave or smaller e.g. rough surfaces, trees, lamp posts. The incident wave is reflected from the object and scattered in many directions.

These propagation mechanisms, in addition to a potential line-of-sight propagation path, mean that the received signal consists of multiple versions of the transmitted signal and each of the signal versions transverse a different propagation path. Due to the different propagation paths, each version of the signal has a different amplitude and phase at the receiver and the composite received signal is the phasor sum of these components. This is commonly referred to as multipath propagation [28].

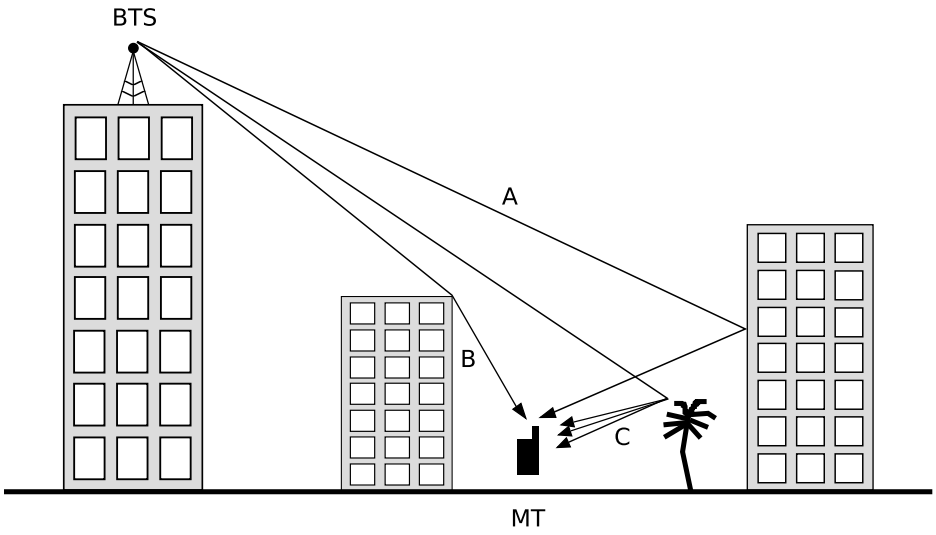

Figure 3.1: Radio wave propagation mechanisms: (A) reflection, (B) diffraction, and (C) scattering.

3.3 Large-Scale Path Loss

Large-scale path loss describes the variation in mean received power as a MT moves over large distances. Both theoretical models and empirical studies indicate that large-scale path loss depends on the transmitter-receiver separation, environmental clutter (e.g. hills, trees, walls), transmission frequency, and antenna heights [38, 39, 40, 41].

The complex and varied nature of cellular propagation environments means that practical path loss models tend to be at least semi-empirical. A generic model that is applicable to a wide range of propagation environments is obviously desirable but there is of course a trade off between generality and accuracy. The following sections describe two large-scale path loss models that are applicable to a wide range of propagation environments.

3.3.1 Distance Dependent Path Loss

Both theoretical models and empirical studies suggest that the mean path loss, $\overline{L_p}(d)$, between a transmitter and receiver as a function of distance, d, between the two can be modelled with the power law function

$$\overline{L_p}(d) = \overline{L_r}(d_0)\left(\frac{d}{d_0}\right)^n \tag{3.1}$$

where $\overline{L_r}(d_0)$ is the mean path loss at a reference distance d_0 (in the antenna's far field) and n is the path loss exponent which determines the rate at which the path loss increases with distance [36]. Mean path loss is often expressed in decibels as

$$\overline{L_p}(d)(\text{dB}) = \overline{L_r}(d_0)(\text{dB}) + 10n\log\left(\frac{d}{d_0}\right) \tag{3.2}$$

The Friis free space model assumes that the transmitter and receiver are located in free space without any obstacles and with this model $n = 2$ [42]. The 2-ray plane earth model is based on geometric optics and assumes a direct path between the transmitter and receiver and a reflected path off the ground and with this model $n = 4$ [43]. These models are not realistic for cellular propagation environments as environmental clutter is not taken into account. A number of empirical studies have been performed to measure the value of n in cellular propagation environments and typical values are listed in Table 3.1. In general, the value of n increases as the propagation environment becomes more cluttered and obstructed.

Environment	Path loss exponent (n)	References
Friis free space model	2	[42]
Plane earth model	4	[43]
Urban (900, 955, and 1845 MHz)	2.1–5.7	[44, 45]
Rural (900 MHz)	2.7–4.4	[46]
In-building (1300 and 914 MHz)	1.8–5.2	[47, 48]
In-building (line-of-sight, 1300 and 910 MHz)	1.5–3	[47, 49]

Table 3.1: Path loss exponents in cellular propagation environments.

3.3.2 Lognormal Shadowing

The distance dependent path loss presented in the previous section describes the mean path loss for a specific transmitter-receiver separation. This does not take into account the fact that with the same transmitter-receiver separation different locations may be surrounded by different obstacles and have vastly different propagation paths and path losses. This variation in path loss with a fixed transmitter-receiver separation is referred to as shadowing and is illustrated in Figure 3.2.

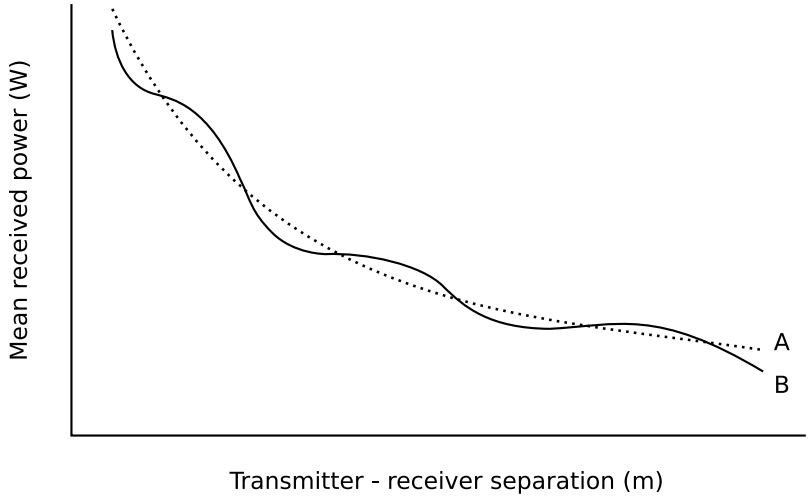

Figure 3.2: Large-scale path loss: (A) distance dependent path loss only, and (B) distance dependent path loss and shadowing.

Empirical studies have shown that with a fixed transmitter-receiver separation the variability in mean path loss (in linear units) can be approximated with a lognormally distributed random variable [44, 45, 46, 50]. Hence, Equation 3.2 can be extended to

$$\overline{L_p}(d)(\text{dB}) = \overline{L_r}(d_0)(\text{dB}) + 10n \log\left(\frac{d}{d_0}\right) + X_\sigma \tag{3.3}$$

where X_σ is a zero-mean Gaussian distributed random variable (in dB) with standard deviation σ (in dB). The value of σ depends on the propagation environment and in general increases as the propagation environment becomes more cluttered and obstructed. A number of empirical studies have been performed to measure the value of σ in cellular propagation environments and typical values are listed in Table 3.2.

Environment	Lognormal variability (σ)	References
Urban (900 MHz)	7.1–13.1 dB	[44]
Urban (955 and 1845 MHz)	5.6–10.3 dB	[45]
Rural (900 MHz)	6.2–11.0 dB	[46]
In-building (1300 and 914 MHz)	4.3–16.3 dB	[47, 48]

Table 3.2: Lognormal shadowing in cellular propagation environments.

3.4 Small-Scale Fading

Small-scale fading describes the rapid and large fluctuation in received power as a MT moves only short distances (in the order of wavelengths) [28]. Fluctuations in excess of 20 dB are common and Figure 3.3 shows a typical small-scale fading receiver power envelope. This phenomenon is due to multipath propagation, described in Section 3.2, and occurs because multiple versions of the transmitted signal arrive at the receiver with different amplitudes and phases. A small MT movement causes a significant change in the phase of the received signal versions and because the composite received signal is the phasor sum of these components a rapid and large fluctuation in received power can occur. Antenna space diversity, described in Section 2.6.2, takes advantage of this phenomenon and uses multiple receiver antennas separated in space to capture multiple uncorrelated samples of the received signal [35].

Multipath propagation leads to time dispersion of the transmitted signal as each of the received signal versions transverse different propagation paths with different propagation delays. A propagation channel's power delay profile can be used to characterise the time dispersive properties of a channel [14]. Figure 3.4 shows a typical power delay profile from an outdoor cellular system. The x-axis represents the time at which different signal versions arrive at the receiver relative to the first received signal version, referred to as the excess delay, and the y-axis represents the received signal power of the different signal versions.

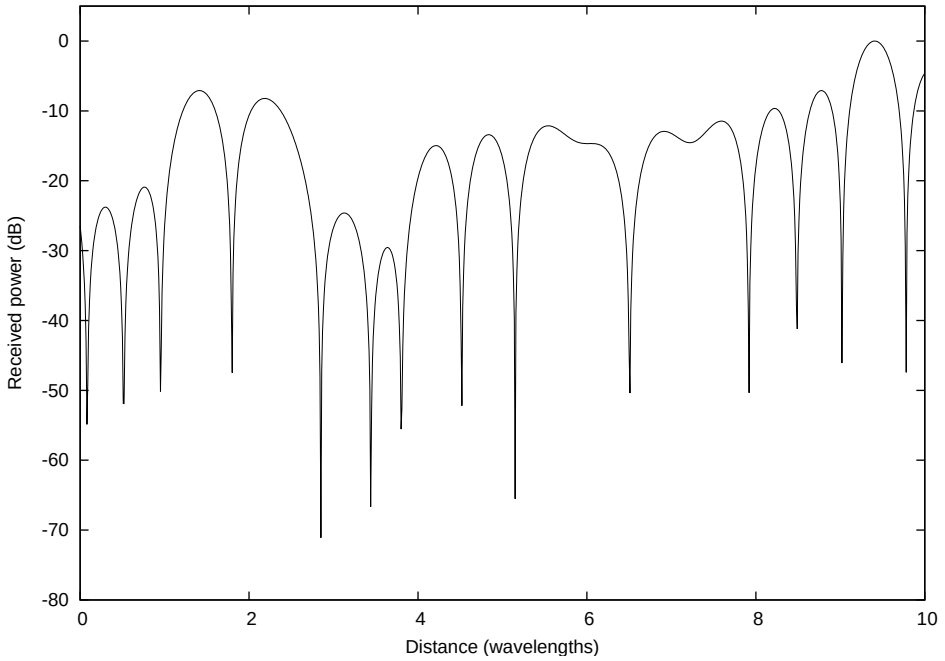

Figure 3.3: Small-scale fading receiver power envelope (Rayleigh fading).

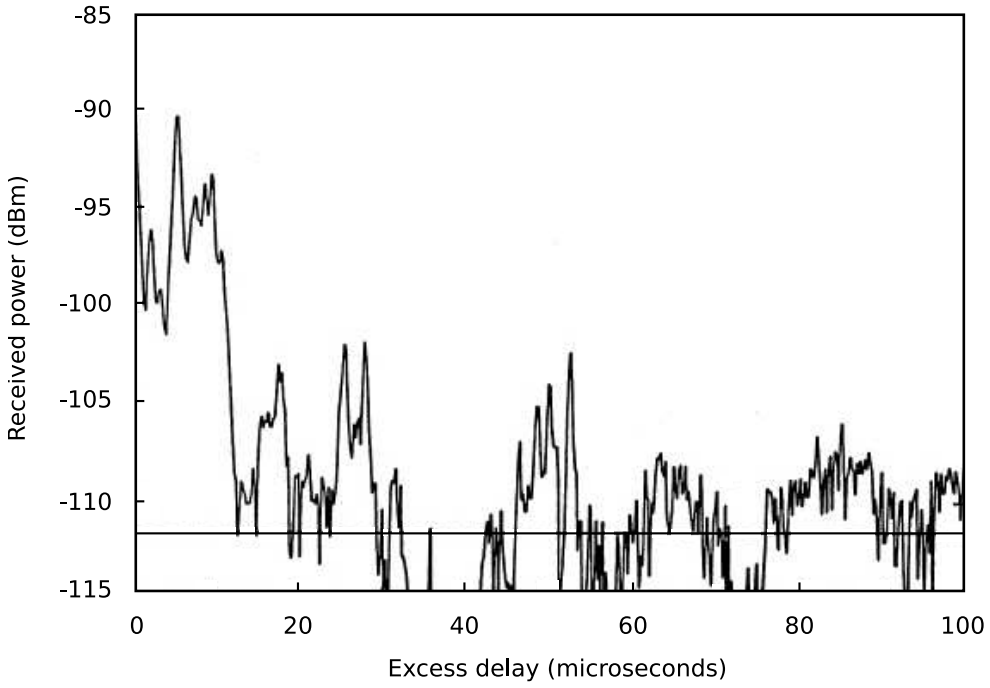

Figure 3.4: Measured multipath power delay profile from a 900 MHz outdoor cellular system in San Francisco [51].

The mean excess delay and root mean square (RMS) delay spread can be used to characterise the time dispersive properties of a propagation channel [14]. The mean excess delay is defined as

$$\overline{\tau} = \frac{\sum_k P(\tau_k)\tau_k}{\sum_k P(\tau_k)} \tag{3.4}$$

where k is the number of received signal versions, τ_k is the excess delay of the k'th signal version, and $P(\tau_k)$ is the received signal power of the k'th signal version. The RMS delay spread is the second central moment of the power delay profile and is defined as

$$\sigma_\tau = \sqrt{\frac{\sum_k P(\tau_k)\tau_k^2}{\sum_k P(\tau_k)} - \overline{\tau}^2} \tag{3.5}$$

Typical values of RMS delay spread in cellular propagation environments are listed Table 3.3. Indoor environments generally have lower delay spreads due to smaller transmitter-receiver separations and shorter propagation paths.

When the system's chip period is much greater than the channel's RMS delay spread, only a single signal version can be resolved at the receiver and the propagation channel is referred to as non-time dispersive or narrowband. When the system's chip period is comparable or less than the channel's RMS delay spread, the time dispersed signal versions cause inter-symbol interference at the receiver and the propagation channel is referred to as time dispersive or wideband. A RAKE receiver, described in Section 2.6.1, takes advantage of the time dispersed signal versions of a wideband propagation channel and uses the uncorrelated power levels of the different signal versions as a source of diversity. The system chip period specified in the 3GPP standards for 3G cellular systems is 260 ns [27] and consequently many 3G cellular system deployments will have wideband propagation channels, especially in outdoor environments (see Table 3.3).

Environment	RMS delay spread (σ_τ)	References
Urban (900 MHz)	2000–8000 ns (typical)	[44, 51]
Urban (910 MHz)	1300 ns avg.	[52]
Urban micro-cellular (900 MHz)	170–1050 ns avg.	[53]
Indoor (915 and 1900 MHz)	70–94 ns avg.	[54]
Indoor (1500 MHz)	25 ns avg.	[55]

Table 3.3: RMS delay spreads in cellular propagation environments.

3.4.1 Rayleigh and Ricean Fading

The Rayleigh distribution is commonly used to describe the amplitude variation (in volts) in the receiver signal envelope caused by small-scale fading and Figure 3.3 shows a typical Rayleigh fading envelope [28]. A theoretical model developed by Clarke shows that when a large number of independent signal versions arrive at the receiver at the same time, each with a random phase and angle of arrival but identical amplitude, the envelope of the received signal is Rayleigh distributed [56]. When expressed in terms of power (Watts), the signal envelope has an exponential distribution given by

$$f(P) = \frac{1}{\overline{P}} \exp(\frac{-P}{\overline{P}}) \qquad \overline{P} \geq 0 \tag{3.6}$$

where P is momentary received power and $\overline{P}$ is the mean received power.

When a line-of-sight path exists between the BTS and MT the received signal comprises of both a deterministic component (i.e. the line-of-sight component) and a random multipath component. In this case, the amplitude variation in the receiver signal envelope caused by small-scale fading is Ricean distributed [14]. As the strength of the deterministic component reduces the Ricean distribution degenerates into a Rayleigh distribution.

3.5 Propagation Models used in this Thesis

This thesis is ultimately concerned about DS-CDMA cellular system performance and this requires an accurate knowledge of the momentary desired signal power and interference power at the receiver. Propagation models for an outdoor macro-cellular system and an indoor pico-cellular system located in an office tower block are presented in the following sections. These models are used in Chapters 6–9 to estimate received signal power at different MT locations.

3.5.1 Outdoor Macro-Cellular Model

The proposed outdoor macro-cellular propagation model assumes that cell radii are in the order of 100's or 1000's of metres and that no single obstacle dominates the propagation environment. Only broad measures of the environmental characteristics are taken into account and this approach is considered reasonable with large cells as it is impractical to individually account for all the physical objects in the system e.g. buildings. A 260 ns system chip period is assumed, which is specified in the 3GPP standards for 3G cellular systems, and in many outdoor environments the propagation channel will be time dispersive and this is factored into the propagation model (see Section 3.4).

The proposed model is shown in Figure 3.5 and is used in Chapters 6, 8, and 9. The transmitted signal experiences large-scale path loss, defined in Equation 3.3, which is common to all the time dispersed signal versions. The path loss exponent n and shadowing parameter σ, defined in Equation 3.3, capture the broad characteristics of the propagation environment. The kth time dispersed signal version has an excess delay of τ_k and static gain of a_k which represents its relative strength. All signal versions experience uncorrelated Rayleigh fading.

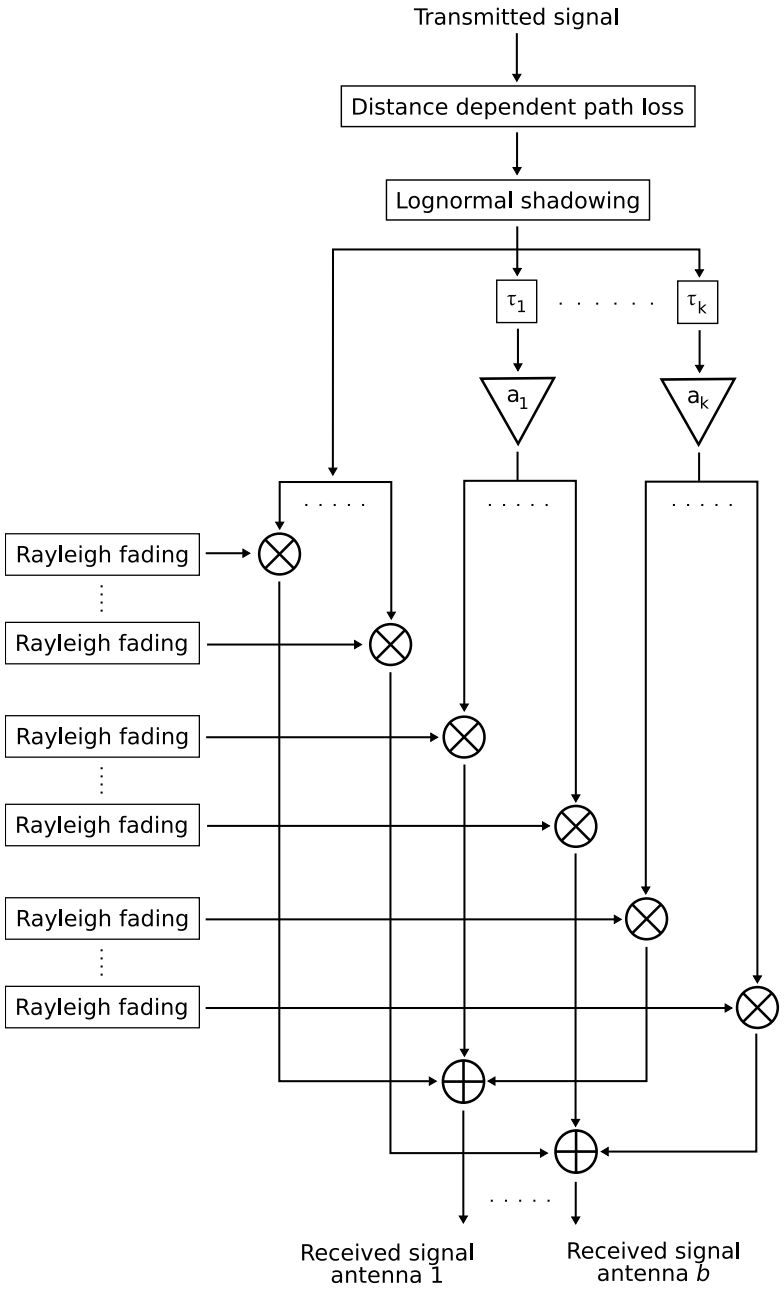

Figure 3.5: Proposed outdoor macro-cellular propagation model with a time dispersive propagation channel. The kth time dispersed signal version has an excess delay of τ_k and static gain of a_k.

3.5.2 Indoor Engineering School Tower Model

Propagation models for indoor pico-cellular environments must account for the architectural properties of the building where the system is deployed (e.g. wall locations, the number of floors, building materials) as this has a significant impact on the propagation characteristics [57]. Because there is an extremely diverse range of potential indoor environments, and because propagation modelling is not the primary focus of this thesis, only a single indoor environment is considered.

An indoor pico-cellular system is assumed to be deployed in the prototypical 12 storey office tower shown in Figure 3.6. The outside of the building consists almost entirely of glass windows with a concrete ledge extending out between floors. Offices are located around the outside of the building and a corridor separates the offices from a central structural core that houses a stairwell and lifts. The office walls are constructed with a mix of wood and plasterboard while the central core and floors are constructed with reinforced concrete. A floor plan of the 8th floor is shown in Figure 3.7 and floors 5–10 all have similar layouts.

Figure 3.6: External view of the Engineering School Tower.

A propagation measurement database is used to calculate the large-scale path loss between 10 potential BTS locations on floors 6–10 and 49 potential MT locations on the 8th floor. These locations are shown in Figure 3.7 and the 10 potential BTS locations are labelled TX-A and TX-B on floors 6–10. Further information about the propagation measurement database can be found in Appendix A. A 260 ns system chip period, which is specified in the 3GPP standards for 3G cellular systems, and non-time dispersive propagation channel are assumed since indoor pico-cellular systems typically have relatively low RMS delay spreads (see Section 3.4).

The proposed indoor pico-cellular propagation model for the Engineering School Tower is shown in Figure 3.8 and is used in Chapter 7. The transmitted signal experiences large-scale path loss and the forementioned propagation measurement database is used to calculate the path loss at different MT locations. All signal versions experience uncorrelated Rayleigh fading.

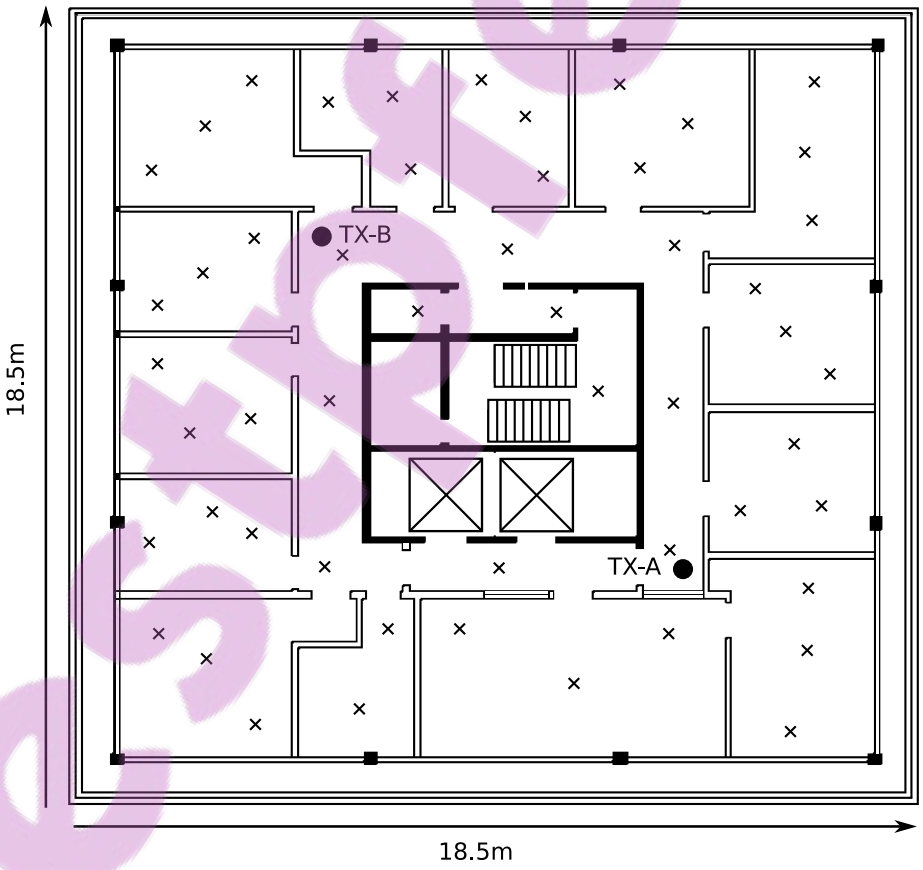

Figure 3.7: Floor plan of the Engineering School Tower 8th floor. Potential BTS locations are TX-A and TX-B and potential MT locations are marked '×'.

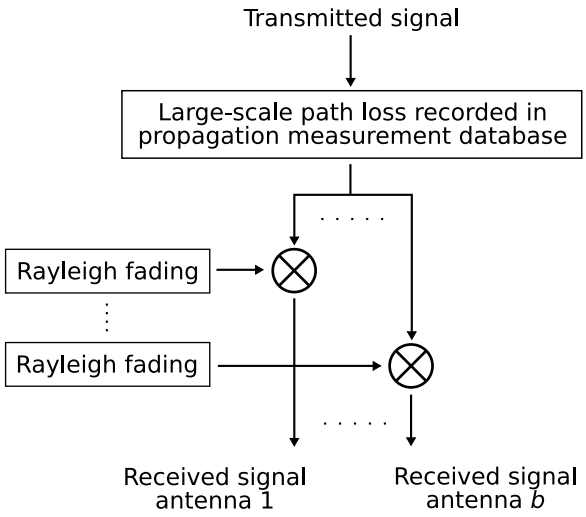

Figure 3.8: Proposed indoor pico-cellular propagation model for the Engineering School Tower.

3.6 Summary

To estimate the performance of DS-CDMA cellular systems the propagation environment must first be modelled so that the desired signal power and interference power at the receiver can be estimated. The propagation environment of a typical cellular system is very hostile as a direct line-of-sight propagation path between the BTS and MT rarely exists and short-term variations in received power in excess of 20 dB are common.

The radio propagation mechanisms of reflection, diffraction, and scattering create a multipath propagation environment in cellular systems where multiple versions of the transmitted signal are received via different propagation paths with different propagation delays. Propagation loss can be explained in terms of both large-scale path loss and small-scale fading. Large-scale path loss describes the variation in mean received power as a MT moves over large distances and is impacted by the transmitter-receiver separation and the level of environmental clutter. Small-scale fading describes the rapid and large fluctuation in received power as a MT moves only short distances (in the order of wavelengths) and is caused by multipath signal versions combining in a phasor fashion at the receiver.

Propagation models for an outdoor macro-cellular system and an indoor pico-cellular system located in an office tower block were presented and these are used in Chapters 6–9 to estimate DS-CDMA cellular system performance.

Chapter 4

Teletraffic and Quality of Service

4.1 Introduction

The prime motivation for the deployment of 3G cellular systems is to offer new packet based services such as high speed Internet, video, and voice over IP (VoIP) just to name a few, and in doing so also compete with traditional fixed line broadband [3, 6]. Packet based services generate discrete variable sized packets and the resultant traffic streams are variable-bit-rate (VBR) in nature [13]. In contrast, the traffic stream generated by the traditional cellular voice service is constant-bit-rate (CBR) in nature. The purpose of this thesis is to investigate the impact of VBR traffic on the performance of DS-CDMA cellular systems. Consequently, the packet based services that could potentially be offered by a cellular system must first be understood and appropriate traffic models developed.

An overview of packet based services and their associated quality of service (QoS) requirements is given in Section 4.2. Traffic characterisation and traffic model development is discussed in Section 4.3 and five traffic models with diverse characteristics are proposed in Section 4.4. These models are used in Chapters 6–9 to evaluate cellular system performance with different types of traffic. Traffic scheduling directly impacts the statistical properties of the aggregate traffic stream transmitted over the radio channel and the impact of traffic scheduling on system performance is discussed in Section 4.5.

4.2 User Services

The traffic generated by a user is directly linked to the service being used and for packet based services the traffic is almost universally VBR in nature [13]. The packet based services that could potentially be offered by a cellular system are numerous and some examples include [6]:

- voice over IP (VoIP)
- audio and video broadcasting
- web browsing
- email
- telemetry
- gaming
- peer-to-peer networking

Even services in the same general category can generate vastly different traffic streams due to different service implementations and configurations. For example, Figure 4.1 shows two video traffic streams encoded with different codecs and the different traffic characteristics are obvious.

Web browsing offers an intuitive example of how a service and its traffic are inter-linked. In a typical web browsing session a user follows the request and response pattern, specifically, a web page is requested and this causes a burst of traffic while the page downloads and this is followed with a period of minimal or no traffic as the user reads the page. This process then

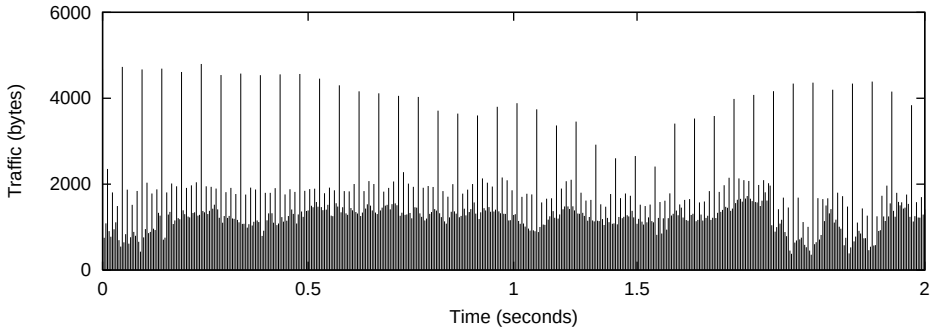

(a) TV sports broadcast – MPEG-4 encoded video with a mean bitrate of 291 kbps.

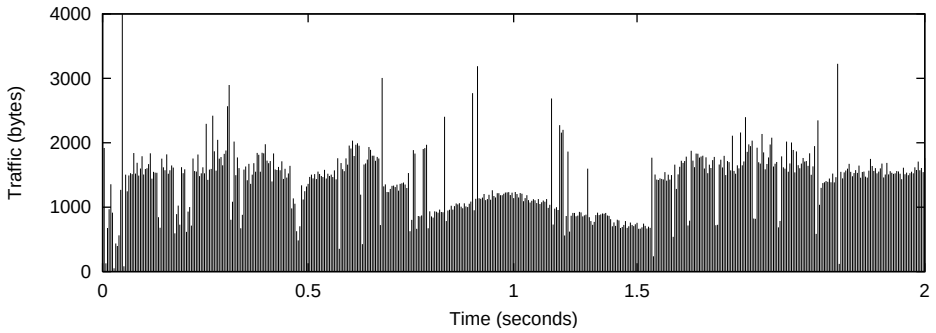

(b) TV news broadcast – H.263 encoded video with a mean bitrate of 64 kbps.

Figure 4.1: Video traffic streams encoded with MPEG-4 and H.263 codecs [15].

repeats itself as a user browses multiple web pages and the overall traffic stream appears very bursty. A web browsing traffic model is presented in following section.

The traffic stream shown in Figure 4.1(a) and the operation of the MPEG-4 codec offers another example of how a service and its traffic are inter-linked. The large periodic spikes observed in the traffic stream are due to the way the MPEG-4 codec encodes certain video frames. For most video frames the codec sends only the difference between the current and previous video frame and this requires relatively little traffic to be sent. However, the codec periodically sends a complete video frame and this requires a relatively large amount of traffic to be sent and leads to the spikes observed[1].

4.2.1 Quality of Service

User services each have their own unique QoS requirements and the system must endeavour to meet these e.g. a voice service requires a low transmission delay so that the conversation does not appear to lag. Four broad QoS classes have been defined in the 3GPP standards for 3G cellular systems and these are listed in Table 4.1.

A system may choose to pre-negotiate a set of QoS guarantees with a user before accepting a service request, or alternatively a service may simply be offered on a best effort basis. Typical quantitative QoS values that a service may request include:

- minimum user bitrate
- maximum packet delay
- maximum packet delay variation (jitter)
- probability of packet loss
- probability of bit error (BER)
- guaranteed packet delivery order

QoS is ideally considered on an end-to-end basis but this is not always possible if part of the transmission path is not controlled by the system operator e.g. traffic originating from the public Internet is generally provided on a best effort basis. In this case, the system can only guarantee QoS for the portion of the transmission path that it controls. QoS metrics that are used in this thesis include the user data rate, packet delay, probability of packet loss, and BER.

[1]These video frames are known as "I-frames" [58].

QoS class	Fundamental characteristics	Example application
Conversational	– Stringent low delay requirements – Low variation in delay (jitter)	Voice over IP
Streaming	– Low variation in delay (jitter)	Video broadcasting
Interactive	– Data integrity must be maintained – Request and response pattern	Web browsing
Background	– Data integrity must be maintained – High delay tolerated	Email

Table 4.1: QoS classes defined in the 3GPP standards for 3G cellular systems [59].

4.3 Traffic Characterisation

Identifying the characteristics of the traffic generated by a user service is important when developing a traffic model [13, 60, 61]. The web browsing model proposed by Anderlind and Zander [62] provides a useful example of how traffic characteristics can be captured in a traffic model. This particular model is illustrated in Figure 4.2 and captures the web browsing request and response pattern described in the previous section (in Figure 4.2 a web packet call corresponds to the burst of traffic that occurs when a user requests and downloads a web page). The traffic characteristics captured in this model are:

- the statistical arrival process of web sessions.
- the statistical distribution of web session time length.
- the statistical arrival process of web packet calls.
- the statistical distribution of web packet call time length.
- the statistical arrival process of packets in a packet call.
- the statistical distribution of packet sizes in a packet call.

Traffic models for packet based services are generally statistical in nature and the use of statistical distributions to model variables such as the number of packets generated per frame or packet size is self explanatory. Five traffic models with diverse statistical properties are presented in Section 4.4 and these are used in Chapters 6–9 to evaluate cellular system performance.

The presence of correlation in a traffic stream is an important characteristic that should be captured in a traffic model [61]. For example, correlation in the number of packets generated per frame can significantly impact system performance as packets then tend to arrive in bursts

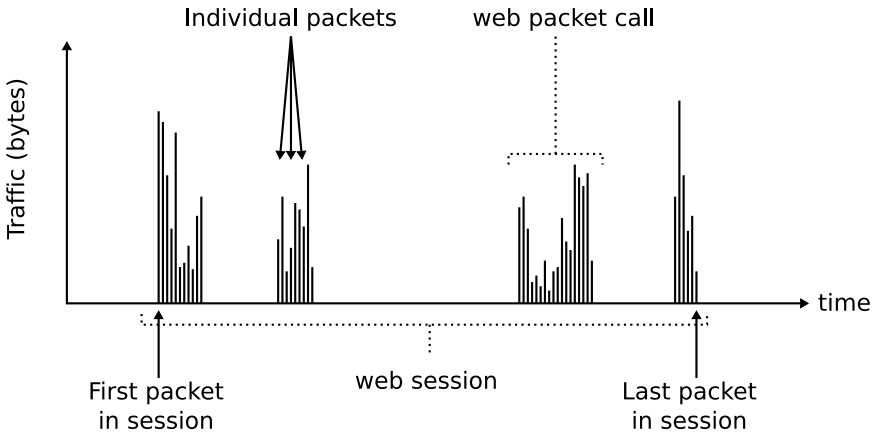

Figure 4.2: Web browsing traffic model [62].

and are more difficult to schedule for transmission (as will become evident in Section 4.5). The DAR traffic model presented in Section 4.4.5 has an auto-correlation function that decays exponentially and the level of correlation in the generated traffic stream can be controlled with a model parameter. The Pareto traffic model presented in Section 4.4.4 has an auto-correlation function that decays slower than exponentially and has a unique characteristic known as long-range dependence which is discussed in the following section.

4.3.1 Long-Range Dependent Traffic

A number of studies have shown that certain types of traffic exhibit a characteristic known as long-range dependence e.g. LAN [63], FTP [64], and video [65] traffic. Traffic that exhibits this characteristic has structural similarities on a wide range of time scales and this means that the generated traffic stream has no natural burst length and instead appears bursty over a wide range of time scales, for example, from milliseconds to minutes [63]. This phenomenon is illustrated in Figure 4.3 where a long-range dependent Pareto traffic stream (see Section 4.4.4) is compared with a non-long-range dependent Poisson traffic stream (see Section 4.4.2) over a range of time scales. The figure shows that the long-range dependent traffic stream maintains its burstiness over a range of time scales while the non-long-range dependent traffic stream does not.

The Hurst parameter, H, describes the level of variability in a long-range dependent traffic stream and a larger value indicates greater variability. Further information about this parameter and long-range dependent processes in general can found in [63]. A long-range dependent Pareto traffic model is presented in Section 4.4.4.

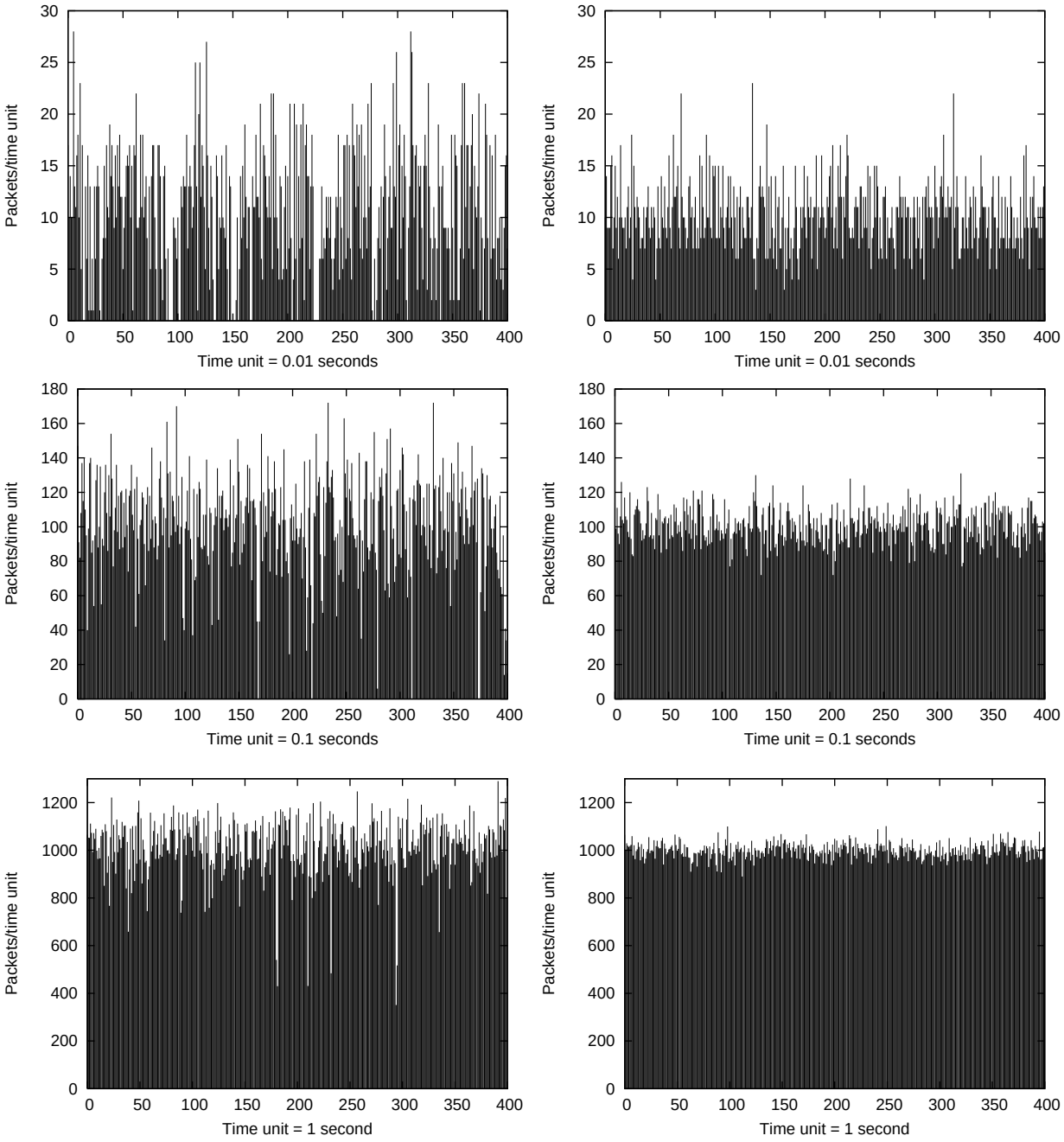

(a) Pareto traffic ($H = 0.6$)

(b) Poisson traffic

Figure 4.3: Comparison of a long-range dependent Pareto ($H = 0.6$) traffic stream and a non-long-range dependent Poisson traffic stream.

4.4 Traffic Model Development

This thesis investigates packet based services and the VBR traffic streams generated by individual users must be captured in a traffic model. Elements on the transmission path between the traffic source and traffic destination can alter the characteristics of the traffic and in many cases these elements will not be under the control of the system operator e.g. traffic originating from the public Internet could be affected by routers and firewalls that are external to the system. From a system operator's point of view, it is best to develop traffic models that describe user traffic at a point within the system that is under the operator's control. The traffic model reference point used in this thesis is shown in Figure 4.4 and this point was chosen because the radio component of a cellular system is the primary focus of this thesis i.e. the traffic offered to the BTS is modelled. Only the downlink is considered in this thesis but on the uplink the traffic model reference point would be at the MT where the traffic is generated.

The packets offered to the BTS have an arbitrary arrival time and size and before transmission over the radio channel the BTS fragments and combines the offered packets into new fixed sized packets that are matched to the radio transmission frame period and available spreading code lengths, as illustrated in Figure 4.4. The traffic models proposed in the following sections describe the number of fixed size packets offered for transmission in each radio frame (i.e. after the system re-packetisation process).

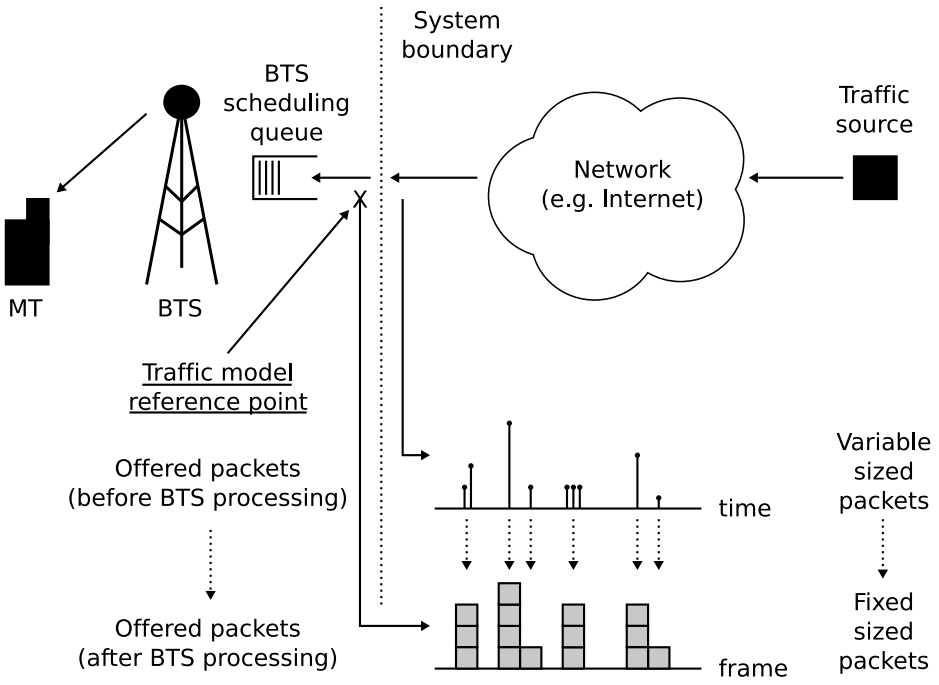

Figure 4.4: Traffic model reference point and traffic re-packetisation.

Since there is a vast number of user services and associated traffic types potentially present in a cellular system the approach taken in this thesis is to consider a small set of reasonably generic traffic models that capture the broad characteristics of VBR traffic. Five traffic models with diverse statistical properties are proposed in the following sections.

4.4.1 CBR Model

A CBR traffic model is by definition non-variable in nature. This model is proposed since it represents the traditional voice service that is dominant in many existing cellular systems and also offers a useful reference point from which to compare system performance. In Chapters 6–9 system performance is compared with CBR traffic and various types of VBR traffic.

As the name implies, the CBR model generates a constant number of packets per frame and has a probability density function given by

$$f_X(x) = \delta(x - \lambda) \tag{4.1}$$

where $\delta(\bullet)$ is the delta function and x represents the number of fixed size packets offered to the BTS scheduling queue in each frame.

4.4.2 Poisson Model

A Poisson process represents a sequence of independent events that occur randomly in time [66]. This process is assumed in many engineering applications and, for example, is the key assumption in the well known Erlang traffic formulae that are used to estimate the probability that a service request is blocked in a telecommunications network [12]. Intuitively, a Poisson process may be an appropriate model for voice call arrivals or web browsing sessions (see Section 4.3) as these could be assumed to be independent events [67]. It is arguable whether such a model is appropriate for packet arrivals but it is still an interesting model to consider because of its simplicity and wide use in many traffic related studies [64].

The sum of multiple Poisson processes is also a Poisson process and the inter-arrival time between events is independent and exponentially distributed. The Poisson model uses a Poisson distribution to represent the number of fixed size packets offered to the BTS scheduling queue in each frame and has a probability density function given by

$$f_X(x) = e^{-\lambda} \sum_{k=0}^{\infty} \frac{\lambda^k}{k!} \delta(x - k) \qquad \lambda \geq 0 \tag{4.2}$$

where λ is the rate parameter, $\delta(\bullet)$ is the delta function, and x is the number of fixed size packets offered to the BTS scheduling queue in each frame. The distribution mean and variance are respectively given by

$$\mu_X = \sigma_x^2 = \lambda \tag{4.3}$$

Figure 4.5 shows the probability density function of the Poisson model and a sample traffic stream with a mean of 1 packet per frame.

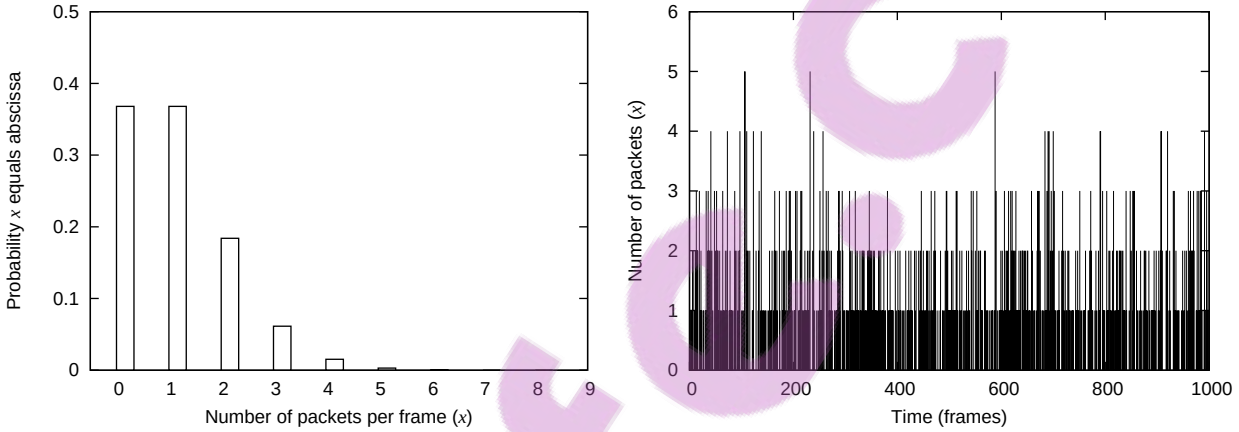

(a) Density function (b) Sample traffic stream

Figure 4.5: Probability density function of the Poisson model and a sample traffic stream with a mean of 1 packet per frame.

4.4.3 Negative Binomial Model

A study of video teleconference traffic by Heyman et al. showed that the distribution of transmitted data per video frame was adequately modelled with a negative binomial distribution [68]. The negative binomial model uses a negative binomial distribution to represent the number of fixed size packets offered to the BTS scheduling queue in each frame and has a probability density function given by

$$f_X(x) = \sum_{k=0}^{\infty} \frac{\Gamma(r+k)}{k!\Gamma(r)} p^r (1-p)^k \delta(x-k) \qquad r > 0,\ 0 < p < 1 \tag{4.4}$$

where $\Gamma(\bullet)$ is the gamma function, $\delta(\bullet)$ is the delta function, and x is the number of fixed size packets offered to the BTS scheduling queue in each frame. The distribution mean and variance are respectively given by

$$\mu_X = \frac{r(1-p)}{p} \tag{4.5}$$

$$\sigma_X^2 = \frac{r(1-p)}{p^2} \tag{4.6}$$

Unlike the Poisson distribution, the mean and variance can be varied independently i.e. there are two degrees of freedom. Figure 4.6 shows the probability density function of the negative binomial model with different levels of variance and a mean of 1 and 2 packets per frame (sub-figures (a) and (b) maintain the same ratios of μ_X/σ_X). Figure 4.7 shows sample traffic streams generated by the negative binomial model with a mean of 1 packet per frame.

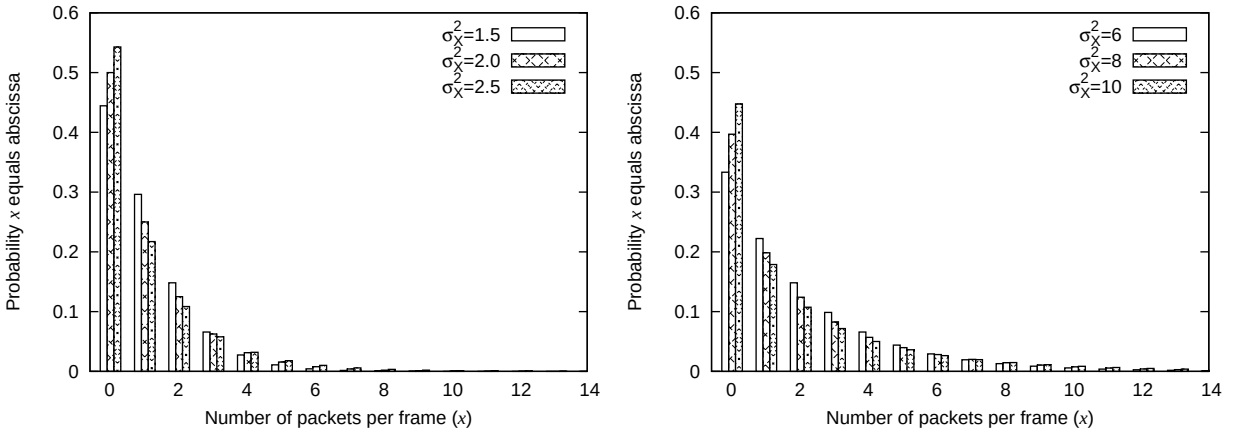

(a) $\mu_X = 1$ (b) $\mu_X = 2$

Figure 4.6: Probability density function of the negative binomial model with variance σ_X^2 and a mean of 1 and 2 packets per frame.

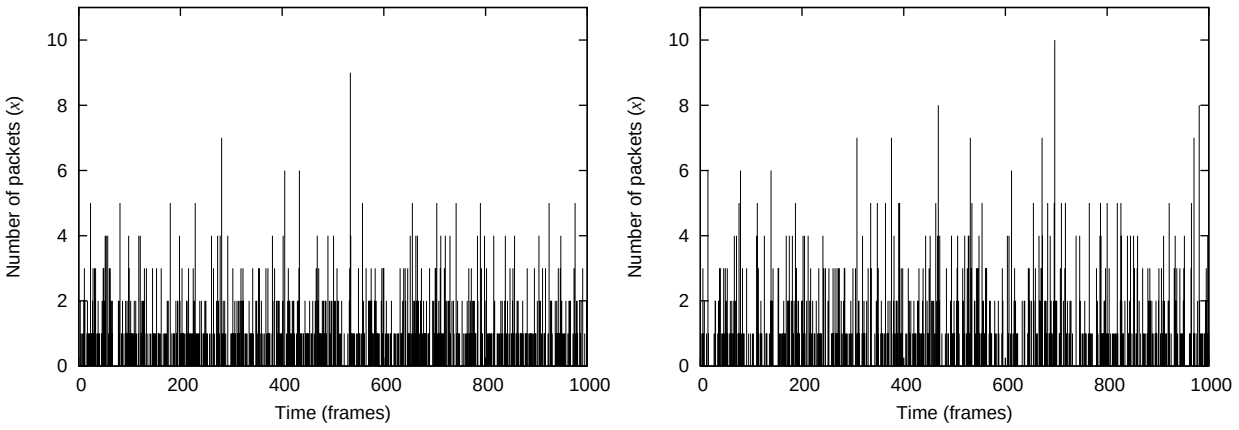

(a) $\sigma_X^2 = 1.5$ (b) $\sigma_X^2 = 2$

Figure 4.7: Sample traffic streams generated by the negative binomial model with variance σ_X^2 and a mean of 1 packet per frame.

4.4.4 Pareto Model

The Pareto model assumes that the inter-arrival time between packets has a Pareto distribution and with an appropriate parameter selection the resultant traffic stream exhibits long-range dependence and appears bursty over a wide range of time scales (see Section 4.3.1) [69]. This characteristic has been observed in a number of different types of traffic [63, 64, 65]. The probability density function of the Pareto distribution is given by

$$f_X(x) = \frac{a}{b}\left(1 + \frac{x}{b}\right)^{-(a+1)} \qquad b > 0 \tag{4.7}$$

where a is the shape parameter, b is the scale parameter, and x represents the inter-arrival time between fixed size packets offered to the BTS scheduling queue. The distribution mean and variance are respectively given by

$$\mu_X = \frac{b}{a-1} \qquad a > 1 \tag{4.8}$$

$$\sigma_X^2 = \frac{b^2}{\left(1 - \frac{1}{a}\right)^2 (a^2 - 2a)} \qquad a > 2 \tag{4.9}$$

and it should be noted that the mean number of packets offered to the BTS scheduling queue in each frame is the inverse of μ_X.

The Hurst parameter, discussed in Section 4.3.1, is commonly used to describe the level of variability in a long-range dependent traffic stream and for the Pareto arrival process this is given by

$$H = \frac{3-a}{2} \tag{4.10}$$

When $H < 0.5$ the Pareto distribution has a finite mean and variance and the resultant traffic stream does **not**exhibit long-range dependence. When $0.5 \leq H < 1$ the Pareto distribution has a finite mean and infinite variance and the resultant traffic stream does exhibit long-range dependence. A larger value of H indicates greater traffic variability. The Hurst parameter has typically been measured in the range 0.7-0.8 for traffic streams in deployed systems [63, 64, 65].

Figure 4.8 shows the probability density function of the Pareto model with different levels of long-range dependence and a mean of 1 and 2 packets per frame. Figure 4.9 shows sample traffic streams generated by the Pareto model with a mean of 1 packet per frame.

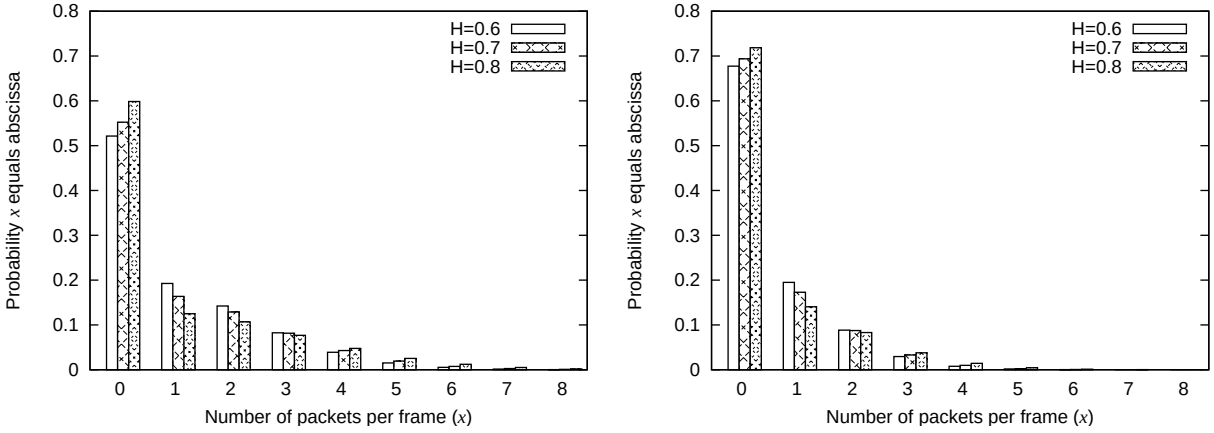

(a) $\mu_X = 1$ (b) $\mu_X = 0.5$

Figure 4.8: Probability density function of the Pareto model with long-range dependence H and a mean of 1 and 2 packets per frame.

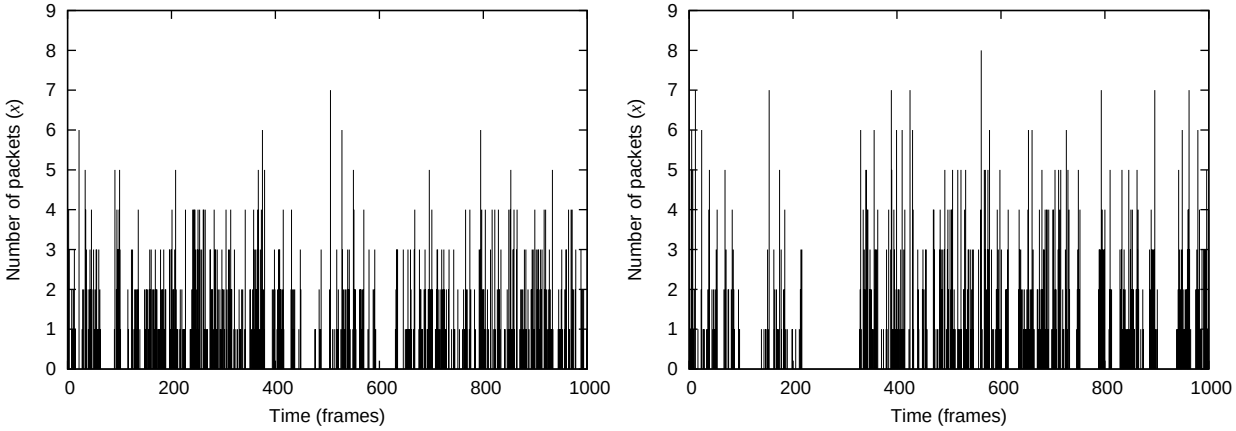

(a) $H = 0.6$ (b) $H = 0.8$

Figure 4.9: Sample traffic streams generated by the Pareto model with long-range dependence H and a mean of 1 packet per frame.

4.4.5 Discrete Auto-Regressive (DAR) Model

The DAR model consists of a time-homogeneous Markov chain i.e. the number of packets offered to the BTS scheduling queue in the current frame depends only on the number of packets offered in the previous frame. This model was proposed by Heyman et al. to model video teleconference traffic [68]. The probability that j packets are offered in a frame, if i packets were offered in the previous frame, is equal to

$$p_{ij} = \Pr(X_n = j | X_{n-1} = i) \tag{4.11}$$

where X_n is a random variable. If the maximum number of packets offered in a frame is finite then the transition probability distribution can be represented as a transition matrix P where the $(i,\ j)$th element is equal to p_{ij}. To minimise the number of model parameters the transition matrix is restricted to the form

$$P = \rho I + (1 - \rho)Q \qquad 0 \leq \rho \leq 1 \tag{4.12}$$

where ρ is the correlation coefficient, I is the identity matrix, and Q is a matrix where each row is the same identical stationary probability distribution that describes the number of packets offered in each frame.

It is assumed that the stationary probability distribution is a truncated version of the negative binomial distribution described in Section 4.4.3 i.e. the maximum number of packets offered in a frame is limited to $x_{\max}$ and the probability that more than $x_{\max}$ packets are offered in a frame is zero. The probability that less than $x_{\max}$ packets are offered in a frame is the same as the non-truncated version of the negative binomial distribution.

Figure 4.10 shows sample traffic streams generated by the DAR model with different levels of correlation and a mean of 1 packet per frame.

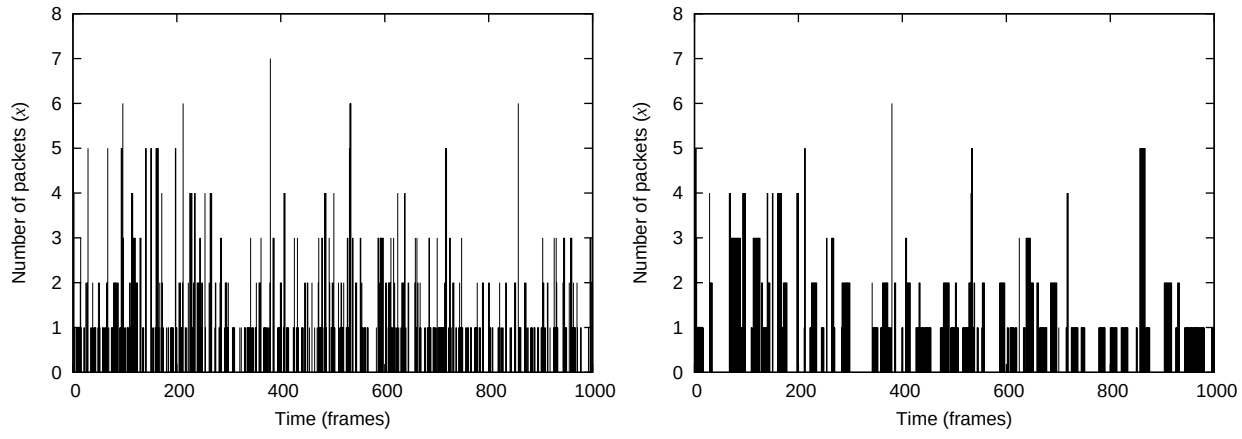

(a) $\rho = 0.4$ (b) $\rho = 0.8$

Figure 4.10: Sample traffic streams generated by the DAR model with correlation ρ and a mean of 1 packet per frame ($\sigma_X^2 = 1.5$, $x_{\max} = 16$).

4.5 Traffic Scheduling

In DS-CDMA cellular systems there is a soft capacity limit on the radio channel and additional spreading codes can be allocated to users at the cost of increased system interference and reduced propagation dependent performance. With dynamic resource allocation, a BTS can vary the number and length of spreading codes allocated to a user on a frame-by-frame basis. This form of dynamic resource allocation is essential for VBR traffic streams as it would be inefficient to allocate a fixed size radio bearer for the duration of a user's service, as there would be periods of time where the allocated bearer capacity would go unused and could be better allocated to another user.

Due to interference constraints on the propagation channel, the system must limit the maximum number of spreading codes allocated in a frame and a traffic scheduling policy is required to determine which packets are transmitted in a frame when the number of offered packets is greater than the available transmission capacity [70, 71]. A deadline sensitive traffic scheduling policy with random packet selection is used exclusively in this thesis and this policy is illustrated in Figure 4.11 [72]. Packets are assumed to have a maximum scheduling delay tolerance and if a packet cannot be transmitted within its delay tolerance then the packet is dropped prior to transmission as it is no longer of use to the end user. The scheduling policy gives highest priority to packets closest to expiry and packets that are equally close to expiry are randomly selected for transmission. Packets that cannot be transmitted in the current frame are delayed for potential transmission in a later frame. This scheduling policy obeys both the work conserving and earliest due date criteria which are known to minimise the probability of packet dropping [73].

In the example shown in Figure 4.11 the scheduling policy limits the maximum number of packets transmitted in a frame to 3 and a fixed spreading code length is assumed. The packets offered by MT 1 must be transmitted in the next available frame or else dropped (delay tolerance of 0) whereas the packets offered by MT 2 can be delayed by a maximum of one frame before they must be dropped (delay tolerance of 1).

The statistical properties of the aggregate traffic stream transmitted over the radio channel are influenced by the traffic scheduling policy and consequently this must be taken into account when evaluating a system's propagation dependent performance.

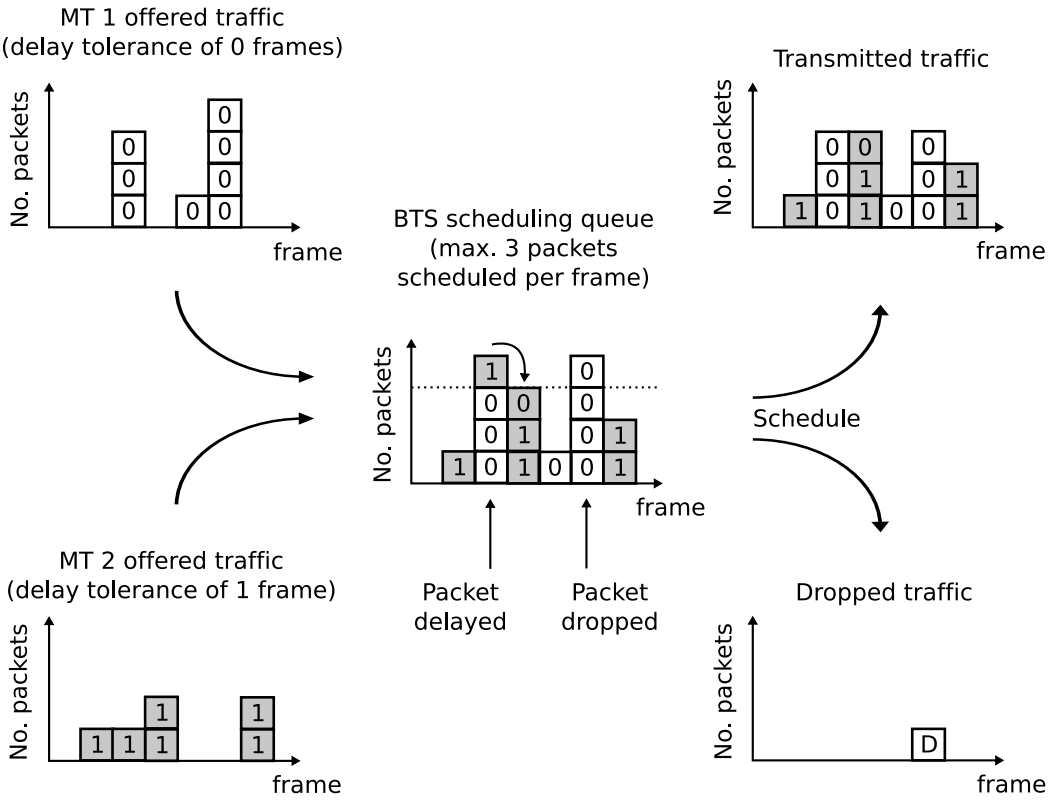

Figure 4.11: Deadline sensitive traffic scheduling policy with random packet selection.

4.6 Summary

The deployment of 3G cellular systems enables a diverse range of new packet based services to be offered to users, for example, high speed Internet, video, and voice over IP (VoIP) just to name a few. To evaluate system performance with these new services the characteristics of the traffic streams they generate must first be understood and appropriate traffic models developed.

Since there is a vast number of potential user services and associated traffic types the approach taken in this thesis is to consider a small set of reasonably generic traffic models that capture the broad characteristics of VBR traffic. Five traffic models with diverse statistical properties have been proposed and these include: a CBR model, a Poisson model, a negative binomial model, a Pareto Model, and a DAR model. These models are used in Chapters 6–9 to evaluate system performance.

In order to efficiently support VBR traffic streams on the radio channel some form of dynamic resource allocation is required. Frame-by-frame traffic scheduling was discussed and a deadline sensitive traffic scheduling policy with random packet selection was proposed.

Chapter 5

Simulation Model Development

5.1 Introduction

The previous three chapters laid the foundation necessary to develop a DS-CDMA cellular system model that can be used to evaluate system performance with VBR traffic. This chapter ties that information together and develops a simulation model that is used in Chapters 6–9 to evaluate the downlink performance of both outdoor macro-cellular systems and an indoor pico-cellular system. Simulation was selected as the performance evaluation method as using a purely theoretical mathematical approach was intractable with all the system components of interest.

A high level overview of the simulation model and simulation procedure is given in Section 5.2. The simulation steps related to traffic generation and traffic scheduling are detailed in Sections 5.3 and 5.4 respectively. The outdoor macro-cellular and indoor pico-cellular system deployment configurations considered in this thesis are described in Section 5.5. The simulation steps related to received power estimation and system performance estimation are detailed in Sections 5.6 and 5.7 respectively.

5.2 Downlink Simulation Model

The proposed simulation model represents a DS-CDMA cellular system with multiple BTS's and multiple non-stationary MT's. The main system components are illustrated in Figure 5.1 and a high level description of each component follows. MT's move within the system according to their own mobility model and connect to the BTS from which they receive the highest mean signal power. An MT traffic model is used to determine the amount of traffic

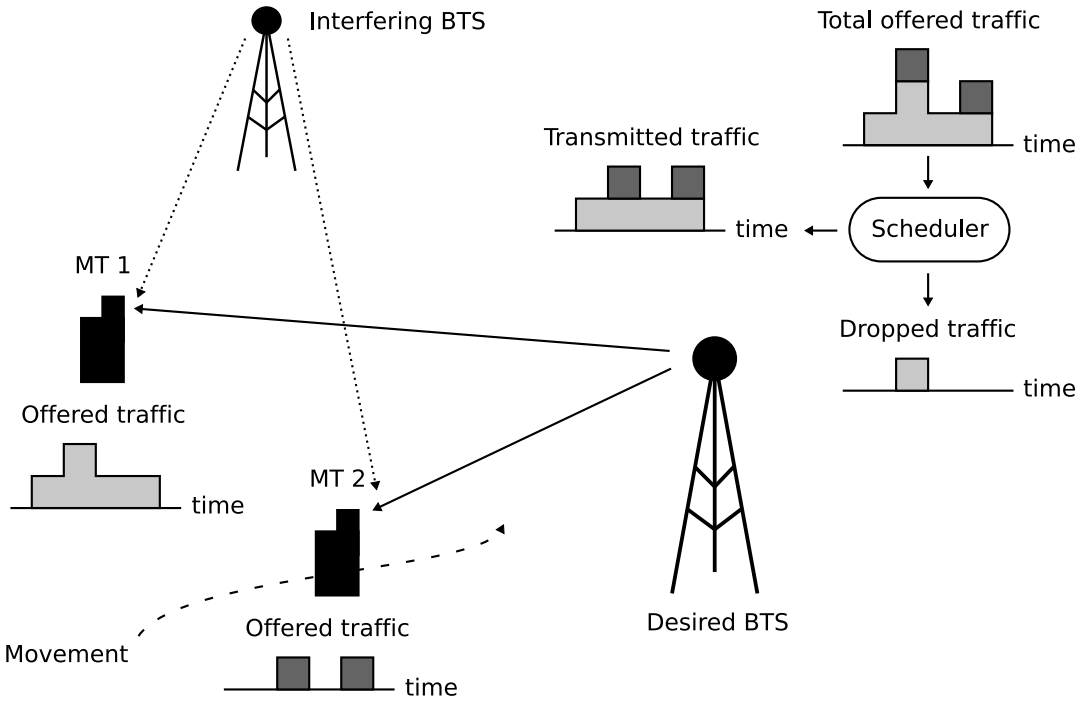

Figure 5.1: DS-CDMA cellular system model components.

that each MT offers to the BTS[1]. The offered traffic is stored in a BTS scheduling queue and is then scheduled for transmission over the radio channel. A propagation model is used to estimate the desired signal power and interference power at the MT receiver and system performance is then estimated.

The simulation procedure for the proposed model is shown in Figure 5.2. Time is broken up into fixed size transmission frames and MT's are dynamically allocated fixed size spreading codes on a frame-by-frame basis. A 2 ms frame period and 260 ns system chip period are assumed as these are specified in the 3GPP standards for high speed downlink packet access (HSDPA) 3G cellular systems [27, 74].

A traffic scheduling queue is maintained at each BTS from which packets are scheduled for transmission over the radio channel. Step (i) in the simulation procedure ensures that expired packets are dropped from the scheduling queue prior to transmission i.e. packets that have been delayed in the scheduling queue longer than their scheduling delay tolerance. Step (ii) adds any newly offered packets to the BTS scheduling queue and the number of new packets is determined by the MT traffic model. The specific details of these two steps are outlined in Sections 5.3 and 5.4.

[1]On the downlink the MT is the traffic destination and not the source but traffic is still referred to as being offered to the BTS by the MT for convenience.

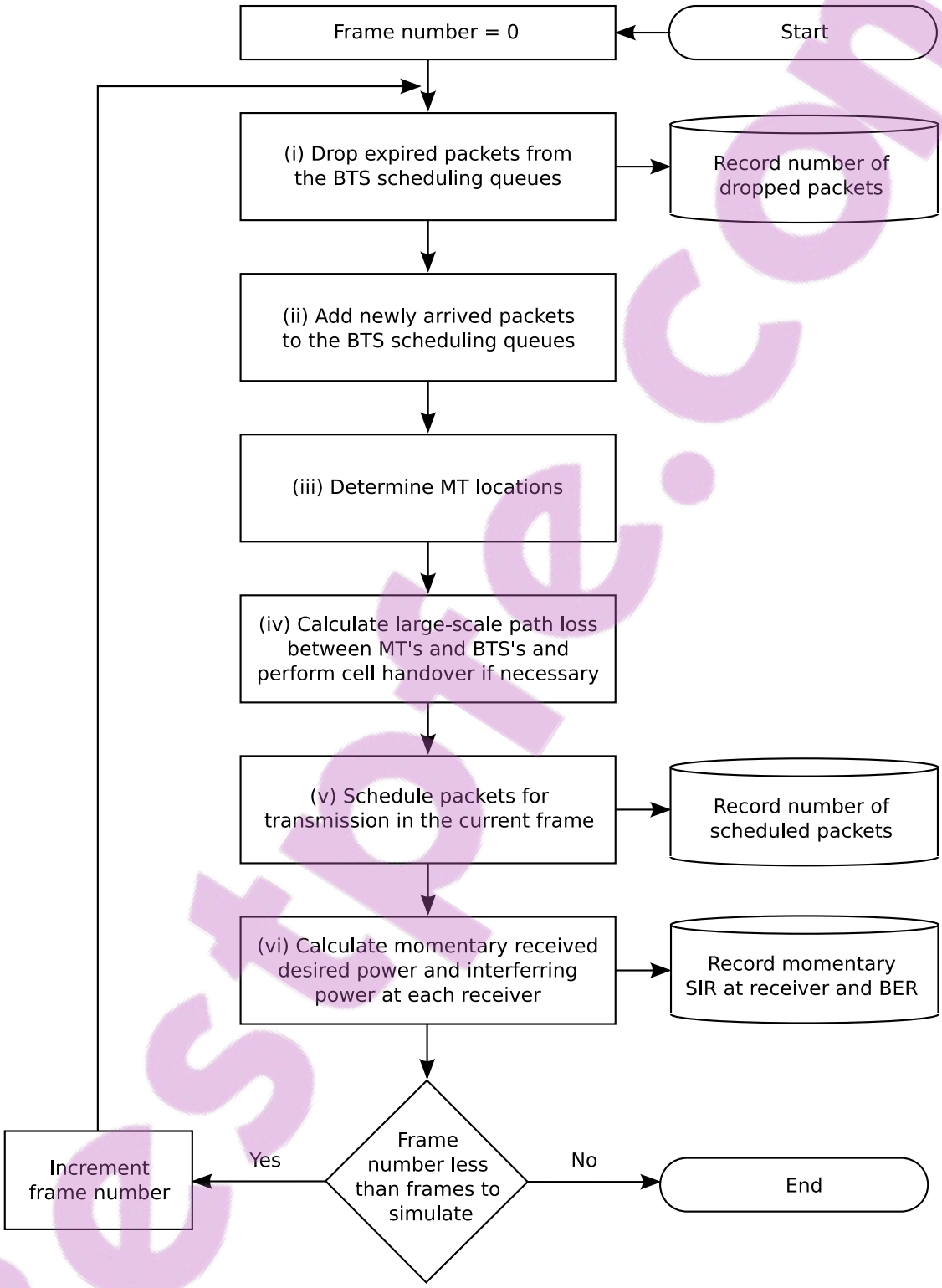

Figure 5.2: Simulation model procedure.

Step (iii) in the simulation procedure determines MT locations in the current frame. The large-scale path loss between the BTS's and MT's is then calculated in step (iv) and if necessary a cell handover is performed so that each MT is connected to the optimal BTS. Step (v) schedules the packets in the BTS scheduling queue for transmission over the radio channel and based on the packets scheduled, step (vi) calculates the momentary desired signal power and interference power at each MT receiver. The specific details of steps (iii), (iv), and (vi) are explained in Sections 5.5 and 5.6 and the specific details of step (v) are explained in Section 5.4.

In each frame iteration the packet scheduling delay, number of dropped packets, momentary SIR at the receiver, and momentary BER are all recorded.

The simulation model was implemented using C++ and an object orientated design e.g. a traffic object was used to generate user packets, a mobility object was used to determine MT location, a propagation object was used to estimate propagation path loss etc. Unit tests were written for each software object to ensure that each generated the expected deterministic or statistical output. This testing approach provided a high level of confidence that the simulation model was implemented without any software bugs. The simulation procedure shown in Figure 5.2 was performed for 100 million frames in each of the scenarios evaluated in Chapters 6–9 and this was sufficient to achieve statistical stability in the measured results (BER and probability of packet loss are measured up to six decimal places).

5.3 Traffic Generation

An MT traffic model is used to determine the number of fixed size packets offered to the BTS scheduling queue in each frame. It is important to note that the traffic model represents the traffic stream offered to the BTS scheduling queue rather than the traffic stream at the actual traffic source, as was discussed in Section 4.4. The traffic model is assumed to represent both the user data and any traffic overhead added by the system e.g. error correcting codes.

If a system was to implement some form of packet re-transmission scheme for lost packets then theoretically there would be an inter-dependency between the traffic model and the system's performance i.e. more dropped packets would create additional traffic. The proposed system model does not implement a packet re-transmission scheme but the user could still implement one themselves within the data they transmit e.g. the widely used TCP/IP protocol includes a re-transmission mechanism [75]. Even if a packet re-transmission scheme was used, the impact on the statistical properties of the traffic stream would likely be minor given the levels of packet loss that are common in actual deployed cellular systems (typically no more than a few percent). Alternatively, it could be assumed that the traffic model represents both user data and also packet re-transmissions.

Packets are assumed to require exactly one fixed size spreading code and one frame for transmission and multiple spreading codes are allocated to users to vary their momentary transmission capacity on the radio channel[2]. One Erlang of traffic is defined in this thesis as a mean traffic load of one code per frame and this is a convenient measure for traffic load as it is independent of the spreading code size. It should however be noted that this measure is only valid if all users use the same fixed size spreading code. Packets are assumed to have a maximum scheduling delay tolerance and this value is associated with the MT traffic model. Packets that are delayed in the BTS scheduling queue longer than their delay tolerance are dropped at the BTS prior to transmission.

The traffic models evaluated in this thesis are listed in Table 5.1. The CBR and Poisson models have one degree of freedom which can be used to control the mean MT traffic load. The negative binomial and Pareto models have two degrees of freedom which can be used to control both the mean MT traffic load and traffic stream variability. The DAR model has a truncated negative binomial distribution and compared to the negative binomial model has an additional degree of freedom that can be used to control the level of correlation in the traffic stream[3].

Model name	Model description	Chapter evaluated
CBR	Section 4.4.1	6–9
Poisson	Section 4.4.2	8
Negative binomial	Section 4.4.3	8–9
Pareto	Section 4.4.4	6–8
DAR	Section 4.4.5	9

Table 5.1: Traffic models evaluated in this thesis.

5.4 Traffic Scheduling

Packets that are offered to the BTS are stored in the BTS scheduling queue and are then scheduled for transmission over the radio channel. Each BTS maintains its own scheduling queue and the queue capacity is assumed to be unlimited. The deadline sensitive scheduling policy presented in Section 4.5 is used exclusively in this thesis. Packets are assumed to have a maximum scheduling delay tolerance and if a packet is delayed in the scheduling queue longer than its delay tolerance then the packet is dropped prior to transmission. Packets closest to expiry have highest priority and packets that are equally close to expiry are randomly selected for transmission.

[2]A variable spreading factor could also be used.

[3]In this thesis the DAR model $x_{\max}$ parameter is not considered a useful degree of freedom.

A fixed size spreading code is assumed and the number of spreading codes that can be allocated in a frame is detailed in each of the scenarios considered in Chapters 6–9. Both the packet scheduling delay and probability of packet dropping are important performance metrics and these are recorded during the simulation procedure.

5.5 Cellular System Deployment

Both outdoor macro-cellular systems and an indoor pico-cellular system are considered in this thesis. Chapters 6, 8, and 9 evaluate the performance of outdoor macro-cellular systems and Chapter 7 evaluates the performance of an indoor pico-cellular system. The system deployment configurations and propagation models used are presented in the following sections.

5.5.1 Outdoor Macro-Cellular System

The outdoor macro-cellular system model assumes an idealised hexagonal cell structure with omni-directional BTS antennas, as illustrated in Figure 5.3. The only significant inter-cell interference is assumed to emanate from the six immediately adjacent co-channel cells and a cell frequency re-use factor of 1 is used.

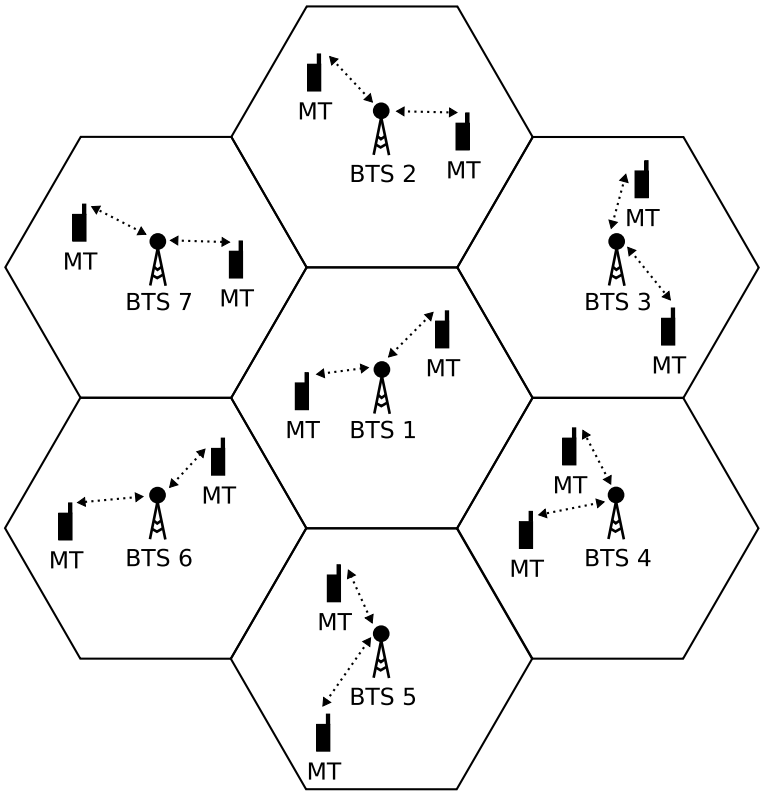

Figure 5.3: Outdoor macro-cellular system with an idealised hexagonal cell structure.

The propagation environment is modelled with the outdoor macro-cellular propagation model presented in Section 3.5.1. A power law distance dependent path loss exponent of $n = 4$ and lognormal shadowing variability of $\sigma = 8\,\text{dB}$ are assumed, unless stated otherwise[4]. Small-scale Rayleigh fading is assumed and both non-time dispersive and time dispersive propagation channels are considered. The combination of lognormal shadowing and Rayleigh fading is referred to as a Suzuki propagation environment [76]. The propagation channel power delay profiles evaluated are listed in Table 5.2 and these are sample profiles recommended in the 3GPP standards for 3G cellular systems.

Fixed size spreading codes are used and each code is allocated the same transmission power. The momentary BTS transmitter power is equal to the sum of the power allocated to each scheduled spreading code and is therefore proportional to the momentary cell traffic load. Receiver noise power is assumed to be insignificant compared to interference power and consequently relative BTS transmitter powers are sufficient to calculate system performance. No power control is used on the downlink.

MT's connect to the BTS from which they receive the highest mean signal power and move only within the cell where they are located. This means that no cell handovers occur as MT's are always connected to the optimal BTS and this simplifies performance analysis as the mean cell traffic load remains constant.

	Excess delay (ns)	Relative mean power (dB)
Delay profile 1	0	0
	976	0
Delay profile 2	0	0
	976	-10
Delay profile 3	0	0
	976	0
	20000	0

Table 5.2: Propagation channel power delay profiles [77].

5.5.2 Indoor Pico-Cellular System

The indoor pico-cellular system model assumes that the system is deployed in the Engineering School Tower described in Section 3.5.2. The system contains 5 BTS's deployed on floors 6–10, one on each floor, and each BTS's coverage area is the floor that it is located on. The building floor plan, shown in Figure 3.7, is similar on floors 6–10 and system performance is

[4]Section 6.5 considers lognormal shadowing variability of $\sigma = 4$, 8, and 12 dB.

evaluated for users on the 8th floor. A cell frequency re-use factor of 1 is used and inter-cell interference emanates from the four cells above and below the 8th floor.

There are 2 potential BTS locations on each floor and 49 potential MT locations on the 8th floor and these are shown in Figure 3.7. The propagation measurement database detailed in Appendix A is used to calculate the large-scale path loss between all potential BTS and MT locations. Small-scale Rayleigh fading and a non-time dispersive propagation channel are assumed.

Fixed size spreading codes are used and each code is allocated the same transmission power. The momentary BTS transmitter power is equal to the sum of the power allocated to each scheduled spreading code and is therefore proportional to the momentary cell traffic load. Receiver noise power is assumed to be insignificant compared to interference power and consequently relative BTS transmitter powers are sufficient to calculate system performance. No power control is used on the downlink.

MT's always connect to the BTS on the floor that they are located on, even if a higher mean signal power is received from another BTS[5]. This may not be optimal but it ensures that no cell handovers occur and this simplifies performance analysis as the mean cell traffic load remains constant. It should also be noted that this non-optimality applies to all traffic types when comparing system performance.

5.6 Received Power Estimation

The desired signal power, intra-cell interference power, and inter-cell interference power at the receiver must all be known to calculate system performance. The generalised procedure used to calculate received power is shown in Figure 5.4 and encompasses both the outdoor macro-cellular system and indoor pico-cellular system propagation environments described in the previous section (also see Figures 3.5 and 3.8). All received signal versions experience a common large-scale path loss and uncorrelated small-scale Rayleigh fading. With a time dispersive propagation channel the relative powers of the signal versions determine the level of self-interference and this is explained in the following section. Receiver noise power is assumed to be insignificant compared to interference power and consequently relative BTS transmitter powers are sufficient to calculate system performance.

[5]Note that the concrete floors do provide a high level of cell isolation.

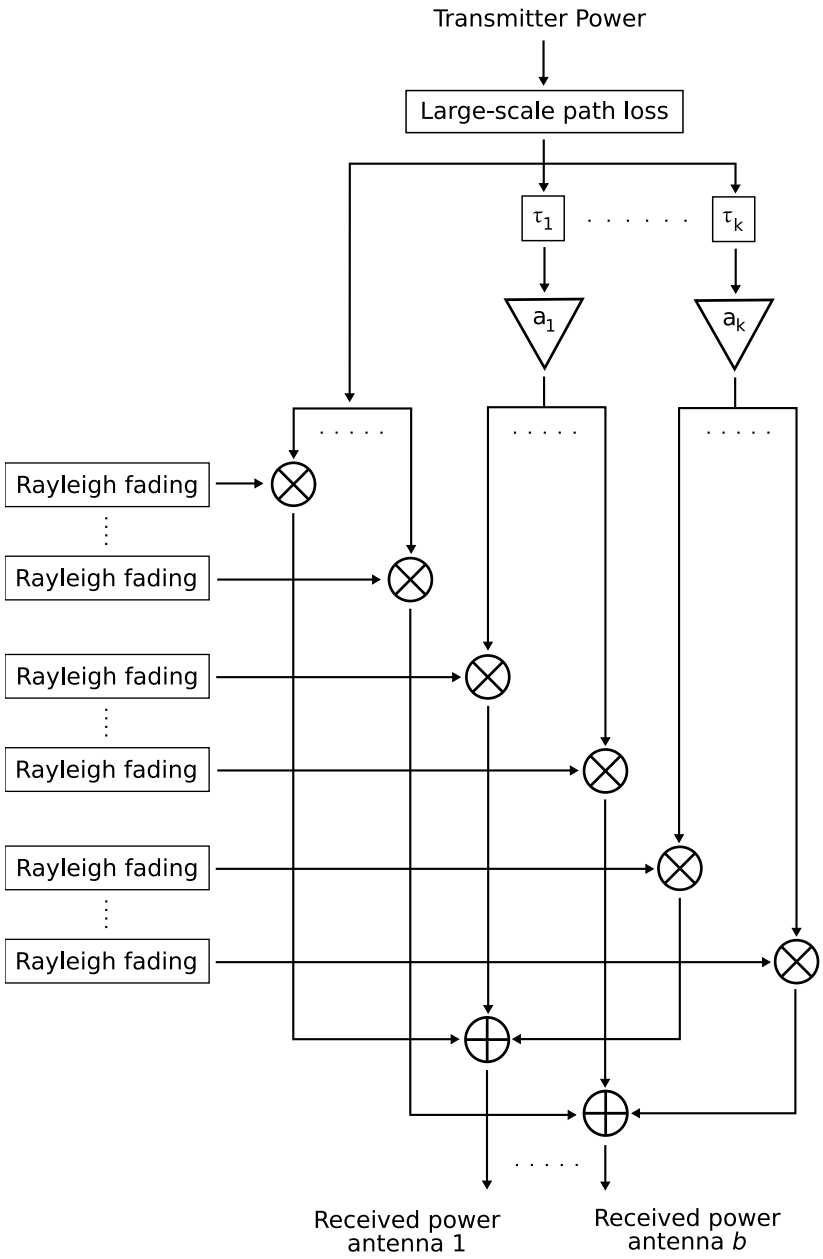

Figure 5.4: Generalised procedure to calculate received power with multiple receiver antennas. The kth time dispersed signal version has an excess delay of τ_k and static gain of a_k.

5.7 Performance Estimation

The performance metrics of interest in this thesis can be broken into two categories, namely, traffic scheduling related metrics and propagation related metrics. The traffic scheduling related metrics of interest are the packet scheduling delay and the probability of packet dropping. The propagation related metrics of interest are the receiver SINR distribution, in particular the probability that the momentary SINR at the receiver is less than the receiver capture ratio[6], and the probability of bit error (BER). The traffic scheduling related metrics were outlined in Section 4.5 and their calculation is self-explanatory. Calculation of the propagation related metrics requires further explanation and this is detailed below.

A mathematical technique to estimate the momentary SINR at the receiver and momentary BER was presented in Section 2.5. This technique is generalised below to take into account the system configurations considered in this thesis. The factors that need to be included in this more generalised technique include the use of OVSF spreading codes (see Section 2.5.1), a potentially time dispersive propagation channel, the use of RAKE receiver and antenna space diversity, and receiver noise power is assumed to be insignificant compared to interference power. Taking this into consideration and generalising Equation 2.17, the signal-to-interference ratio (SIR) on the bth antenna and fth finger of a RAKE receiver can be expressed as

$$SIR_{b,f} = c \cdot s_f \cdot \frac{P_{desired,b,f}}{I_{inter,b} + I_{intra,b,f} + I_{self,b,f}} \tag{5.1}$$

where c is a constant that depends on the cross correlation properties of the spreading codes used, s_f is the spreading factor, $P_{desired,b,f}$ is the desired signal power on the bth antenna that is synchronised with the fth finger of the RAKE receiver, $I_{inter,b}$ is the total inter-cell interference power on the bth antenna, $I_{intra,b,f}$ is the total intra-cell interference power on the bth antenna that is not synchronised with the fth finger of the RAKE receiver, and $I_{self,b,f}$ is the desired signal power on the bth antenna that is not synchronised with the fth finger of the RAKE receiver (i.e. self interference)[7]. It is assumed that $c = 1$ and values in the range $1 \leq c \leq 3$ are commonly used in the literature [16, 30, 31].

Figure 5.5 illustrates the signal power components defined in Equation 5.1. With a time dispersive propagation channel only the desired signal power that is synchronised with the RAKE receiver finger is useful. Any desired signal power that is not synchronised with the RAKE receiver finger acts as a source of self-interference. With a non-time dispersive propagation channel there is no self-interference and only the first RAKE receiver finger is

[6]The receiver capture ratio is defined as the minimum required SINR at the receiver to successfully capture the transmitted spreading code.

[7]Spreading code synchronisation was discussed in Section 2.5.

useful. Intra-cell interference originates from the same BTS as the desired signal and the intra-cell interference that is synchronised with the RAKE receiver finger is cancelled out due to the orthogonal properties of the OVSF spreading codes. Intra-cell interference that is not synchronised with the RAKE receiver finger acts as a source of interference. Inter-cell interference originates from other BTS's and because it is not synchronised with the RAKE receiver finger it acts as a source of interference.

The number of desired signal components that a RAKE receiver can resolve depends on the time separation between the signal components and this must be greater than the system chip period. If the signal components on each RAKE receiver finger and antenna are combined using maximal ratio combining (see Section 2.6) then the composite SIR at the receiver output is given by

$$SIR = \sum_{b=1}^{B} \sum_{f=1}^{F} SIR_{b,f} \tag{5.2}$$

where B is the number of antennas and F is the number of RAKE receiver fingers. The composite interference is assumed to be Gaussian distributed and with a BPSK or QPSK modulation scheme the BER can be derived from Equation 2.18.

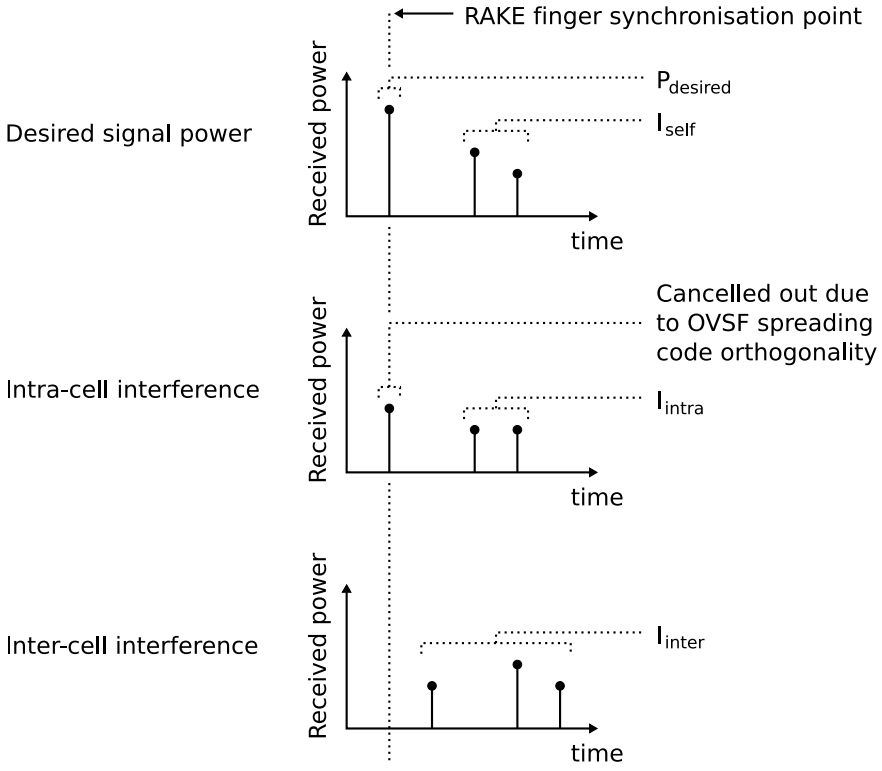

Figure 5.5: The power received on a RAKE receiver finger with a time dispersive propagation channel. Spreading codes transmitted from the same BTS are synchronised and OVSF spreading codes are used.

5.8 Summary

A DS-CDMA cellular system simulation model has been developed to evaluate the downlink performance of both outdoor macro-cellular systems and an indoor pico-cellular system with VBR traffic. Simulation was selected as the performance evaluation method as using a purely theoretical mathematical approach was intractable with all the system components of interest.

The proposed simulation model represents a cellular system with multiple BTS's and multiple non-stationary MT's. The key system model components are an MT traffic model that is used to determine the amount of traffic offered to each BTS, a BTS traffic scheduling policy that performs frame-by-frame dynamic resource allocation on the radio channel, and a radio channel propagation model. The system performance metrics that are measured are the packet scheduling delay, probability of packet dropping, receiver SIR distribution, and BER.

Chapter 6

Downlink Performance in Outdoor Macro-Cellular Environments

6.1 Introduction

This chapter identifies scenarios where the downlink performance of a typical DS-CDMA outdoor macro-cellular system is sensitive to the statistical properties of the user traffic. A typical system in this environment has cell diameters in the order of 100's or 1000's of metres and obstacles such as hills and buildings obstruct the propagation path between the BTS and MT. System performance is evaluated with two statistically dissimilar traffic models in order to obtain a measure of performance sensitivity to traffic type and the system model developed in Chapter 5 is used to evaluate system performance. The scenarios that are identified as sensitive to traffic type are investigated in further detail in Chapter 8 where an emphasis is placed on how specific traffic types affect performance.

The two traffic models considered in this chapter are outlined in Section 6.2. The downlink performance of the outdoor macro-cellular system described in Section 5.5.1 is then evaluated in Sections 6.3 and 6.4. Section 6.3 considers a non-time dispersive propagation environment while Section 6.4 considers a time dispersive propagation environment and receiver diversity. The impact of the propagation environment hostility on system performance is evaluated in Section 6.5.

6.2 BTS Transmitter Power Distribution

Two statistically dissimilar traffic models are used in this chapter to evaluate system performance and these models represent individual MT traffic streams offered to the BTS. The first model is the simple deterministic CBR model presented in Section 4.4.1 and the second

model is the bursty Pareto ($H = 0.8$) model presented in Section 4.4.4[1]. The CBR model represents a traditional voice service that requires a fixed size radio bearer for the duration of the service while the Pareto model represents a bursty VBR packet service.

It is assumed that the BTS allocates the same transmission power to each spreading code and therefore the momentary BTS transmitter power is proportional to the number of spreading codes (i.e. packets) transmitted in a frame. Hence, variability in the aggregate transmitted traffic stream directly translates into variability in the BTS transmitter power and this in turn leads to variability in the system interference power. Figure 6.1 shows the BTS transmitter power probability density function with m MT's per BTS and the Pareto ($H = 0.8$) traffic model. It is assumed that each MT offers 1 Erlang of traffic and that the BTS limits the maximum number of spreading codes transmitted per frame[2]. Note that the discontinuity in Figure 6.1(a) with $m = 8$ and a normalised transmitter power of 16 is due to the non-negligible probability that more than 16 packets are offered in a frame and the fact that the BTS limits the maximum number of spreading codes transmitted in a frame to 16.

The shape of the probability density function obviously depends on the statistical properties of the aggregate transmitted traffic stream and this is inherently linked to the statistical properties of the individual MT traffic streams. The probability density function with the CBR traffic model is simply a delta function as the number of spreading codes transmitted in each frame is constant. As the number of MT's per BTS increases the central limit theorem comes into effect and the probability density function becomes more Gaussian [66].

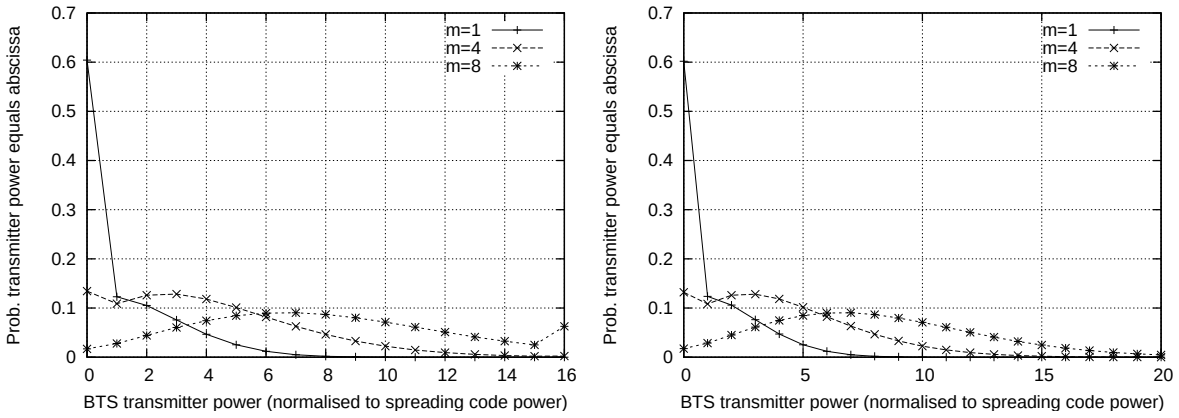

(a) max. 16 codes per frame

(b) max. 64 codes per frame

Figure 6.1: BTS transmitter power probability density function with m MT's per BTS and the Pareto ($H = 0.8$) traffic model. Each MT offers 1 Erlang of traffic and the BTS limits the maximum number of spreading codes transmitted per frame and drops any excess offered packets.

[1] A value of $H = 0.8$ was selected as this has been measured for traffic streams in deployed systems (see Section 4.4.4).

[2] An Erlang of traffic is defined in Section 5.3 and is equal to a mean traffic load of one packet per frame.

Table 6.1 shows the probability that the BTS drops an offered packet with the Pareto ($H = 0.8$) traffic model and a maximum of 16 and 64 available spreading codes per frame, which are the two scenarios considered in this chapter. Packets are assumed to have zero scheduling delay tolerance and with 8 MT's per BTS the probability of packet dropping is less than 2% with 16 available spreading codes and less than 10^{-6} with 64 available spreading codes. No packet dropping occurs with the CBR traffic model if the number of MT's per BTS is less than or equal to the number of available spreading codes. The significance of the level of packet dropping needs to be considered in conjunction with the level of packet loss due to propagation as both of these sources determine overall packet loss.

In the scenarios considered in this chapter the system traffic scheduling policy has minimal impact on the BTS transmitter power distribution. This is due to the low level of packet dropping, which is shown in Table 6.1, and the assumed zero packet scheduling delay tolerance. Consequently, the statistical properties of the aggregate transmitted traffic stream are similar to the statistical properties of the aggregate offered traffic stream. Chapter 9 considers a number of different scheduling policies that deliberately alter the statistical properties of the aggregate transmitted traffic stream, which is also known as traffic shaping.

No. MT's (m)	Max. 16 codes per frame	Max. 64 codes per frame
1	0.000000	0.000000
2	0.000009	0.000000
3	0.000123	0.000000
4	0.000656	0.000000
5	0.001999	0.000000
6	0.004695	0.000000
7	0.009269	0.000000
8	0.016418	0.000000

Table 6.1: Probability the BTS drops an offered packet with m MT's per BTS and the Pareto ($H = 0.8$) traffic model. Each MT offers 1 Erlang of traffic and all packets have zero scheduling delay tolerance.

6.3 A Non-Time Dispersive Suzuki Propagation Environment

This section evaluates the downlink performance of the outdoor macro-cellular system detailed in Section 5.5.1. A non-time dispersive propagation channel, large-scale path loss exponent of $n = 4$, and lognormal shadowing variability of $\sigma = 8\,\text{dB}$ are assumed[3]. Section 6.4

[3]Full details of the system model and propagation model can be found in Chapter 5.

considers a time dispersive propagation channel with receiver diversity and Section 6.5 considers different levels of lognormal shadowing variability.

BTS's with omni-directional antennas are located on a regular hexagonal grid and the only significant inter-cell interference is assumed to emanate from the 6 immediately adjacent co-channel cells. OVSF spreading codes are used exclusively and their orthogonal nature, in conjunction with the non-time dispersive propagation channel, means that no intra-cell interference occurs i.e. only inter-cell interference. BTS's use a fixed spreading factor and allocate the same transmission power to each spreading code. Packets are assumed to have zero scheduling delay tolerance and each BTS limits the maximum number of codes transmitted per frame to the value of the spreading factor i.e. a maximum of 16 or 64 spreading codes per frame in the scenarios considered (excess packets are dropped).

Unless stated otherwise, MT's move randomly within their own cell and all potential cell locations are equally likely. MT's connect to the BTS from which they receive the highest mean signal power and the MT mobility model ensures that no cell handovers occur. Each MT offers 1 Erlang of traffic and spreading factors of 16 and 64 are considered. A QPSK modulation scheme and system chip rate of 3.84 Mcps is assumed and this translates into a radio bearer bitrate of 480 kbps per code with a spreading factor of 16 and a radio bearer bitrate of 120 kbps per code with a spreading factor of 64. Performance is evaluated with the CBR and Pareto ($H = 0.8$) traffic models discussed in the previous section.

6.3.1 Random MT Location Within Own Cell

Figures 6.2–6.7 show system downlink performance when all MT's move randomly within their own cell and there are m MT's per cell. In all cases the Pareto traffic model has superior BER and coverage performance than the CBR traffic model, especially at low loads[4]. As the number of users and traffic load increases the level of performance difference reduces. Table 6.2 compares BER performance with the two traffic models and shows that the percentage difference between the two models is similar with both spreading factors of 16 and 64 (the larger discrepancy when $m = 1$ is explained below). Note that Figures 6.2–6.7 and Table 6.2 only show values of m up to $m = 8$ as for values greater than this the performance difference between the traffic models is negligible.

To understand how a performance difference manifests itself consideration must be given to the receiver's SIR distribution. Regardless of the traffic model, the SIR distribution will naturally have some degree of spread due to the random nature of the propagation channel e.g. MT location, lognormal shadowing, and Rayleigh fading all influence the received desired signal power and interference power. The average BER is a function of the receiver SIR

[4]Coverage performance is defined as the probability the momentary SIR at the receiver is less than the receiver capture ratio.

distribution and BER vs. SIR curve of the modulation scheme used, which in this case is QPSK. The traffic model impacts the BTS transmitter power distribution, which in turn impacts the interference power distribution, and this in turn impacts the receiver SIR distribution and leads to a potential performance difference between the traffic models.

The actual performance difference between the traffic models depends on the level of non-linearity in the BER vs. SIR curve and how the receiver SIR distribution weights the various points on the curve. For example, the SIR distribution spread with the Pareto traffic model is larger than with the CBR traffic model due to the greater BTS transmitter power variability and interference variability associated with the Pareto model. In the scenarios considered, the Pareto model has superior performance than the CBR model because the benefit of having a greater probability of high SIR values exceeds the cost of also having a greater probability of low SIR values.

Different sections of the BER vs. SIR curve have different levels of non-linearity and this impacts the performance results. For example, the only material difference between the spreading factor of 16 and spreading factor of 64 scenarios is a 6 dB difference in receiver processing gain. This can be seen in Figures 6.4 and 6.7 which show an identical SIR distribution except for a horizontal shift equal to the 6 dB difference in receiver processing gain i.e. there is a 6 dB shift in the SIR distribution mean. Table 6.2 shows that when $m = 4$ and $m = 8$ a 6 dB shift in the SIR distribution mean has minimal impact on the performance difference between the two traffic models but when $m = 1$ the impact is more significant.

As the number of MT's increases the central limit theorem comes into effect and the aggregate offered traffic stream statistically becomes more Gaussian and the variability of the traffic stream reduces relative to the mean. In general, this reduces the performance difference between the two traffic models as the receiver SIR distributions associated with the traffic models statistically become more similar. This can be seen in Figures 6.2–6.7 and Table 6.2 which show a reduced performance difference between the traffic models as the number of MT's increases.

System coverage performance is measured in terms of the probability that the momentary SIR at the receiver is less than the receiver capture ratio. Figures 6.3 and 6.6 show that the Pareto traffic model has superior coverage performance than the CBR traffic model with the receiver capture ratios considered. Coverage performance obviously depends on the receiver's SIR distribution and it should be noted that the probability of extremely low SIR values is actually greater with the Pareto model due to the potential for bursts of interference. The receiver SIR cumulative distribution functions shown in Figures 6.4 and 6.7 show coverage performance in a more generalised form and the vertical difference between the CBR and Pareto curves corresponds to the difference in coverage performance between the traffic models if the receiver capture ratio is equal to the x-axis value.

Spreading factor	No. MT's	Prob. of bit error (BER)		% difference
		CBR	Pareto	
$s_f = 16$	$m = 1$	0.047466	0.033996	-53.8%
	$m = 4$	0.090013	0.083398	-7.3%
	$m = 8$	0.117958	0.113678	-3.6%
$s_f = 64$	$m = 1$	0.021754	0.015998	-26.5%
	$m = 4$	0.047395	0.043408	-8.4%
	$m = 8$	0.066397	0.064161	-3.4%

Table 6.2: Comparison of the BER with CBR and Pareto ($H = 0.8$) traffic models. MT's move randomly within their own cell.

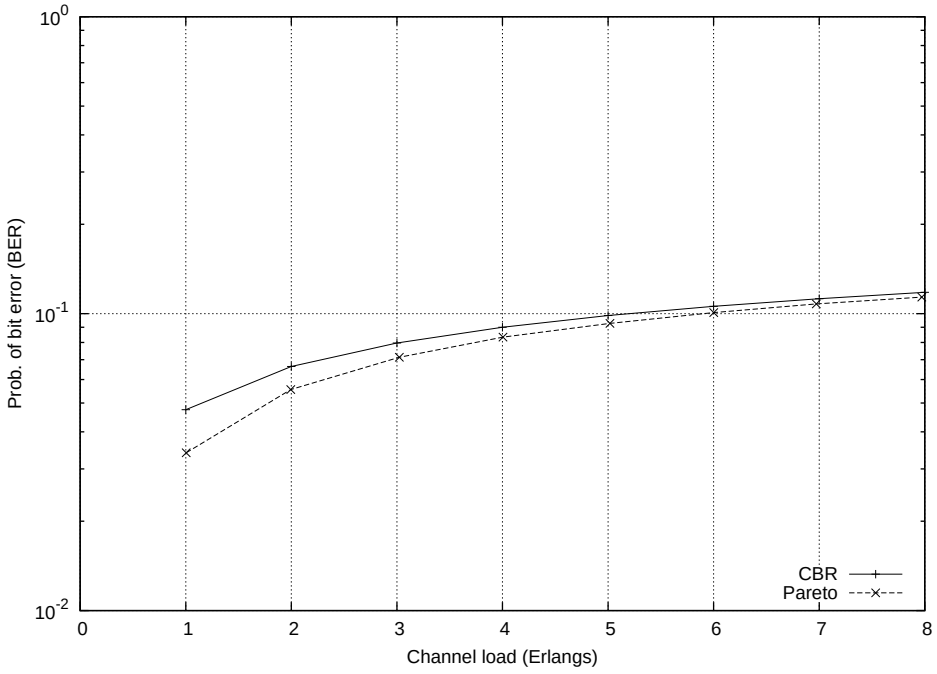

Figure 6.2: BER with CBR and Pareto ($H = 0.8$) traffic models. MT's move randomly within their own cell and use a fixed spreading factor of 16.

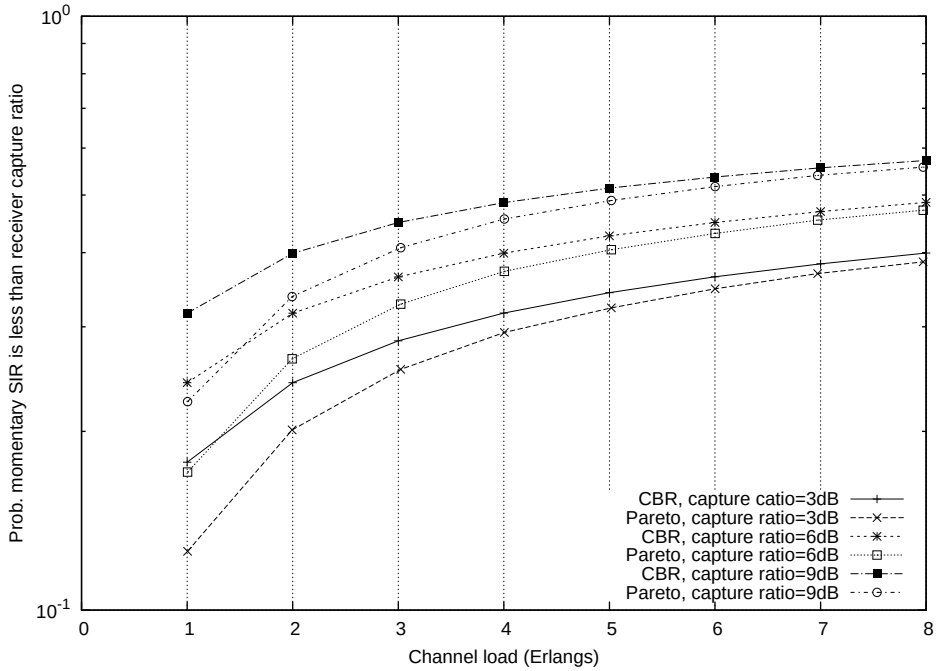

Figure 6.3: Probability the momentary SIR at the receiver is less than the receiver capture ratio with CBR and Pareto ($H = 0.8$) traffic models. MT's move randomly within their own cell and use a fixed spreading factor of 16.

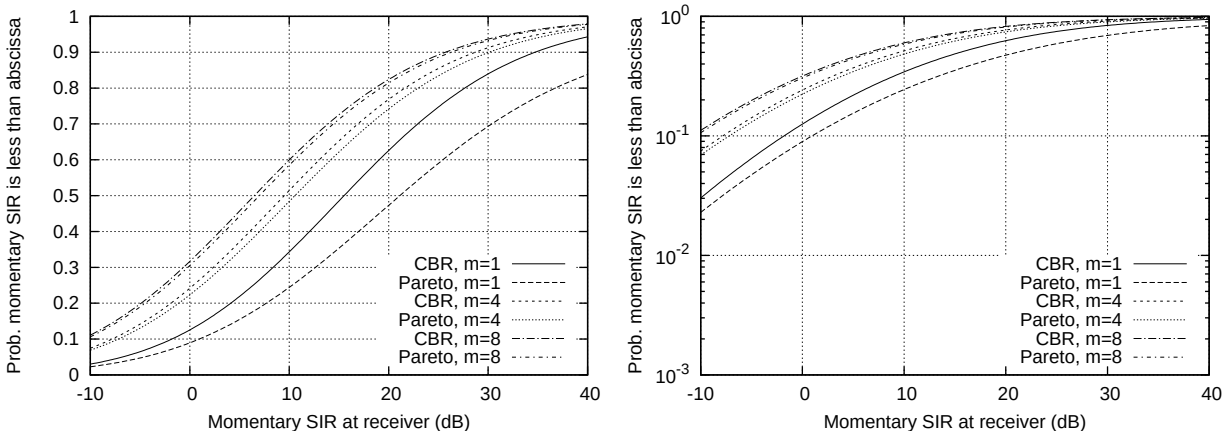

(a) linear scale (b) logarithmic scale

Figure 6.4: Cumulative distribution function of the momentary SIR at the receiver with CBR and Pareto ($H = 0.8$) traffic models (m MT's per cell). MT's move randomly within their own cell and use a fixed spreading factor of 16.

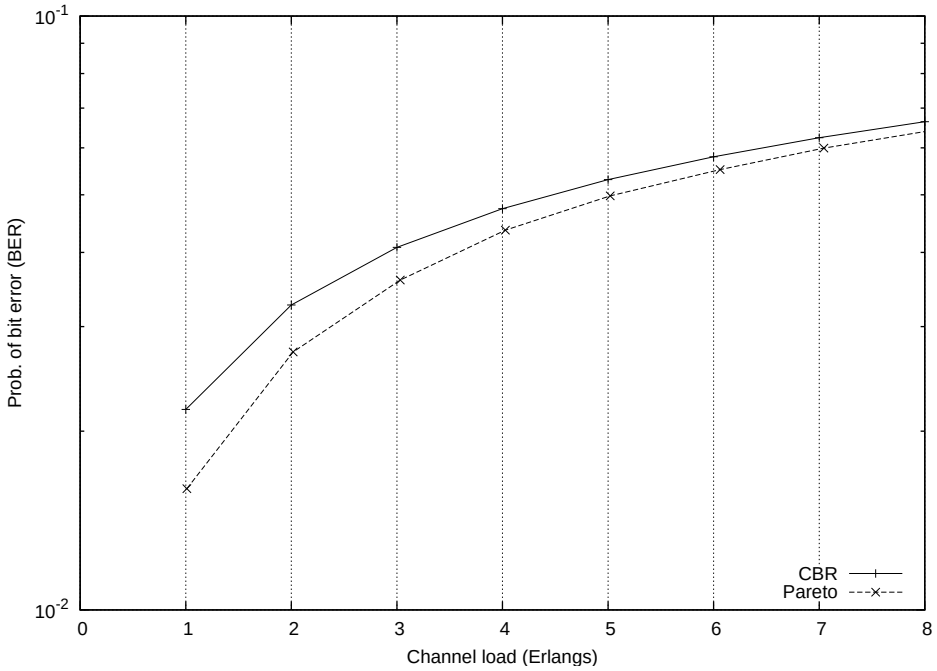

Figure 6.5: BER with CBR and Pareto ($H = 0.8$) traffic models. MT's move randomly within their own cell and use a fixed spreading factor of 64.

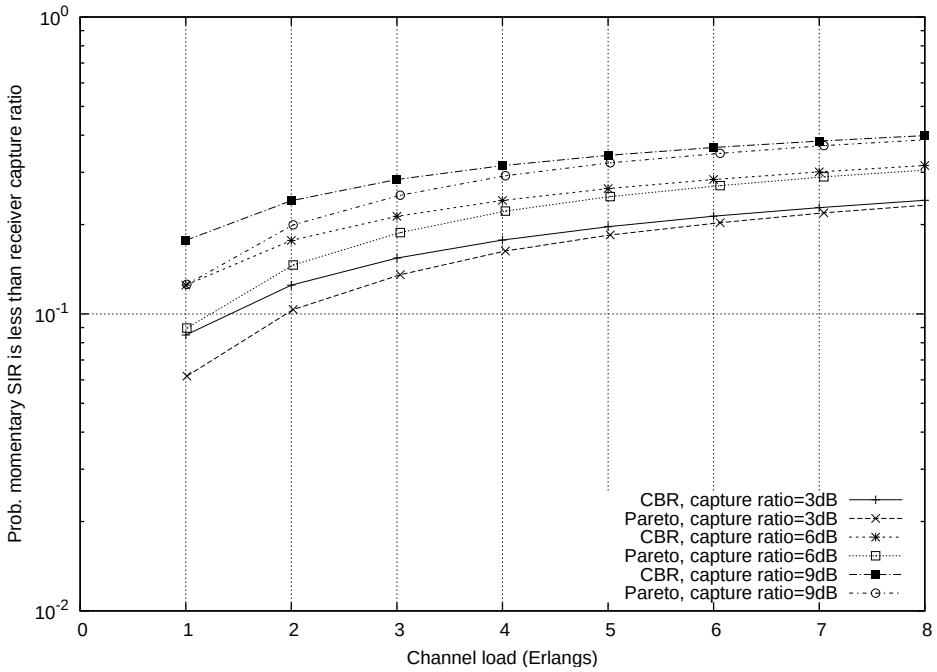

Figure 6.6: Probability the momentary SIR at the receiver is less than the receiver capture ratio with CBR and Pareto ($H = 0.8$) traffic models. MT's move randomly within their own cell and use a fixed spreading factor of 64.

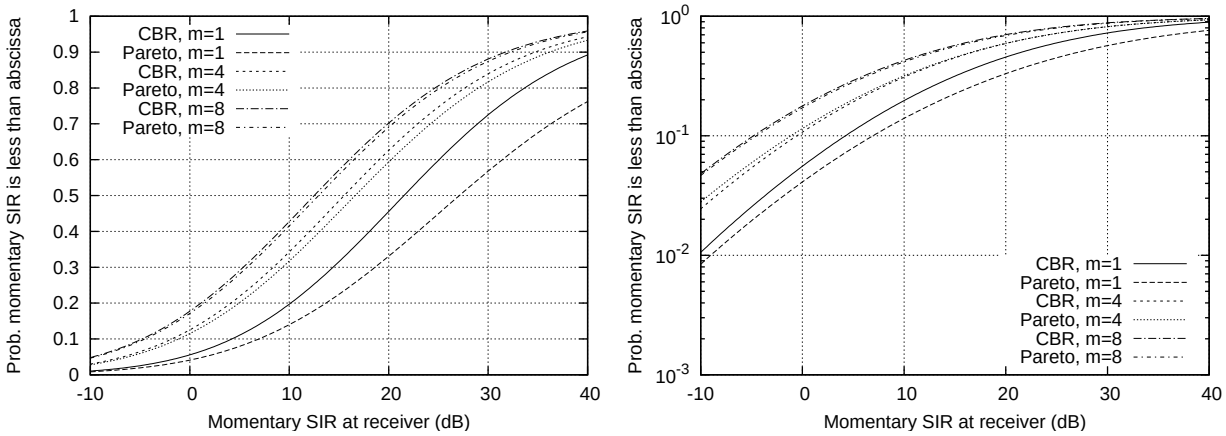

(a) linear scale (b) logarithmic scale

Figure 6.7: Cumulative distribution function of the momentary SIR at the receiver with CBR and Pareto ($H = 0.8$) traffic models (m MT's per cell). MT's move randomly within their own cell and use a fixed spreading factor of 64.

6.3.2 Fixed MT Location Near the Cell Centre

Figures 6.8–6.13 show downlink performance for a stationary MT located 0.2 radii from the cell centre. All other MT's move randomly within their own cell and there are m MT's per cell. This location is considered to be in a good coverage area with a relatively high mean desired signal power and only 5% of the total cell coverage area will receive a higher mean desired signal power.

Trends similar to those observed in the random MT location scenario are also observed in this scenario. Absolute performance levels are better in this case as the MT being evaluated is permanently located in a good coverage area. Table 6.3 shows that a BER performance difference still exists between the CBR and Pareto traffic models but to a lesser extent. The reduced performance difference is due to the higher mean SIR at the receiver which causes the receiver SIR distributions to be concentrated around a more linear section of the BER vs. SIR curve i.e. the difference in the benefit of having a greater probability of high SIR values and the cost of having a greater probability of low SIR values is reduced compared to the random MT location scenario.

Coverage performance is shown in Figures 6.9 and 6.12 and once again the Pareto traffic model has superior coverage performance than the CBR traffic model with the receiver capture ratios considered, but to a lesser extent than in the random MT location scenario. Figures 6.10 and 6.13 show that the receiver SIR cumulative distribution function curves have shifted to the right when compared to Figures 6.4 and 6.7 in the random MT location scenario i.e. the shape of the receiver SIR distributions is the same but the mean is higher due to the desirable MT location. With receiver capture ratios of 3, 6, and 9 dB the vertical difference between

the CBR and Pareto cumulative distribution function curves is less than in the random MT location case as these values are closer to the tail region of the curves and this is reflected in Figures 6.9 and 6.12.

Spreading factor	No. MT's	Prob. of bit error (BER)		% difference
		CBR	Pareto	
$s_f = 16$	$m = 1$	0.000889	0.000822	-7.6%
	$m = 4$	0.003043	0.002919	-4.1%
	$m = 8$	0.005421	0.005241	-3.3%
$s_f = 64$	$m = 1$	0.000247	0.000243	-1.6%
	$m = 4$	0.000890	0.000872	-2.1%
	$m = 8$	0.001658	0.001643	-0.9%

Table 6.3: Comparison of the BER for a stationary MT located 0.2 radii from the cell centre with CBR and Pareto ($H = 0.8$) traffic models.

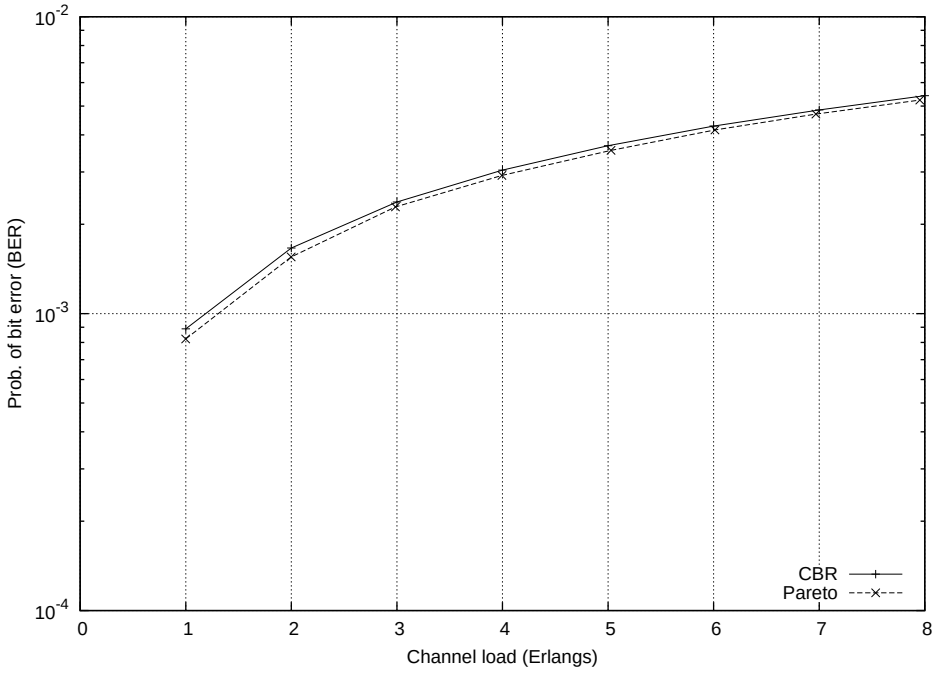

Figure 6.8: BER for a stationary MT located 0.2 radii from the cell centre with CBR and Pareto ($H = 0.8$) traffic models. All MT's use a fixed spreading factor of 16.

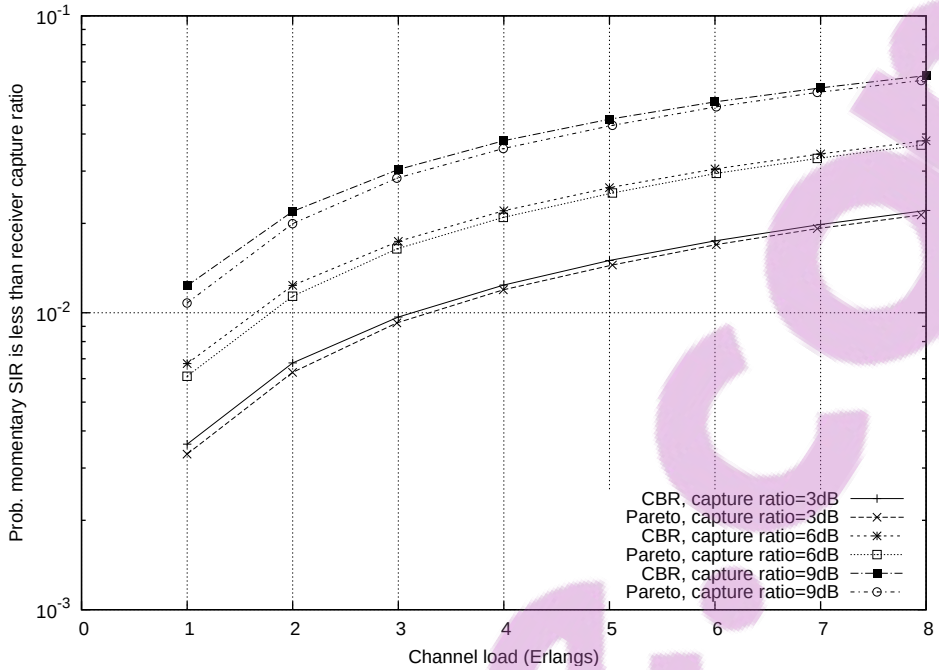

Figure 6.9: Probability the momentary SIR at the receiver is less than the receiver capture ratio for a stationary MT located 0.2 radii from the cell centre with CBR and Pareto ($H = 0.8$) traffic models. All MT's use a fixed spreading factor of 16.

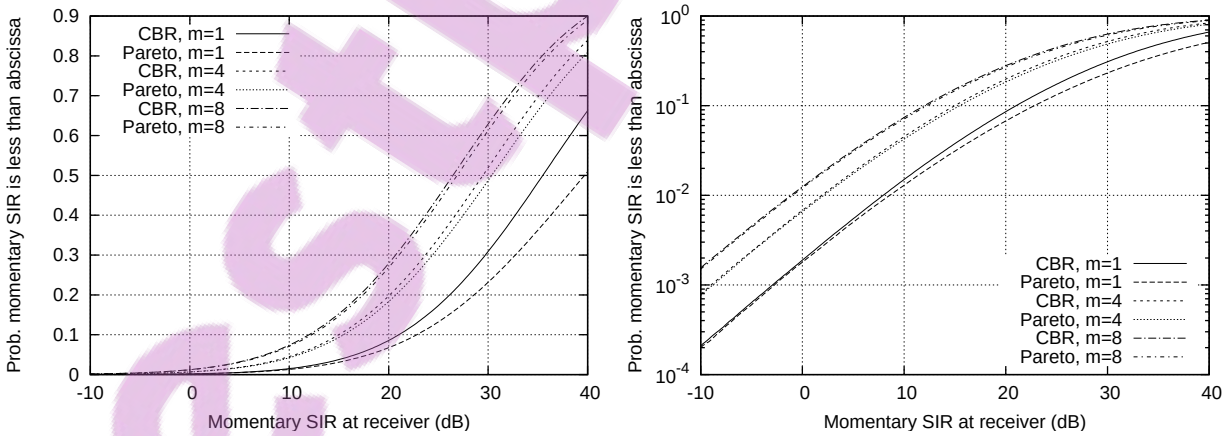

(a) linear scale

(b) logarithmic scale

Figure 6.10: Cumulative distribution function of the momentary SIR at the receiver for a stationary MT located 0.2 radii from the cell centre with CBR and Pareto ($H = 0.8$) traffic models (m MT's per cell). All MT's use a fixed spreading factor of 16.

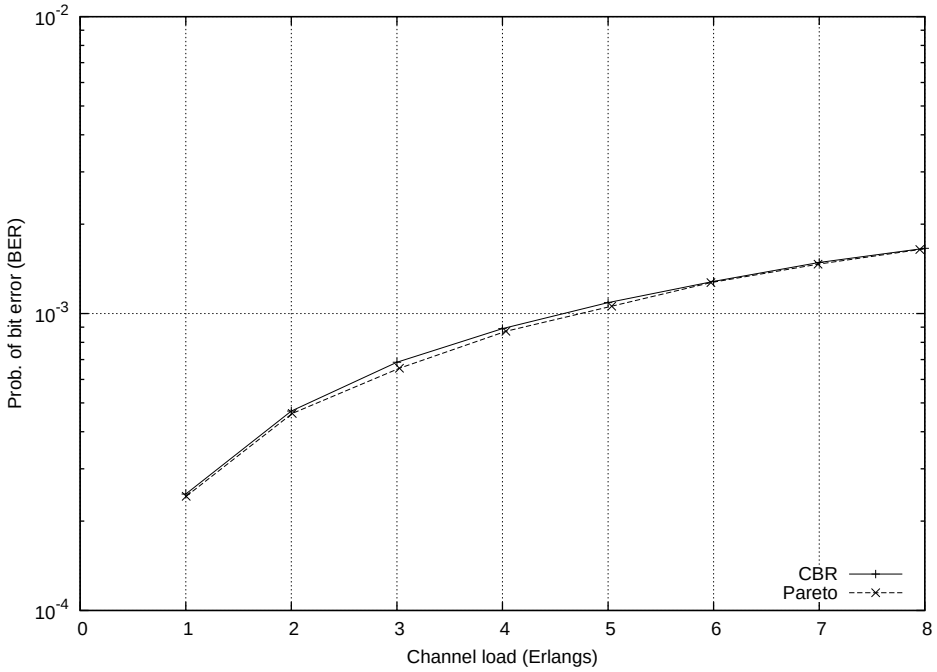

Figure 6.11: BER for a stationary MT located 0.2 radii from the cell centre with CBR and Pareto ($H = 0.8$) traffic models. All MT's use a fixed spreading factor of 64.

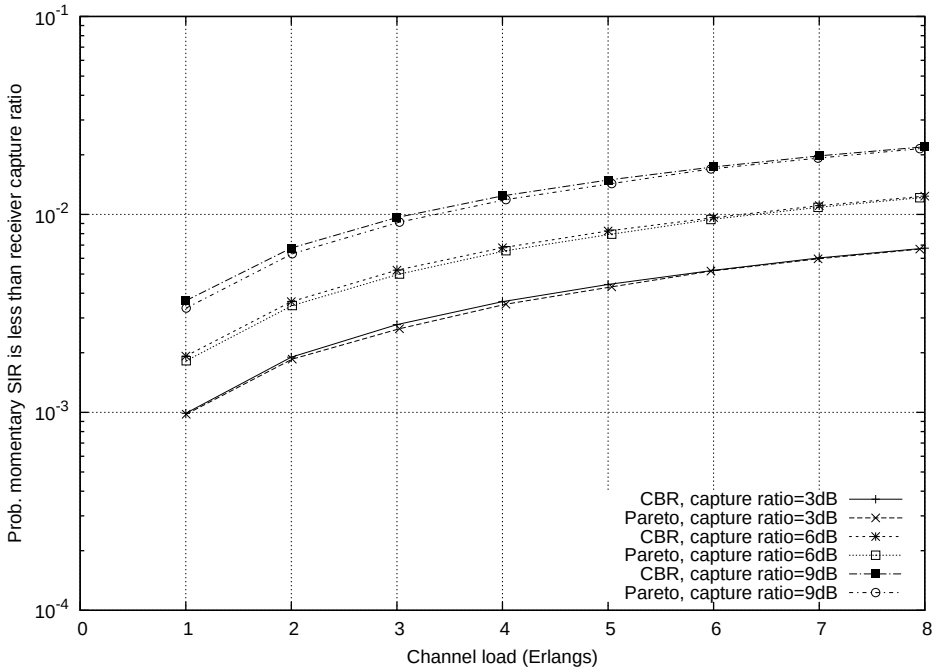

Figure 6.12: Probability the momentary SIR at the receiver is less than the receiver capture ratio for a stationary MT located 0.2 radii from the cell centre with CBR and Pareto ($H = 0.8$) traffic models. All MT's use a fixed spreading factor of 64.

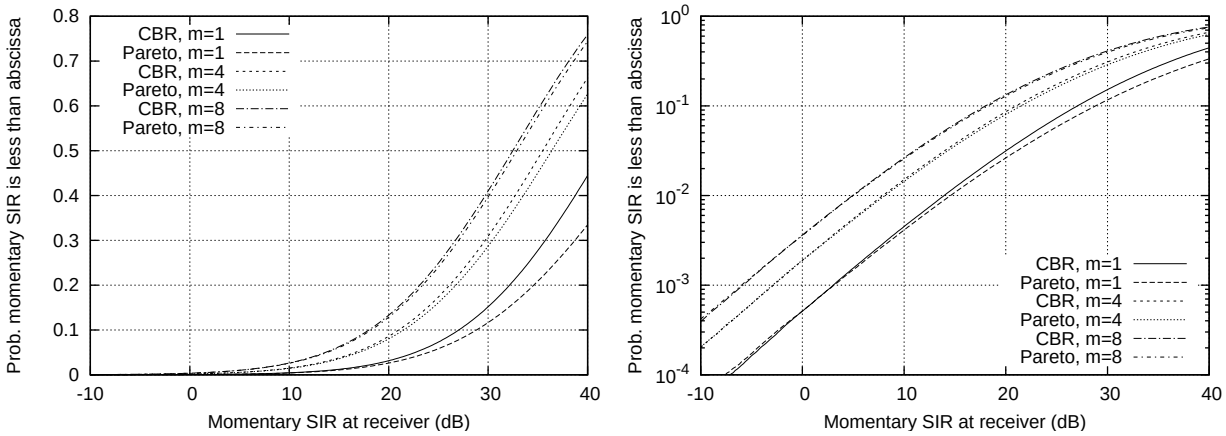

(a) linear scale (b) logarithmic scale

Figure 6.13: Cumulative distribution function of the momentary SIR at the receiver for a stationary MT located 0.2 radii from the cell centre with CBR and Pareto ($H = 0.8$) traffic models (m MT's per cell). All MT's use a fixed spreading factor of 64.

6.3.3 Fixed MT Location Far Away from the Cell Centre

Figures 6.14–6.19 show downlink performance for a stationary MT located 0.85 radii from the cell centre. All other MT's move randomly within their own cell and there are m MT's per cell. This location is considered to be in a poor coverage area with a relatively low mean desired signal power and 87% of the total cell coverage area will receive a higher mean desired signal power.

Trends similar to those observed in the random MT location scenario are also observed in this scenario. Absolute performance levels are worse in this case as the MT being evaluated is permanently located in a poor coverage area. Table 6.4 compares BER performance with the CBR and Pareto traffic models and once again the Pareto model has superior performance, as expected.

Coverage performance is shown in Figures 6.15 and 6.18. Figures 6.16 and 6.19 show that the receiver SIR cumulative distribution function curves have shifted to the left when compared to Figures 6.4 and 6.7 in the random MT location scenario i.e. the shape of the receiver SIR distributions is the same but the mean is lower due to the undesirable MT location. With receiver capture ratios of 3, 6, and 9 dB the vertical difference between the CBR and Pareto cumulative distribution function curves is greater than in the random MT location case as these values are further away from the tail region of the curves and this is reflected in Figures 6.15 and 6.18.

Spreading factor	No. MT's	Prob. of bit error (BER)		% difference
		CBR	Pareto	
$s_f = 16$	$m = 1$	0.090266	0.063914	-29.2%
	$m = 4$	0.158882	0.146729	-7.6%
	$m = 8$	0.199486	0.192788	-3.4%
$s_f = 64$	$m = 1$	0.044116	0.031381	-28.9%
	$m = 4$	0.090287	0.082855	-8.2%
	$m = 8$	0.122050	0.118057	-3.3%

Table 6.4: Comparison of the BER for a stationary MT located 0.85 radii from the cell centre with CBR and Pareto ($H = 0.8$) traffic models.

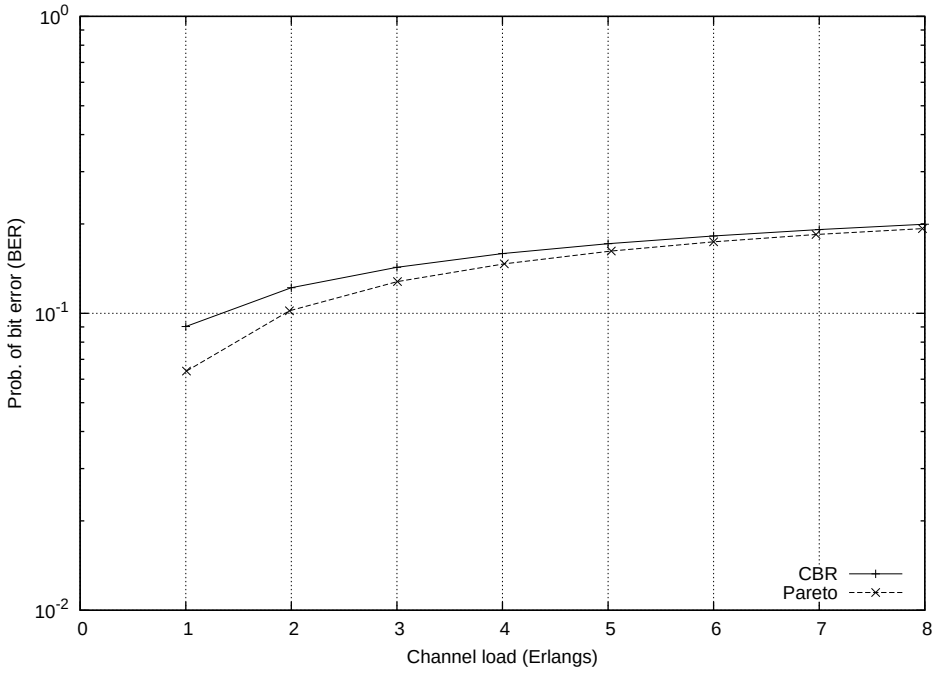

Figure 6.14: BER for a stationary MT located 0.85 radii from the cell centre with CBR and Pareto ($H = 0.8$) traffic models. All MT's use a fixed spreading factor of 16.

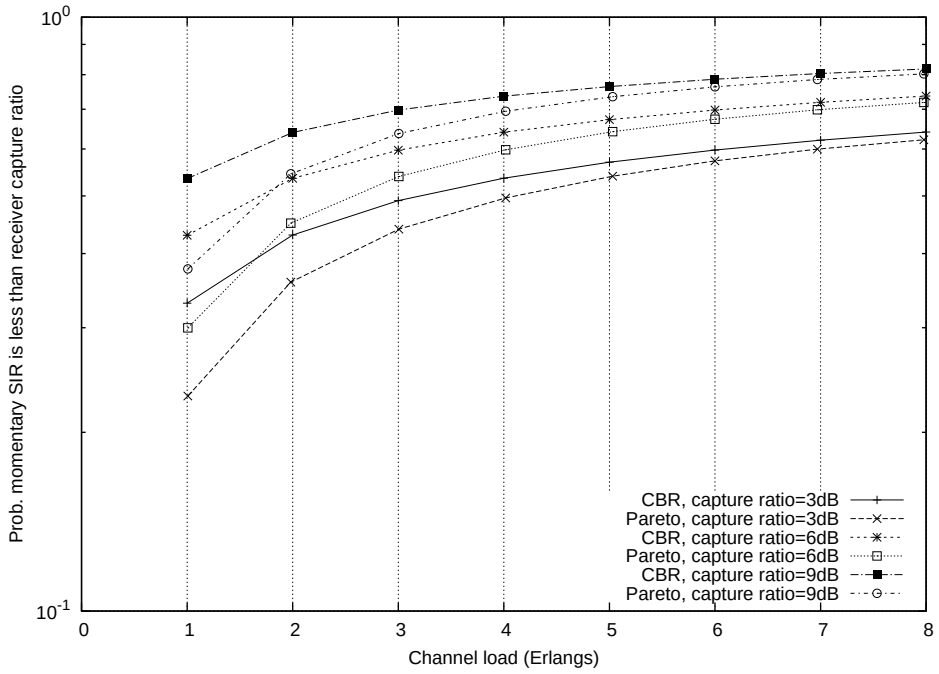

Figure 6.15: Probability the momentary SIR at the receiver is less than the receiver capture ratio for a stationary MT located 0.85 radii from the cell centre with CBR and Pareto ($H = 0.8$) traffic models. Other MT's move randomly within their own cell and all MT's use a fixed spreading factor of 16.

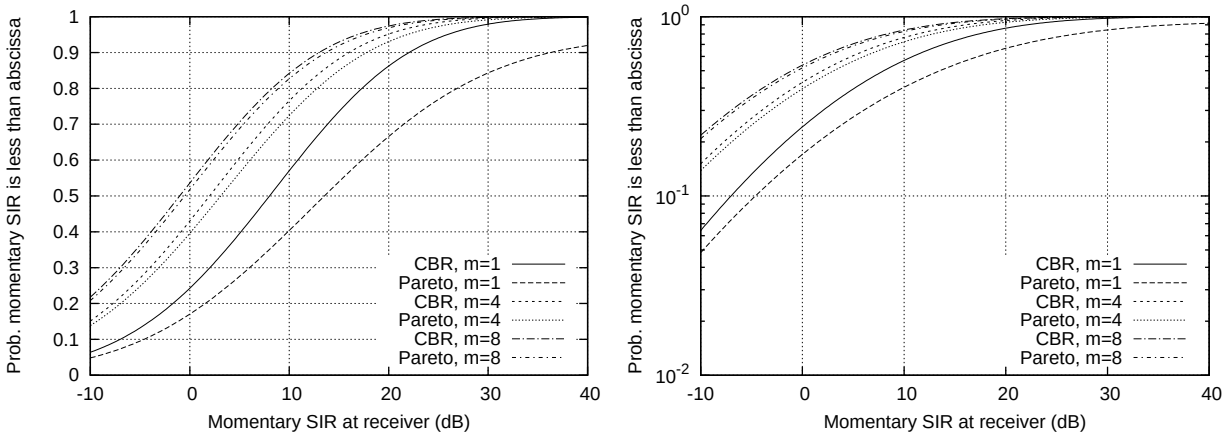

(a) linear scale (b) logarithmic scale

Figure 6.16: Cumulative distribution function of the momentary SIR at the receiver for a stationary MT located 0.85 radii from the cell centre with CBR and Pareto ($H = 0.8$) traffic models (m MT's per cell). All MT's use a fixed spreading factor of 16.

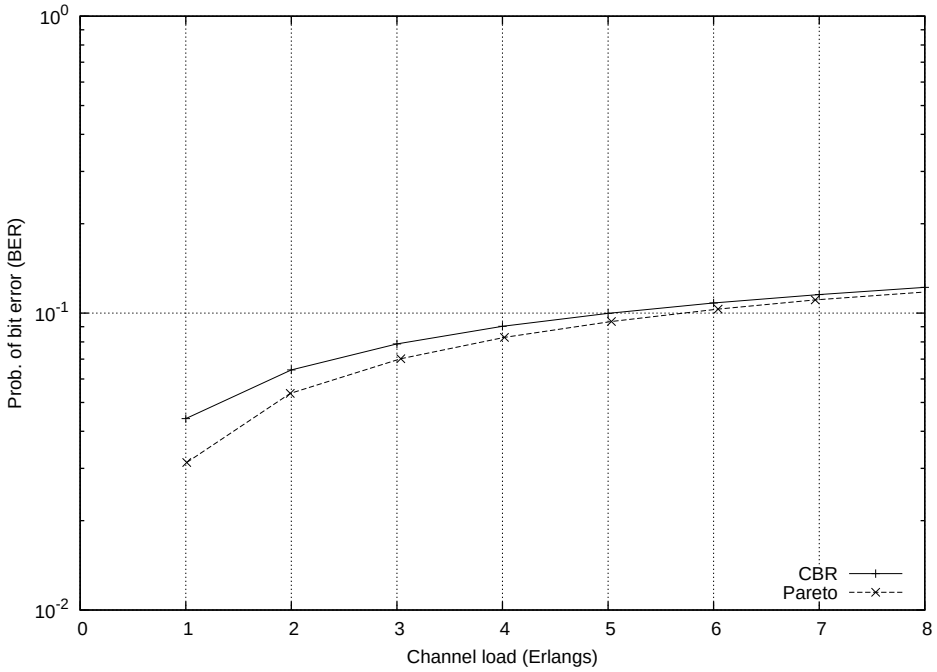

Figure 6.17: BER for a stationary MT located 0.85 radii from the cell centre with CBR and Pareto ($H = 0.8$) traffic models. All MT's use a fixed spreading factor of 64.

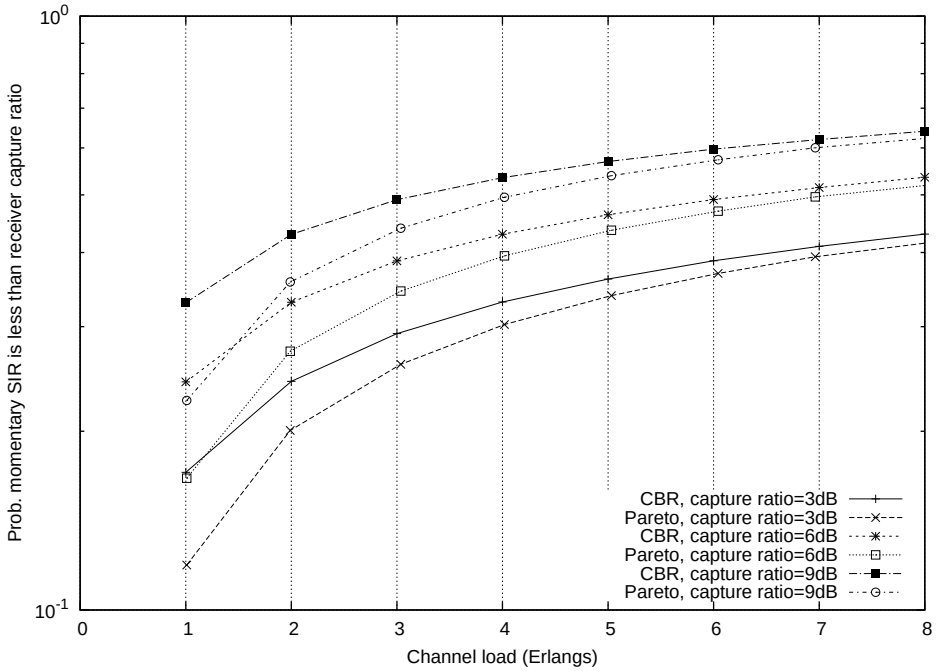

Figure 6.18: Probability the momentary SIR at the receiver is less than the receiver capture ratio for a stationary MT located 0.85 radii from the cell centre with CBR and Pareto ($H = 0.8$) traffic models. All MT's use a fixed spreading factor of 64.

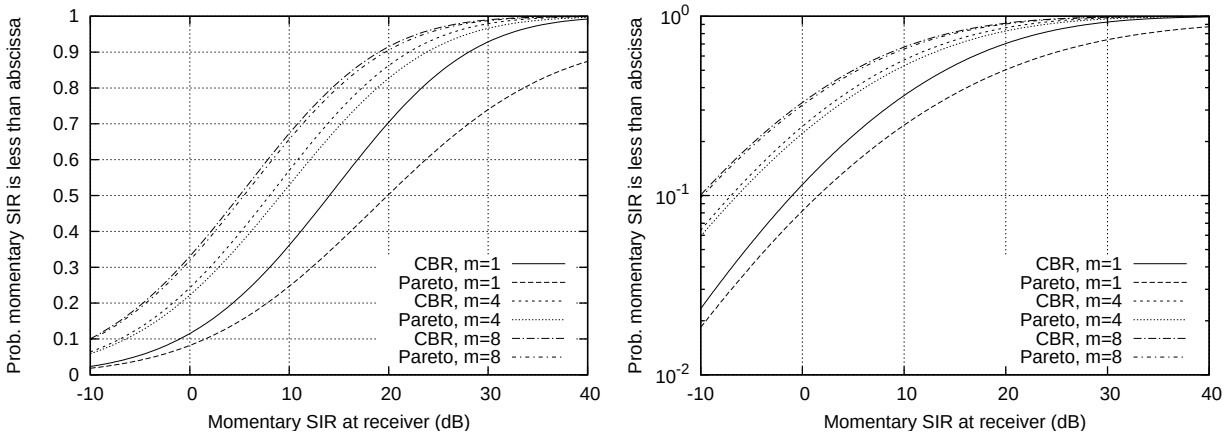

(a) linear scale (b) logarithmic scale

Figure 6.19: Cumulative distribution function of the momentary SIR at the receiver for a stationary MT located 0.85 radii from the cell centre with CBR and Pareto ($H = 0.8$) traffic models (m MT's per cell). All MT's use a fixed spreading factor of 64.

6.4 A Time Dispersive Suzuki Propagation Environment

This section evaluates the downlink performance of the same system considered in the previous section but with a time dispersive propagation channel and receiver diversity. A perfect RAKE receiver and two receiver antennas are assumed and maximal ratio combining is used for both receiver diversity techniques i.e. the SIR at the receiver output is the sum of the SIR's on each RAKE finger on both antennas (see Section 5.7)[5]. All other system parameters are identical to those in Section 6.3. The propagation channel power delay profiles evaluated are detailed in Table 5.2 and the relative mean powers received on each RAKE finger are listed in Table 6.5.

When a BTS transmits multiple spreading codes in a non-time dispersive propagation environment only one version of the transmitted signal arrives at the receiver. Because orthogonal OVSF spreading codes are assumed this means that codes transmitted from the same BTS are effectively transparent to one another i.e. there is no intra-cell interference or self-interference. However, in a time dispersive propagation environment multiple versions of the transmitted signal arrive at the receiver with different time delays and only the signal version synchronised with the receiver provides useful signal power. All other signal versions appear as either intra-cell interference or self-interference, as detailed in Section 5.7.

[5]The RAKE receiver is assumed to have at least 3 fingers.

	RAKE finger	Relative mean power (dB)
Delay profile 1	1	0
	2	0
Delay profile 2	1	0
	2	-10
Delay profile 3	1	0
	2	0
	3	0

Table 6.5: Propagation channel power delay profiles (derived from Table 5.2).

6.4.1 Random MT Location Within Own Cell

Figures 6.20–6.25 show system downlink performance when all MT's move randomly within their own cell and there are m MT's per cell. When compared to the non-time dispersive propagation environment evaluated in Section 6.3 the absolute performance levels are superior due to the benefits of receiver diversity. Table 6.6 compares BER performance with the CBR and Pareto traffic models and propagation channel delay profile 1. Once again, the Pareto model has superior BER and coverage performance than the CBR model, especially at low loads, and as the number of users and traffic load increases the performance difference reduces.

The same mechanisms that were identified in Section 6.3 explain most of the observations in this scenario but further consideration must be given to the impact of the time dispersive propagation channel. In a time dispersive propagation environment there is intra-cell interference in addition to inter-cell interference. The level of intra-cell interference at an MT receiver is positively correlated with the number of spreading codes allocated to the MT[6]. The mean received desired signal power remains constant and is independent of the number of spreading codes allocated to the MT, but the level of intra-cell interference is directly proportional to the number of spreading codes allocated to the MT. Hence, a burst of traffic in a time dispersive propagation environment can potentially degrade MT performance since all packets in the burst will on average experience higher levels of intra-cell interference than if they were transmitted in separate frames. However, Figures 6.20 and 6.23 show that the effect of correlated intra-cell interference is not significant enough to override the basic trends that were observed in Section 6.3 with the non-time dispersive propagation channel.

Both the time dispersive propagation channel and use of receiver diversity alter the receiver's SIR distribution and this can be seen in Figures 6.22 and 6.25 when compared to the corresponding figures in Section 6.3 i.e. Figures 6.4 and 6.7. The receiver SIR cumulative

[6]Multiple spreading codes allocated to an MT are treated independently and are considered a source of intra-cell interference to one another i.e. not self-interference. See Section 5.7 for the definition of self-interference.

distribution function curves shown in Figures 6.22 and 6.25 have visible crossover points and these points determine which traffic model has superior coverage performance with different receiver capture ratios. Figure 6.21 shows that with capture ratios of 3 and 6 dB the Pareto traffic model has superior coverage performance at low loads but inferior coverage performance at high loads when compared to the CBR traffic model. The results presented in this section also show that the situation can arise where one traffic model has superior BER performance but inferior coverage performance when compared to another traffic model.

Figures 6.22 and 6.25 show that there is a greater probability of mid to high receiver SIR values with the CBR traffic model than with the Pareto traffic model. This is in contrast to the results in Section 6.3 with a non-time dispersive propagation channel and is due to the correlated intra-cell interference identified above. The stepping phenomenon observed in these figures, which is especially noticeable when $m = 1$, is due to the fact that the ratio of the desired signal power to intra-cell interference power is an integer value that is equal to the number of spread codes transmitted minus one. With the Pareto traffic model the number of spreading codes transmitted is variable and this causes "jumps" in the ratio of the desired signal power to intra-cell interference power and this in turn causes the receiver SIR values to cluster around specific points. This stepping phenomenon does not occur with the CBR traffic model since the number of spreading codes transmitted is constant.

Spreading factor	No. MT's	Prob. of bit error (BER)		% difference
		CBR	Pareto	
$s_f = 16$	$m = 1$	0.009012	0.007110	-21.1%
	$m = 4$	0.027520	0.026586	-3.4%
	$m = 8$	0.045934	0.045999	0.1%
$s_f = 64$	$m = 1$	0.002550	0.002092	-18.0%
	$m = 4$	0.009223	0.008546	-7.3%
	$m = 8$	0.016378	0.015908	-2.9%

Table 6.6: Comparison of the BER with propagation channel delay profile 1 and CBR and Pareto ($H = 0.8$) traffic models. MT's move randomly within their own cell.

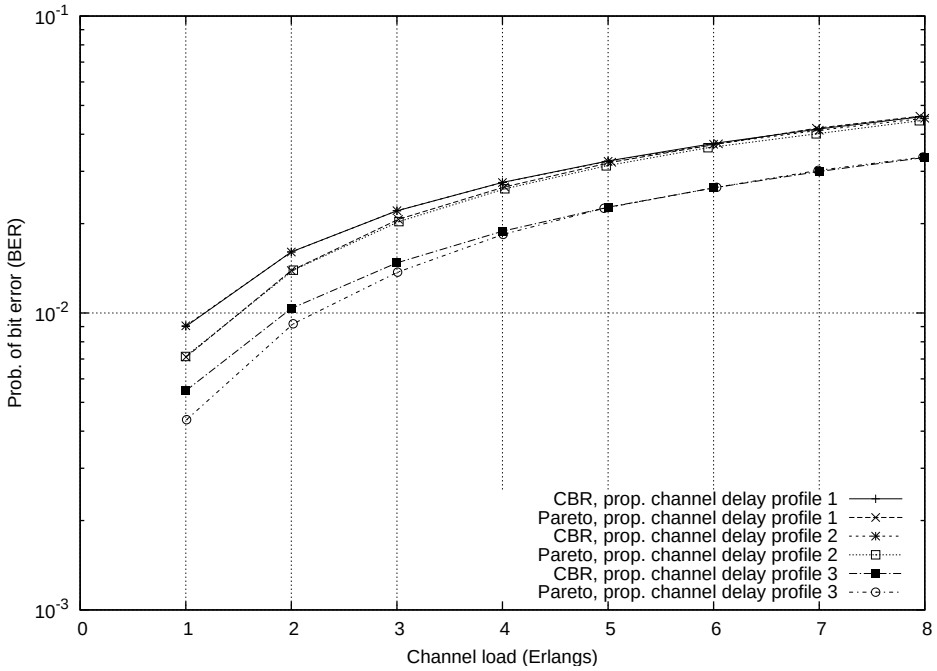

Figure 6.20: BER with CBR and Pareto ($H = 0.8$) traffic models. MT's move randomly within their own cell and use a fixed spreading factor of 16.

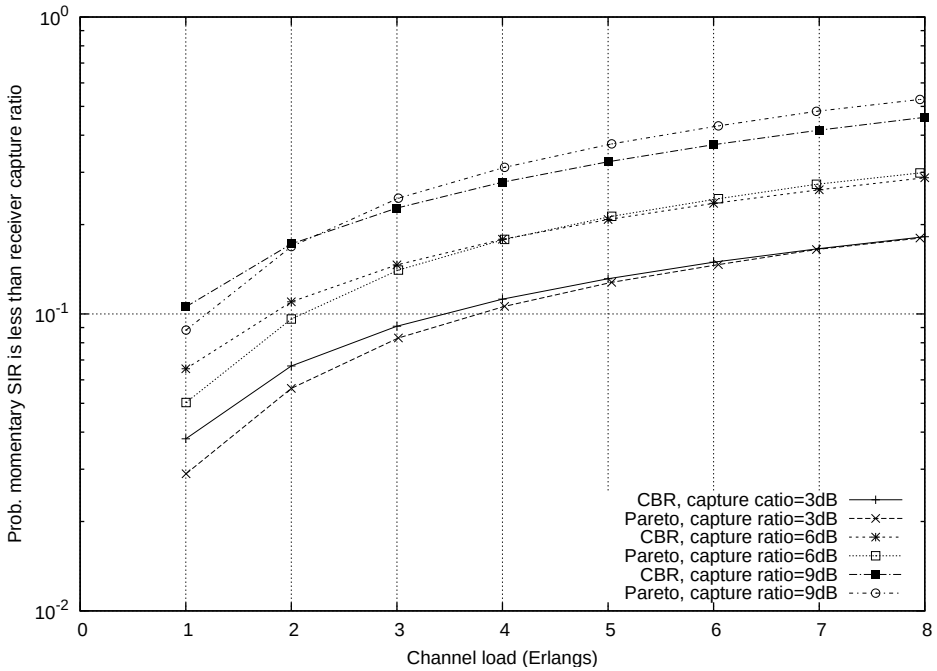

Figure 6.21: Probability the momentary SIR at the receiver is less than the receiver capture ratio with propagation channel delay profile 1 and CBR and Pareto ($H = 0.8$) traffic models. MT's move randomly within the same cell and use a fixed spreading factor of 16.

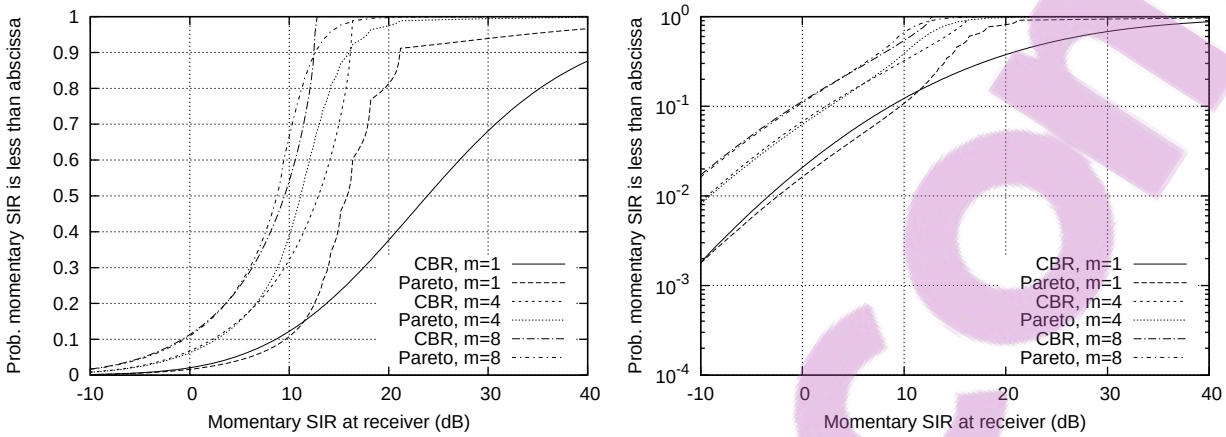

(a) linear scale (b) logarithmic scale

Figure 6.22: Cumulative distribution function of the momentary SIR at the receiver with propagation channel delay profile 1 and CBR and Pareto ($H = 0.8$) traffic models (m MT's per cell). MT's move randomly within their own cell and use a fixed spreading factor of 16.

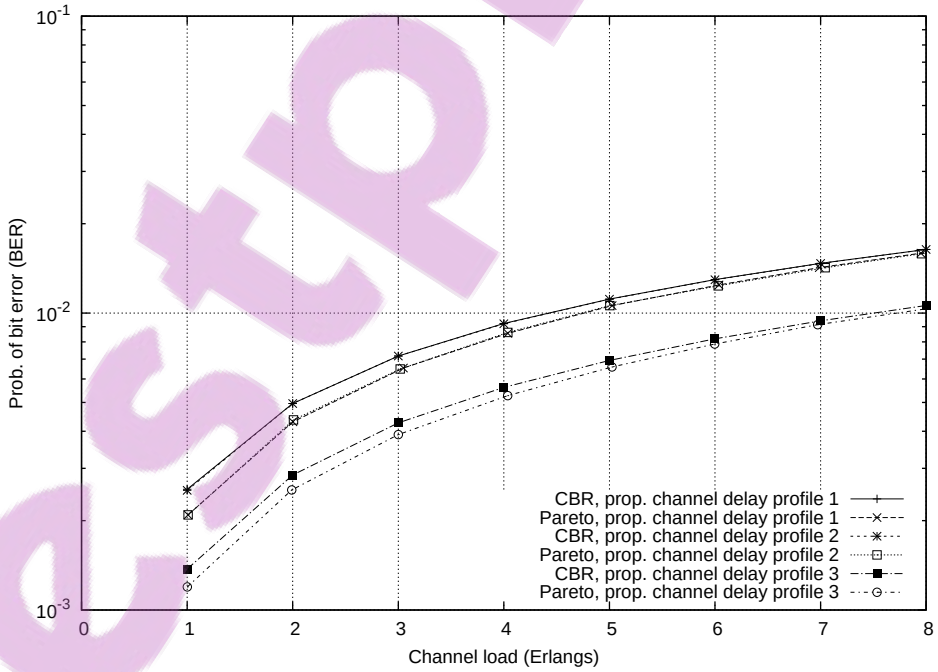

Figure 6.23: BER with CBR and Pareto ($H = 0.8$) traffic models. MT's move randomly within their own cell and use a fixed spreading factor of 64.

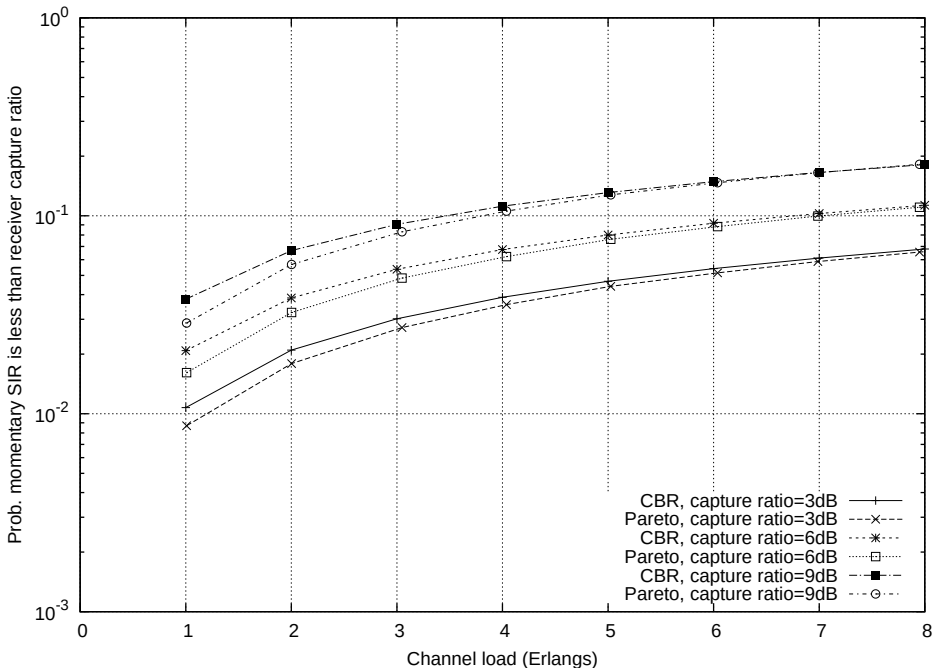

Figure 6.24: Probability the momentary SIR at the receiver is less than the receiver capture ratio with propagation channel delay profile 1 and CBR and Pareto ($H = 0.8$) traffic models. MT's move randomly within their own cell and use a fixed spreading factor of 64.

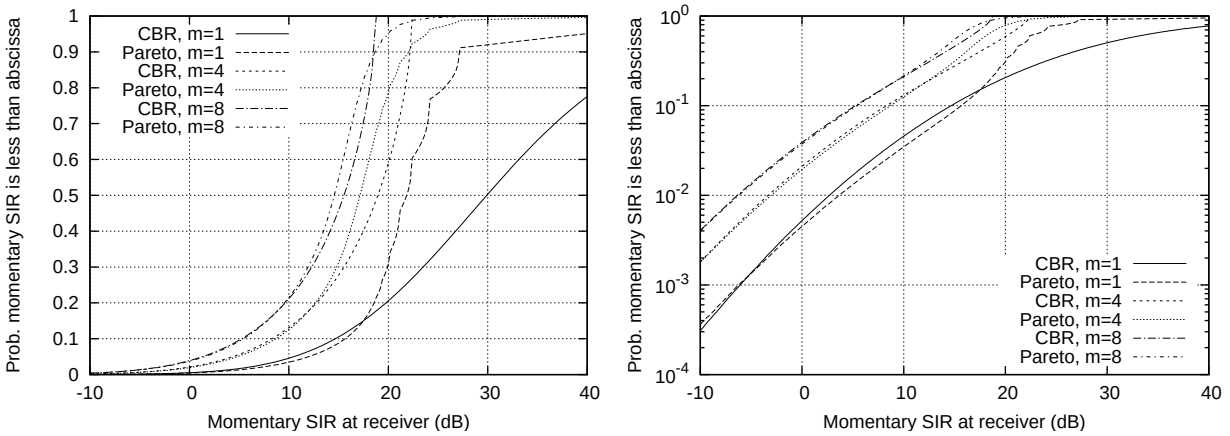

(a) linear scale

(b) logarithmic scale

Figure 6.25: Cumulative distribution function of the momentary SIR at the receiver with propagation channel delay profile 1 and CBR and Pareto ($H = 0.8$) traffic models (m MT's per cell). MT's move randomly within their own cell and use a fixed spreading factor of 64.

6.4.2 Fixed MT Location Near the Cell Centre

Figures 6.26–6.31 show downlink performance for a stationary MT located 0.2 radii from the cell centre. All other MT's move randomly within their own cell and there are m MT's per cell. This location is considered to be in a good coverage area with a relatively high mean desired signal power and only 5% of the total cell coverage area will receive a higher mean desired signal power.

Table 6.7 compares BER performance with the CBR and Pareto traffic models and propagation channel delay profile 1. The CBR model has significantly superior BER performance than the Pareto model and this is in contrast to the results presented in previous sections. This is due to the correlated intra-cell interference phenomenon identified in the previous section and occurs because intra-cell interference is much more dominant in this scenario i.e. bursts of traffic are positively correlated with higher levels of intra-cell interference and this degrades performance.

Figures 6.28 and 6.31 show that the stepping phenomenon identified in the previous section is much more pronounced in this scenario and again this is due to the much more dominant intra-cell interference.

Spreading factor	No. MT's	Prob. of bit error (BER)		% difference
		CBR	Pareto	
$s_f = 16$	$m = 1$	0.000005	0.000011	108.1%
	$m = 4$	0.000068	0.000197	189.5%
	$m = 8$	0.000321	0.000916	185.3%
$s_f = 64$	$m = 1$	0.000000	0.000001	95.6%
	$m = 4$	0.000006	0.000007	22.8%
	$m = 8$	0.000020	0.000024	20.4%

Table 6.7: Comparison of the BER for a stationary MT located 0.2 radii from the cell centre with propagation channel delay profile 1 and CBR and Pareto ($H = 0.8$) traffic models.

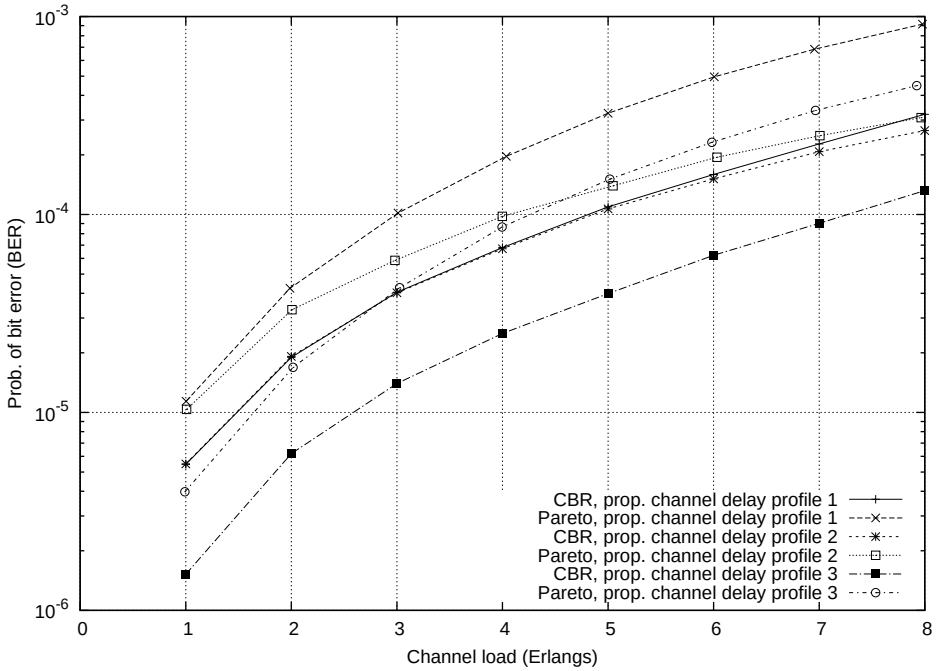

Figure 6.26: BER for a stationary MT located 0.2 radii from the cell centre with CBR and Pareto ($H = 0.8$) traffic models. All MT's use a fixed spreading factor of 16.

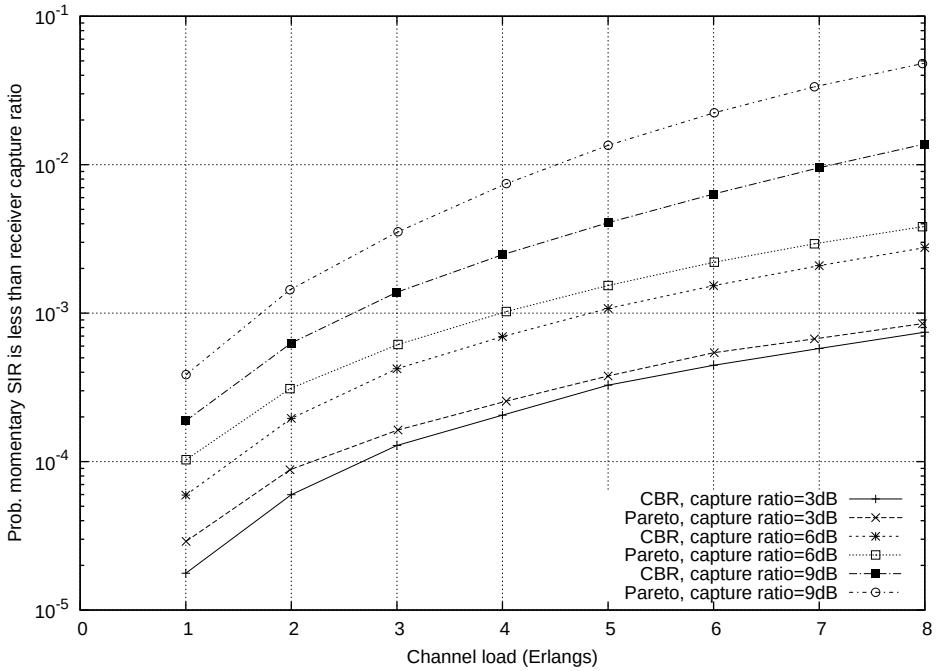

Figure 6.27: Probability the momentary SIR at the receiver is less than the receiver capture ratio for a stationary MT located 0.2 radii from the cell centre with propagation channel delay profile 1 and CBR and Pareto ($H = 0.8$) traffic models. All MT's use a fixed spreading factor of 16.

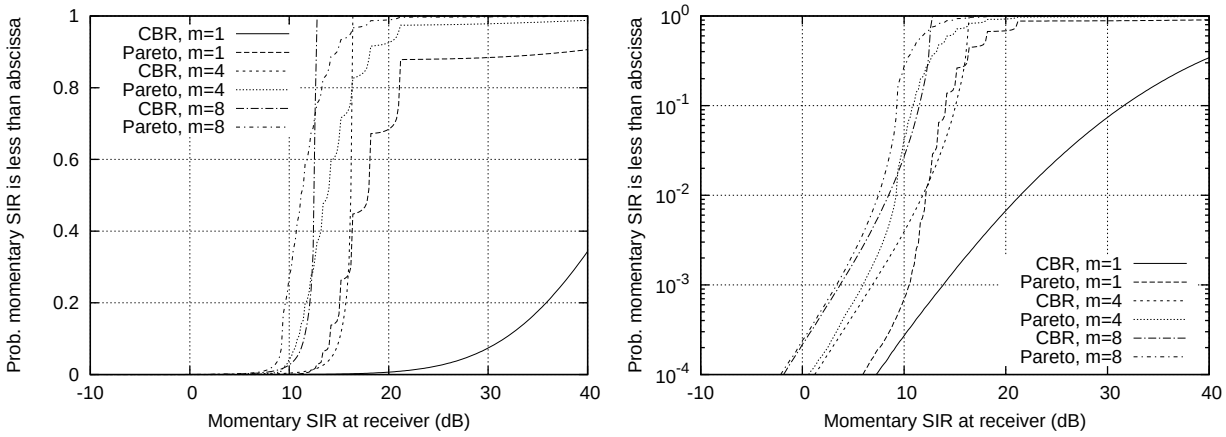

(a) linear scale (b) logarithmic scale

Figure 6.28: Cumulative distribution function of the momentary SIR at the receiver for a stationary MT located 0.2 radii from the cell centre with propagation channel delay profile 1 and CBR and Pareto ($H = 0.8$) traffic models (m MT's per cell). All MT's use a fixed spreading factor of 16.

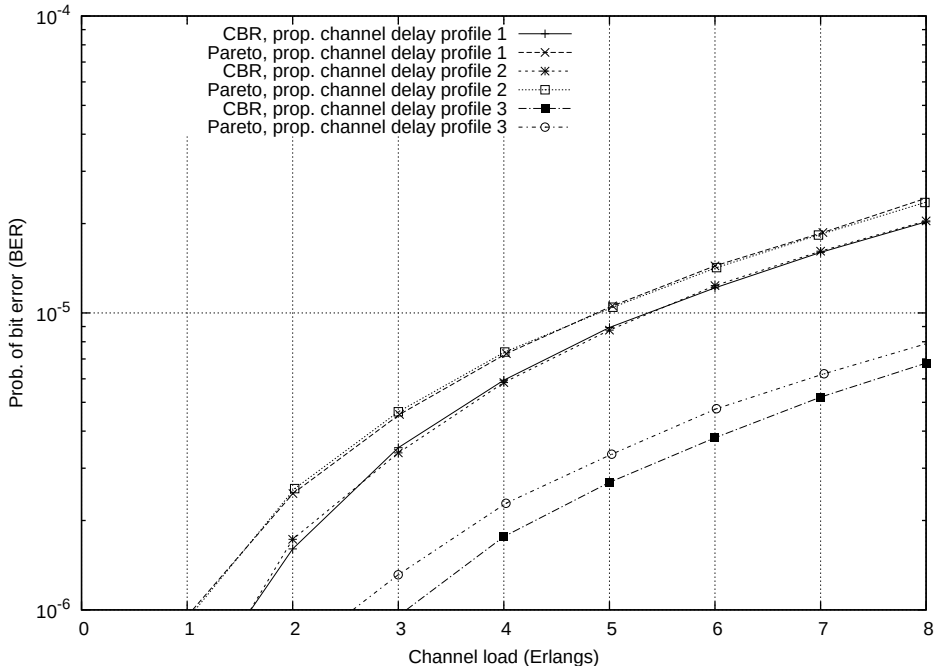

Figure 6.29: BER for a stationary MT located 0.2 radii from the cell centre with CBR and Pareto ($H = 0.8$) traffic models. All MT's use a fixed spreading factor of 64.

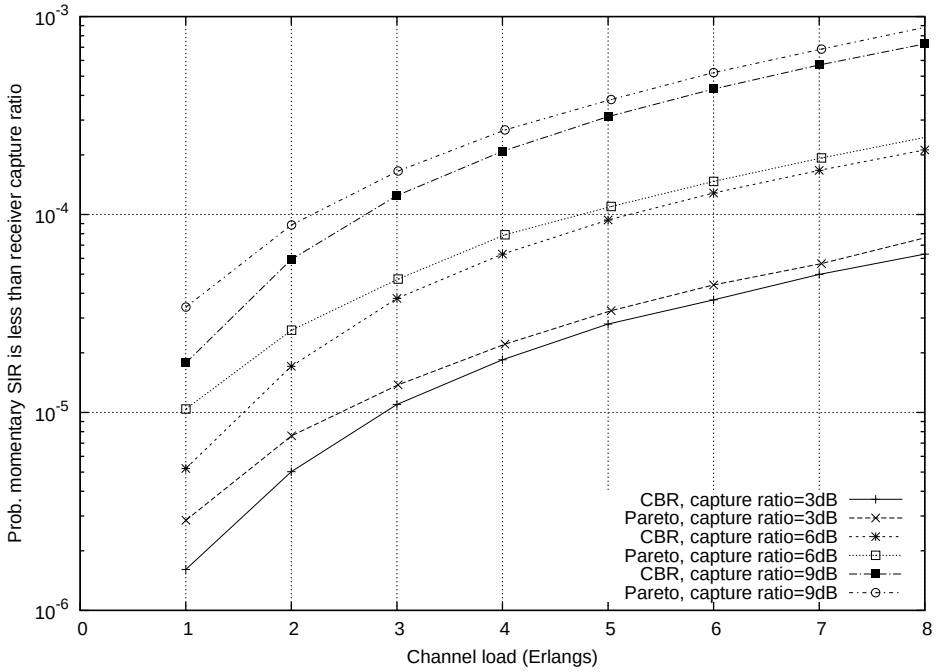

Figure 6.30: Probability the momentary SIR at the receiver is less than the receiver capture ratio for a stationary MT located 0.2 radii from the cell centre with propagation channel delay profile 1 and CBR and Pareto ($H = 0.8$) traffic models. All MT's use a fixed spreading factor of 64.

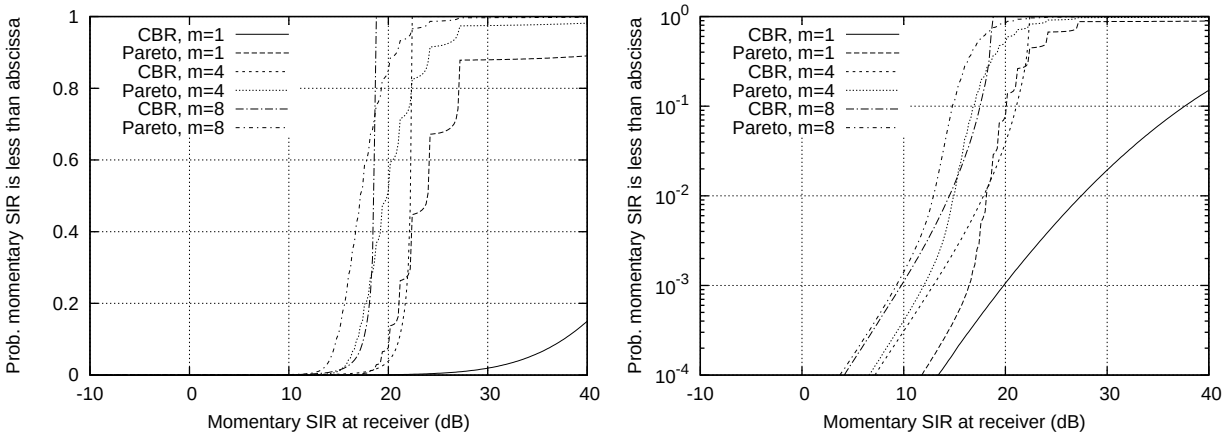

(a) linear scale (b) logarithmic scale

Figure 6.31: Cumulative distribution function of the momentary SIR at the receiver for a stationary MT located 0.2 radii from the cell centre with propagation channel delay profile 1 and CBR and Pareto ($H = 0.8$) traffic models (m MT's per cell). All MT's use a fixed spreading factor of 64.

6.4.3 Fixed MT Location Far Away from the Cell Centre

Figures 6.32–6.37 show downlink performance for a stationary MT located 0.85 radii from the cell centre. All other MT's move randomly within their own cell and there are m MT's per cell. This location is considered to be in a poor coverage area with a relatively low mean desired signal power and 87% of the total cell coverage area will receive a higher mean desired signal power.

Trends similar to those observed in the random MT location scenario are also observed in this scenario and this is expected. It should however be noted that inter-cell interference is more dominant in this scenario. Table 6.8 compares BER performance with the CBR and Pareto traffic models and propagation channel delay profile 1.

Spreading factor	No. MT's	Prob. of bit error (BER)		% difference
		CBR	Pareto	
$s_f = 16$	$m = 1$	0.020571	0.015689	-23.7%
	$m = 4$	0.058003	0.054867	-5.4%
	$m = 8$	0.091100	0.089860	-1.4%
$s_f = 64$	$m = 1$	0.006055	0.004832	-20.2%
	$m = 4$	0.020941	0.019305	-7.8%
	$m = 8$	0.035923	0.034617	-3.6%

Table 6.8: Comparison of the BER for a stationary MT located 0.85 radii from the cell centre with propagation channel delay profile 1 and CBR and Pareto ($H = 0.8$) traffic models.

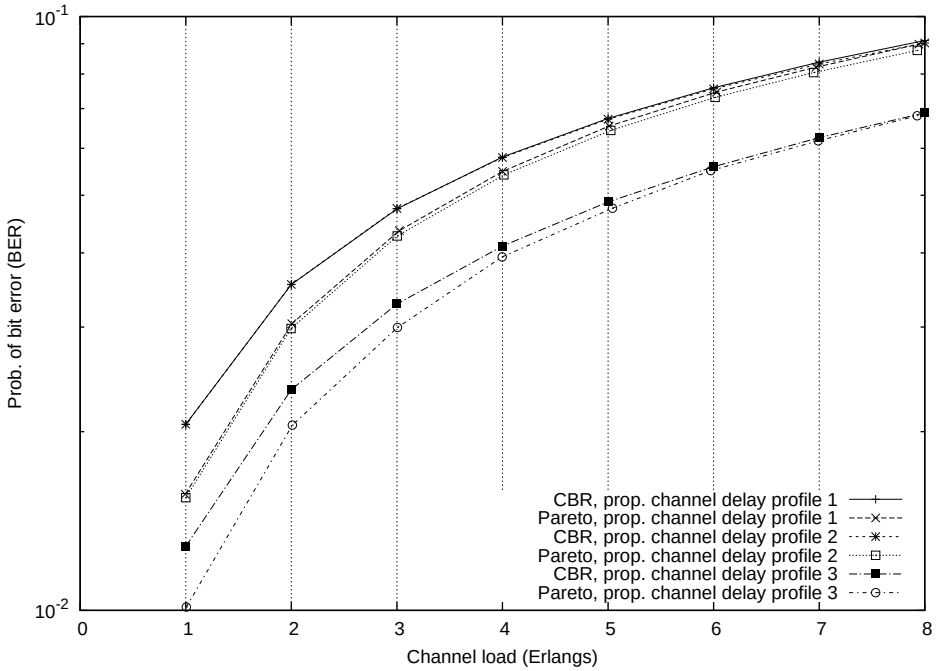

Figure 6.32: BER for a stationary MT located 0.85 radii from the cell centre with CBR and Pareto ($H = 0.8$) traffic models. All MT's use a fixed spreading factor of 16.

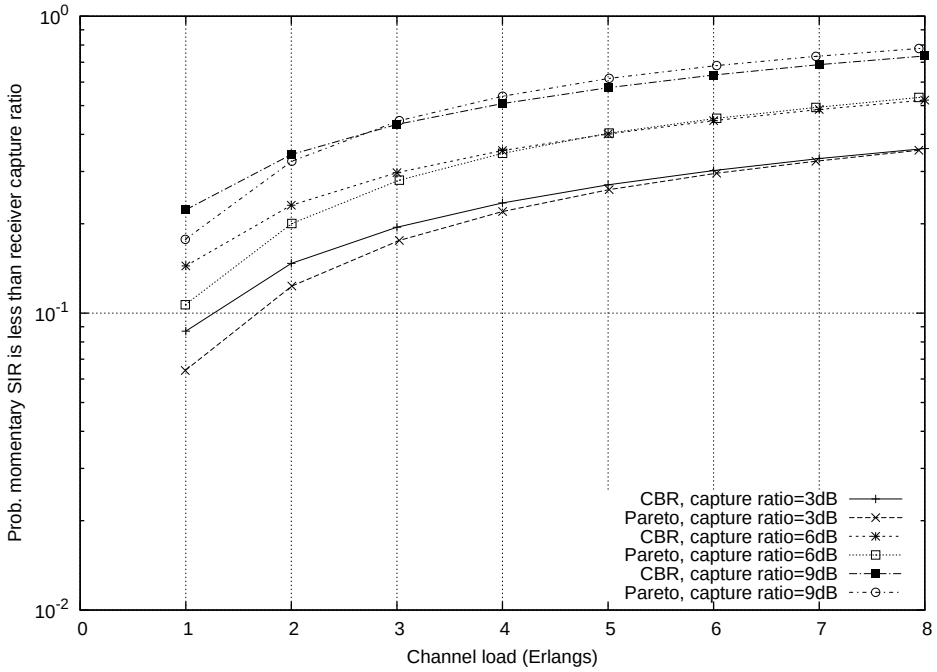

Figure 6.33: Probability the momentary SIR at the receiver is less than the receiver capture ratio for a stationary MT located 0.85 radii from the cell centre with propagation channel delay profile 1 and CBR and Pareto ($H = 0.8$) traffic models. All MT's use a fixed spreading factor of 16.

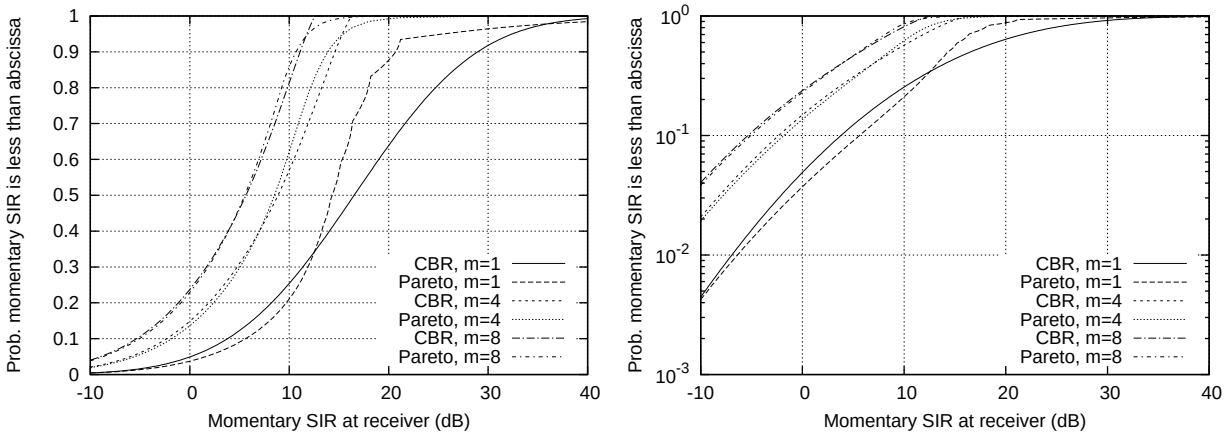

(a) linear scale (b) logarithmic scale

Figure 6.34: Cumulative distribution function of the momentary SIR at the receiver for a stationary MT located 0.85 radii from the cell centre with propagation channel delay profile 1 and CBR and Pareto ($H = 0.8$) traffic models (m MT's per cell). All MT's use a fixed spreading factor of 16.

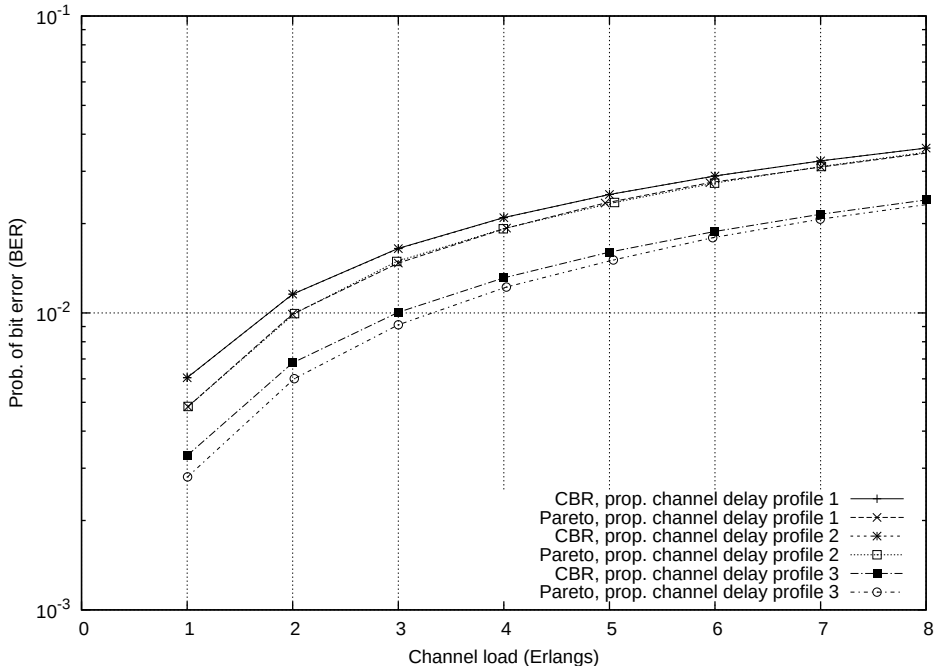

Figure 6.35: BER for a stationary MT located 0.85 radii from the cell centre with CBR and Pareto ($H = 0.8$) traffic models. All MT's use a fixed spreading factor of 64.

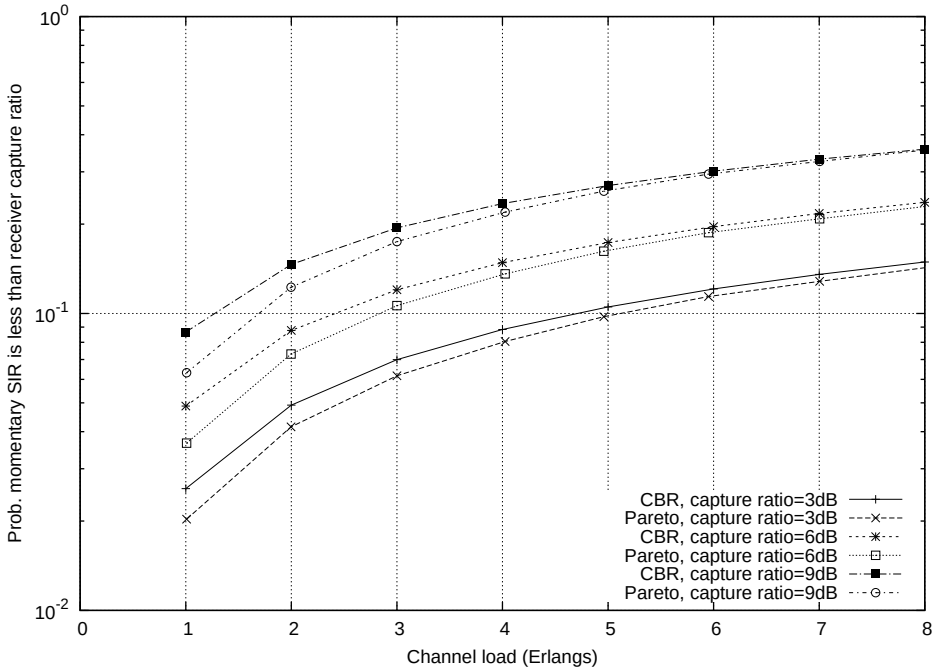

Figure 6.36: Probability the momentary SIR at the receiver is less than the receiver capture ratio for a stationary MT located 0.85 radii from the cell centre with propagation channel delay profile 1 and CBR and Pareto ($H = 0.8$) traffic models. All MT's use a fixed spreading factor of 64.

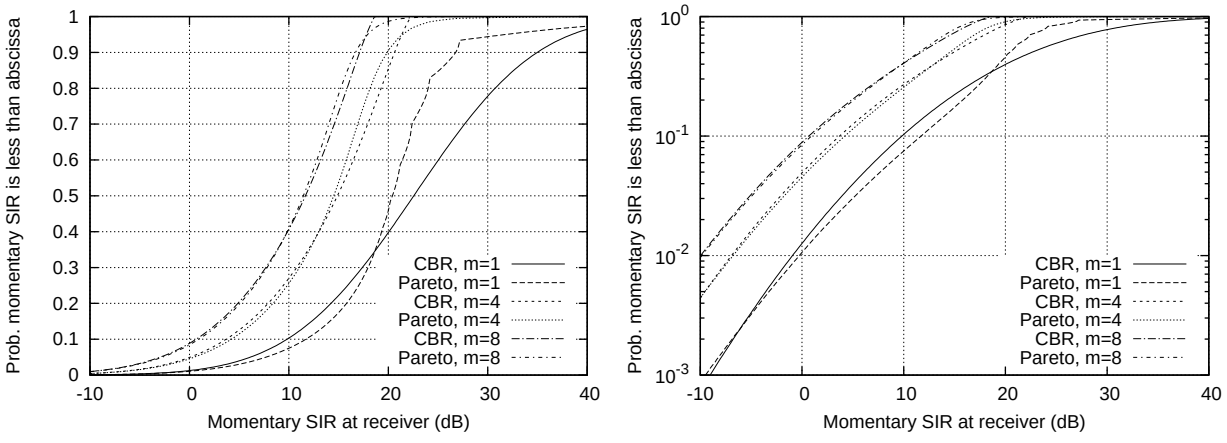

(a) linear scale

(b) logarithmic scale

Figure 6.37: Cumulative distribution function of the momentary SIR at the receiver for a stationary MT located 0.85 radii from the cell centre with propagation channel delay profile 1 and CBR and Pareto ($H = 0.8$) traffic models (m MT's per cell). All MT's use a fixed spreading factor of 64.

6.4.4 A Variable Spreading Factor vs. Multiple Spreading Codes

The system considered in this chapter dynamically allocates fixed size spreading codes on a frame-by-frame basis and multiple spreading codes are allocated to a user to vary their momentary transmission capacity on the radio channel. An alternative method to vary a user's momentary transmission capacity is to use a variable spreading factor and adjust the transmission power allocated to each spreading code as necessary.

The results presented in this chapter show that allocating multiple spreading codes to a user may not be optimal and in a time dispersive propagation environment the use of a variable spreading factor may be a better choice. As was explained in Section 6.4.1, in a time dispersive propagation environment the level of intra-cell interference at an MT receiver is positively correlated with the number of spreading codes allocated to the MT. Consequently, it is best to minimise the number of spreading codes allocated to any one MT. With a non-time dispersive propagation environment and orthogonal spreading codes there is no intra-cell interference and the choice of multiple spreading codes or a variable spreading factor has no impact on performance.

One drawback of a variable spreading factor is the reduced granularity of available transmission capacities. For example, OVSF spreading codes have fixed lengths of 2^n, where n is a positive integer, and if an MT requires the equivalent of 3 spreading codes with a spreading factor of 64, and a variable spreading factor is used, then the first adequate OVSF spreading code has a spreading factor of 16 i.e. 25% of the allocated transmission capacity is wasted.

6.5 Propagation Environment Shadowing Variability

The lognormal shadowing parameter σ in the propagation model used in Sections 6.3 and 6.4 influences the variability of the received signal power and can be considered a measure of the hostility of the propagation environment. A larger value of σ causes greater variability in the received signal power and implies a more hostile propagation environment[7]. A change in the variability of the desired signal power or interference power impacts the receiver SIR distribution and this in turn impacts system performance.

Tables 6.9 and 6.10 compare BER performance with the CBR and Pareto traffic models with different levels of lognormal shadowing variability. Table 6.9 considers the scenario in Section 6.3.1 (a non-time dispersive propagation channel) and Table 6.10 considers the scenario in Section 6.4.1 (a time dispersive propagation channel with propagation channel delay profile 1). In both cases MT's move randomly within their own cell and use a spreading factor of 16. The tables show that the lognormal shadowing variability does impact the BER

[7]Typical values of σ in cellular propagation environments are listed in Table 3.2.

performance difference between the traffic models to a small extent but there is no definitive pattern.

Shadowing variability (dB)	No. MT's	Prob. of bit error (BER)		% difference
		CBR	Pareto	
$\sigma = 4$	$m = 1$	0.018781	0.015401	-18.0%
	$m = 4$	0.049732	0.046211	-7.1%
	$m = 8$	0.074781	0.071941	-3.8%
$\sigma = 8$	$m = 1$	0.047466	0.033996	-53.8%
	$m = 4$	0.090013	0.083398	-7.3%
	$m = 8$	0.117958	0.113678	-3.6%
$\sigma = 12$	$m = 1$	0.092702	0.062944	-32.1%
	$m = 4$	0.140697	0.130184	-7.5%
	$m = 8$	0.168299	0.163102	-3.1%

Table 6.9: Comparison of the BER with CBR and Pareto ($H = 0.8$) traffic models in a non-time dispersive propagation environment with different levels of lognormal shadowing variability σ. MT's move randomly within their own cell.

Shadowing variability (dB)	No. MT's	Prob. of bit error (BER)		% difference
		CBR	Pareto	
$\sigma = 4$	$m = 1$	0.018828	0.015402	-18.2%
	$m = 4$	0.049736	0.046328	-6.9%
	$m = 8$	0.074725	0.071788	-3.9%
$\sigma = 8$	$m = 1$	0.009012	0.007110	-21.1%
	$m = 4$	0.027520	0.026586	-3.4%
	$m = 8$	0.045934	0.045999	0.1%
$\sigma = 12$	$m = 1$	0.092660	0.063259	-31.7%
	$m = 4$	0.140730	0.129943	-7.7%
	$m = 8$	0.168312	0.163444	-2.9%

Table 6.10: Comparison of the BER with CBR and Pareto ($H = 0.8$) traffic models in a time dispersive propagation environment (propagation channel delay profile 1) with different levels of lognormal shadowing variability σ. MT's move randomly within their own cell.

6.6 Summary

The downlink performance of a typical DS-CDMA outdoor macro-cellular system has been evaluated with two statistically dissimilar traffic models, specifically, a CBR traffic model and a bursty Pareto ($H = 0.8$) traffic model. These models were selected to obtain a measure of system performance sensitivity to traffic type and both non-time dispersive and time dispersive propagation environments were evaluated.

In the non-time dispersive propagation environment evaluated the Pareto traffic model had between 1–54% superior BER performance than the CBR traffic model. A performance difference manifested itself because the traffic models generate different traffic streams and this impacts the BTS transmitter power distribution, which in turn impacts the interference power distribution, and this in turn impacts the receiver SIR distribution and system performance. In general, as the number of users and traffic load increased the level of performance difference between the traffic models reduced and eventually reached a negligible level.

Similar performance trends were observed with a time dispersive propagation environment but with one important exception. In the scenario where intra-cell interference was dominant the CBR traffic model had between 20–190% superior BER performance than the Pareto traffic model. This is due to the fact that in a time dispersive propagation environment the level of intra-cell interference at an MT receiver is positively correlated with the number of spreading codes allocated to the MT. The use of a variable spreading factor rather than multiple spreading codes avoids this detrimental correlation effect.

Chapter 7

Downlink Performance in an Indoor Pico-Cellular Environment

7.1 Introduction

This chapter identifies scenarios where the downlink performance of a DS-CDMA indoor pico-cellular system is sensitive to the statistical properties of the user traffic. As in Chapter 6, system performance is evaluated with two statistically dissimilar traffic models in order to obtain a measure of performance sensitivity to traffic type.

Because the propagation environments of indoor pico-cellular systems are varied, due to the diverse range of buildings where an indoor pico-cellular system can be deployed, the approach taken in this thesis is to evaluate system performance for only a single indoor pico-cellular system and use this as a representative example of other indoor pico-cellular systems. The system considered is deployed in the Engineering School Tower described in Section 3.5.2.

An overview of the system evaluated is given in Section 7.2 and two in-building BTS deployment configurations are presented. System downlink performance is then evaluated and the use of higher order modulation schemes is considered in Section 7.3.

7.2 Engineering School Tower

The indoor pico-cellular system evaluated is deployed in the Engineering School Tower described in Section 3.5.2 and the system model developed in Chapter 5 is used to evaluate system performance. The same two statistically dissimilar traffic models that were used in Chapter 6 to evaluate system performance are also used in this chapter i.e. the CBR traffic model and bursty Pareto ($H = 0.8$) traffic model. The Engineering School Tower is a prototypical 12 storey office tower and the floor plan of the 8th floor is shown in Figure 7.1

(floors 5–10 all have a similar layout). The system contains 5 BTS's deployed on floors 6–10, one on each floor, and each BTS's coverage area is the floor that it is located on. System performance is evaluated for users on the 8th floor.

There are 2 potential BTS locations on each floor and 49 potential MT locations on the 8th floor and these are shown in Figure 7.1. A propagation measurement database is used to calculate the mean propagation path loss between BTS's and MT's and Rayleigh fading is applied to the mean received signal power to determine the momentary received signal power. Information about the propagation measurement database can be found in Appendix A. A non-time dispersive propagation channel is assumed since indoor propagation environments typically have small propagation channel delay spreads (see Section 3.4). Two BTS configurations are considered and these are shown in Figure 7.2. In the aligned configuration, floors 6–10 each have a BTS located at position TX-A while in the offset configuration, floors 6, 8, and 10 each have a BTS located at position TX-A and floors 7 and 9 each have a BTS located at position TX-B. MT's always connect to the BTS on the same floor and no cell handovers occur.

OVSF spreading codes are used exclusively and their orthogonal nature, in conjunction with the non-time dispersive propagation channel, means that no intra-cell interference occurs i.e. only inter-cell interference. BTS's use a fixed spreading factor and allocate the same transmission power to each spreading code. Packets are assumed to have zero scheduling delay tolerance and each BTS limits the maximum number of codes transmitted per frame to the value of the spreading factor i.e. a maximum of 16 or 64 spreading codes per frame in the scenarios considered (excess packets are dropped). The BTS transmitter power distribution and traffic scheduling performance presented in Section 6.2 also applies to the system considered in this chapter.

Unless stated otherwise, MT's move randomly on their own floor and all 49 potential MT locations are equally likely. Two specific MT locations are considered in later sections and these are labelled RX-A and RX-B in Figure 7.1. Location RX-A has a relatively high mean received signal power from TX-A (a path loss of 64 dB) while location RX-B has a relatively low mean received signal power from TX-A (a path loss of 90 dB)[1]. Each MT offers 1 Erlang of traffic and spreading factors of 16 and 64 are considered. A QPSK modulation scheme and system chip rate of 3.84 Mcps is assumed and this translates into a radio bearer bitrate of 480 kbps per code with a spreading factor of 16 and a radio bearer bitrate of 120 kbps per code with a spreading factor of 64.

[1] A complete table of path losses is included in Appendix A.

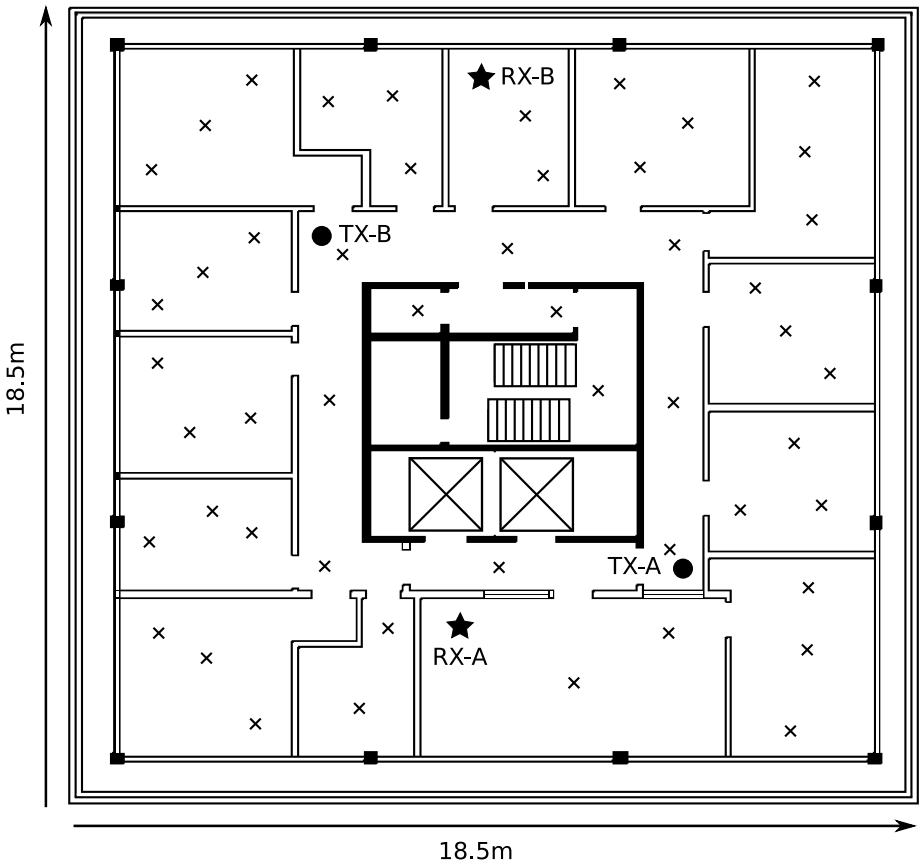

Figure 7.1: Floor plan of the Engineering School Tower 8th floor. Potential BTS locations are TX-A and TX-B and potential MT locations are RX-A, RX-B, and locations marked '×'.

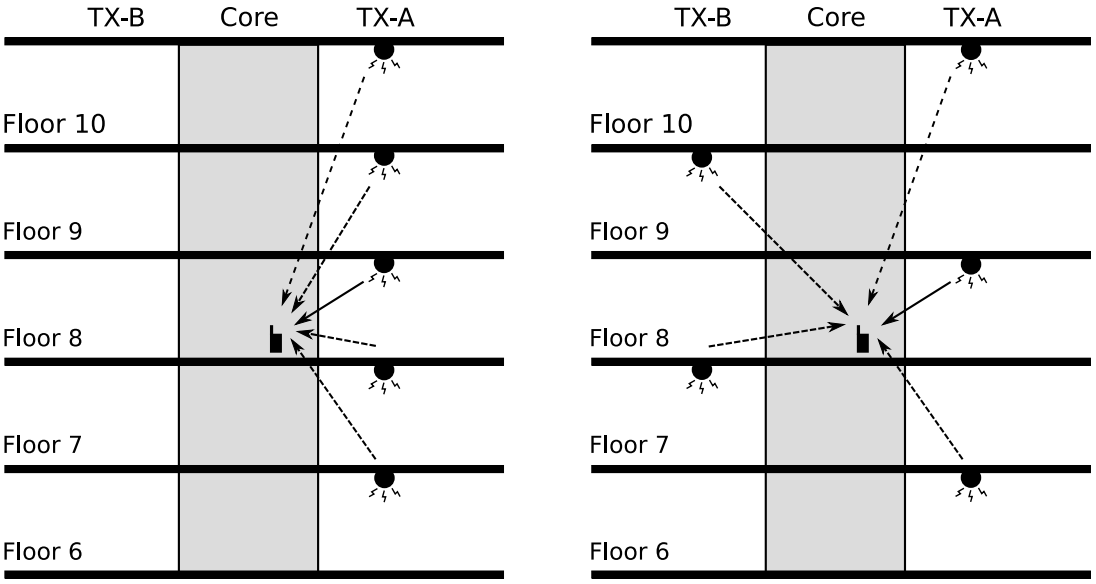

(a) aligned (b) offset

Figure 7.2: Cross-section of the Engineering School Tower with aligned and offset BTS configurations.

7.2.1 Correlated Shadowing

Correlated shadowing refers to a correlation in the level of desired signal power and interference power at the receiver. It has been shown that a positive correlation can significantly improve system performance and that a negative correlation can significantly degrade it [78]. Correlation is generally understood to occur when there are commonalities in the propagation paths between the receiver and the desired and interfering transmitters. In outdoor macro-cellular environments the potential for correlation is relatively low whereas in indoor pico-cellular environments the potential is relatively high [79, 80].

The aligned and offset BTS configurations shown in Figure 7.2 provide a useful illustration of correlated shadowing. In the aligned configuration both the desired and interfering signals experience similar levels of path loss due to the similar propagation paths and this leads to a positive correlation. In the offset configuration the desired signal tends to experience relatively little path loss when the interfering signals from the two immediately adjacent floors tend to experience relatively high path loss, and vice versa, and this leads to a negative correlation. It was shown in [81] that the Engineering School Tower exhibits significant positive correlation with the aligned BTS configuration and significant negative correlation with the offset BTS configuration. The impact of this is evident in the performance results presented in the following sections.

7.2.2 Random MT Location on the Same Floor

Figures 7.3–7.8 show system downlink performance when all MT's move randomly on their own floor and there are m MT's per floor/cell. In all cases the Pareto traffic model has superior BER and coverage performance than the CBR traffic model, especially at low loads[2]. As discussed in Chapter 6, the BER performance difference between the traffic models depends on the level of non-linearity in the BER vs. SIR curve and how the receiver SIR distribution associated with each traffic model weights the various points on the curve. As the number of MT's increases the central limit theorem comes into effect and the aggregate offered traffic stream statistically becomes more Gaussian and the variability of the traffic stream reduces relative to the mean. This reduces the performance difference between the two traffic models as the receiver SIR distributions associated with the traffic models statistically become more similar. The trends observed with the indoor pico-cellular environment are similar to those seen in Chapter 6 where an outdoor macro-cellular environment was considered and this is not unexpected as the fundamental propagation mechanisms are similar.

Table 7.1 compares BER performance with the two traffic models when using both aligned

[2]Coverage performance is defined as the probability the momentary SIR at the receiver is less than the receiver capture ratio.

and offset BTS configurations. As a comparison, in the non-time dispersive propagation environment scenario evaluated in Chapter 6 the Pareto traffic model had between 1–54% superior BER performance than the CBR traffic model. The aligned BTS configuration achieves vastly superior performance than the offset BTS configuration and this is due to the correlated shadowing described in the previous section. Figures 7.5 and 7.8 show the receiver SIR distributions with the different BTS configurations and in the aligned case the receiver SIR distribution spread is much smaller. This reconciles with the positively correlated shadowing associated with the aligned configuration i.e. a positive correlation tends to reduce the difference between the desired signal power and interference power. The different BTS configurations also impact the level of performance difference between the two traffic models, because of the different receiver SIR distributions, and this implies that the choice of BTS configuration during system design impacts how the system will perform with different types of traffic.

The contrasting receiver SIR distributions with the two BTS configurations is also evident in the coverage performance shown in Figures 7.4 and 7.7. The performance difference between the two traffic models is relatively low with the aligned configuration and receiver capture ratios of 3, 6, and 9 dB since these values are in the tail region of the cumulative distribution function curves shown in Figures 7.5 and 7.8. With the offset configuration the performance difference is more significant as the receiver capture ratios of 3, 6, and 9 dB are further away from the tail region of the cumulative distribution function curves due to the larger receiver SIR distribution spread.

BTS configuration	No. MT's	Prob. of bit error (BER)		% difference
		CBR	Pareto	
SPREADING FACTOR $s_f = 16$				
Aligned	$m = 1$	0.008464	0.007541	-10.9%
	$m = 4$	0.027146	0.025511	-6.0%
	$m = 8$	0.044865	0.043396	-3.3%
Offset	$m = 1$	0.092385	0.059201	-35.9%
	$m = 4$	0.131152	0.122843	-6.3%
	$m = 8$	0.152719	0.149253	-2.3%
SPREADING FACTOR $s_f = 64$				
Aligned	$m = 1$	0.002296	0.002153	-6.2%
	$m = 4$	0.008467	0.008175	-3.4%
	$m = 8$	0.015520	0.015222	-1.9%
Offset	$m = 1$	0.057939	0.038232	-34.0%
	$m = 4$	0.092388	0.085023	-8.0%
	$m = 8$	0.111067	0.107999	-2.8%

Table 7.1: Comparison of the BER with CBR and Pareto ($H = 0.8$) traffic models using aligned and offset BTS configurations. MT's move randomly on their own floor.

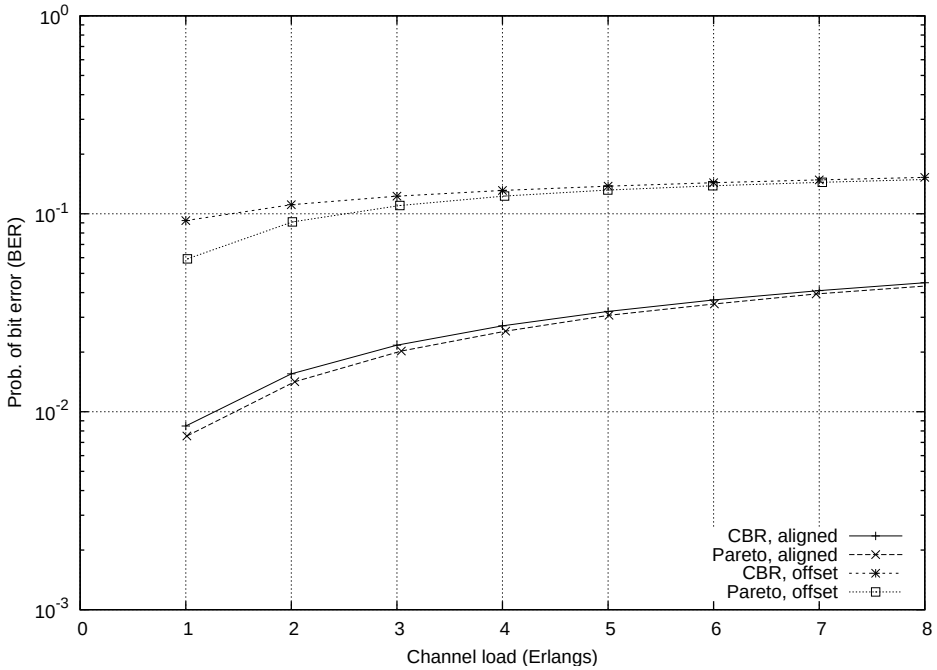

Figure 7.3: BER with CBR and Pareto ($H = 0.8$) traffic models using aligned and offset BTS configurations. MT's move randomly on their own floor and use a fixed spreading factor of 16.

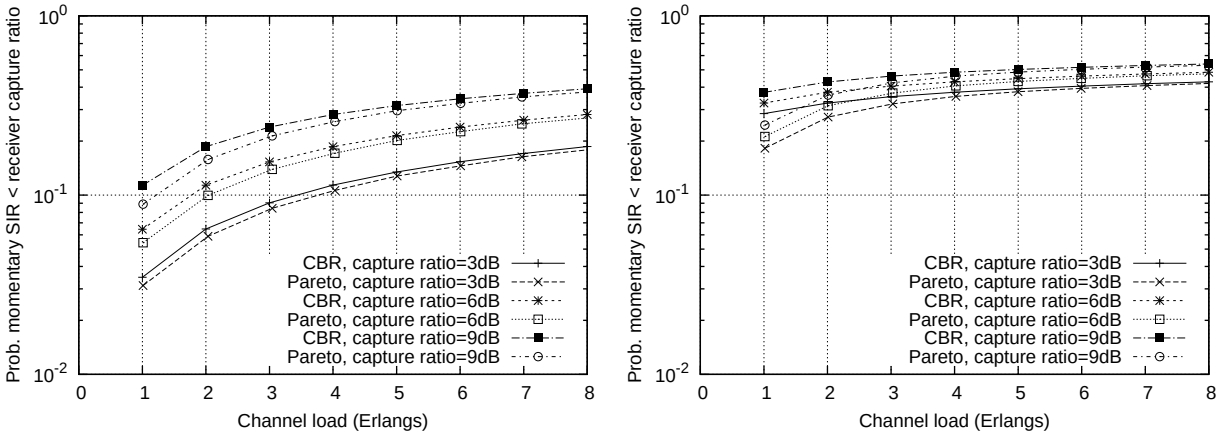

(a) aligned (b) offset

Figure 7.4: Probability the momentary SIR at the receiver is less than the receiver capture ratio with CBR and Pareto ($H = 0.8$) traffic models using aligned and offset BTS configurations. MT's move randomly on their own floor and use a fixed spreading factor of 16.

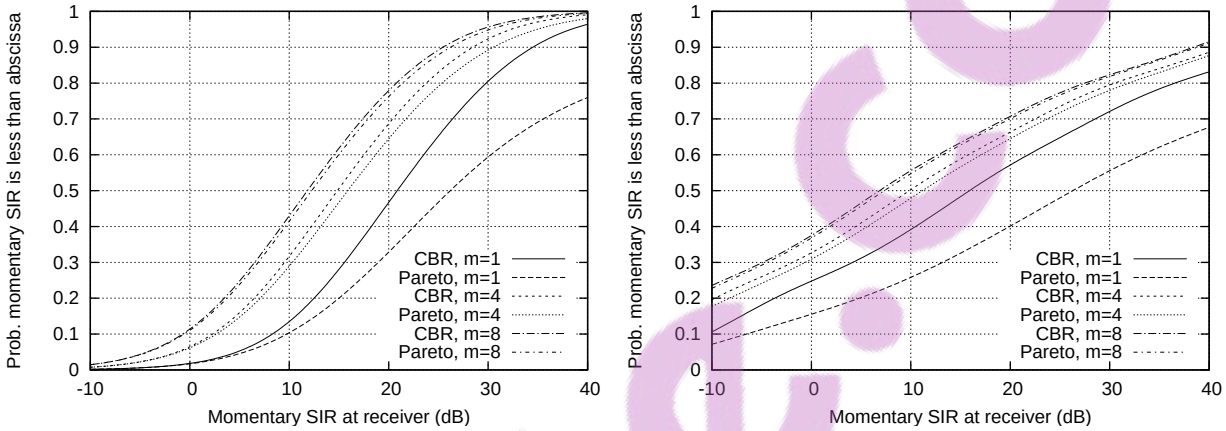

(a) aligned, linear scale

(b) offset, linear scale

(c) aligned, logarithmic scale

(d) offset, logarithmic scale

Figure 7.5: Cumulative distribution function of the momentary SIR at the receiver with CBR and Pareto ($H = 0.8$) traffic models using aligned and offset BTS configurations (m MT's per cell). MT's move randomly on their own floor and use a fixed spreading factor of 16.

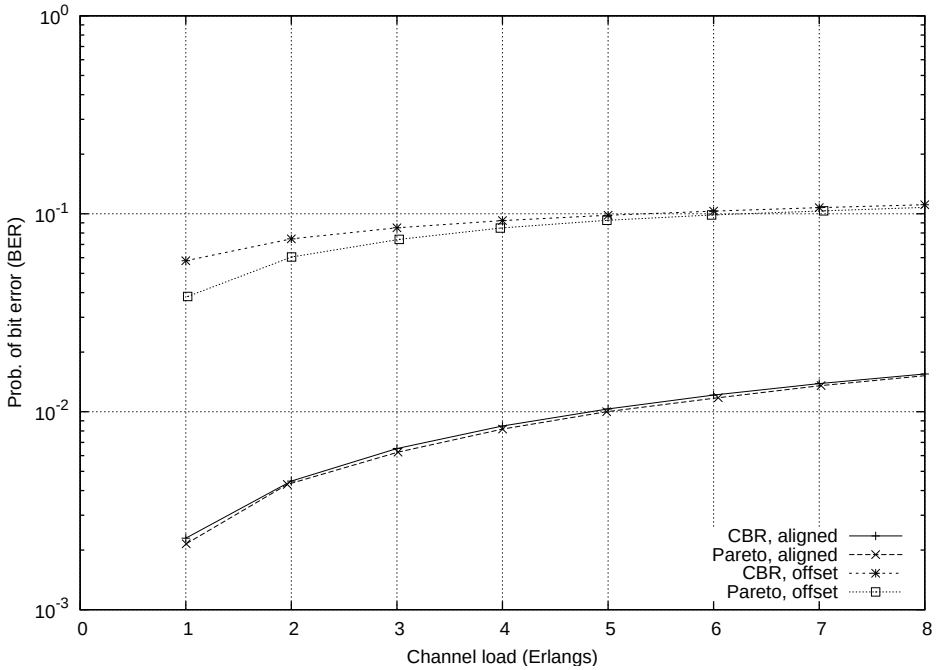

Figure 7.6: BER with CBR and Pareto ($H = 0.8$) traffic models using aligned and offset BTS configurations. MT's move randomly on their own floor and use a fixed spreading factor of 64.

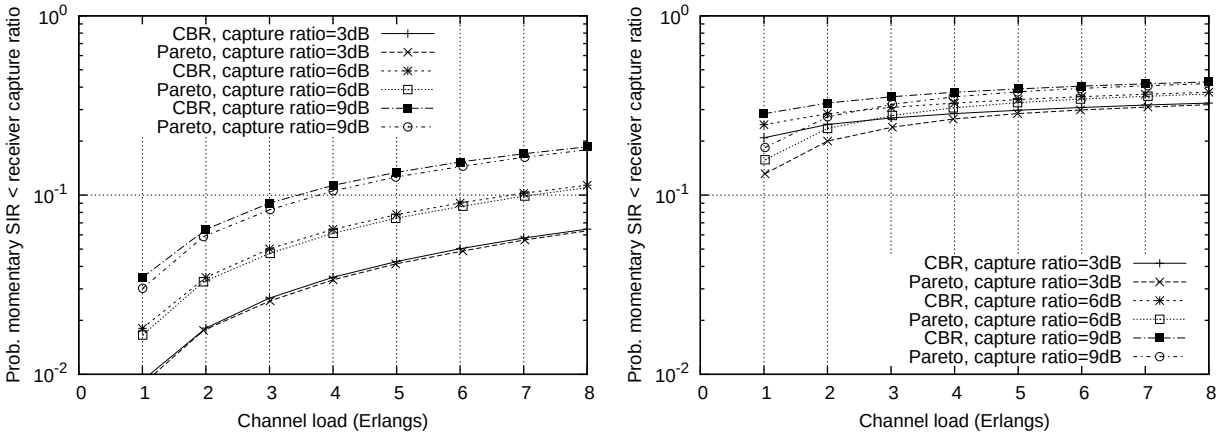

(a) aligned (b) offset

Figure 7.7: Probability the momentary SIR at the receiver is less than the receiver capture ratio with CBR and Pareto ($H = 0.8$) traffic models using aligned and offset BTS configurations. MT's move randomly on their own floor and use a fixed spreading factor of 64.

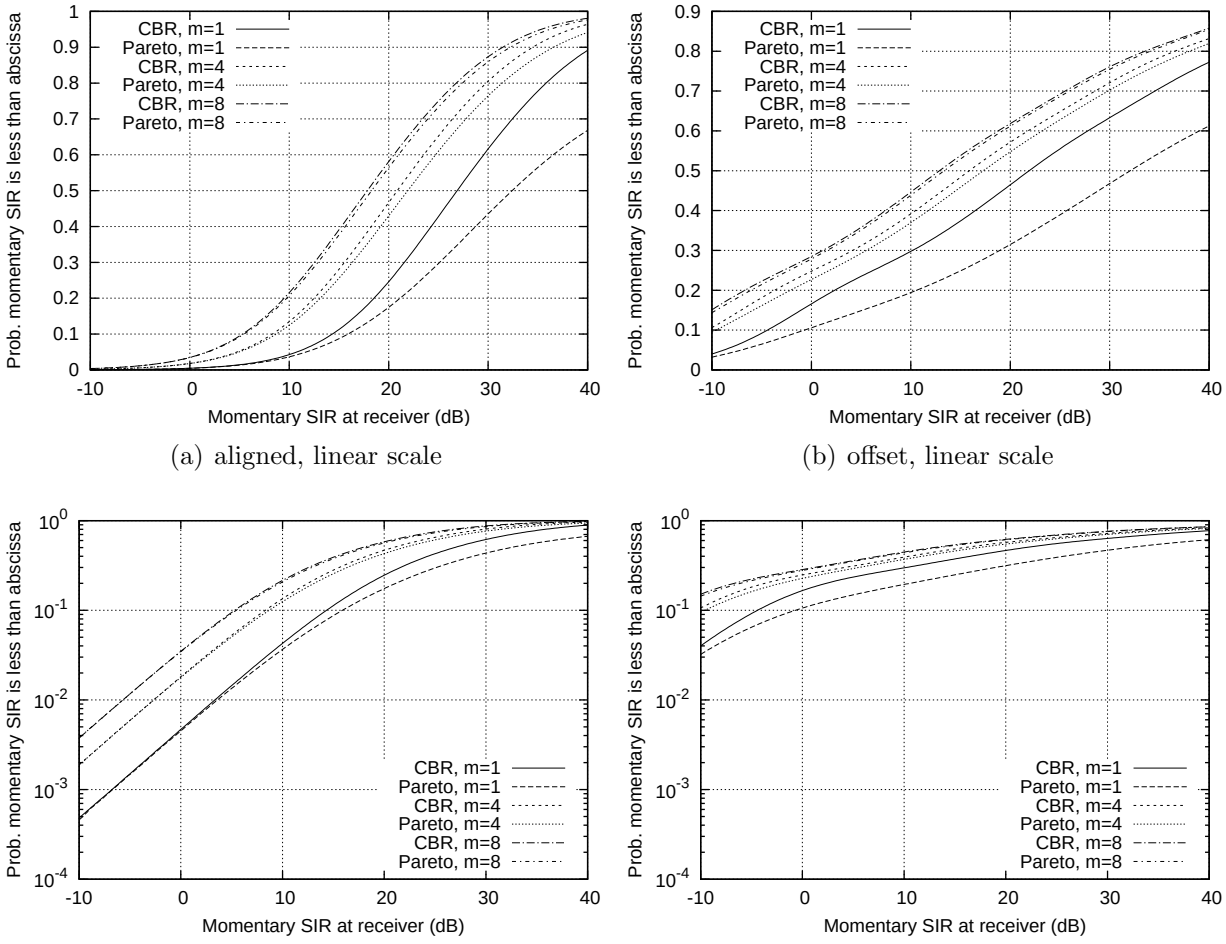

(a) aligned, linear scale

(b) offset, linear scale

(c) aligned, logarithmic scale

(d) offset, logarithmic scale

Figure 7.8: Cumulative distribution function of the momentary SIR at the receiver with CBR and Pareto ($H = 0.8$) traffic models using aligned and offset BTS configurations (m MT's per cell). MT's move randomly on their own floor and use a fixed spreading factor of 64.

7.2.3 Fixed MT Location with a High Mean Desired Signal Power

Figures 7.9–7.14 show downlink performance for a stationary MT located at position RX-A (see Figure 7.1). All other MT's move randomly on their own floor and there are m MT's per floor/cell. This location is considered to be in a good coverage area with a relatively high mean desired signal power from TX-A (a path loss of 64 dB). Absolute performance levels are better in this scenario than in the random MT location scenario as the MT being evaluated is permanently located in a good coverage area. The offset BTS configuration has superior performance than the aligned configuration because the path loss between the MT and position TX-B on floors 7 and 9 (102 dB and 98 dB respectively) is significantly more than the path loss between the MT and position TX-A on floors 7 and 9 (81 dB and 80 dB respectively) i.e. there is less interference from the two adjacent floors.

Table 7.2 shows that the BER performance difference between the two traffic models is minimal with both the aligned and offset BTS configurations. In some cases the CBR traffic model actually has slightly superior BER performance than the Pareto traffic model which is in contrast to the results in the previous section. The minimal performance difference occurs because the mean SIR at the receiver is relatively high and the receiver's SIR distribution is concentrated around a relatively linear section of the BER vs. SIR curve where the traffic model has little impact. This mirrors the results observed in the equivalent scenario in Chapter 6 where an outdoor macro-cellular environment was considered i.e. Section 6.3.2.

Coverage performance is shown in Figures 7.10 and 7.13 and again the performance difference between the two traffic models is minimal. This is because the mean SIR at the receiver is relatively high and the receiver capture ratios of 3, 6, and 9 dB are in the tail region of the receiver SIR cumulative distribution function curves shown in Figures 7.11 and 7.14.

BTS configuration	No. MT's	Prob. of bit error (BER)		% difference
		CBR	Pareto	
SPREADING FACTOR $s_f = 16$				
Aligned	$m = 1$	0.001612	0.001606	-0.4%
	$m = 4$	0.006311	0.006193	-1.9%
	$m = 8$	0.012315	0.012192	-1.0%
Offset	$m = 1$	0.000107	0.000108	0.8%
	$m = 4$	0.000417	0.000431	3.4%
	$m = 8$	0.000843	0.000837	-0.7%
SPREADING FACTOR $s_f = 64$				
Aligned	$m = 1$	0.000405	0.000396	-2.4%
	$m = 4$	0.001612	0.001615	0.2%
	$m = 8$	0.003194	0.003196	0.1%
Offset	$m = 1$	0.000027	0.000028	4.7%
	$m = 4$	0.000103	0.000104	0.2%
	$m = 8$	0.000211	0.000202	-4.2%

Table 7.2: Comparison of the BER for a stationary MT located at position RX-A with CBR and Pareto ($H = 0.8$) traffic models using aligned and offset BTS configurations.

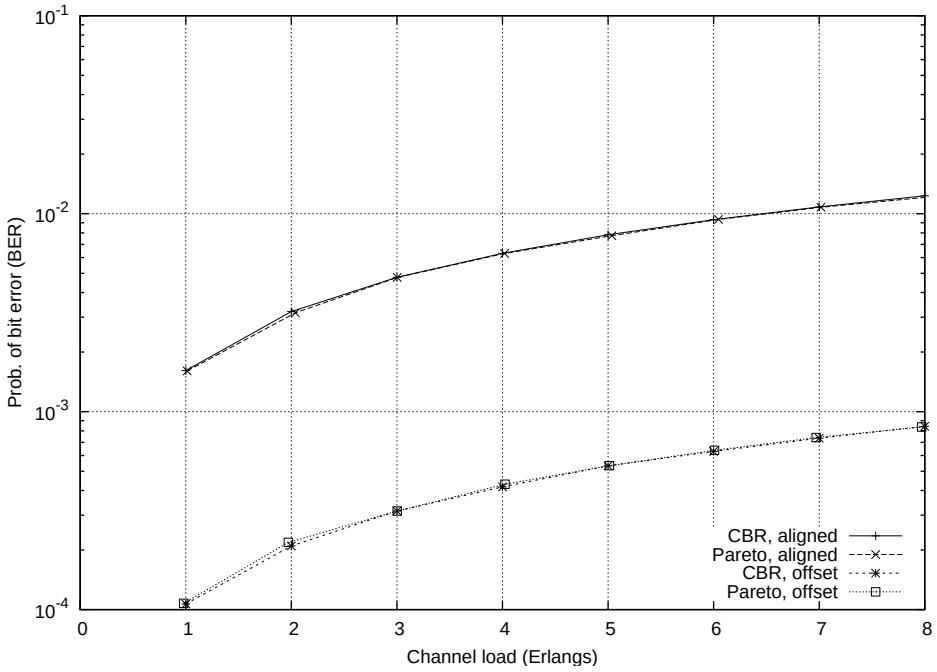

Figure 7.9: BER for a stationary MT located at position RX-A with CBR and Pareto ($H = 0.8$) traffic models using aligned and offset BTS configurations. All MT's use a fixed spreading factor of 16.

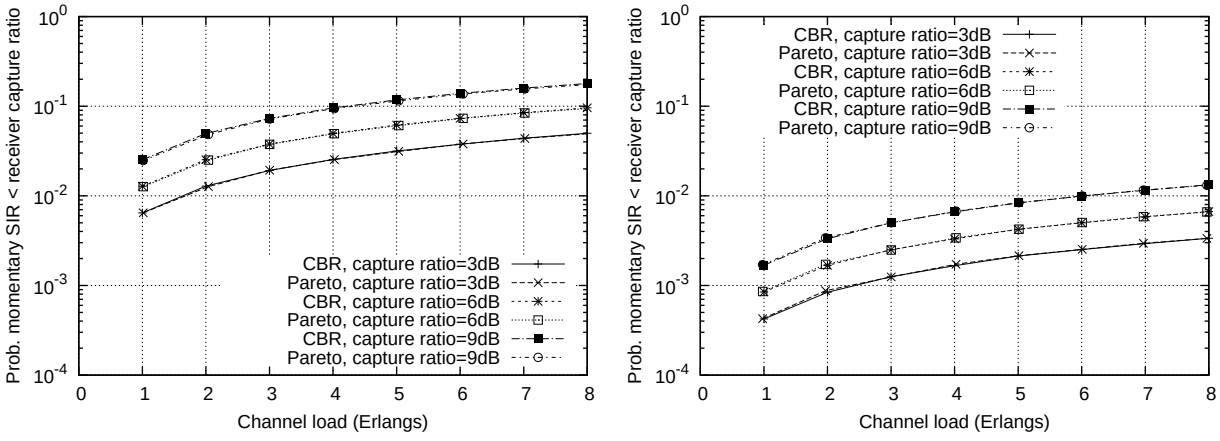

(a) aligned (b) offset

Figure 7.10: Probability the momentary SIR at the receiver is less than the receiver capture ratio for a stationary MT located at position RX-A with CBR and Pareto ($H = 0.8$) traffic models using aligned and offset BTS configurations. All MT's use a fixed spreading factor of 16.

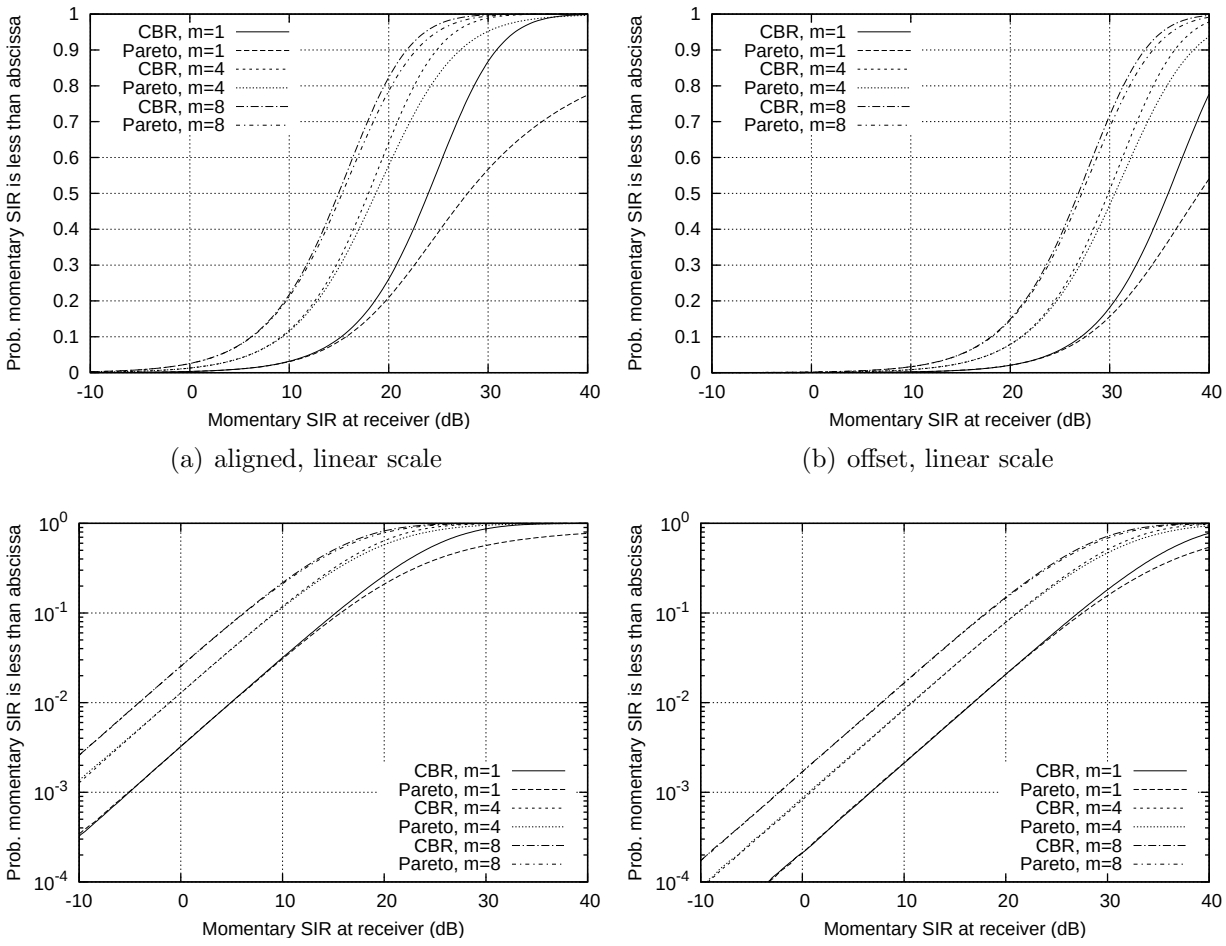

(a) aligned, linear scale

(b) offset, linear scale

(c) aligned, logarithmic scale

(d) offset, logarithmic scale

Figure 7.11: Cumulative distribution function of the momentary SIR at the receiver for a stationary MT located at position RX-A with CBR and Pareto ($H = 0.8$) traffic models using aligned and offset BTS configurations (m MT's per cell). All MT's use a fixed spreading factor of 16.

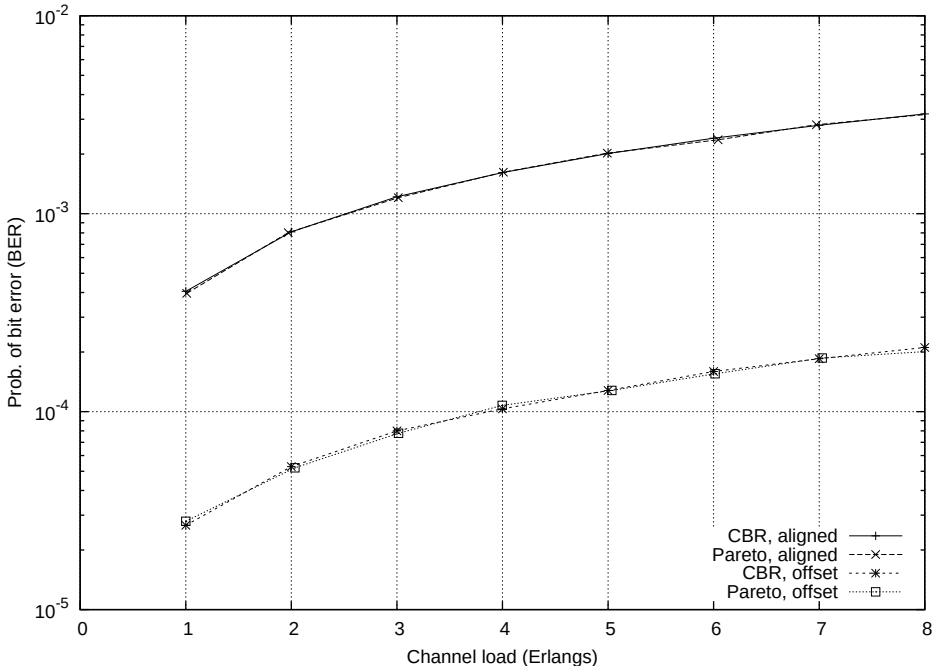

Figure 7.12: BER for a stationary MT located at position RX-A with CBR and Pareto ($H = 0.8$) traffic models using aligned and offset BTS configurations. All MT's use a fixed spreading factor of 64.

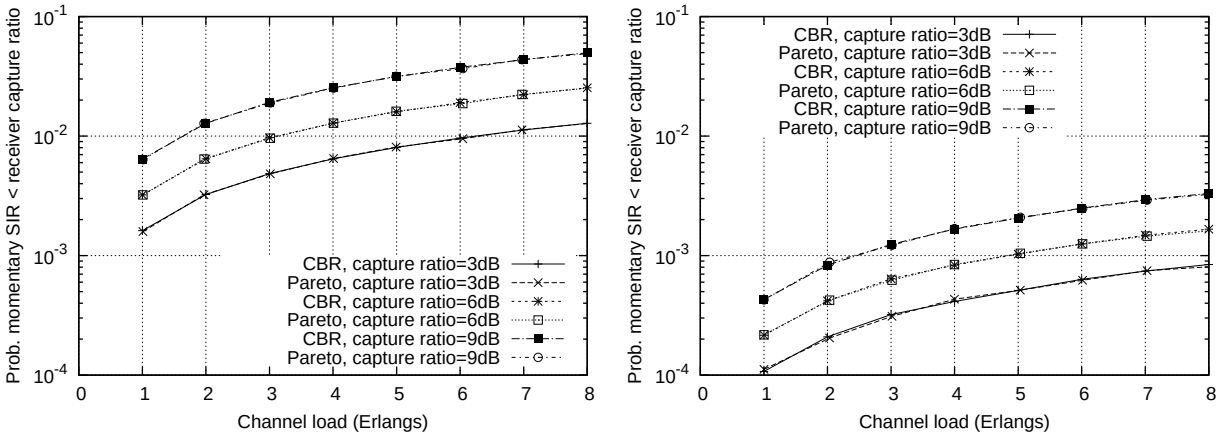

(a) aligned (b) offset

Figure 7.13: Probability the momentary SIR at the receiver is less than the receiver capture ratio for a stationary MT located at position RX-A with CBR and Pareto ($H = 0.8$) traffic models using aligned and offset BTS configurations. All MT's use a fixed spreading factor of 64.

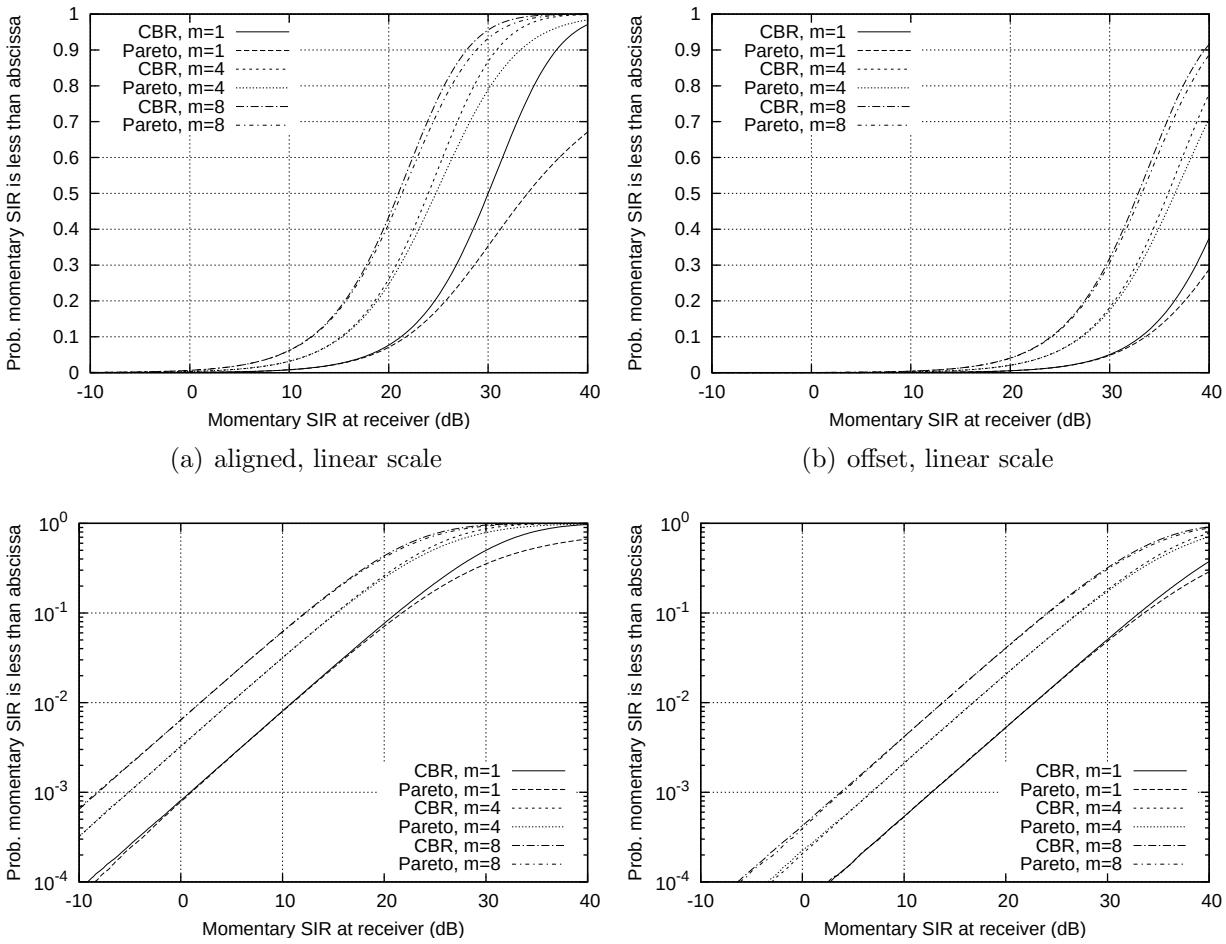

(a) aligned, linear scale

(b) offset, linear scale

(c) aligned, logarithmic scale

(d) offset, logarithmic scale

Figure 7.14: Cumulative distribution function of the momentary SIR at the receiver for a stationary MT located at position RX-A with CBR and Pareto ($H = 0.8$) traffic models using aligned and offset BTS configurations (m MT's per cell). All MT's use a fixed spreading factor of 64.

7.2.4 Fixed MT Location with a Low Mean Desired Signal Power

Figures 7.15–7.20 show downlink performance for a stationary MT located at position RX-B (see Figure 7.1). All other MT's move randomly on their own floor and there are m MT's per floor/cell. This location is considered to be in a poor coverage area with a relatively low mean desired signal power from TX-A (a path loss of 90 dB). Absolute performance levels are worse in this scenario than in the random MT location scenario as the MT being evaluated is permanently located in a poor coverage area. The aligned BTS configuration has superior performance than the offset configuration because the path loss between the MT and position TX-A on floors 7 and 9 (107 dB and 101 dB respectively) is significantly more than the path loss between the MT and position TX-B on floors 7 and 9 (88 dB and 85 dB respectively) i.e. there is less interference from the two adjacent floors.

Table 7.3 shows that the BER performance difference between the two traffic models is minimal with the aligned BTS configuration and moderate with the offset BTS configuration. This is because in the aligned case the mean SIR at the receiver is relatively high and the receiver's SIR distribution is concentrated around a relatively linear section of the BER vs. SIR curve where the traffic model has little impact. In the offset case the mean SIR at the receiver is lower and the receiver's SIR distribution is concentrated around a more non-linear section of the BER vs. SIR curve where the traffic model has a greater impact. The receiver's SIR distribution spread is also greater in the offset case.

Coverage performance is shown in Figures 7.16 and 7.19 and trends similar to those seen in the BER performance are observed i.e. in the aligned BTS configuration the performance difference between the traffic models is minimal but in the offset BTS configuration the performance difference is more significant. As explained in previous sections, this is due to the proximity of the receiver capture ratios of 3, 6, and 9 dB to the tail regions of the receiver SIR cumulative distribution function curves shown in Figures 7.17 and 7.20.

BTS configuration	No. MT's	Prob. of bit error (BER)		% difference
		CBR	Pareto	
SPREADING FACTOR $s_f = 16$				
Aligned	$m = 1$	0.004880	0.004678	-4.1%
	$m = 4$	0.018484	0.018141	-1.9%
	$m = 8$	0.034600	0.034261	-1.0%
Offset	$m = 1$	0.090881	0.068304	-24.8%
	$m = 4$	0.198749	0.180651	-9.1%
	$m = 8$	0.259227	0.248582	-4.1%
SPREADING FACTOR $s_f = 64$				
Aligned	$m = 1$	0.001244	0.001210	-2.7%
	$m = 4$	0.004906	0.004862	-0.9%
	$m = 8$	0.009606	0.009589	-0.2%
Offset	$m = 1$	0.030358	0.026333	-13.3%
	$m = 4$	0.090878	0.083342	-8.3%
	$m = 8$	0.140398	0.134558	-4.2%

Table 7.3: Comparison of the BER for a stationary MT located at position RX-B with CBR and Pareto ($H = 0.8$) traffic models using aligned and offset BTS configurations.

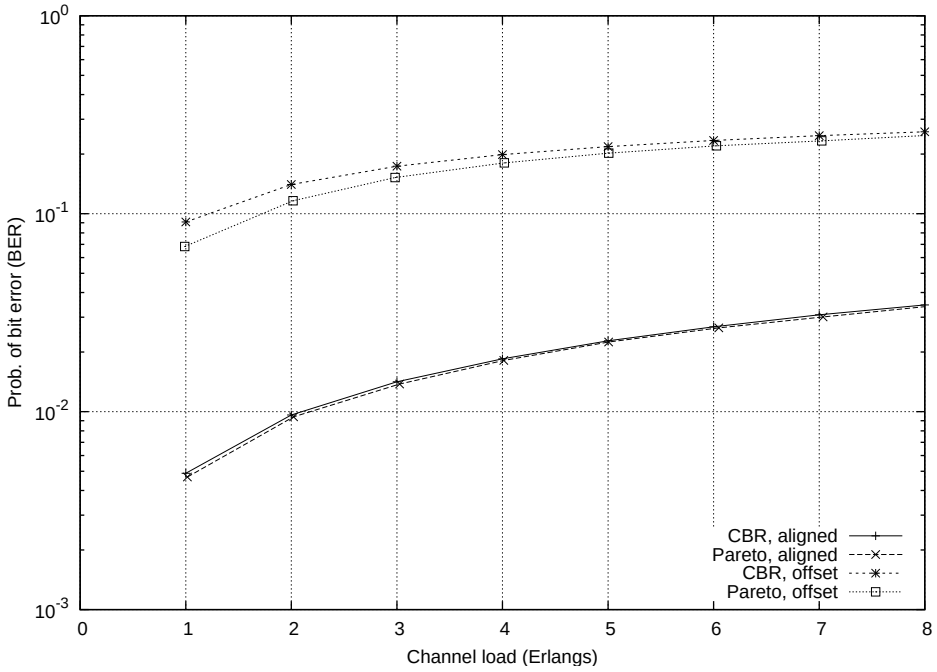

Figure 7.15: BER for a stationary MT located at position RX-B with CBR and Pareto ($H = 0.8$) traffic models using aligned and offset BTS configurations. All MT's use a fixed spreading factor of 16.

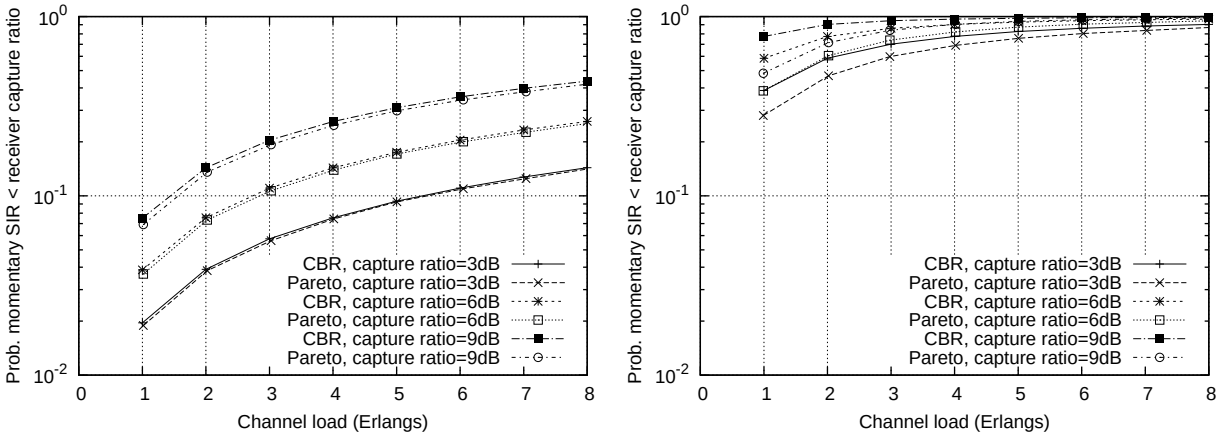

(a) aligned (b) offset

Figure 7.16: Probability the momentary SIR at the receiver is less than the receiver capture ratio for a stationary MT located at position RX-B with CBR and Pareto ($H = 0.8$) traffic models using aligned and offset BTS configurations. All MT's use a fixed spreading factor of 16.

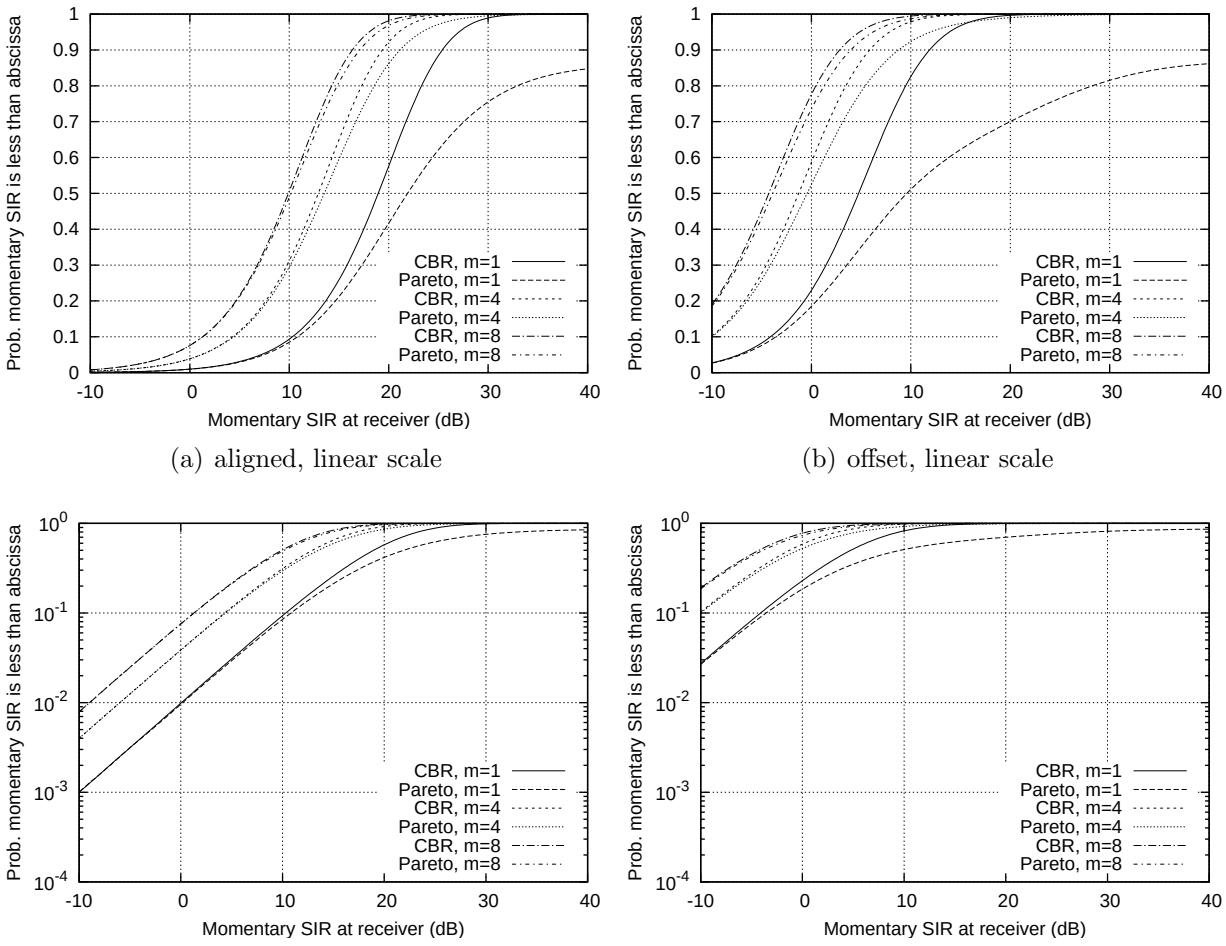

(a) aligned, linear scale

(b) offset, linear scale

(c) aligned, logarithmic scale

(d) offset, logarithmic scale

Figure 7.17: Cumulative distribution function of the momentary SIR at the receiver for a stationary MT located at position RX-B with CBR and Pareto ($H = 0.8$) traffic models using aligned and offset BTS configurations (m MT's per cell). All MT's use a fixed spreading factor of 16.

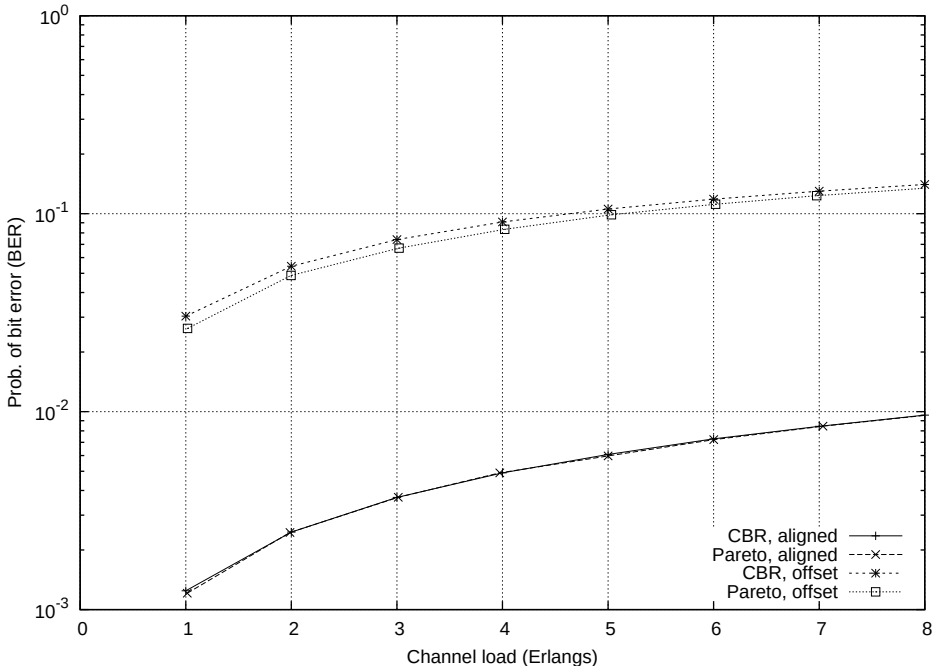

Figure 7.18: BER for a stationary MT located at position RX-B with CBR and Pareto ($H = 0.8$) traffic models using aligned and offset BTS configurations. All MT's use a fixed spreading factor of 64.

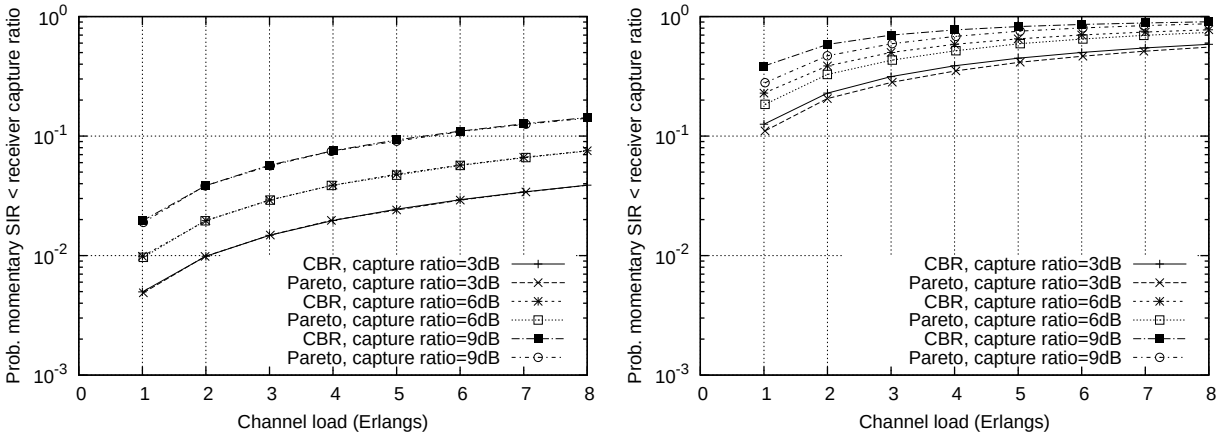

(a) aligned (b) offset

Figure 7.19: Probability the momentary SIR at the receiver is less than the receiver capture ratio for a stationary MT located at position RX-B with CBR and Pareto ($H = 0.8$) traffic models using aligned and offset BTS configurations. All MT's use a fixed spreading factor of 64.

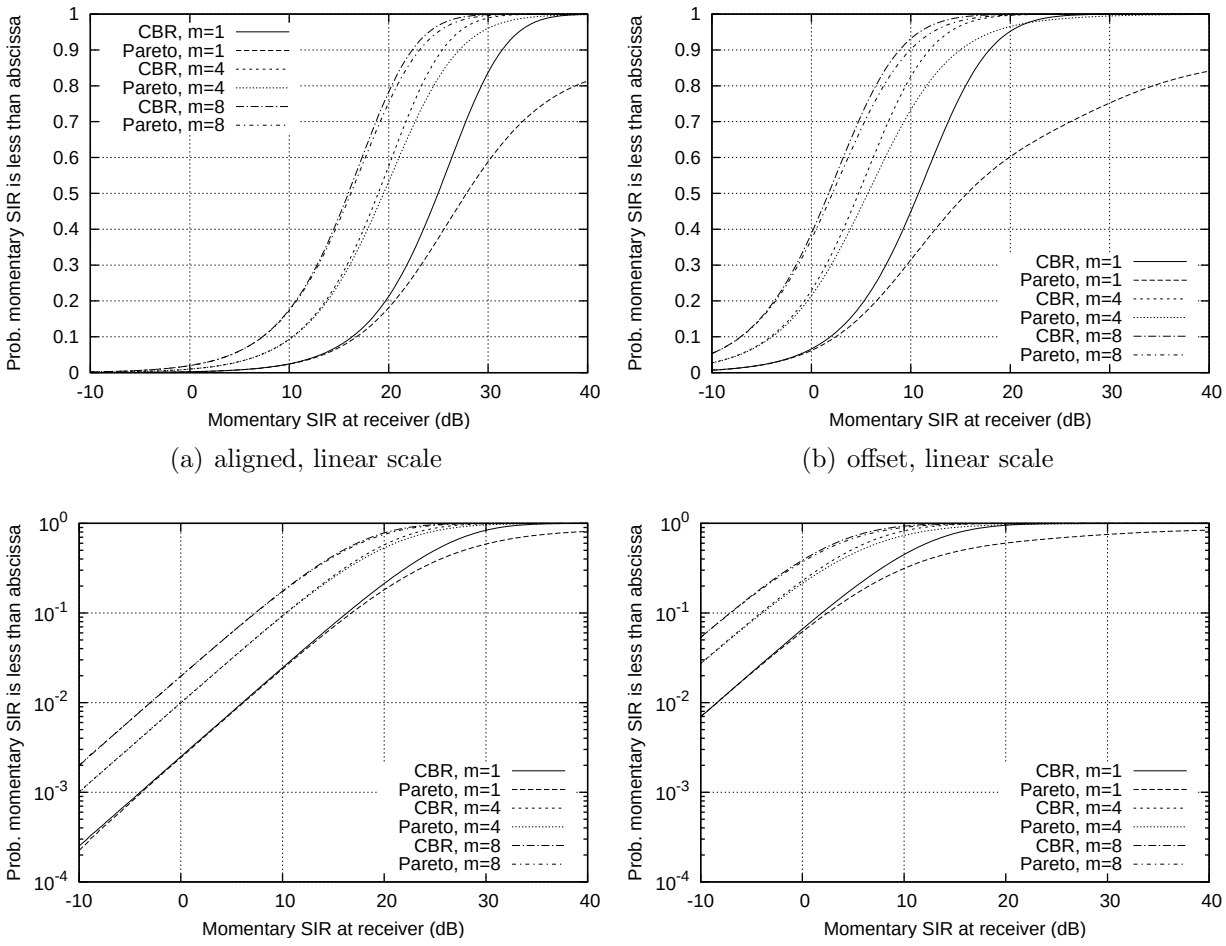

(a) aligned, linear scale

(b) offset, linear scale

(c) aligned, logarithmic scale

(d) offset, logarithmic scale

Figure 7.20: Cumulative distribution function of the momentary SIR at the receiver for a stationary MT located at position RX-B with CBR and Pareto ($H = 0.8$) traffic models using aligned and offset BTS configurations (m MT's per cell). All MT's use a fixed spreading factor of 64.

7.3 Higher Order Modulation Schemes

In systems or at MT locations where relatively high mean SIR values are attainable at the receiver it may be beneficial to use higher order modulation schemes to encode more user information bits per transmitted symbol [25]. Figure 7.21 shows the BER vs. SIR curves of the QPSK and 16QAM modulation schemes which encode 2 and 4 user information bits per symbol respectively i.e. 16QAM provides twice the throughput of QPSK[3].

Figures 7.22–7.24 show downlink performance for the scenario considered in Section 7.2 with the aligned BTS configuration and both QPSK and 16QAM modulation schemes. Table 7.4 compares the BER performance of the CBR and Pareto traffic models and in general the Pareto model has superior BER performance than the CBR model and the performance difference between the traffic models is larger with the 16QAM modulation scheme. Changing the modulation scheme from QPSK to 16QAM alters the BER vs. SIR curve and effectively shifts the BER vs. SIR curve to the right. This tends to concentrate the receiver SIR distribution in a more non-linear section of the BER vs. SIR curve where the traffic model has a greater impact on performance. This explains the larger performance difference between the traffic models with the 16QAM modulation scheme.

The receiver SIR distribution is independent of the modulation scheme. However, a higher order modulation scheme requires a higher receiver capture ratio in order to maintain acceptable performance and this reduces the system's coverage performance.

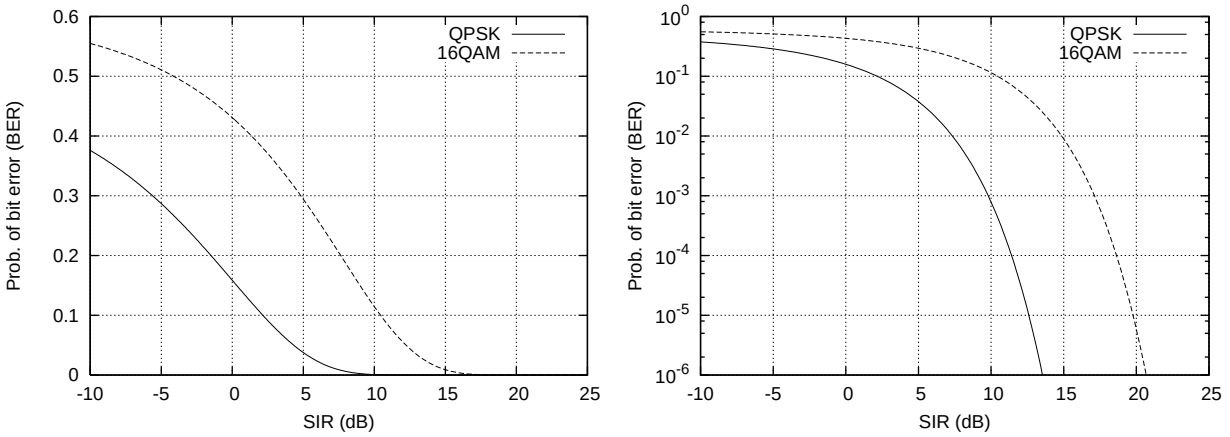

(a) linear scale (b) logarithmic scale

Figure 7.21: QPSK and 16QAM modulation schemes.

[3]Gray coding is assumed for the assignment of information bits to symbols.

Spreading factor	No. MT's	Prob. of bit error (BER) CBR	Prob. of bit error (BER) Pareto	% difference 16QAM	% difference QPSK
RANDOM MT LOCATION					
$s_f = 16$	$m = 1$	0.008464	0.007541	-21.6%	-10.9%
	$m = 4$	0.027146	0.025511	-7.9%	-6.0%
	$m = 8$	0.044865	0.043396	-3.5%	-3.3%
$s_f = 64$	$m = 1$	0.014367	0.012211	-15.0%	-6.2%
	$m = 4$	0.044232	0.041214	-6.8%	-3.4%
	$m = 8$	0.071131	0.068755	-3.3%	-1.9%
STATIONARY MT LOCATED AT POSITION RX-A					
$s_f = 16$	$m = 1$	0.010946	0.010493	-4.1%	-0.4%
	$m = 4$	0.039778	0.037985	-4.5%	-1.9%
	$m = 8$	0.071501	0.069491	-2.8%	-1.0%
$s_f = 64$	$m = 1$	0.002812	0.002762	-1.8%	-2.4%
	$m = 4$	0.010961	0.010865	-0.9%	0.2%
	$m = 8$	0.021175	0.020926	-1.2%	0.1%
STATIONARY MT LOCATED AT POSITION RX-B					
$s_f = 16$	$m = 1$	0.031629	0.028259	-10.7%	-4.1%
	$m = 4$	0.101065	0.095681	-5.3%	-1.9%
	$m = 8$	0.162248	0.157642	-2.8%	-1.0%
$s_f = 64$	$m = 1$	0.008507	0.008154	-4.1%	-2.7%
	$m = 4$	0.031737	0.030891	-2.7%	-0.9%
	$m = 8$	0.058233	0.057326	-1.6%	-0.2%

Table 7.4: Comparison of the BER with CBR and Pareto ($H = 0.8$) traffic models using the aligned BTS configuration and QPSK and 16QAM modulation schemes. (Full BER results for QPSK can be found in Section 7.2).

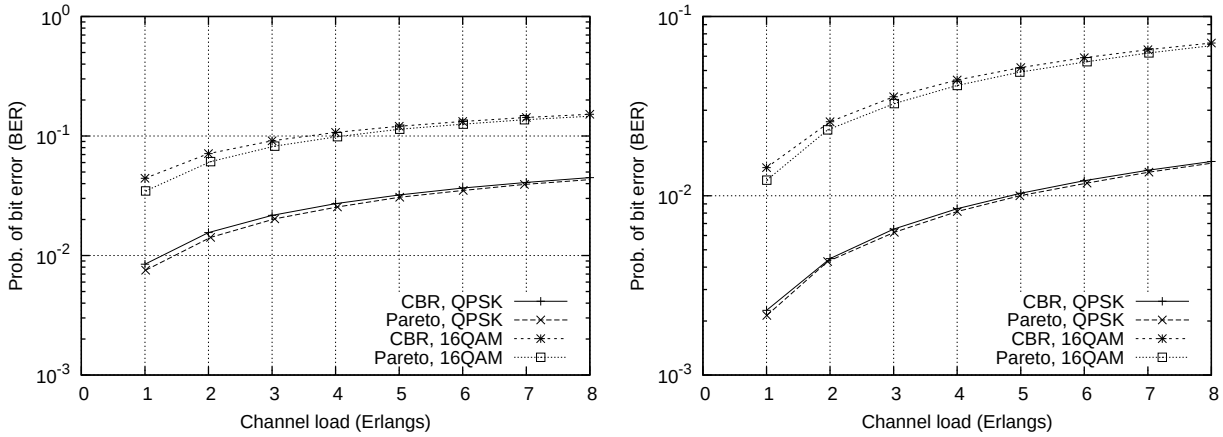

(a) spreading factor = 16

(b) spreading factor = 64

Figure 7.22: BER with CBR and Pareto ($H = 0.8$) traffic models using the aligned BTS configuration and QPSK and 16QAM modulation schemes. MT's move randomly on their own floor.

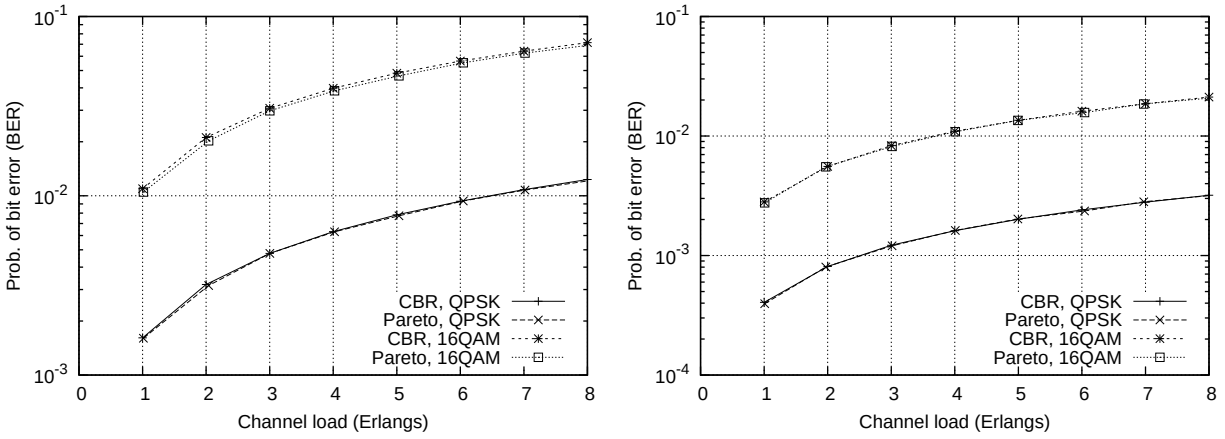

(a) spreading factor = 16 (b) spreading factor = 64

Figure 7.23: BER for a stationary MT located at position RX-A with CBR and Pareto ($H = 0.8$) traffic models using the aligned BTS configuration and QPSK and 16QAM modulation schemes.

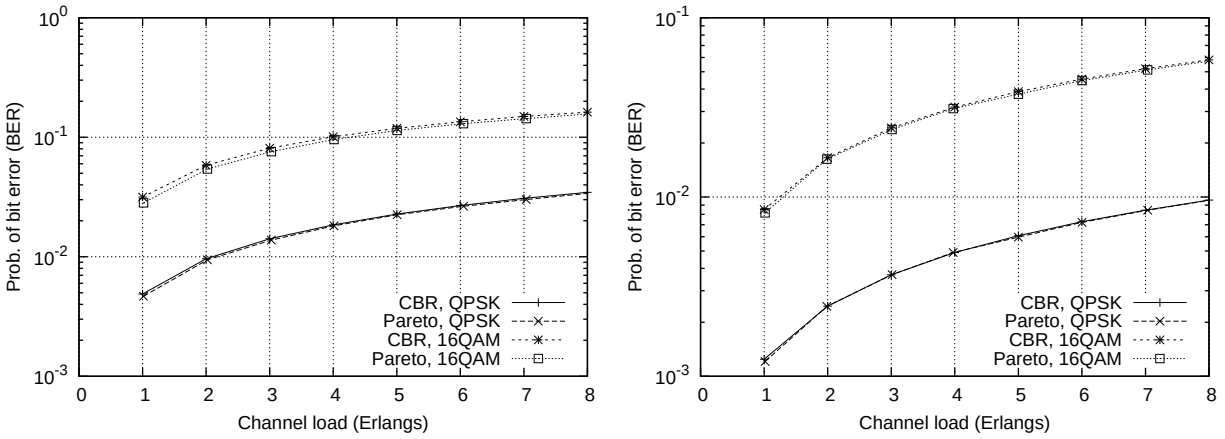

(a) spreading factor = 16 (b) spreading factor = 64

Figure 7.24: BER for a stationary MT located at position RX-B with CBR and Pareto ($H = 0.8$) traffic models using the aligned BTS configuration and QPSK and 16QAM modulation schemes.

7.4 Summary

The downlink performance of a DS-CDMA indoor pico-cellular system has been evaluated with two statistically dissimilar traffic models, specifically, a CBR traffic model and a bursty Pareto ($H = 0.8$) traffic model. These models were selected to obtain a measure of system performance sensitivity to traffic type. The system evaluated is deployed in the Engineering School Tower described in Section 3.5.2 and is considered a representative example of indoor pico-cellular systems.

Similar performance trends to those observed in Chapter 6 where an outdoor macro-cellular environment was considered were also observed in this chapter. This is not unexpected as the fundamental propagation mechanisms are similar in both propagation environments. In the scenarios evaluated, the Pareto traffic model had between -5% and 36% superior BER performance than the CBR traffic model. As a comparison, in the non-time dispersive propagation environment scenario evaluated in Chapter 6 the Pareto traffic model had between 1–54% superior BER performance than the CBR traffic model.

Two BTS deployment configurations were considered and it was shown that in addition to impacting the absolute system performance level the BTS configuration also impacts the level of performance difference between different traffic types. Hence, the choice of BTS configuration during system design impacts how the system will perform with different types of traffic. Both QPSK and 16QAM modulation schemes were considered and the choice of modulation scheme was also shown to impact the level of performance difference between different traffic types.

Chapter 8

Downlink Performance Sensitivity to Traffic Type

8.1 Introduction

Chapters 6 and 7 identified scenarios where the downlink performance of both outdoor and indoor DS-CDMA cellular systems is sensitive to the statistical properties of the user traffic. The approach taken in those chapters was to evaluate system performance with two statistically dissimilar traffic models in order to obtain a measure of performance sensitivity to traffic type. Both the indoor and outdoor systems considered exhibited varying levels of performance sensitivity. The outdoor system scenarios that were identified as sensitive to traffic type are investigated in further detail in this chapter with a wider variety of traffic types. The indoor system scenarios that were identified as sensitive to traffic type are not investigated as the same basic trends were observed for both outdoor and indoor systems.

The four traffic models considered in this chapter are presented in Section 8.2 and the impact of their diverse statistical properties on the BTS transmitter power distribution and system scheduling performance is evaluated. The relationship between the system's traffic scheduling policy, scheduling performance, and propagation dependent performance is also discussed. The downlink performance of the outdoor macro-cellular system considered in Chapter 6 is evaluated in Sections 8.3 and 8.4 with the four proposed traffic models. Section 8.3 considers a non-time dispersive propagation environment while Section 8.4 considers a time dispersive propagation environment and receiver diversity.

8.2 Traffic Statistical Properties

The traffic models considered in this chapter are:

- the CBR model
- the Poisson model
- the negative binomial model
- the Pareto model

and these are described in Section 4.4 and represent individual MT traffic streams offered to the BTS. The CBR and Pareto ($H = 0.8$) traffic models were evaluated in Chapters 6 and 7 and the other proposed traffic models offer a greater variety of traffic types for evaluation. The CBR and Poisson models have one degree of freedom which can be used to control the mean MT traffic load. The negative binomial and Pareto models have two degrees of freedom which can be used to control both the mean MT traffic load and traffic stream variability.

Six specific traffic models are focused on in this chapter, namely, CBR, Poisson, negative binomial ($\sigma_X^2 = 1.5$), Pareto ($H = 0.6$), negative binomial ($\sigma_X^2 = 2.1$), and Pareto ($H = 0.8$) traffic models. The Pareto ($H = 0.8$) model was considered in Chapters 6 and 7 and a value of $H = 0.8$ was selected as this has been measured for traffic streams in deployed systems (see Section 4.4.4). The parameter values selected for the negative binomial ($\sigma_X^2 = 1.5$), Pareto ($H = 0.6$), and negative binomial ($\sigma_X^2 = 2.1$) models were chosen so that the resultant traffic streams had a range of variabilities between the extremes of the CBR and Pareto ($H = 0.8$) models and this is evident in Figure 8.2.

It is assumed that the BTS allocates the same transmission power to each spreading code and therefore the momentary BTS transmitter power is proportional to the number of spreading codes (i.e. packets) transmitted in a frame. Figure 8.1 shows the BTS transmitter power probability density function with m MT's per BTS and the proposed traffic models. It is assumed that each MT offers 1 Erlang of traffic and that the BTS limits the maximum number of spreading codes transmitted per frame to 16[1]. Note that the discontinuity in Figure 8.1(d) with $m = 8$ and a normalised transmitter power of 16 is due to the non-negligible probability that more than 16 packets are offered in a frame and the fact that the BTS limits the maximum number of spreading codes transmitted in a frame to 16.

The shape of the BTS transmitter power probability density function obviously depends on the statistical properties of the aggregate transmitted traffic stream and this is inherently linked to the statistical properties of the individual MT traffic streams. The probability

[1] An Erlang of traffic is defined in Section 5.3 and is equal to a mean traffic load of one packet per frame.

density function with the CBR traffic model is simply a delta function as the number of spreading codes transmitted in each frame is constant. As the number of MT's per BTS increases the central limit theorem comes into effect and the probability density function becomes more Gaussian.

Figures 8.2 and 8.3 show the BTS transmitter power variance with the proposed traffic models. The BTS transmitter power with the CBR traffic model inherently has zero variance.

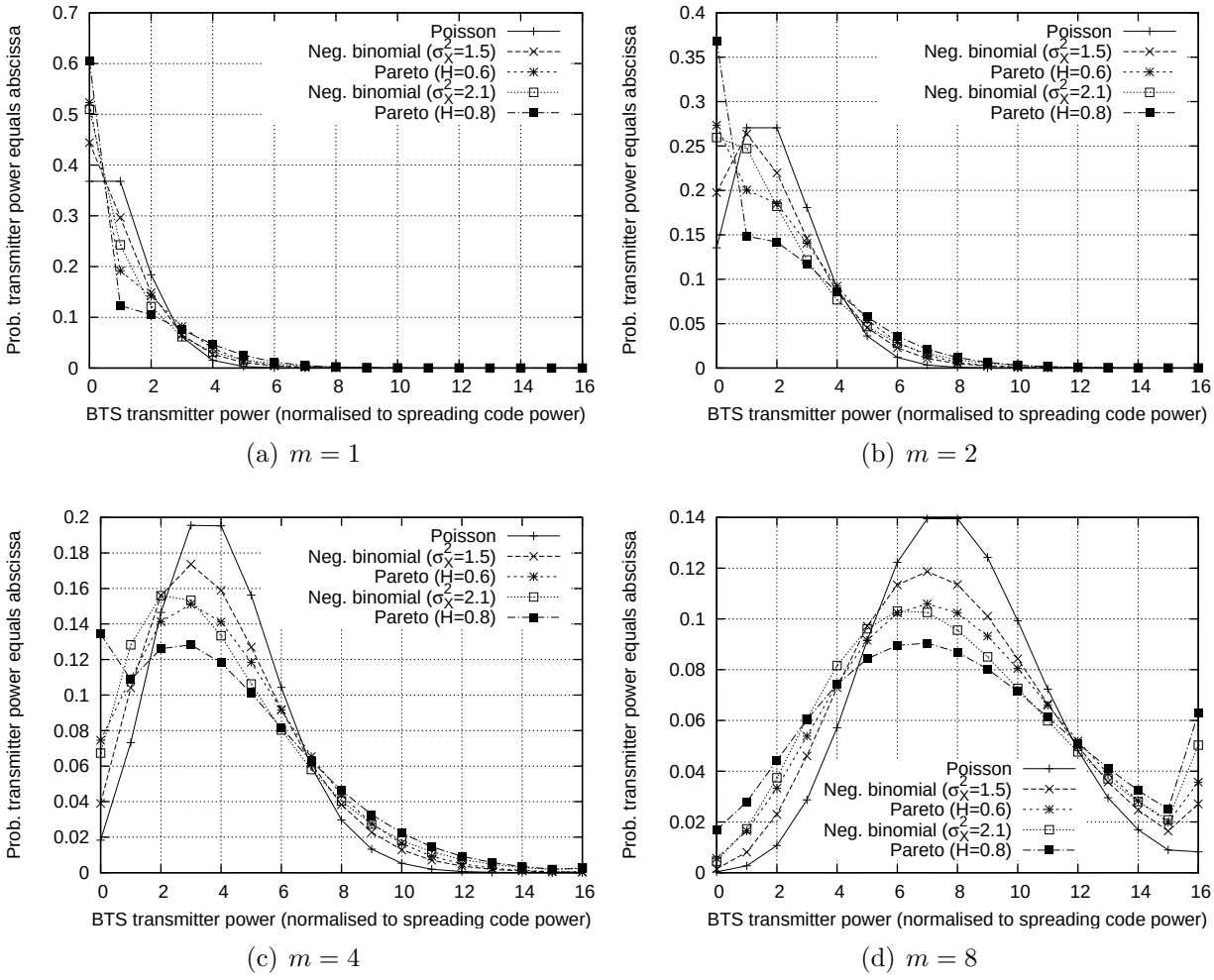

(a) $m = 1$ (b) $m = 2$

(c) $m = 4$ (d) $m = 8$

Figure 8.1: BTS transmitter power probability density function with m MT's per BTS and Poisson, negative binomial, and Pareto traffic models. Each MT offers 1 Erlang of traffic and the BTS limits the maximum number of codes transmitted per frame to 16 and drops any excess offered packets.

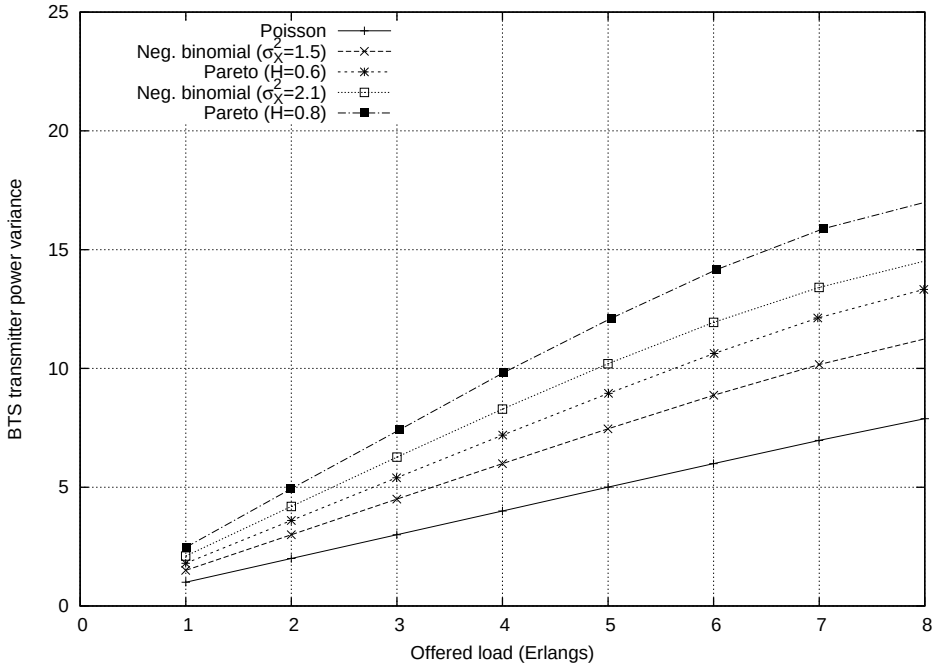

Figure 8.2: BTS transmitter power variance with Poisson, negative binomial, and Pareto traffic models. Each MT offers 1 Erlang of traffic and the BTS limits the maximum number of codes transmitted per frame to 16 and drops any excess offered packets. (BTS transmitter power is normalised to the spreading code power.)

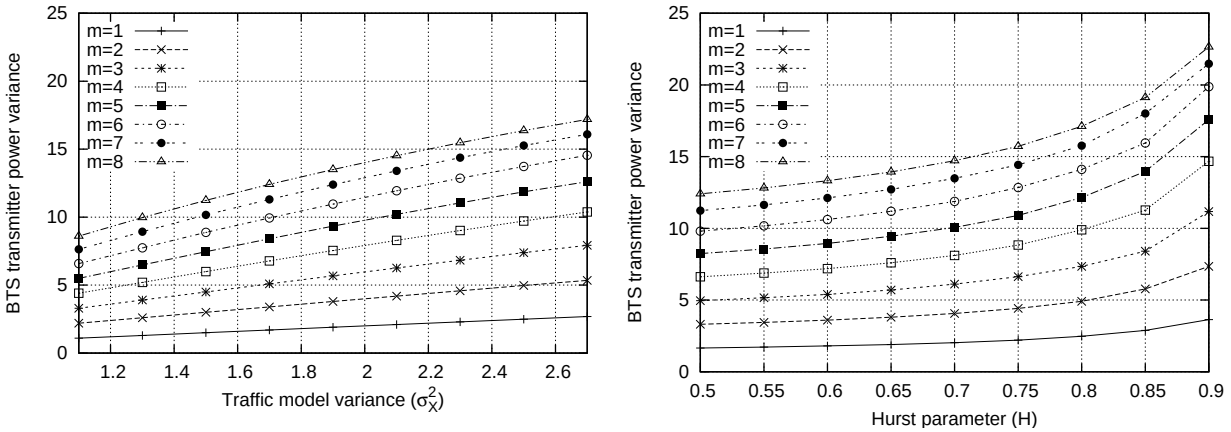

(a) negative binomial (b) Pareto

Figure 8.3: BTS transmitter power variance with negative binomial and Pareto traffic models. Each MT offers 1 Erlang of traffic and the BTS limits the maximum number of codes transmitted per frame to 16 and drops any excess offered packets. (BTS transmitter power is normalised to the spreading code power.)

8.2.1 Scheduling Performance

The system traffic scheduling policy impacts the statistical properties of the aggregate transmitted traffic stream and this in turn impacts the BTS transmitter power distribution and the system's propagation dependent performance. The traffic scheduling policy determines the number of packets transmitted in each frame and there is a trade off between scheduling performance and propagation dependent performance. If the scheduling policy reduces the maximum number of spreading codes that can transmitted in a frame then this reduces the interference on the propagation channel, which improves propagation dependent performance, but comes at the cost of either increased packet scheduling delay or increased packet dropping, which degrades scheduling performance.

The traffic scheduling policy used in Chapters 6 and 7 is also used in this chapter and a zero packet scheduling delay tolerance is assumed. Figures 8.4 and 8.5 show the probability that the BTS drops an offered packet with the proposed traffic models when the BTS limits the maximum number of spreading codes transmitted per frame to 16, which is the scenario considered throughout this chapter. No packet dropping occurs with the CBR traffic model if the number of MT's per BTS is less than or equal to the number of available spreading codes. The significance of the level of packet dropping needs to be considered in conjunction with the level of packet loss due to propagation as both of these sources determine overall packet loss.

Chapter 9 considers a number of different scheduling policies that deliberately alter the statistical properties of the aggregate transmitted traffic stream, which is also known as traffic shaping.

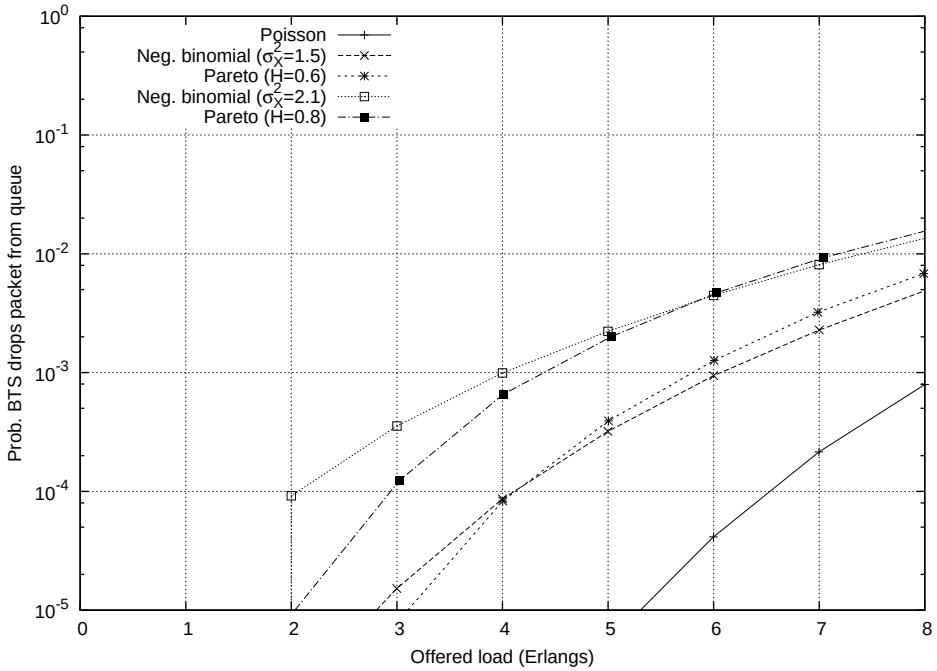

Figure 8.4: Probability the BTS drops an offered packet with Poisson, negative binomial, and Pareto traffic models. Each MT offers 1 Erlang of traffic and all packets have zero scheduling delay tolerance. The BTS transmits a maximum of 16 spreading codes per frame.

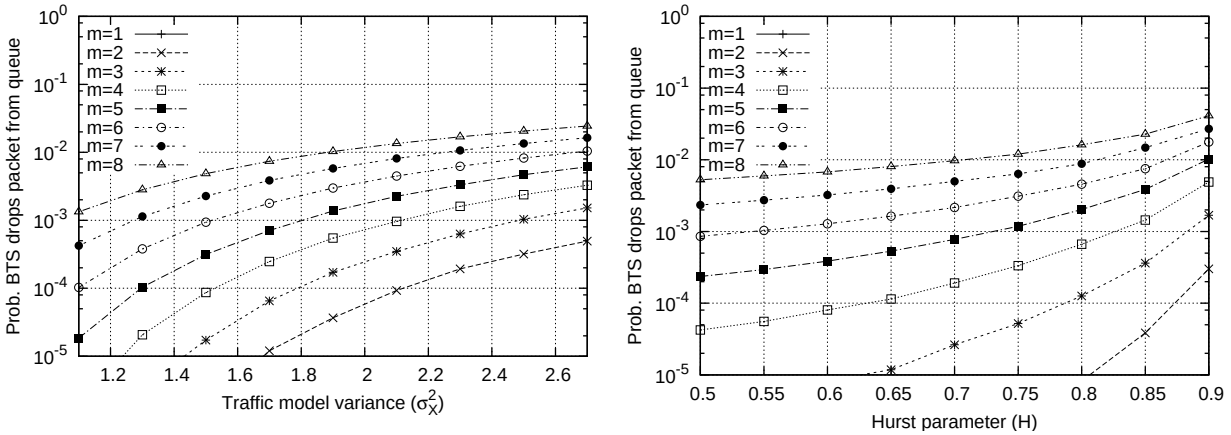

(a) negative binomial (b) Pareto

Figure 8.5: Probability the BTS drops an offered packet with negative binomial and Pareto traffic models. Each MT offers 1 Erlang of traffic and all packets have zero scheduling delay tolerance. The BTS transmits a maximum of 16 spreading codes per frame.

8.3 An Outdoor Non-Time Dispersive Suzuki Propagation Environment

This section evaluates the downlink performance of the same outdoor macro-cellular system evaluated in Chapter 6 but with the traffic models proposed in Section 8.2. A non-time dispersive propagation channel, large-scale path loss exponent of $n = 4$, and lognormal shadowing variability of $\sigma = 8\,\text{dB}$ are assumed[2]. Section 8.4 considers a time dispersive propagation channel and receiver diversity.

BTS's with omni-directional antennas are located on a regular hexagonal grid and the only significant inter-cell interference is assumed to emanate from the 6 immediately adjacent co-channel cells. OVSF spreading codes are used exclusively and their orthogonal nature, in conjunction with the non-time dispersive propagation channel, means that no intra-cell interference occurs i.e. only inter-cell interference. BTS's use a fixed spreading factor of 16 and allocate the same transmission power to each spreading code. Packets are assumed to have zero scheduling delay tolerance and each BTS limits the maximum number of codes transmitted per frame to the value of the spreading factor i.e. 16 (excess packets are dropped). Only a spreading factor of 16 is considered in this chapter as similar trends were observed with both spreading factors of 16 and 64 in Chapters 6 and 7.

Unless stated otherwise, MT's move randomly within their own cell and all potential cell locations are equally likely. MT's connect to the BTS from which they receive the highest mean signal power and the MT mobility model ensures that no cell handovers occur. Each MT offers 1 Erlang of traffic and uses a spreading factor of 16. A QPSK modulation scheme and system chip rate of 3.84 Mcps is assumed and this translates into a radio bearer bitrate of 480 kbps per code.

8.3.1 Random MT Location Within Own Cell

Figures 8.6–8.10 and Table 8.1 show system downlink performance when all MT's move randomly within their own cell and there are m MT's per cell. The results for the CBR and Pareto ($H = 0.8$) traffic models are identical to those presented in Section 6.3.1. The most striking result is that with a fixed traffic load, the BTS transmitter power variance provides a good indication of the level of propagation dependent performance, independent of the specific traffic model. This is evident in Table 8.1 where there is an approximately linear relationship between the BTS transmitter power variance and BER (with a fixed number of MT's per cell).

[2]Full details of the system model and propagation model can be found in Chapter 5.

The observations made in Section 6.3.1 with the CBR and Pareto ($H = 0.8$) traffic models also apply to the additional traffic models considered in this chapter. As discussed in Chapter 6, the BER performance difference between the traffic models depends on the level of non-linearity in the BER vs. SIR curve and how the receiver SIR distribution associated with each traffic model weights the various points on the curve. As the number of MT's increases the central limit theorem comes into effect and the aggregate offered traffic stream statistically becomes more Gaussian and the variability of the traffic stream reduces relative to the mean. This reduces the performance difference between the traffic models as the receiver SIR distributions associated with the traffic models statistically become more similar.

No. MT's	Traffic model	BTS transmitter power variance	Prob. of bit error (BER)	BER % diff. relative to CBR
$m = 1$	CBR	0.00	0.047466	
	Poisson	1.00	0.040503	-14.7%
	Neg. binomial ($\sigma_X^2 = 1.5$)	1.50	0.038440	-19.0%
	Pareto ($H = 0.6$)	1.80	0.036593	-22.9%
	Neg. binomial ($\sigma_X^2 = 2.1$)	2.10	0.036517	-23.1%
	Pareto ($H = 0.8$)	2.48	0.033996	-28.4%
$m = 4$	CBR	0.00	0.090013	
	Poisson	4.00	0.087460	-2.8%
	Neg. binomial ($\sigma_X^2 = 1.5$)	5.99	0.086235	-4.2%
	Pareto ($H = 0.6$)	7.19	0.085023	-5.5%
	Neg. binomial ($\sigma_X^2 = 2.1$)	8.29	0.084742	-5.9%
	Pareto ($H = 0.8$)	9.82	0.083398	-7.3%
$m = 8$	CBR	0.00	0.117958	
	Poisson	7.88	0.116435	-1.3%
	Neg. binomial ($\sigma_X^2 = 1.5$)	11.24	0.115645	-2.0%
	Pareto ($H = 0.6$)	13.32	0.115057	-2.5%
	Neg. binomial ($\sigma_X^2 = 2.1$)	14.52	0.114500	-2.9%
	Pareto ($H = 0.8$)	17.11	0.113678	-3.6%

Table 8.1: Comparison of the BER with CBR, Poisson, negative binomial, and Pareto traffic models. MT's move randomly within their own cell and use a fixed spreading factor of 16. (BTS transmitter power is normalised to the spreading code power.)

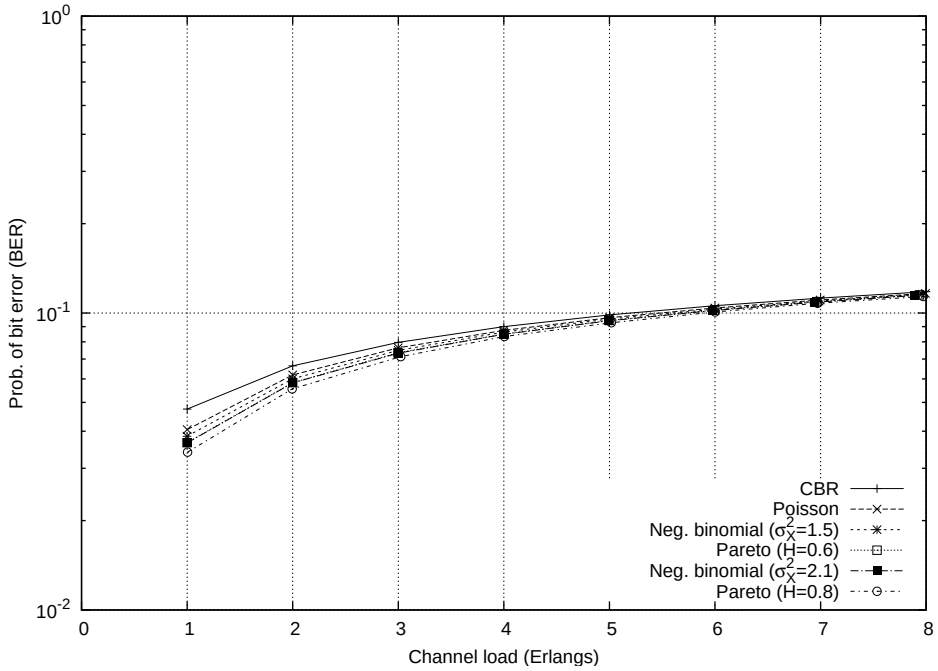

Figure 8.6: BER with CBR, Poisson, negative binomial, and Pareto traffic models. MT's move randomly within their own cell and use a fixed spreading factor of 16.

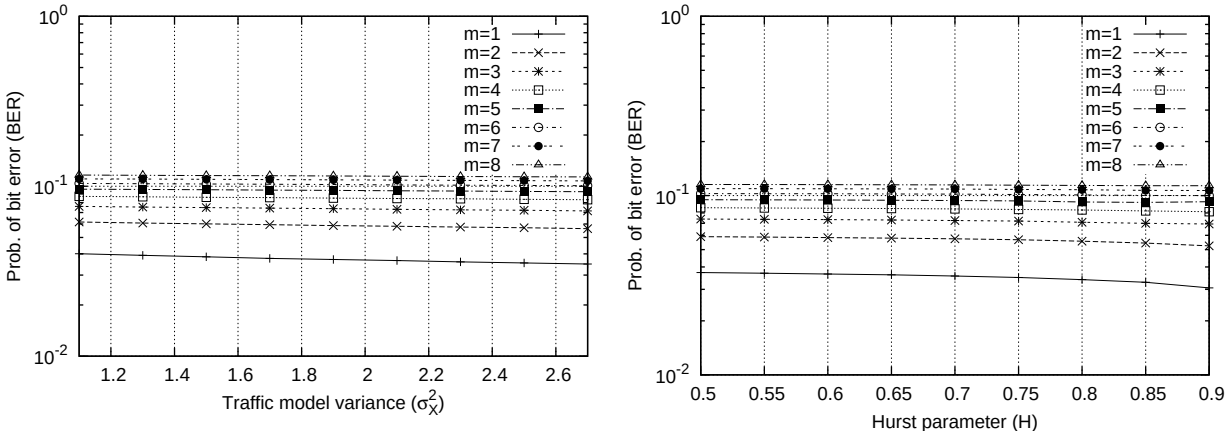

(a) negative binomial (b) Pareto

Figure 8.7: BER with negative binomial and Pareto traffic models (m MT's per cell). MT's move randomly within their own cell and use a fixed spreading factor of 16.

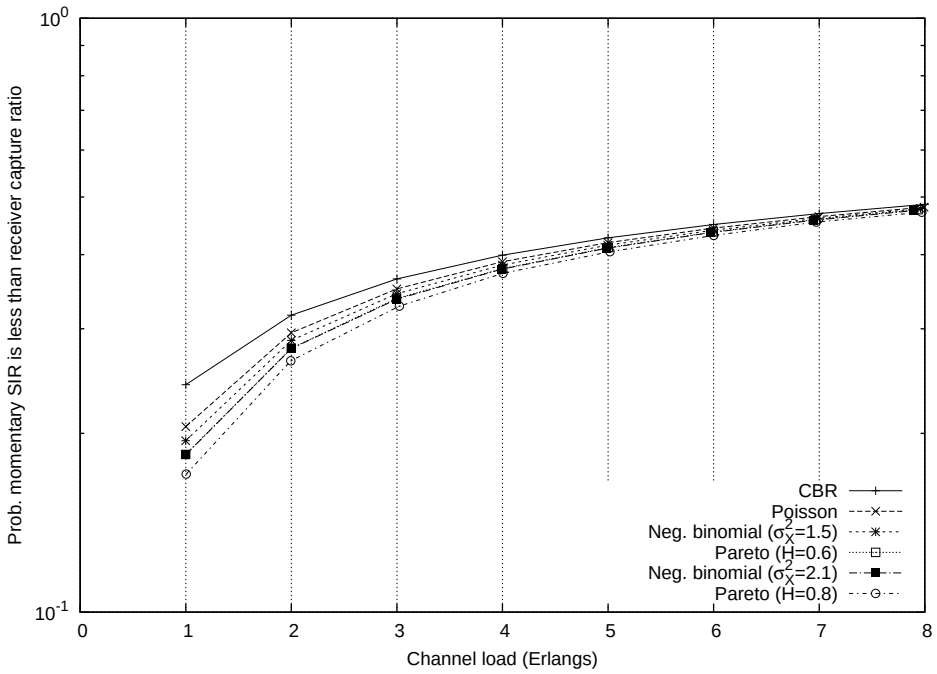

Figure 8.8: Probability the momentary SIR at the receiver is less than a 6 dB receiver capture ratio with CBR, Poisson, negative binomial, and Pareto traffic models. MT's move randomly within their own cell and use a fixed spreading factor of 16.

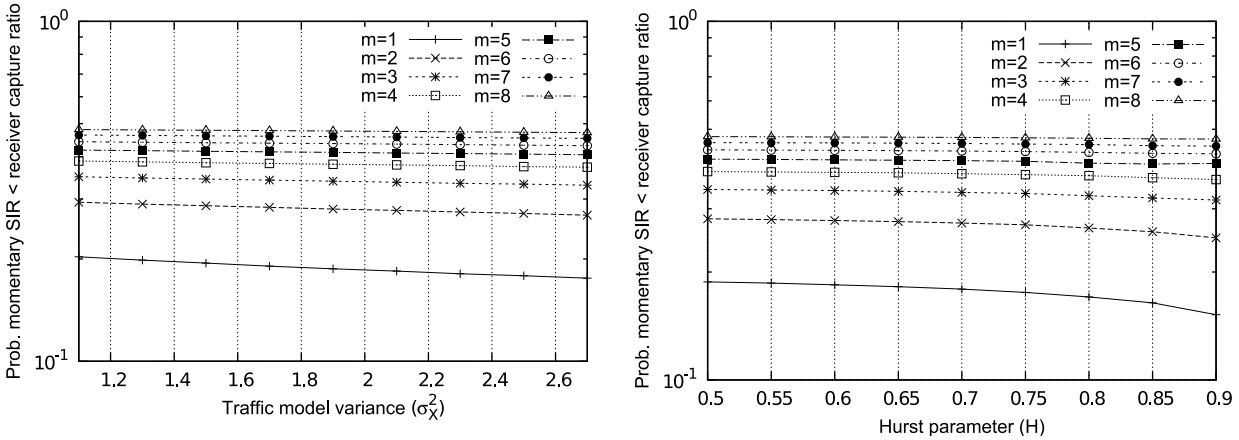

(a) negative binomial (b) Pareto

Figure 8.9: Probability the momentary SIR at the receiver is less than a 6 dB receiver capture ratio with negative binomial and Pareto traffic models (m MT's per cell). MT's move randomly within their own cell and use a fixed spreading factor of 16.

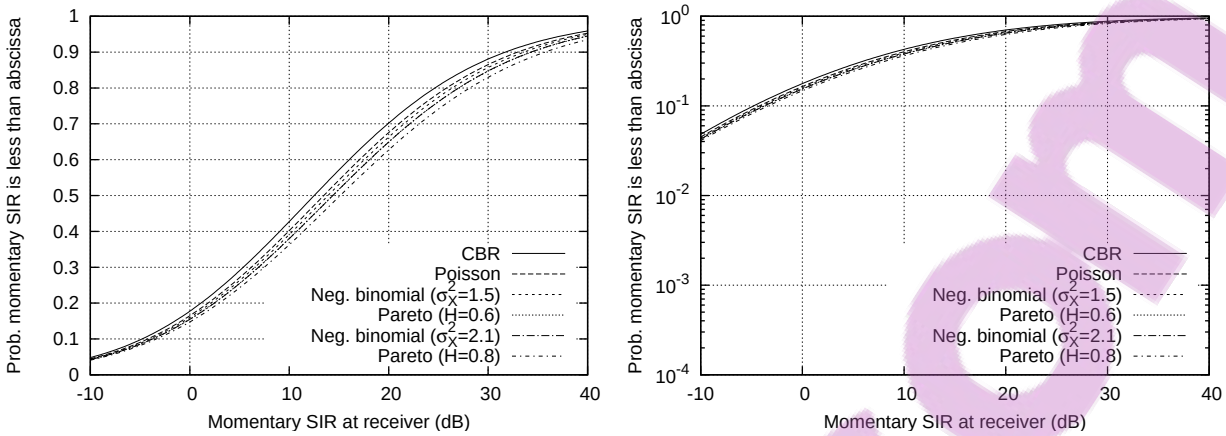

(a) linear scale (b) logarithmic scale

Figure 8.10: Cumulative distribution function of the momentary SIR at the receiver with CBR, Poisson, negative binomial, and Pareto traffic models. Each cell contains 2 MT's which move randomly within their own cell and use a fixed spreading factor of 16.

8.3.2 Fixed MT Location Near the Cell Centre

Figures 8.11–8.15 and Table 8.2 show system downlink performance for a stationary MT located 0.2 radii from the cell centre. All other MT's move randomly within their own cell and there are m MT's per cell. This location is considered to be in a good coverage area with a relatively high mean desired signal power and only 5% of the total cell coverage area will receive a higher mean desired signal power. The results for the CBR and Pareto ($H = 0.8$) traffic models are identical to those presented in Section 6.3.2.

As was the case in the previous section, with a fixed traffic load the BTS transmitter power variance provides a good indication of the level of propagation dependent performance, independent of the specific traffic model. This is evident in Table 8.2 where there is an approximately linear relationship between the BTS transmitter power variance and BER (with a fixed number of MT's per cell). The observations made in Section 6.3.2 with the CBR and Pareto ($H = 0.8$) traffic models also apply to the additional traffic models considered in this chapter, with the most important observation being that traffic type has minimal impact on propagation dependent performance when the mean SIR at the receiver is relatively high.

It should be noted that in Table 8.2 when $m = 1$, the negative binomial ($\sigma_X^2 = 2.1$) model has slightly superior BER performance than the Pareto ($H = 0.8$) model even though the negative binomial ($\sigma_X^2 = 2.1$) model has a lower BTS transmitter power variance. This is because the relationship between BTS transmitter power variance and BER performance is only approximately linear and the actual BER depends on the specific receiver SIR distribution and BER vs. SIR curve.

No. MT's	Traffic model	BTS transmitter power variance	Prob. of bit error (BER)	BER % diff. relative to CBR
$m = 1$	CBR	0.00	0.000889	
	Poisson	1.00	0.000854	-4.0%
	Neg. binomial ($\sigma_X^2 = 1.5$)	1.50	0.000840	-5.5%
	Pareto ($H = 0.6$)	1.80	0.000831	-6.6%
	Neg. binomial ($\sigma_X^2 = 2.1$)	2.10	0.000817	-8.1%
	Pareto ($H = 0.8$)	2.48	0.000822	-7.6%
$m = 4$	CBR	0.00	0.003043	
	Poisson	4.00	0.002978	-2.1%
	Neg. binomial ($\sigma_X^2 = 1.5$)	5.99	0.002970	-2.4%
	Pareto ($H = 0.6$)	7.19	0.002958	-2.8%
	Neg. binomial ($\sigma_X^2 = 2.1$)	8.29	0.002938	-3.5%
	Pareto ($H = 0.8$)	9.82	0.002919	-4.1%
$m = 8$	CBR	0.00	0.005421	
	Poisson	7.88	0.005361	-1.1%
	Neg. binomial ($\sigma_X^2 = 1.5$)	11.24	0.005346	-1.4%
	Pareto ($H = 0.6$)	13.32	0.005287	-2.5%
	Neg. binomial ($\sigma_X^2 = 2.1$)	14.52	0.005262	-2.9%
	Pareto ($H = 0.8$)	17.11	0.005241	-3.3%

Table 8.2: Comparison of the BER for a stationary MT located 0.2 radii from the cell centre with CBR, Poisson, negative binomial, and Pareto traffic models. All MT's use a fixed spreading factor of 16. (BTS transmitter power is normalised to the spreading code power.)

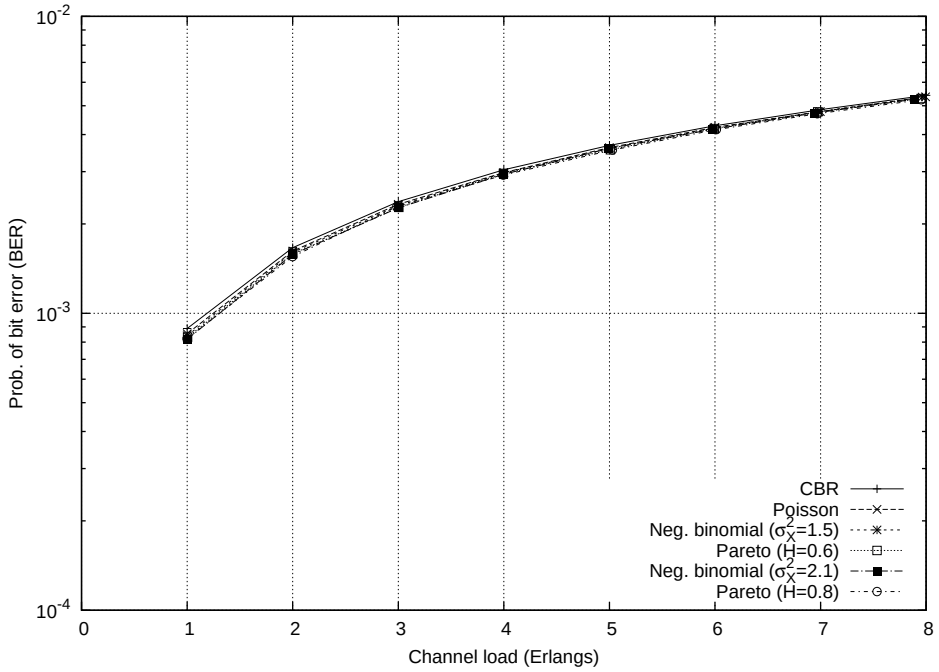

Figure 8.11: BER for a stationary MT located 0.2 radii from the cell centre with CBR, Poisson, negative binomial, and Pareto traffic models. All MT's use a fixed spreading factor of 16.

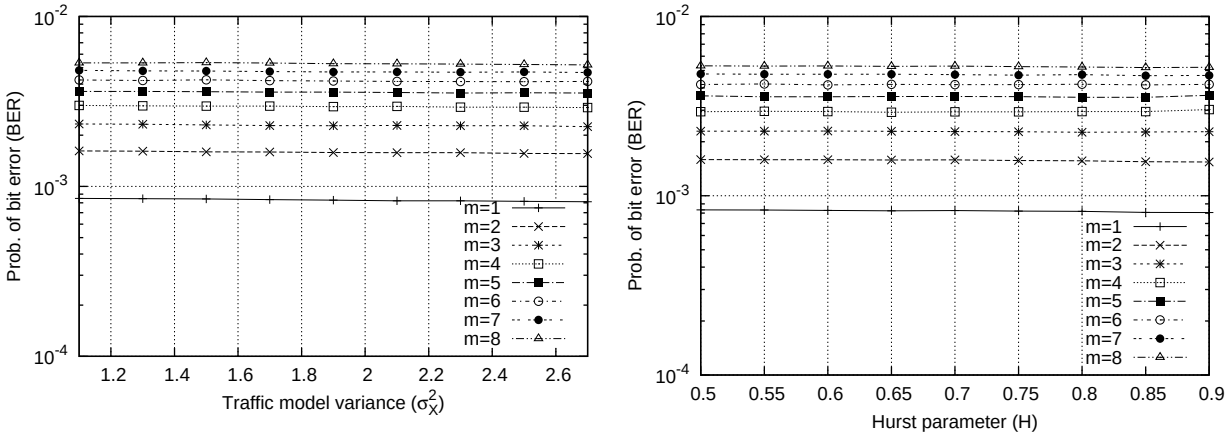

(a) negative binomial (b) Pareto

Figure 8.12: BER for a stationary MT located 0.2 radii from the cell centre with negative binomial and Pareto traffic models (m MT's per cell). All MT's use a fixed spreading factor of 16.

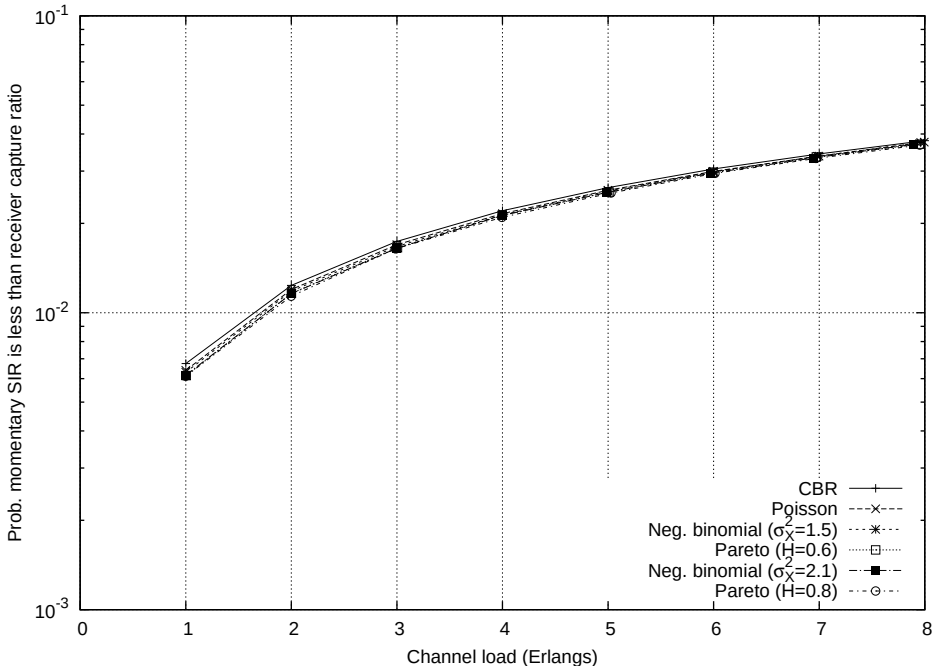

Figure 8.13: Probability the momentary SIR at the receiver is less than a 6 dB receiver capture ratio for a stationary MT located 0.2 radii from the cell centre with CBR, Poisson, negative binomial, and Pareto traffic models. All MT's use a fixed spreading factor of 16.

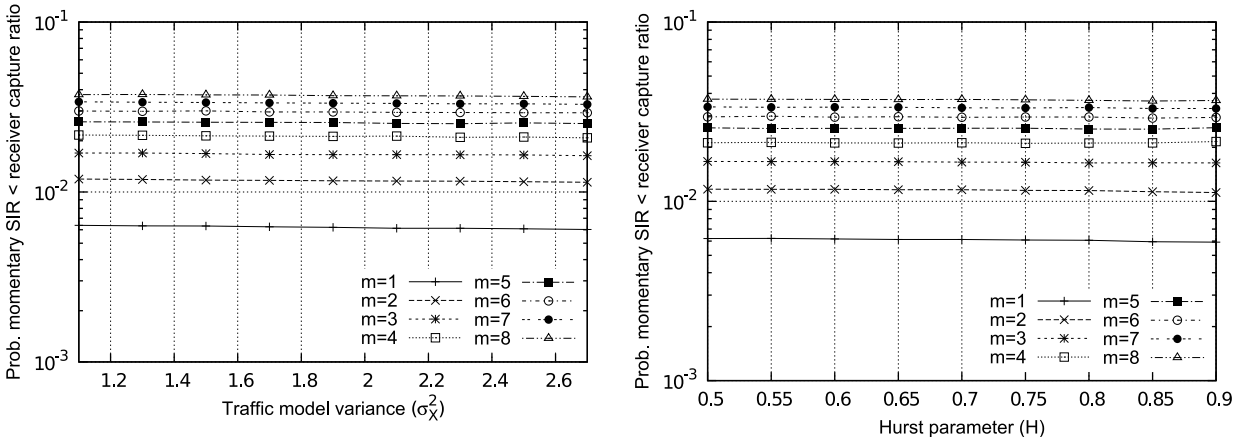

(a) negative binomial

(b) Pareto

Figure 8.14: Probability the momentary SIR at the receiver is less than a 6 dB receiver capture ratio for a stationary MT located 0.2 radii from the cell centre with negative binomial and Pareto traffic models (m MT's per cell). All MT's use a fixed spreading factor of 16.

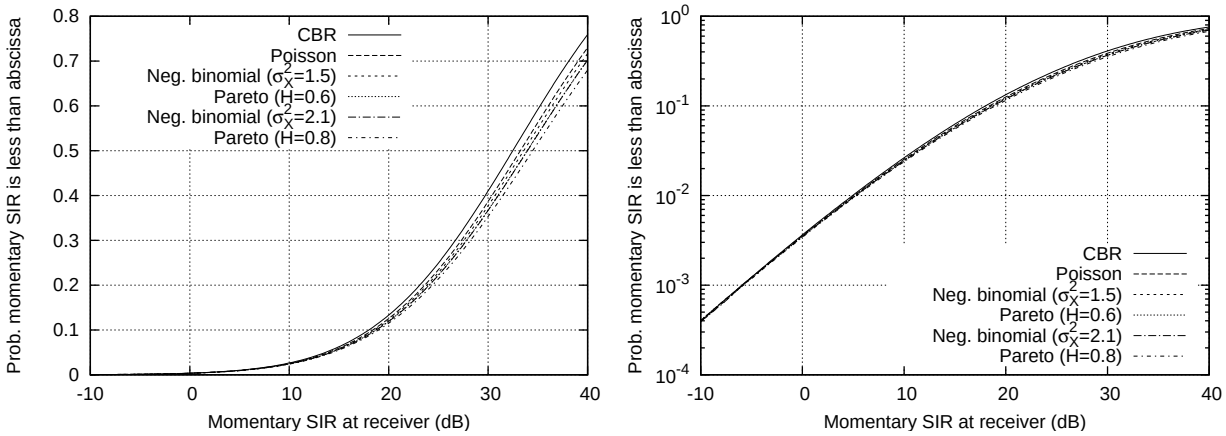

(a) linear scale (b) logarithmic scale

Figure 8.15: Cumulative distribution function of the momentary SIR at the receiver for a stationary MT located 0.2 radii from the cell centre with CBR, Poisson, negative binomial, and Pareto traffic models. Each cell contains 2 MT's and all MT's use a fixed spreading factor of 16.

8.4 An Outdoor Time Dispersive Suzuki Propagation Environment

This section evaluates the downlink performance of the same outdoor macro-cellular system evaluated in Chapter 6 but with the traffic models proposed in Section 8.2. Compared to the previous section, a time dispersive propagation channel and receiver diversity are considered while all other parameters are identical. A perfect RAKE receiver and two receiver antennas are assumed and maximal ratio combining is used for both receiver diversity techniques i.e. the SIR at the receiver output is the sum of the SIR's on each RAKE finger on both antennas (see Section 5.7)[3]. Propagation channel delay profile 1 listed in Table 6.5 is evaluated.

8.4.1 Random MT Location Within Own Cell

Figures 8.16–8.20 and Table 8.3 show system downlink performance when all MT's move randomly within their own cell and there are m MT's per cell. The results for the CBR and Pareto ($H = 0.8$) traffic models are identical to those presented in Section 6.4.1. When compared to the non-time dispersive propagation environment evaluated in Section 8.3 the absolute performance levels are superior due to the benefits of receiver diversity.

As was the case in the previous section, with a fixed traffic load the BTS transmitter power variance provides a good indication of the level of propagation dependent performance, inde-

[3]The RAKE receiver is assumed to have at least 3 fingers.

pendent of the specific traffic model. This is evident in Table 8.3 where there is an approximately linear relationship between the BTS transmitter power variance and BER (with a fixed number of MT's per cell). The observations made in Section 6.4.1 with the CBR and Pareto ($H = 0.8$) traffic models also apply to the additional traffic models considered in this chapter. At low to medium traffic loads the traffic type has a small to moderate impact on propagation dependent performance while at medium to high traffic loads the traffic type has minimal impact on propagation dependent performance.

No. MT's	Traffic model	BTS transmitter power variance	Prob. of bit error (BER)	BER % diff. relative to CBR
$m = 1$	CBR	0.00	0.009012	
	Poisson	1.00	0.007902	-12.3%
	Neg. binomial ($\sigma_X^2 = 1.5$)	1.50	0.007622	-15.4%
	Pareto ($H = 0.6$)	1.80	0.007353	-18.4%
	Neg. binomial ($\sigma_X^2 = 2.1$)	2.10	0.007384	-18.1%
	Pareto ($H = 0.8$)	2.48	0.007110	-21.1%
$m = 4$	CBR	0.00	0.027520	
	Poisson	4.00	0.027182	-1.2%
	Neg. binomial ($\sigma_X^2 = 1.5$)	5.99	0.027058	-1.7%
	Pareto ($H = 0.6$)	7.19	0.026768	-2.7%
	Neg. binomial ($\sigma_X^2 = 2.1$)	8.29	0.026926	-2.2%
	Pareto ($H = 0.8$)	9.82	0.026586	-3.4%
$m = 8$	CBR	0.00	0.045934	
	Poisson	7.88	0.046256	0.7%
	Neg. binomial ($\sigma_X^2 = 1.5$)	11.24	0.046281	0.8%
	Pareto ($H = 0.6$)	13.32	0.046230	0.6%
	Neg. binomial ($\sigma_X^2 = 2.1$)	14.52	0.046056	0.3%
	Pareto ($H = 0.8$)	17.11	0.045999	0.1%

Table 8.3: Comparison of the BER with CBR, Poisson, negative binomial, and Pareto traffic models. MT's move randomly within their own cell and use a fixed spreading factor of 16. (BTS transmitter power is normalised to the spreading code power.)

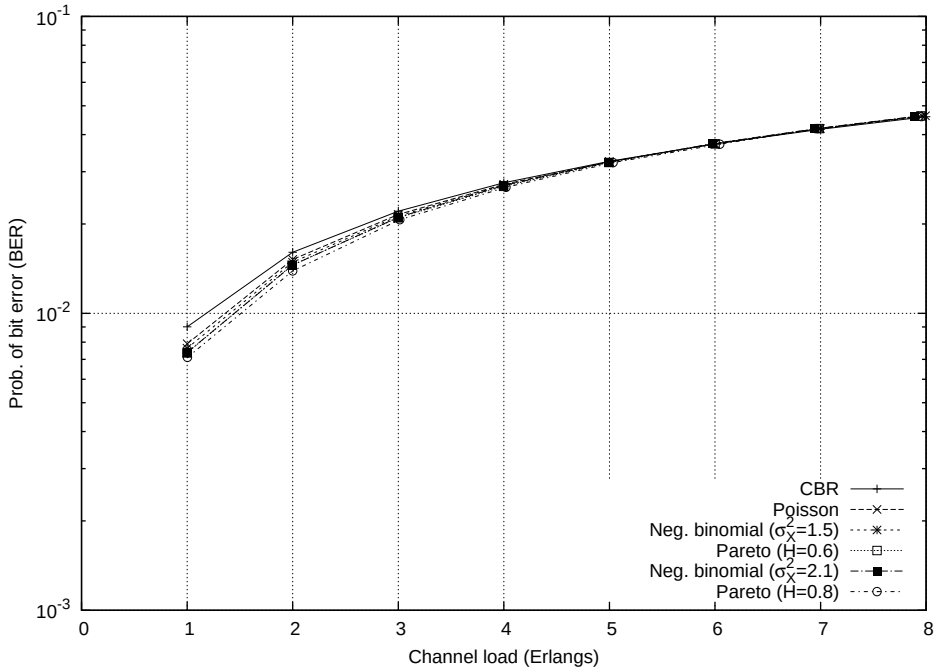

Figure 8.16: BER with CBR, Poisson, negative binomial, and Pareto traffic models. MT's move randomly within their own cell and use a fixed spreading factor of 16.

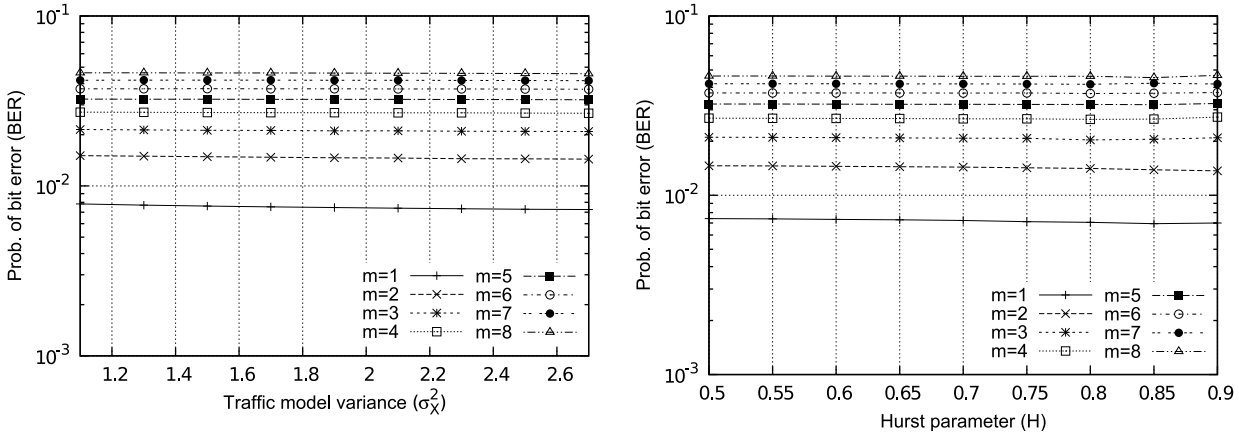

(a) negative binomial (b) Pareto

Figure 8.17: BER with negative binomial and Pareto traffic models (m MT's per cell). MT's move randomly within their own cell and use a fixed spreading factor of 16.

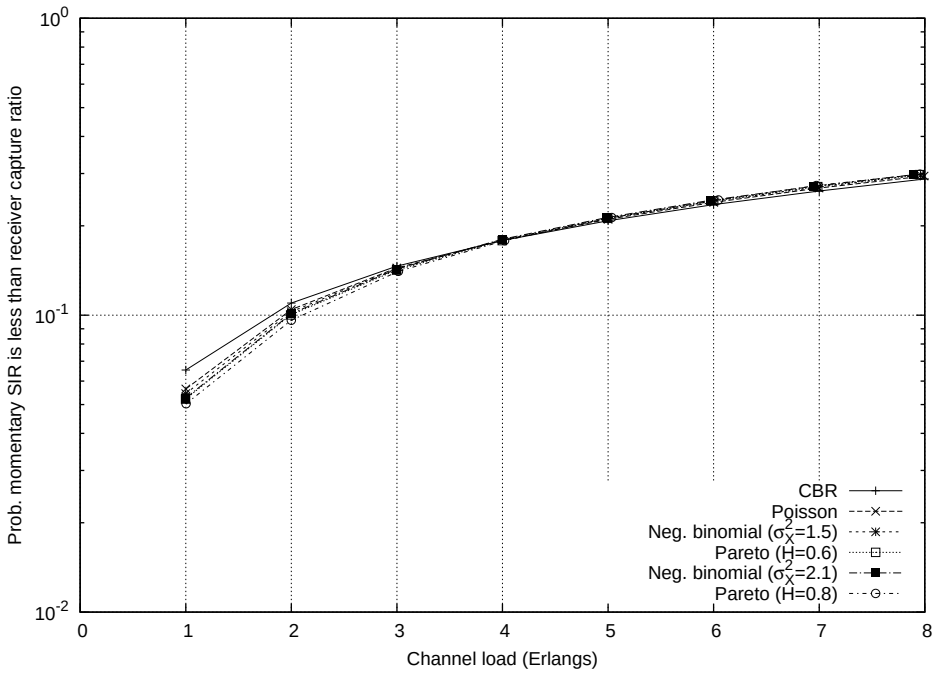

Figure 8.18: Probability the momentary SIR at the receiver is less than a 6 dB receiver capture ratio with CBR, Poisson, negative binomial, and Pareto traffic models. MT's move randomly within their own cell and use a fixed spreading factor of 16.

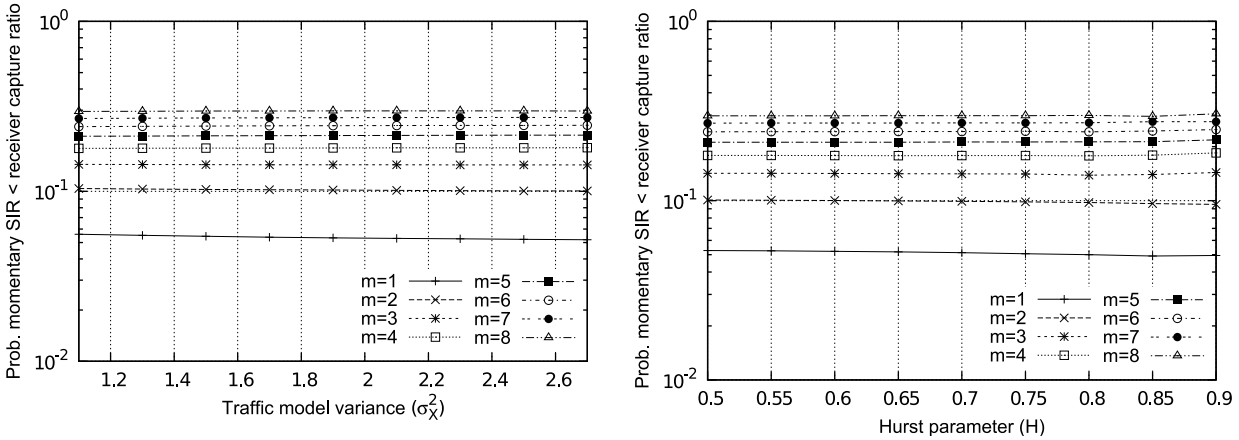

(a) negative binomial

(b) Pareto

Figure 8.19: Probability the momentary SIR at the receiver is less than a 6 dB receiver capture ratio with negative binomial and Pareto traffic models (m MT's per cell). MT's move randomly within their own cell and use a fixed spreading factor of 16.

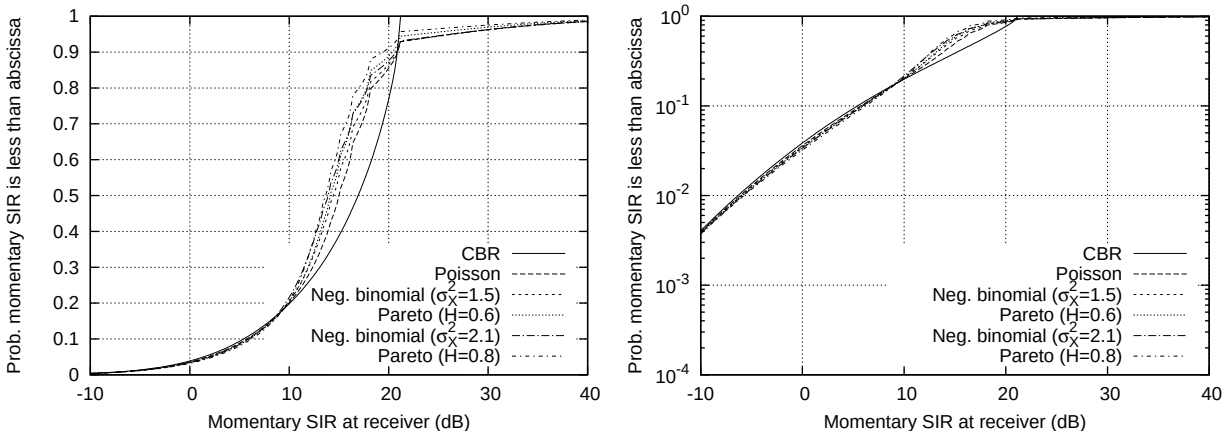

(a) linear scale (b) logarithmic scale

Figure 8.20: Cumulative distribution function of the momentary SIR at the receiver with CBR, Poisson, negative binomial, and Pareto traffic models. Each cell contains 2 MT's which move randomly within their own cell and use a fixed spreading factor of 16.

8.4.2 Fixed MT Location Near the Cell Centre

Figures 8.21–8.25 and Table 8.4 show system downlink performance for a stationary MT located 0.2 radii from the cell centre. All other MT's move randomly within their own cell and there are m MT's per cell. This location is considered to be in a good coverage area with a relatively high mean desired signal power and only 5% of the total cell coverage area will receive a higher mean desired signal power. The results for the CBR and Pareto ($H = 0.8$) traffic models are identical to those presented in Section 6.4.2.

As was the case in the previous sections, with a fixed traffic load the BTS transmitter power variance provides a good indication of the level of propagation dependent performance, independent of the specific traffic model. This is evident in Table 8.4 where there is an approximately linear relationship between the BTS transmitter power variance and BER (with a fixed number of MT's per cell). The observations made in Section 6.4.2 with the CBR and Pareto ($H = 0.8$) traffic models also apply to the additional traffic models considered in this chapter, with the most important observation being that in a time dispersive propagation environment where intra-cell interference is dominant, the correlated intra-cell interference phenomenon identified in Section 6.4.1 significantly degrades the propagation dependent performance of bursty traffic.

No. MT's	Traffic model	BTS transmitter power variance	Prob. of bit error (BER)	BER % diff. relative to CBR
$m = 1$	CBR	0.00	0.000005	
	Poisson	1.00	0.000008	45.1%
	Neg. binomial ($\sigma_X^2 = 1.5$)	1.50	0.000009	69.7%
	Pareto ($H = 0.6$)	1.80	0.000010	78.5%
	Neg. binomial ($\sigma_X^2 = 2.1$)	2.10	0.000015	178.0%
	Pareto ($H = 0.8$)	2.48	0.000011	108.1%
$m = 4$	CBR	0.00	0.000068	
	Poisson	4.00	0.000091	34.1%
	Neg. binomial ($\sigma_X^2 = 1.5$)	5.99	0.000122	79.3%
	Pareto ($H = 0.6$)	7.19	0.000134	96.5%
	Neg. binomial ($\sigma_X^2 = 2.1$)	8.29	0.000180	164.7%
	Pareto ($H = 0.8$)	9.82	0.000197	189.1%
$m = 8$	CBR	0.00	0.000321	
	Poisson	7.88	0.000563	75.6%
	Neg. binomial ($\sigma_X^2 = 1.5$)	11.24	0.000694	116.4%
	Pareto ($H = 0.6$)	13.32	0.000762	137.4%
	Neg. binomial ($\sigma_X^2 = 2.1$)	14.52	0.000819	155.2%
	Pareto ($H = 0.8$)	17.11	0.000916	185.5%

Table 8.4: Comparison of the BER for a stationary MT located 0.2 radii from the cell centre with CBR, Poisson, negative binomial, and Pareto traffic models. All MT's use a fixed spreading factor of 16. (BTS transmitter power is normalised to the spreading code power.)

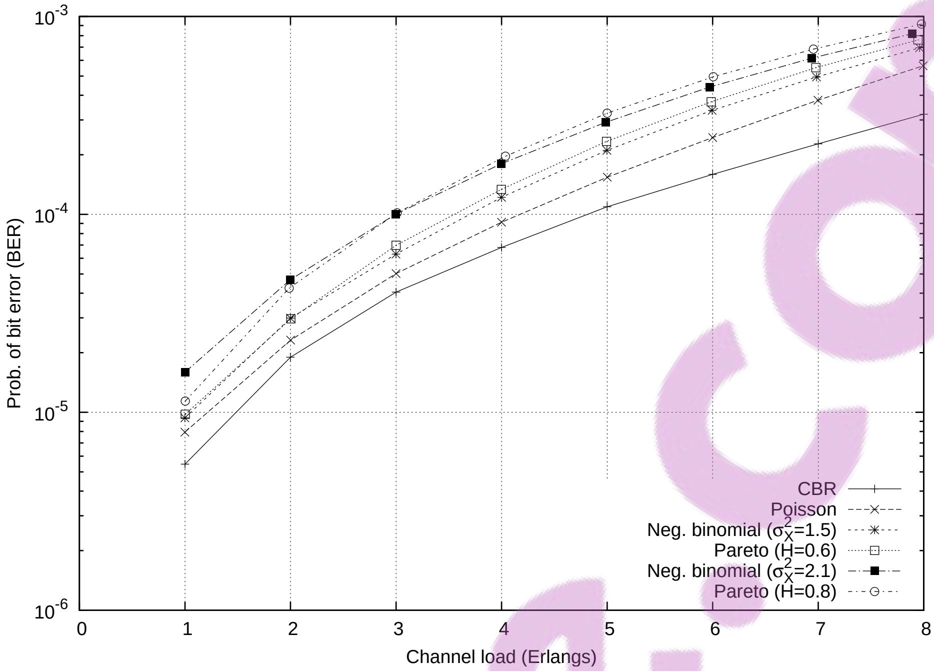

Figure 8.21: BER for a stationary MT located 0.2 radii from the cell centre with CBR, Poisson, negative binomial, and Pareto traffic models. All MT's use a fixed spreading factor of 16.

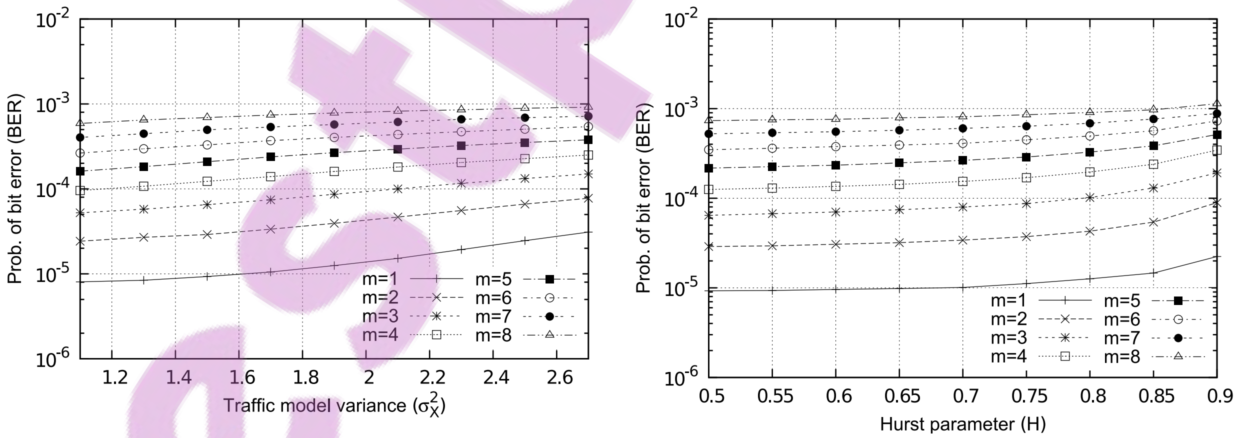

(a) negative binomial

(b) Pareto

Figure 8.22: BER for a stationary MT located 0.2 radii from the cell centre with negative binomial and Pareto traffic models (m MT's per cell). All MT's use a fixed spreading factor of 16.

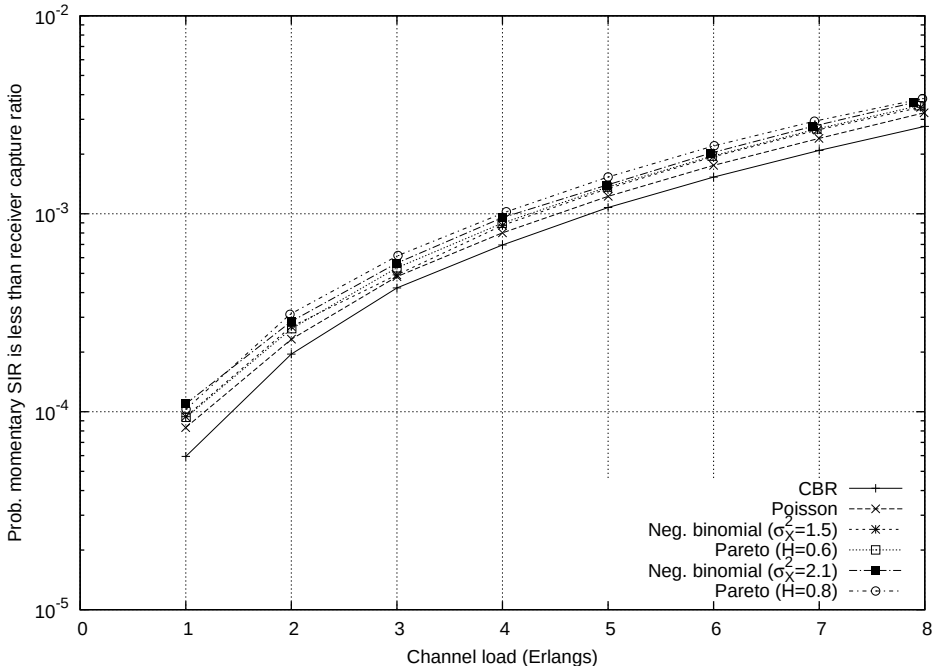

Figure 8.23: Probability the momentary SIR at the receiver is less than a 6 dB receiver capture ratio for a stationary MT located 0.2 radii from the cell centre with CBR, Poisson, negative binomial, and Pareto traffic models. All MT's use a fixed spreading factor of 16.

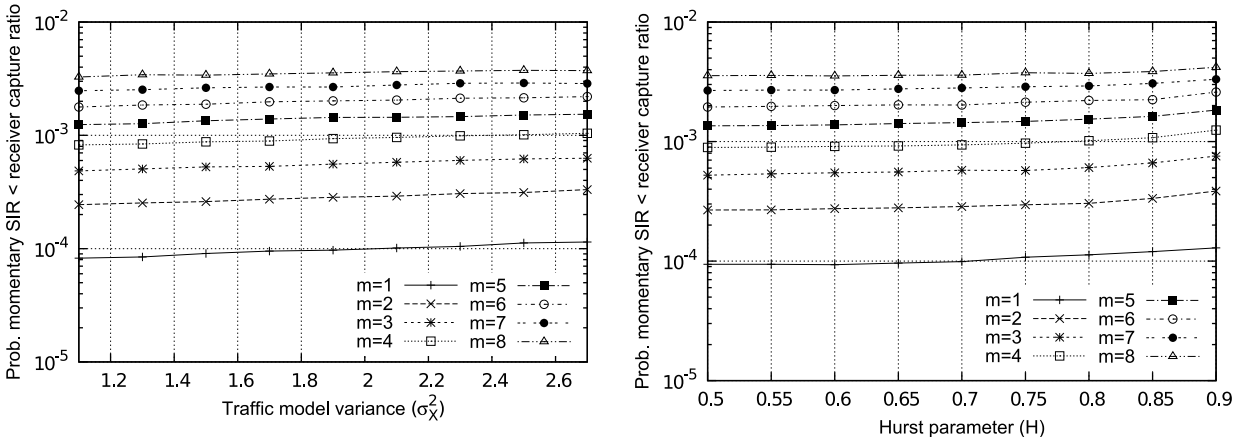

(a) negative binomial

(b) Pareto

Figure 8.24: Probability the momentary SIR at the receiver is less than a 6 dB receiver capture ratio for a stationary MT located 0.2 radii from the cell centre with negative binomial and Pareto traffic models (m MT's per cell). All MT's use a fixed spreading factor of 16.

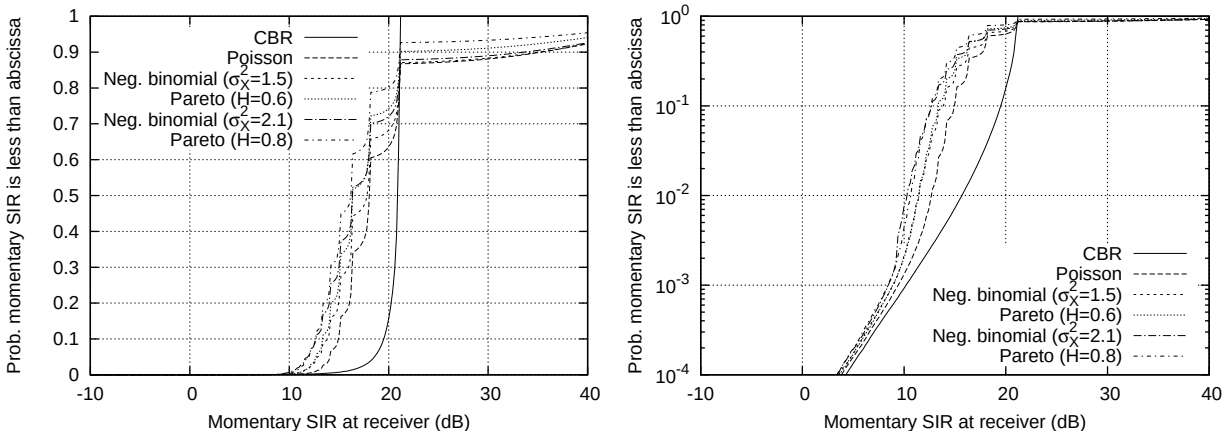

(a) linear scale (b) logarithmic scale

Figure 8.25: Cumulative distribution function of the momentary SIR at the receiver for a stationary MT located 0.2 radii from the cell centre with CBR, Poisson, negative binomial, and Pareto traffic models. Each cell contains 2 MT's and all MT's use a fixed spreading factor of 16.

8.5 Summary

The downlink performance of the outdoor macro-cellular system evaluated in Chapter 6 has been re-evaluated in this chapter with a wider variety of traffic models to access how specific traffic types impact system performance. The traffic models considered were a CBR model, a Poisson model, a negative binomial model, and a Pareto model.

The BTS transmitter power distribution and system scheduling performance were evaluated with the four proposed traffic models and the system's propagation dependent performance was then evaluated. The most striking result was that with a fixed traffic load, the BTS transmitter power variance provides a good indication of the level of propagation dependent performance, independent of the specific traffic model. Hence, if the propagation dependent performance of a system is known for at least a few traffic types then interpolation or extrapolation can be used to estimate propagation dependent performance with other traffic types. This also implies that a detailed traffic model may be unnecessary to estimate propagation dependent performance and knowledge of the BTS transmitter power mean and variance may be sufficient.

The general observations made in Chapter 6 with the CBR and Pareto ($H = 0.8$) traffic models were also shown to apply to the additional traffic models considered in this chapter.

Chapter 9

Traffic Shaping and Quality of Service

9.1 Introduction

Chapters 6–8 evaluated the downlink performance of DS-CDMA cellular systems which used a traffic scheduling policy that had minimal impact on the statistical properties of the transmitted traffic stream. Specifically, the scheduling policy limited the maximum number of spreading codes that could be transmitted in a frame, but a sufficiently high limit was selected to ensure that the statistical properties of the aggregate transmitted traffic stream were similar to the statistical properties of the aggregate offered traffic stream. This allowed the system's propagation dependent performance to be compared with a variety of traffic types without the traffic scheduling policy significantly influencing the results.

When selecting a traffic scheduling policy for a DS-CDMA cellular system there is a trade-off between scheduling performance and propagation dependent performance. Transmitting more spreading codes in a frame improves scheduling performance (i.e. a lower packet scheduling delay and reduced packet dropping) but comes at the cost of increased system interference and reduced propagation dependent performance.

A commonly used technique in telecommunication networks is to "shape" the carried traffic stream in order to reduce its variability [70, 71, 82]. To shape a traffic stream some packets must be delayed for transmission in a later frame and the level of shaping that can be achieved depends on the maximum tolerable scheduling delay and the user quality of service (QoS) requirements[1]. This chapter investigates the impact of traffic shaping on the performance of DS-CDMA cellular systems with different types of traffic.

A number of different traffic scheduling policies are presented in Section 9.2 and their impact on system scheduling performance is evaluated with a negative binomial ($\sigma_X^2 = 2.1$) traffic

[1]Packets can also be dropped to shape a traffic stream but obviously this is not desirable.

model. The downlink performance of the outdoor macro-cellular system considered in Chapters 6 and 8 is then evaluated in Section 9.3 with the proposed traffic scheduling policies and the CBR traffic model, negative binomial ($\sigma_X^2 = 2.1$) traffic model, and DAR traffic model which were presented in Section 4.4.

9.2 Traffic Scheduling Policies

In Chapters 6–8 it was assumed that the traffic scheduling policy limited the maximum number of spreading codes transmitted per frame to the value of the spreading factor used e.g. a maximum of 16 codes per frame with a spreading factor of 16. All user traffic was assumed to have zero scheduling delay tolerance ($D = 0$) and any excess packets offered to the BTS were dropped. In the scenarios that were considered, the level of packet dropping was insignificant and the statistical properties of the aggregate transmitted traffic stream were similar to the statistical properties of the aggregate offered traffic stream.

In this chapter, different limits on the maximum number of spreading codes that can be transmitted per frame and different packet scheduling delay tolerances are considered. A fixed spreading factor of 16 is assumed and limits of 16, 10, and 6 codes per frame are evaluated along with packet scheduling delay tolerances of 0, 1, and 2 frames. Figure 9.1 illustrates how different scheduling policies can shape the transmitted traffic stream and alter its statistical properties.

Table 9.1 shows both the probability that the BTS drops an offered packet and the BTS transmitter power variance with the negative binomial ($\sigma_X^2 = 2.1$) traffic model that was evaluated in Chapter 8 and the proposed traffic scheduling policies. Reducing the maximum number of codes that can be transmitted per frame reduces the variability of the transmitted traffic stream and this is reflected in Table 9.1 in the form of a reduced BTS transmitter power variance. The probability of packet dropping increases as the maximum number of spreading codes per frame is reduced and decreases as the scheduling delay tolerance is increased. In Table 9.1, the only scenarios where the level of packet dropping exceeds 2% is when there is a scheduling delay tolerance of 0 frames and either a maximum of 10 codes per frame ($m = 4, 8$) or 6 codes per frame ($m = 4$).

When the level of packet dropping is already small, increasing the scheduling delay tolerance has minimal impact on the statistical properties of the aggregate transmitted traffic stream and BTS transmitter power distribution as the number of packets affected by the change is relatively small. This is evident in Table 9.1 where in most cases there is a minimal change in the BTS transmitter power variance as the scheduling delay tolerance is increased.

Increasing the scheduling delay tolerance can either increase or decrease the BTS transmitter power variance, as shown in Table 9.1 when there is a maximum of 10 codes per frame and

$m = 4$ and $m = 8$. If the mean traffic load is relatively high compared to the maximum number of available codes per frame, then increasing the scheduling delay tolerance reduces the BTS transmitter power variance as packets that would have been dropped are now potentially transmitted in the next frame, where the number of packets transmitted will now tend to be closer to the mean. If the mean traffic load is relatively low compared to the maximum number of available codes per frame, then increasing the scheduling delay tolerance increases the BTS transmitter power variance as packets that would have been dropped are now potentially transmitted in the next frame, where the number of packets transmitted will now tend to be further away from the mean.

It should be noted that a higher level of packet dropping leads to a lower traffic load on the propagation channel, which reduces system interference and improves propagation dependent performance. The propagation dependent performance of the outdoor macro-cellular system considered in Chapters 6 and 8 is evaluated in the following section and needs to be considered in conjunction with the results in Table 9.1.

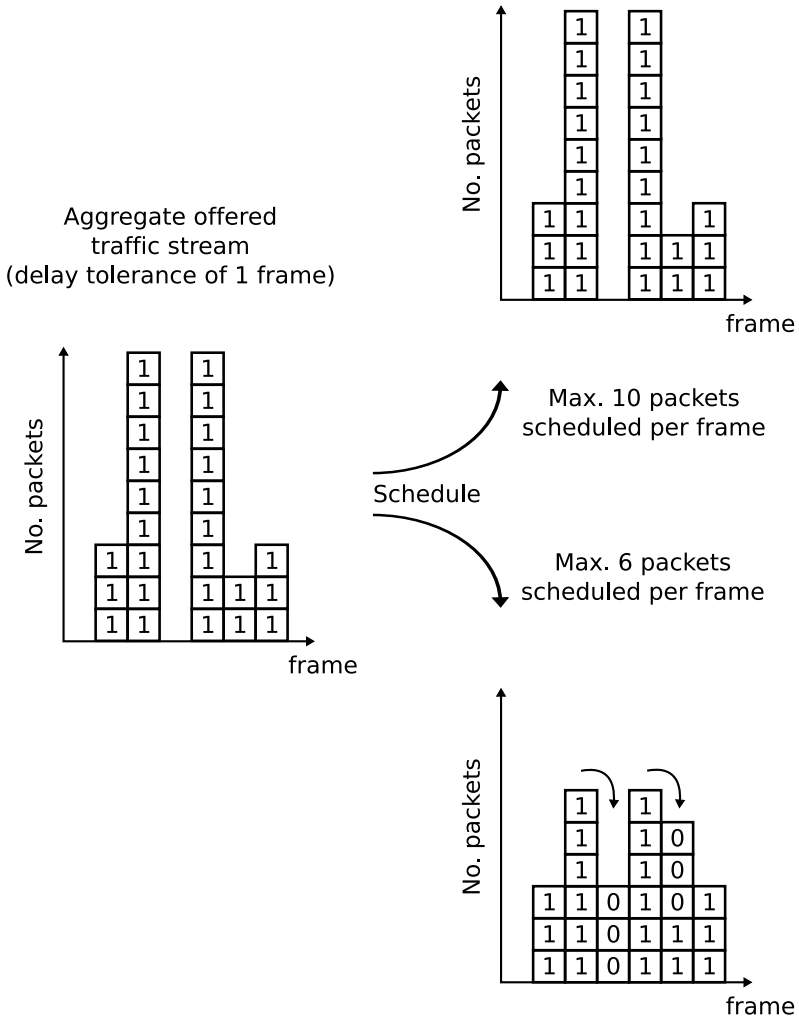

Figure 9.1: Traffic shaping with different traffic scheduling policies.

No. MT's	Prob. packet dropped			BTS transmitter power variance		
	$D = 0$	$D = 1$	$D = 2$	$D = 0$	$D = 1$	$D = 2$
MAX. 16 CODES PER FRAME						
$m = 1$	0.000000	0.000000	0.000000	2.10	2.10	2.10
$m = 4$	0.000987	0.000000	0.000000	8.29	8.29	8.29
$m = 8$	0.013499	0.000015	0.000000	14.51	14.81	14.81
MAX. 10 CODES PER FRAME						
$m = 1$	0.001313	0.000000	0.000000	2.07	2.07	2.07
$m = 4$	0.020455	0.000144	0.000000	7.06	7.25	7.25
$m = 8$	0.111422	0.013266	0.001906	7.23	6.47	6.37
MAX. 6 CODES PER FRAME						
$m = 1$	0.018530	0.000362	0.000000	1.85	1.90	1.90
$m = 4$	0.125448	0.017583	0.002642	3.89	3.85	3.86

Table 9.1: Probability the BTS drops an offered packet and the BTS transmitter power variance with m MT's per BTS and the negative binomial ($\sigma_X^2 = 2.1$) traffic model. Each MT offers 1 Erlang of traffic and all packets have a scheduling delay tolerance of D frames. (BTS transmitter power is normalised to the spreading code power.)

9.3 An Outdoor Time Dispersive Suzuki Propagation Environment

This section evaluates the downlink performance of the same outdoor macro-cellular system evaluated in Chapters 6 and 8 but with the traffic scheduling policies proposed in Section 9.2. A time dispersive propagation channel (delay profile 1 listed in Table 6.5) with receiver diversity and a fixed spreading factor of 16 are considered.

System performance is evaluated with the same CBR traffic model and negative binomial ($\sigma_X^2 = 2.1$) traffic model that were considered in Chapter 8. The DAR traffic model presented in Section 4.4.5 is also evaluated and it is assumed to have a truncated negative binomial ($\sigma_X^2 = 2.1$) stationary probability distribution ($x_{\max} = 16$). The DAR traffic model has the property that the number of packets generated in the current frame depends on the number of packets generated in the previous frame i.e. there is correlation in the traffic stream. The correlation coefficient, ρ, controls the level of correlation and when $\rho = 0$ the DAR traffic model is approximately equal to the negative binomial ($\sigma_X^2 = 2.1$) traffic model[2].

[2]At least for the parameter values assumed in this chapter.

9.3.1 Random MT Location Within Own Cell

Table 9.2 shows system downlink performance with the CBR and negative binomial ($\sigma_X^2 = 2.1$) traffic models when all MT's move randomly within their own cell and there are m MT's per cell. These results need to be considered in conjunction with the scheduling performance results in Table 9.1.

Increasing the scheduling delay tolerance has minimal impact on the propagation dependent performance in most cases. This is because the level of packet dropping is already less than 2% in most cases and increasing the scheduling delay tolerance has minimal impact on the BTS transmitter power distribution. The exceptional cases are when there is a maximum of 10 codes per frame ($m = 4$, 8) and 6 codes per frame ($m = 4$) and in these cases the change in propagation dependent performance is primarily due to the increased traffic load on the propagation channel as the scheduling delay tolerance is increased i.e. the level of packet dropping has reduced.

Reducing the maximum number of available codes per frame has minimal impact on the BER performance difference between the traffic models. At low traffic loads, reducing the maximum number of available codes per frame has minimal impact on the BER performance difference because the level of packet dropping is low and there is little impact on the BTS transmitter power distribution. At high traffic loads, Chapter 8 showed that there was already a minimal BER performance difference between the traffic models and consequently reducing the maximum number of available codes per frame has little effect.

Figures 9.2 and 9.3 show system downlink performance with the CBR and DAR ($\sigma_X^2 = 2.1$) traffic models when all MT's move randomly within their own cell. As predicted by basic queueing theory, the level of packet dropping increases as the DAR traffic model correlation coefficient increases ($D \neq 0$) as packets tend to increasingly arrive in bursts which is more difficult to schedule within the scheduling delay tolerance. In Figure 9.2 with 1 MT per cell, the level of packet dropping is relatively small regardless of the correlation coefficient and consequently the correlation coefficient has little impact on the BTS transmitter power distribution and propagation dependent performance. In Figure 9.3 with 4 MT's per cell and a maximum of 6 codes per frame, the level of packet dropping is more significant and the change in the propagation dependent performance as the correlation coefficient is varied is primarily due to the change in the traffic load on the propagation channel. Appendix B shows the BER performance results in Figures 9.2 and 9.3 in a tabular form for easier comparison.

No. MT's	Prob. of bit error (BER)				BER % diff. relative to CBR		
	CBR	Neg. binomial ($\sigma_X^2 = 2.1$)					
		$D = 0$	$D = 1$	$D = 2$	$D = 0$	$D = 1$	$D = 2$
MAX. 16 CODES PER FRAME							
$m = 1$	0.009012	0.007384	0.007362	0.007377	-18.1%	-18.3%	-18.1%
$m = 4$	0.027520	0.026926	0.026938	0.026926	-2.2%	-2.1%	-2.2%
$m = 8$	0.045934	0.046056	0.046561	0.046548	0.3%	1.4%	1.3%
MAX. 10 CODES PER FRAME							
$m = 1$	0.009012	0.007360	0.007392	0.007345	-18.3%	-18.0%	-18.5%
$m = 4$	0.027520	0.026372	0.026840	0.026839	-4.2%	-2.5%	-2.5%
$m = 8$	0.045934	0.042209	0.045533	0.045950	-8.1%	-0.9%	0.0%
MAX. 6 CODES PER FRAME							
$m = 1$	0.009012	0.007249	0.007388	0.007365	-19.6%	-18.0%	-18.3%
$m = 4$	0.027520	0.024099	0.026518	0.026809	-12.4%	-3.6%	-2.6%

Table 9.2: BER with CBR and negative binomial ($\sigma_X^2 = 2.1$) traffic models. MT's move randomly within their own cell and use a fixed spreading factor of 16. The BTS limits the maximum number of codes transmitted per frame and all packets have a scheduling delay tolerance of D frames.

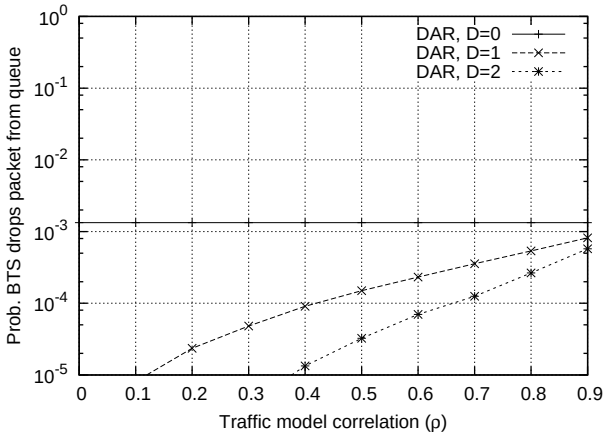

(a) Prob. packet dropped – max. 10 codes per frame

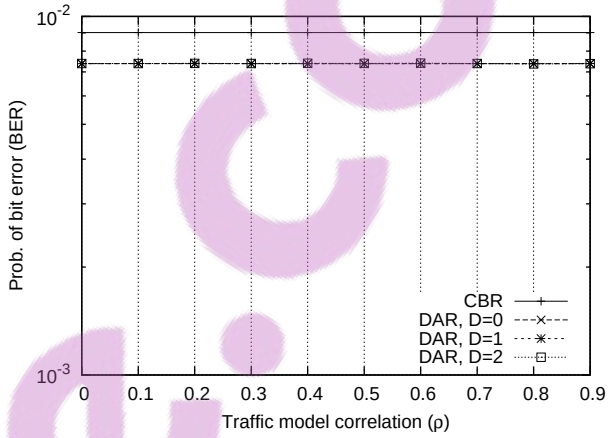

(b) BER – max. 10 codes per frame

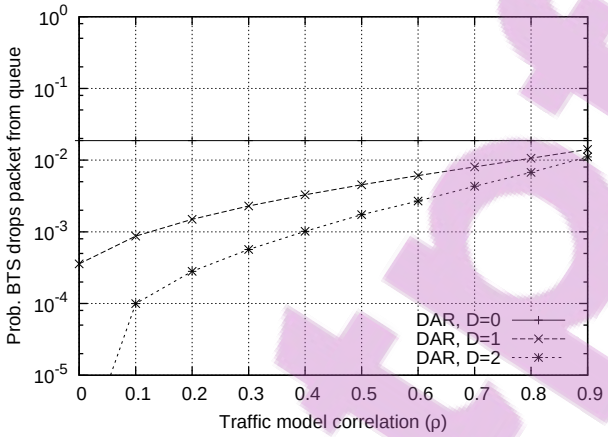

(c) Prob. packet dropped – max. 6 codes per frame

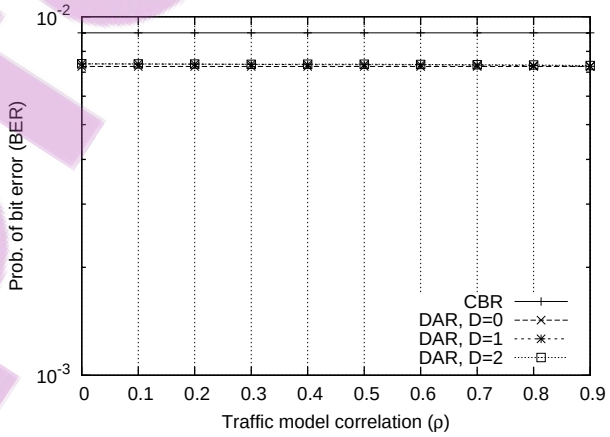

(d) BER – max. 6 codes per frame

Figure 9.2: Probability the BTS drops an offered packet and BER with the DAR ($\sigma_X^2 = 2.1$) traffic model and varying levels of traffic stream correlation. **Each cell contains 1 MT** that uses a fixed spreading factor of 16. The BTS limits the maximum number of codes transmitted per frame and all packets have a scheduling delay tolerance of D frames.

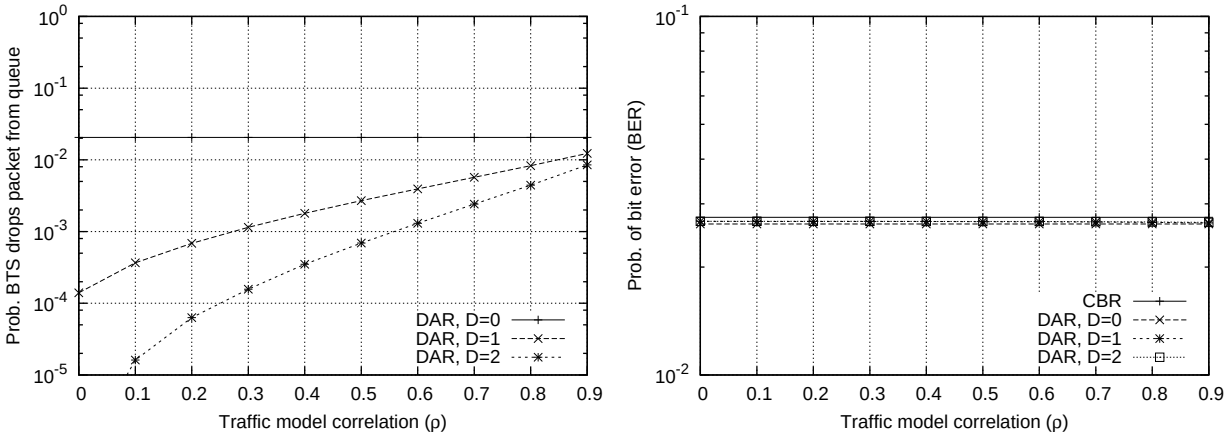

(a) Prob. packet dropped – max. 10 codes per frame

(b) BER – max. 10 codes per frame

(c) Prob. packet dropped – max. 6 codes per frame

(d) BER – max. 6 codes per frame

Figure 9.3: Probability the BTS drops an offered packet and BER with the DAR ($\sigma_X^2 = 2.1$) traffic model and varying levels of traffic stream correlation. **Each cell contains 4 MT's** that use a fixed spreading factor of 16. The BTS limits the maximum number of codes transmitted per frame and all packets have a scheduling delay tolerance of D frames.

9.3.2 Fixed MT Location Near the Cell Centre

Table 9.3 shows system downlink performance with the CBR and negative binomial ($\sigma_X^2 = 2.1$) traffic models for a stationary MT located 0.2 radii from the cell centre. All other MT's move randomly within their own cell and there are m MT's per cell. These results need to be considered in conjunction with the scheduling performance results in Table 9.1. It was shown in Chapter 8 that in this particular scenario the CBR traffic model had significantly superior BER performance than the negative binomial ($\sigma_X^2 = 2.1$) traffic model.

As was the case in the previous section, increasing the scheduling delay tolerance has minimal impact on the propagation dependent performance in most cases. This is because the level of packet dropping is already less than 2% in most cases and increasing the scheduling delay tolerance has minimal impact on the BTS transmitter power distribution. The exceptional cases are when there is a maximum of 10 codes per frame ($m = 8$) and 6 codes per frame ($m = 4$) and in these cases the change in propagation dependent performance is primarily due to the increased traffic load on the propagation channel as the scheduling delay tolerance is increased i.e. the level of packet dropping has reduced.

It was shown in Chapter 8 that in a time dispersive propagation environment where intra-cell interference is dominant, the correlated intra-cell interference phenomenon identified in Section 6.4.1 significantly degrades the propagation dependent performance of bursty traffic at both low and high traffic loads. Reducing the maximum number of codes that can be transmitted per frame reduces the variability of the transmitted traffic stream, especially at high traffic loads, and Table 9.3 shows a reduced BER performance difference between the traffic models as the transmitted traffic streams statistically become more similar.

Figures 9.4 and 9.5 show system downlink performance with the CBR and DAR ($\sigma_X^2 = 2.1$) traffic models for a stationary MT located 0.2 radii from the cell centre while all other MT's move randomly within their own cell. Similar trends to those observed in the previous section are also observed in this case. Appendix B shows the BER performance results in Figures 9.4 and 9.5 in a tabular form for easier comparison.

No. MT's	Prob. of bit error (BER)				BER % diff. relative to CBR		
	CBR	Neg. binomial ($\sigma_X^2 = 2.1$)					
		$D = 0$	$D = 1$	$D = 2$	$D = 0$	$D = 1$	$D = 2$
MAX. 16 CODES PER FRAME							
$m = 1$	0.000005	0.000016	0.000015	0.000016	191.6%	173.3%	187.8%
$m = 4$	0.000068	0.000180	0.000182	0.000183	164.7%	167.5%	168.4%
$m = 8$	0.000321	0.000819	0.000857	0.000862	155.2%	167.2%	168.8%
MAX. 10 CODES PER FRAME							
$m = 1$	0.000005	0.000013	0.000012	0.000012	133.4%	123.6%	119.6%
$m = 4$	0.000068	0.000115	0.000119	0.000119	69.5%	75.6%	75.4%
$m = 8$	0.000321	0.000333	0.000415	0.000422	3.9%	29.3%	31.6%
MAX. 6 CODES PER FRAME							
$m = 1$	0.000005	0.000010	0.000010	0.000010	76.9%	85.3%	85.3%
$m = 4$	0.000068	0.000064	0.000079	0.000084	-6.6%	16.6%	23.5%

Table 9.3: BER for a stationary MT located 0.2 radii from the cell centre with CBR and negative binomial ($\sigma_X^2 = 2.1$) traffic models. MT's use a fixed spreading factor of 16. The BTS limits the maximum number of codes transmitted per frame and all packets have a scheduling delay tolerance of D frames.

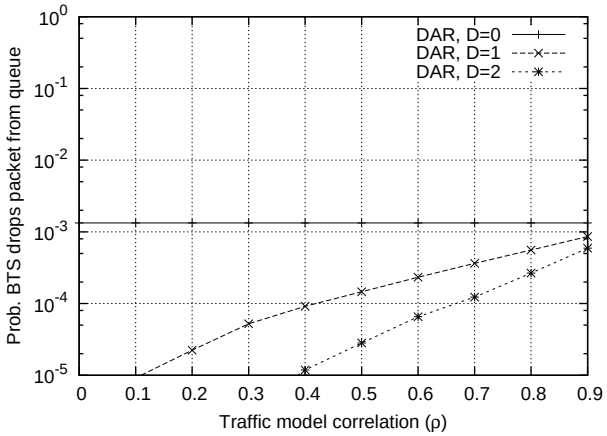

(a) Prob. packet dropped – max. 10 codes per frame

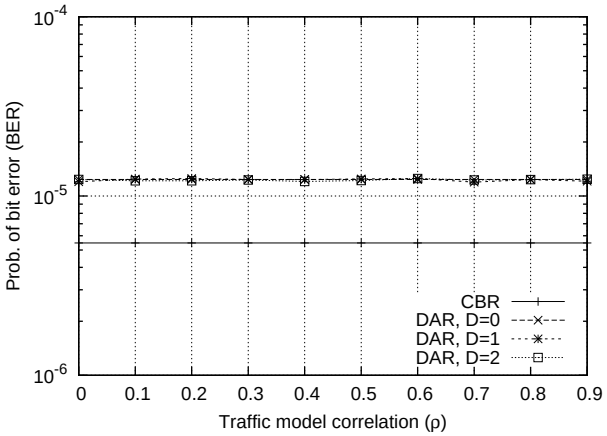

(b) BER – max. 10 codes per frame

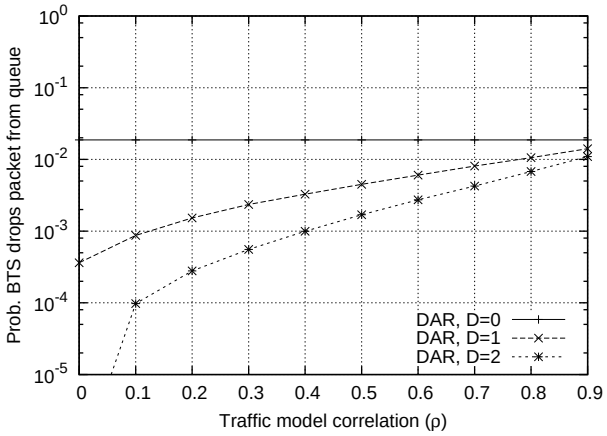

(c) Prob. packet dropped – max. 6 codes per frame

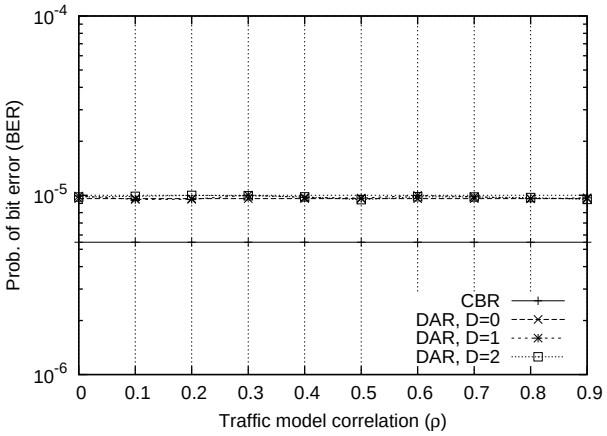

(d) BER – max. 6 codes per frame

Figure 9.4: Probability the BTS drops an offered packet and BER for a stationary MT located 0.2 radii from the cell centre with the DAR ($\sigma_X^2 = 2.1$) traffic model and varying levels of traffic stream correlation. **Each cell contains 1 MT** that uses a fixed spreading factor of 16. The BTS limits the maximum number of codes transmitted per frame and all packets have a scheduling delay tolerance of D frames.

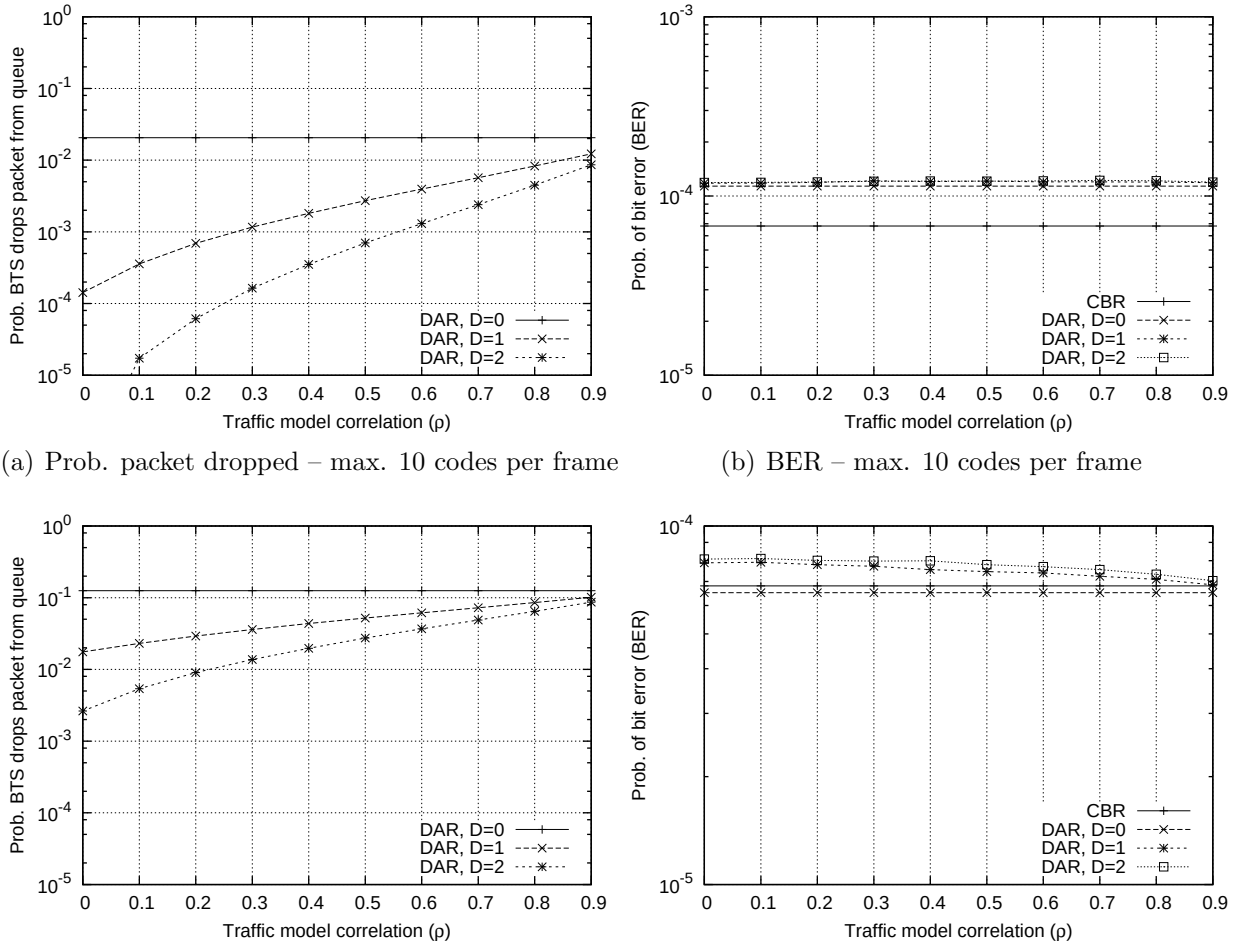

(a) Prob. packet dropped – max. 10 codes per frame

(b) BER – max. 10 codes per frame

(c) Prob. packet dropped – max. 6 codes per frame

(d) BER – max. 6 codes per frame

Figure 9.5: Probability the BTS drops an offered packet and BER for a stationary MT located 0.2 radii from the cell centre with the DAR ($\sigma_X^2 = 2.1$) traffic model and varying levels of traffic stream correlation. **Each cell contains 4 MT's** that use a fixed spreading factor of 16. The BTS limits the maximum number of codes transmitted per frame and all packets have a scheduling delay tolerance of D frames.

9.4 Summary

When selecting a traffic scheduling policy for a DS-CDMA cellular system there is a trade-off between scheduling performance and propagation dependent performance. Transmitting more spreading codes in a frame improves scheduling performance (i.e. a lower packet scheduling delay and reduced packet dropping) but comes at the cost of increased system interference and reduced propagation dependent performance. A commonly used technique in telecommunication networks is to select a traffic scheduling policy that deliberately shapes the transmitted traffic stream in order to improve system performance.

This chapter has evaluated the performance of the outdoor macro-cellular system considered in Chapters 6 and 8 with a number of different traffic scheduling policies, specifically, scheduling policies with different limits on the maximum number of spreading codes that can be transmitted per frame and also different packet scheduling delay tolerances. A CBR traffic model, negative binomial ($\sigma_X^2 = 2.1$) traffic model, and DAR traffic model were all evaluated.

In general, reducing the maximum number of spreading codes that can be transmitted per frame and increasing the traffic scheduling delay tolerance has minimal impact on the BER performance difference between different traffic types. However, it can make a significant difference in a time dispersive propagation environment when intra-cell interference is dominant and in this case reducing the variability of the transmitted traffic stream reduces the BER performance difference between different traffic types. In general though, traffic shaping that reduces the variability of a transmitted traffic stream is in most cases undesirable as burstier traffic has generally been shown to have superior propagation dependent performance. In many scenarios it may even be beneficial to implement a traffic scheduling policy that deliberately increases the variability of the transmitted traffic stream.

Chapter 10

Implications of Variable-Bit-Rate Traffic on System Design

10.1 Introduction

This thesis has investigated the impact of VBR traffic on the downlink performance of DS-CDMA cellular systems that utilise frame-by-frame dynamic resource allocation on the radio channel. This chapter consolidates the results presented in Chapters 6–9 and outlines the implications of VBR traffic on DS-CDMA cellular system design, in particular, the propagation related aspects.

The deployment of 3G DS-CDMA cellular systems is resulting in a transition from cellular systems that predominantly carry CBR voice traffic to multi-service packet based systems that predominantly carry VBR traffic. This has significant implications for cellular system design as the statistical properties of the individual user traffic streams must now be taken into account. For systems that carry VBR traffic in addition to CBR traffic, additional design considerations include: anticipating the services and traffic types that will be present in a system, developing traffic models that capture the statistical properties of the user traffic streams, supporting the diverse quality of service (QoS) requirements associated with each user service, selecting a traffic scheduling policy that schedules and prioritises traffic for transmission over the radio channel, and determining what impact different traffic types have on the system's performance.

Section 10.2 consolidates the results presented in Chapters 6–9 and outlines the implications of VBR traffic on DS-CDMA cellular system design. Section 10.3 discusses traffic modelling requirements for system design and Section 10.4 lists recommendations for future work based on the findings of this thesis.

10.2 CBR Traffic vs. VBR Traffic

Cellular systems have traditionally been designed assuming CBR traffic, often because a CBR voice service was assumed [16, 17, 18, 19, 20]. In this case, a fixed size radio bearer was simply allocated to a user for the duration of their service and the statistical properties of the user traffic streams were not a relevant consideration. With VBR traffic and dynamic resource allocation on the radio channel, the statistical properties of the user traffic streams impact both the system's traffic scheduling performance and propagation dependent performance and these performance components are illustrated in Figure 10.1.

From a design perspective, it would be convenient if VBR traffic could be approximated as CBR traffic as this would eliminate the need to develop detailed traffic models and existing design procedures could be reused. The propagation related aspects of system design are the primary focus of this thesis but consideration must also be given to traffic scheduling as this impacts propagation dependent performance.

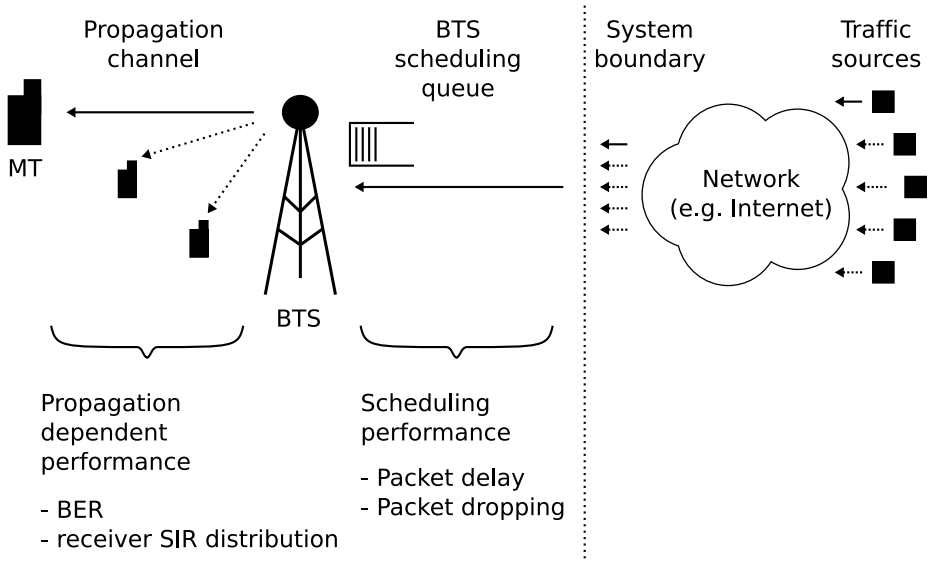

Figure 10.1: Cellular system performance components.

10.2.1 Scheduling Performance

In DS-CDMA cellular systems there is a soft capacity limit on the radio channel and additional spreading codes can be allocated to users at the cost of increased system interference and reduced propagation dependent performance. With dynamic resource allocation, a BTS can vary the number and length of spreading codes allocated to a user on a frame-by-frame basis. This form of dynamic resource allocation is essential for VBR traffic streams as it would be inefficient to allocate a fixed size radio bearer for the duration of a user's service,

as there would be periods of time where the allocated bearer capacity would go unused and could be better allocated to another user.

Due to interference constraints on the propagation channel, the system must limit the maximum number of spreading codes allocated in a frame and a traffic scheduling policy is required to determine which packets are transmitted in a frame when the number of offered packets is greater than the available transmission capacity. For systems that carry only CBR traffic, a scheduling policy is unnecessary as the number of packets (or quantity of data) offered to the BTS in each frame is constant. Instead, the system ensures that there is enough spare transmission capacity before accepting a service request and once accepted the user is allocated a fixed size radio bearer for the duration of their service. Hence, scheduling performance is not a design consideration for systems that carry only CBR traffic.

For systems that carry VBR traffic, scheduling performance is a design consideration as user traffic is inherently variable and there is the potential for more packets to be offered in a frame than there is available transmission capacity. During the system design process a traffic scheduling policy must be selected that takes into account system interference constraints and user QoS requirements e.g. maximum packet scheduling delay. Selecting a traffic scheduling policy and estimating scheduling performance is effectively a traditional queueing problem and there is already a large body of knowledge related to this field [67, 71, 83]. It is known that burstier more variable traffic tends to result in greater levels of packet dropping and scheduling delay and this was observed in Chapters 6–9 where scheduling performance was evaluated.

From a propagation dependent performance point of view, important traffic scheduling design considerations are:

- the level of packet dropping i.e. does packet dropping significantly impact the traffic load on the propagation channel and level of system interference?
- the level of packet dropping compared to the level of packet loss due to propagation i.e. is packet dropping significant in terms of overall system packet loss?
- the impact of the traffic scheduling policy on the statistical properties of the transmitted traffic stream i.e. does the scheduling policy shape the transmitted traffic stream in a way that affects propagation dependent performance?

Standard queueing theory techniques can be used to answer these questions and evaluate scheduling performance [83].

10.2.2 Propagation Dependent Performance

Chapters 6–9 identified scenarios where the propagation dependent performance of both outdoor and indoor DS-CDMA cellular systems is sensitive to the statistical properties of the user traffic streams. If a system's propagation dependent performance is sensitive to the statistical properties of the user traffic streams then this must be factored into the system design process and traffic models must be developed that capture the characteristics of the user traffic streams. The major findings of this thesis related to propagation dependent performance are as follows:

- There is the potential for a significant difference in propagation dependent performance with different traffic types.
- With a non-time dispersive propagation environment, a bursty Pareto ($H = 0.8$) traffic model had between -5% and 54% superior BER performance than a CBR traffic model in the scenarios considered in Chapters 6 and 7.
- With a time dispersive propagation environment, a bursty Pareto ($H = 0.8$) traffic model had between 0–24% superior BER performance than a CBR traffic model in the scenarios considered in Chapter 6. The one exceptional case was when intra-cell interference was dominant relative to inter-cell interference. In this case, a bursty Pareto ($H = 0.8$) traffic model had between 20–190% inferior BER performance than a CBR traffic model in the scenarios considered. This was due to the detrimental correlated intra-cell interference phenomenon identified in Section 6.4.1.
- A variable spreading factor rather than multiple spreading codes is a preferable method to vary a user's momentary data rate as this avoids the detrimental correlated intra-cell interference phenomenon identified in Section 6.4.1.
- In general, when there is a significant difference in propagation dependent performance between different traffic types, burstier more variable traffic has superior propagation dependent performance. Chapter 8 showed that the BTS transmitter power mean and variance provides a good indication of the level of propagation dependent performance regardless of the specific traffic type.
- In general, as the number of users per cell increases, the difference in propagation dependent performance between different traffic types reduces and eventually becomes negligible. In the scenarios considered in Chapters 6–9, the BER performance difference between different traffic types generally became minor (less than 10%) with more than 4 MT's per cell.
- A relatively high mean SIR at the receiver tends to result in a negligible difference in propagation dependent performance between different traffic types. This is because the

receiver's SIR distribution tends to be concentrated around a relatively linear section of the BER vs. SIR curve. Hence, a larger spreading factor or desirable MT location tend to reduce the difference in propagation dependent performance between different traffic types.

- It was shown in Chapter 6 that the level of propagation environment hostility, in particular the level of lognormal shadowing, has minimal impact on the BER performance difference between different traffic types.

- A system's BTS deployment configuration impacts the receiver SIR distribution and in addition to impacting absolute performance levels also impacts the difference in propagation dependent performance between different traffic types. This was observed in Chapter 7 where two BTS deployment configurations were considered for an indoor pico-cellular system.

- It was shown in Chapter 9 that the system's traffic scheduling policy generally has minimal impact on the difference in propagation dependent performance between different traffic types. This is because in the scenarios where the difference in propagation dependent performance is significant, the traffic scheduling policy has minimal impact on the transmitted traffic stream which is ultimately what determines the level of system interference and propagation dependent performance.

- In the scenarios where VBR traffic has superior propagation dependent performance, it may be beneficial to implement a traffic scheduling policy that deliberately increases the variability of the transmitted traffic stream. Additional traffic scheduling delay would however need to be incurred to implement such a scheduling policy.

10.3 Traffic Modelling Requirements

For the propagation related aspects of DS-CDMA cellular system design, a traffic model that captures the statistical properties of the user traffic streams is in many cases unnecessary, as outlined in the previous section. In general, with more than 4 MT's per cell the difference in propagation dependent performance between different traffic types is relatively minor and approximating VBR traffic as CBR traffic is a reasonable approximation that simplifies system design and performance evaluation. In the cases where a significant performance difference exists between different traffic types, it was shown in Chapter 8 that the BTS transmitter power mean and variance provides a good indication of the level of propagation dependent performance regardless of the specific traffic type. Hence, a detailed traffic model is not necessarily required even when a significant performance difference exists between different traffic types.

For outdoor macro-cellular systems that have a relatively high number of users per cell, there is likely to be a minimal difference in propagation dependent performance between different traffic types and knowledge of the expected mean traffic load is sufficient for system design. For indoor pico-cellular systems the number of users per cell is likely to be less and the difference in propagation dependent performance between different traffic types may be more significant and the statistical properties of the user traffic streams may need to be factored into the system design process. It has been shown that VBR traffic generally has superior propagation dependent performance than CBR traffic and for convenience VBR traffic could still be approximated as CBR traffic and this would provide a worst case performance scenario. Indoor pico-cellular systems are expected to become more prevalent as packet based services are embraced and user data throughput requirements increase.

Regardless of whether the statistical properties of the user traffic streams need to be modelled, the statistical properties of the arrival process of service requests still need to be modelled in order to determine service availability and this applies to both CBR traffic and VBR traffic. When a user makes a service request for a packet based service the system must negotiate with the user a set of acceptable QoS guarantees or else block the service request. Service availability can be evaluated with standard queueing theory techniques [83].

10.3.1 Time Scale Granularity

This thesis has considered frame-by-frame dynamic resource allocation on the radio channel and a 2 ms frame period was assumed as this is specified in the 3GPP standards for high speed downlink packet access (HSDPA) 3G cellular systems [74]. The results presented in Chapters 6–9 apply equally to dynamic resource allocation schemes that use different time resolutions but the traffic models used for performance evaluation must be adapted accordingly i.e. the traffic models must describe the number of packets offered to the BTS in each scheduling interval.

Only the downlink was considered in this thesis as frame-by-frame dynamic resource allocation is more suited to the downlink where the BTS has complete and immediate information about all traffic requiring transmission. On the uplink, dynamic resource allocation is still feasible but a coarser time resolution is required. In this case, an MT would send periodic reports to the BTS about its current traffic requirements and the BTS would dynamically allocate an appropriate transmission capacity.

10.3.2 Mixed Traffic Types

Because there is a diverse range of potential packet based services there is also likely to be a diverse range of traffic types present in a cellular system. From an MT's perspective,

propagation dependent performance depends only on the aggregate transmitted traffic stream as this determines the level of system interference. Hence, a traffic model of the aggregate transmitted traffic stream is also sufficient to evaluate propagation dependent performance and the composition of the aggregate transmitted traffic stream is irrelevant.

10.4 Recommendations for Future Work

It was identified in Chapter 6 that in a time dispersive propagation environment, the use of a variable spreading factor rather than multiple spreading codes is a preferable method to vary a user's momentary data rate as this avoids the detrimental correlated intra-cell interference phenomenon identified in Section 6.4.1. Investigation into the use of a variable spreading factor rather than multiple spreading codes would be a useful extension to the work presented. With a non-time dispersive propagation environment a variable spreading factor and multiple spreading codes perform equally well.

Fixed size spreading codes and an identical spreading code transmission power have been assumed throughout this thesis. Dynamic spreading code power allocation and downlink power control, discussed in Section 2.4.1, can be used to minimise system interference and improve propagation dependent performance. Investigation of this technique with different traffic types would be a useful contribution.

Propagation dependent performance has been identified as more sensitive to traffic type when there are fewer users per cell. Because indoor pico-cellular systems tend to have a relatively low number of users per cell, additional investigation into indoor pico-cellular systems would be a useful extension to the work presented as only a single indoor propagation environment was considered in this thesis.

It has been shown that VBR traffic has superior propagation dependent performance in many scenarios and the results presented in Chapter 9 suggest that it may be beneficial to implement a traffic scheduling policy that deliberately increases the variability of the transmitted traffic stream. This would be an interesting area for further study.

This thesis has investigated the impact of VBR traffic on downlink performance and consideration of uplink performance would also be useful. A method for dynamic resource allocation on the radio channel would first need to be developed as frame-by-frame dynamic resource allocation, which was assumed on the downlink, is not feasible on the uplink. Because spreading code synchronisation cannot be maintained on the uplink the use of non-orthogonal spreading codes would also need to be considered.

10.5 Summary

This thesis has investigated the impact of VBR traffic on the performance of DS-CDMA cellular systems that utilise frame-by-frame dynamic resource allocation on the radio channel. This chapter has consolidated the results presented in Chapters 6–9 and outlined the implications of VBR traffic on DS-CDMA cellular system design, in particular, the propagation related aspects.

The scenarios where traffic type has a significant impact on propagation dependent performance were summarised and design guidelines were presented for DS-CDMA cellular systems with VBR traffic. Scenarios where VBR traffic can be approximated as CBR traffic were identified and this is a convenient approximation as it simplifies system design and detailed traffic models do not need to be developed. Traffic modelling requirements for system design were discussed and recommendations for future work were presented.

Chapter 11

Summary

Cellular systems have traditionally been designed to support only a single user service, namely, constant-bit-rate (CBR) voice. Modern cellular systems must however support multiple packet based services, and their associated quality of service (QoS) requirements, in addition to the traditional CBR voice service. The traffic generated by packet based services is variable-bit-rate (VBR) in nature and dynamic resource allocation on the radio channel is essential in order to efficiently support packet based services. With DS-CDMA based cellular systems there is a soft capacity limit on the radio channel, specifically, additional capacity can be allocated to users at the cost of increased system interference and it is up to the system to ensure that an acceptable level of system interference is maintained. Hence, in DS-CDMA cellular systems there is a direct relationship between user traffic and propagation dependent performance.

This thesis has investigated the impact of VBR traffic on the downlink performance of DS-CDMA cellular systems that utilise frame-by-frame dynamic resource allocation on the radio channel. The primary objectives of this thesis were:

- to identify and model different types of VBR traffic that could potentially be present in 3G cellular systems.
- to develop a DS-CDMA cellular system model that can be used to estimate system performance with different types of traffic.
- to determine whether traffic type has a significant influence on system performance, in particular propagation dependent performance, and if so under what circumstances.
- to identify the implications of VBR traffic on DS-CDMA cellular system performance and develop a set of system design guidelines.

A simulation model was developed to evaluate the downlink performance of both outdoor and indoor DS-CDMA cellular systems and the performance metrics measured include the

probability of packet dropping at the BTS, packet scheduling delay, coverage performance (i.e. the receiver SIR distribution), and probability of bit error (BER). The main components of the simulation model are:

- a traffic model that is used to represent the number of fixed size packets offered to a BTS in a frame.
- a BTS traffic scheduling policy that allocates fixed size spreading codes to users on a frame-by-frame basis.
- a propagation model that is used to estimate the desired signal power and interference power at an MT receiver.

Since there is a vast number of packet based services and associated traffic types that could potentially be present in a cellular system the approach taken in this thesis was to consider a small set of reasonably generic traffic models that capture the broad characteristics of VBR traffic.

An outdoor macro-cellular system was initially considered and system performance was evaluated with two statistically dissimilar traffic models, namely, a CBR traffic model and a bursty Pareto traffic model. A BTS traffic scheduling policy was selected so that minimal BTS packet dropping occurred and the statistical properties of the aggregate traffic stream transmitted over the propagation channel were similar to the statistical properties of the aggregate traffic stream offered to the BTS. System performance was compared with the two traffic models and the sensitivity of system performance to traffic type was measured.

With orthogonal spreading codes and a non-time dispersive propagation environment it was shown that BER performance with the bursty Pareto ($H = 0.8$) traffic model was between -5% and 54% superior than with the CBR traffic model in the scenarios considered. A performance difference manifested itself because the BTS transmitter power distribution and receiver SIR distribution were different with the two traffic models. As the number of MT's in the system increased the performance difference between the traffic models reduced and with 4 or less MT's per cell the performance difference was generally significant.

System performance was evaluated with the following mobility scenarios:

1. All MT's move randomly within their own cell.
2. A stationary MT located near the cell centre, considered to be in a good coverage location, while all other MT's move randomly within their own cell.
3. A stationary MT located far away from the cell centre, considered to be in a poor coverage location, while all other MT's move randomly within their own cell.

Scenarios (1) and (3) yielded similar results and these were consistent with the results described above. However, in scenario (2) the relatively high mean SIR at the receiver resulted in a minimal BER performance difference between the traffic models, regardless of the number of MT's per cell. Fixed spreading factors of 16 and 64 were considered and these shifted the mean SIR at the receiver but did not significantly impact the BER performance difference between the traffic models.

Similar trends were observed with a time dispersive propagation environment but with one important exception. The spreading codes received from the same BTS were no longer perfectly synchronised and the intra-cell interference at an MT receiver was positively correlated with the number of spreading codes allocated to the MT. In the scenarios where intra-cell interference was dominant, for example in mobility scenario (2) listed above, it was shown that the correlated intra-cell interference had a detrimental impact on performance and BER performance with the CBR traffic model was between 20–190% superior than with the bursty Pareto ($H = 0.8$) traffic model. The use of a variable spreading factor rather than multiple spreading codes avoids this detrimental correlation effect.

The performance of an indoor pico-cellular system deployed in a prototypical office tower was then evaluated with the same CBR and Pareto traffic models considered with the outdoor macro-cellular system. Because propagation channel delay spreads are typically small in indoor environments only a non-time dispersive propagation environment was considered. Performance trends similar to those observed with the outdoor macro-cellular system were also observed with the indoor pico-cellular system and this was not unexpected as the fundamental propagation mechanisms are similar in both environments.

Two BTS deployment configurations were considered in the indoor pico-cellular system and it was observed that the BTS configuration impacts both the absolute system performance level and also the BER performance difference between the traffic models. This was due to the different receiver SIR distributions with the two BTS configurations. Both QPSK and 16QAM modulation schemes were evaluated and the 16QAM modulation scheme resulted in a slightly larger BER performance difference between the traffic models.

Because similar performance trends were observed with both the outdoor macro-cellular system and the indoor pico-cellular system, only the outdoor system was selected for further investigation with additional traffic types. The performance of the outdoor macro-cellular system was then re-evaluated with CBR, Poisson, negative binomial, and Pareto traffic models and also a variety of traffic model parameter values. Traffic was assumed to have zero scheduling delay tolerance (i.e. packets offered to the BTS had to be transmitted immediately or else dropped) and the probability of BTS packet dropping was evaluated with the different traffic models. As expected, the bursty more variable traffic experienced higher packet dropping.

It was shown that with a fixed mean traffic load the BTS transmitter power variance provides

a good indication of the level of BER performance, regardless of the specific traffic type, and there is an approximately linear relationship between the two. Hence, in many cases the BTS transmitter power mean and variance may be sufficient to estimate propagation dependent performance and a detailed traffic model may be unnecessary.

A number of different BTS traffic scheduling policies were considered and these reduced the maximum number of available spreading codes per frame and increased the traffic scheduling delay tolerance, in effect, shaping the aggregate transmitted traffic stream and reducing its variability. The impact of the scheduling policies on system performance was evaluated with both a negative binomial traffic model and a DAR traffic model with varying levels of traffic correlation. It was shown that in the scenarios where propagation dependent performance was previously identified as sensitive to traffic type the different scheduling policies generally had minimal impact on BER performance. In these scenarios, the traffic load was generally low and relatively few packets needed to be delayed or dropped by the scheduler, hence, the statistical properties of the transmitted traffic stream and propagation dependent performance remained largely unaffected. It was however shown that the use a traffic scheduling policy that deliberately increases the variability of the transmitted traffic stream may be beneficial in many scenarios as this can improve propagation dependent performance.

Based on the results presented in this thesis the implications of VBR traffic on DS-CDMA cellular system design were then outlined. It was shown that in many scenarios VBR traffic can be approximated as CBR traffic when considering the propagation related aspects of system design and this is a convenient approximation as it simplifies system design and detailed traffic models do not need to be developed.

In summary, the unique contributions of this thesis are:

- the development of a DS-CDMA cellular system model that can be used to estimate system performance with different traffic types.
- the identification of scenarios where the downlink performance of both outdoor and indoor DS-CDMA cellular systems is sensitive to the statistical properties of the user traffic streams.
- the evaluation of DS-CDMA cellular system performance with diverse traffic types.
- the evaluation of DS-CDMA cellular system performance with different traffic scheduling policies that deliberately alter the statistical properties of the user traffic.
- the development of design guidelines for DS-CDMA cellular systems with VBR traffic.

Appendix A

Engineering School Tower Propagation Measurement Database

This appendix provides additional information about the Engineering School Tower propagation measurement database described in Section 3.5.2 and used in Chapter 7 to evaluate the performance of an indoor pico-cellular system. The measurement database is based on a 1.8 GHz propagation study performed in the Engineering School Tower at the University of Auckland and a detailed report about the study can be found in [81].

The measurement database includes large-scale path losses between 10 potential BTS locations and 49 potential MT locations on the 8th floor of the Engineering School Tower. The 10 potential BTS locations are marked TX-A and TX-B in Figure 3.7 and are located on floors 6–10. The 49 potential MT locations are marked '×' in Figure 3.7 and are located on the 8th floor. Table A.1 lists the large-scale path losses between the BTS's and MT locations and the origin of the MT coordinates is shown in Figure 3.7 and is in the bottom left hand corner of the figure.

Two specific MT locations are considered in Chapter 7 and these are marked RX-A and RX-B in Figure 7.1. In Table A.1, location RX-A corresponds to MT location 12 and location RX-B corresponds to MT location 48.

MT location			Path loss to BTS TX-A (dB)					Path loss to BTS TX-B (dB)				
Coordinate			Floor					Floor				
No.	x (m)	y (m)	6	7	8	9	10	6	7	8	9	10
1	13.5	5.1	99.3	79.7	43.1	77.6	96.0	110.6	102.5	90.4	101.3	111.6
2	9.3	5.2	92.8	76.6	50.9	72.2	93.1	113.3	98.8	87.4	98.5	107.9
3	5.2	5.2	94.9	87.7	59.9	80.5	97.6	97.2	73.4	57.8	75.0	88.7
4	5.1	9.4	106.9	104.9	89.7	93.7	110.5	96.2	71.9	50.9	72.0	91.2
5	5.1	13.4	106.8	102.4	89.5	88.2	107.5	99.2	76.7	44.2	77.0	96.4
6	9.5	13.4	108.8	100.7	79.8	92.0	108.7	97.4	75.8	51.6	69.5	91.3
7	13.4	13.4	91.5	80.8	61.3	76.5	90.3	92.8	82.6	58.1	75.5	92.5
8	13.4	9.3	97.1	77.9	50.3	68.4	89.9	110.3	102.4	86.1	99.1	111.1
9	7.4	11.7	118.6	111.8	92.6	108.0	120.2	117.3	95.6	77.6	97.1	116.2
10	10.8	11.7	107.3	98.7	76.5	95.2	109.7	114.2	101.8	85.5	96.7	113.8
11	11.7	9.6	116.7	106.4	80.5	95.0	113.7	116.3	102.3	95.7	102.6	114.1
12	8.5	3.4	91.0	80.8	64.4	80.3	97.0	105.5	102.0	90.2	98.3	111.5
13	13.1	3.4	95.1	79.2	54.6	77.5	97.3	105.6	105.8	93.2	106.4	112.0
14	16.6	3.0	96.3	82.7	58.1	89.2	100.5	103.3	108.8	100.9	113.6	116.2
15	16.6	1.3	92.7	82.3	68.7	90.2	102.1	105.9	108.7	103.0	113.0	117.0
16	16.6	4.2	98.3	83.0	56.0	88.9	99.9	103.2	108.3	101.0	113.0	115.2
17	4.7	1.4	87.8	87.7	79.5	88.0	98.7	102.2	87.3	77.7	89.0	102.4
18	6.1	3.3	89.7	87.6	75.0	84.4	101.3	102.9	83.2	68.6	87.1	97.2
19	5.6	2.2	87.7	87.4	74.8	90.0	100.8	102.8	89.9	71.5	88.2	100.8
20	3.0	6.0	103.8	98.2	63.6	85.5	100.5	101.1	89.2	72.2	87.3	100.5
21	1.4	5.7	99.0	97.7	73.5	91.4	106.5	99.9	90.3	79.3	94.6	103.6
22	2.3	6.7	101.7	97.6	68.6	89.3	103.6	99.2	88.9	74.4	88.8	101.3
23	16.7	8.3	99.7	90.0	65.2	78.5	98.7	106.8	105.4	91.2	105.9	114.7
24	15.5	7.2	97.7	82.3	58.1	82.1	101.3	105.1	108.4	92.0	107.9	116.2
25	17.0	7.0	100.3	88.5	65.1	80.0	100.1	105.6	107.0	90.9	107.0	115.5
26	16.7	17.1	103.6	101.0	87.8	95.8	106.4	98.4	94.4	77.5	91.7	106.0
27	16.7	14.7	105.7	102.6	86.4	98.7	105.9	101.0	92.5	65.8	89.3	97.3
28	16.7	16.0	100.3	101.0	85.7	95.9	105.5	98.0	92.5	73.4	89.6	101.8
29	13.0	15.1	99.4	92.5	70.2	80.7	89.0	102.1	91.9	75.5	87.9	101.9
30	13.0	17.2	96.6	91.8	70.4	80.5	94.6	97.7	96.1	81.5	93.6	104.5
31	13.9	16.0	100.7	91.7	74.6	81.5	91.8	99.5	93.4	76.0	89.3	102.9
32	1.2	10.6	104.9	107.9	87.4	104.6	117.4	96.1	88.3	71.2	88.6	101.9
33	3.5	9.5	108.8	109.5	88.1	102.7	116.7	101.5	85.1	67.8	84.9	100.3
34	2.2	9.4	106.1	109.2	87.1	104.6	116.6	98.8	85.5	65.5	87.1	99.8

continued on next page

MT location			Path loss to BTS TX-A (dB)					Path loss to BTS TX-B (dB)				
Coordinate			Floor					Floor				
No.	x (m)	y (m)	6	7	8	9	10	6	7	8	9	10
35	3.4	13.4	111.7	111.8	95.1	93.3	113.2	100.5	78.0	49.0	80.4	100.3
36	1.5	12.3	111.6	113.3	98.2	98.3	117.2	98.0	75.8	52.2	82.6	102.2
37	2.4	13.0	111.9	113.4	97.0	97.6	115.5	97.7	77.1	53.8	80.9	101.3
38	3.0	1.7	93.2	90.2	85.1	92.3	101.0	96.3	95.5	85.5	95.6	101.9
39	1.2	3.3	90.9	89.3	87.9	92.2	102.8	93.0	95.4	82.6	95.4	103.6
40	2.3	3.0	92.2	89.6	84.3	92.7	102.0	96.8	93.8	82.1	95.5	102.4
41	1.0	15.0	109.0	113.2	102.3	111.2	117.6	96.9	86.7	66.5	85.7	101.6
42	3.0	17.2	105.8	111.9	101.2	110.7	114.6	98.5	84.1	67.9	87.5	101.8
43	2.5	16.0	108.6	112.4	101.5	107.7	115.1	99.7	86.1	66.2	86.1	100.7
44	4.9	17.1	106.4	111.0	99.3	100.4	114.4	98.6	73.3	56.5	80.9	100.1
45	6.1	15.6	107.7	110.1	95.5	102.9	116.9	102.5	75.9	58.9	83.1	103.2
46	6.0	17.2	107.9	111.0	98.4	101.4	114.4	100.3	77.7	59.1	81.2	100.5
47	10.0	15.0	103.8	107.5	88.6	100.8	109.0	102.9	87.5	67.7	85.4	102.7
48	8.5	17.0	102.5	106.6	89.9	101.3	110.3	101.2	87.9	73.2	85.5	99.8
49	9.5	16.5	103.0	107.1	90.4	100.9	110.7	103.2	87.9	69.2	85.8	101.7

Table A.1: Large-scale path losses.

Appendix B

Additional Traffic Shaping Results

This appendix shows the results presented in Figures 9.2–9.5 in a tabular form for easier comparison. An analysis of the results presented is included in the relevant sections in Chapter 9.

- Table B.1 corresponds to Figure 9.2.
- Table B.2 corresponds to Figure 9.3.
- Table B.3 corresponds to Figure 9.4.
- Table B.4 corresponds to Figure 9.5.

Traffic model correlation (ρ)	Prob. of bit error (BER)				BER % diff. relative to CBR		
	CBR	DAR ($\sigma_X^2 = 2.1$)					
		$D = 0$	$D = 1$	$D = 2$	$D = 0$	$D = 1$	$D = 2$
MAX. 10 CODES PER FRAME							
0	0.009012	0.007386	0.007385	0.007390	-18.0%	-18.1%	-18.0%
0.1	0.009012	0.007386	0.007391	0.007393	-18.0%	-18.0%	-18.0%
0.2	0.009012	0.007386	0.007396	0.007394	-18.0%	-17.9%	-17.9%
0.3	0.009012	0.007386	0.007383	0.007392	-18.0%	-18.1%	-18.0%
0.4	0.009012	0.007386	0.007386	0.007402	-18.0%	-18.0%	-17.9%
0.5	0.009012	0.007386	0.007377	0.007397	-18.0%	-18.1%	-17.9%
0.6	0.009012	0.007386	0.007387	0.007407	-18.0%	-18.0%	-17.8%
0.7	0.009012	0.007386	0.007384	0.007389	-18.0%	-18.1%	-18.0%
0.8	0.009012	0.007386	0.007383	0.007373	-18.0%	-18.1%	-18.2%
0.9	0.009012	0.007386	0.007388	0.007386	-18.0%	-18.0%	-18.0%
MAX. 6 CODES PER FRAME							
0	0.009012	0.007263	0.007384	0.007393	-19.4%	-18.1%	-18.0%
0.1	0.009012	0.007263	0.007377	0.007385	-19.4%	-18.1%	-18.1%
0.2	0.009012	0.007263	0.007370	0.007380	-19.4%	-18.2%	-18.1%
0.3	0.009012	0.007263	0.007363	0.007368	-19.4%	-18.3%	-18.2%
0.4	0.009012	0.007263	0.007347	0.007372	-19.4%	-18.5%	-18.2%
0.5	0.009012	0.007263	0.007344	0.007371	-19.4%	-18.5%	-18.2%
0.6	0.009012	0.007263	0.007338	0.007361	-19.4%	-18.6%	-18.3%
0.7	0.009012	0.007263	0.007326	0.007346	-19.4%	-18.7%	-18.5%
0.8	0.009012	0.007263	0.007310	0.007332	-19.4%	-18.9%	-18.6%
0.9	0.009012	0.007263	0.007269	0.007311	-19.4%	-19.3%	-18.9%

Table B.1: BER with the DAR ($\sigma_X^2 = 2.1$) traffic model and varying levels of traffic stream correlation. **Each cell contains 1 MT** that uses a fixed spreading factor of 16 and MT's move randomly within their own cell. The BTS limits the maximum number of codes transmitted per frame and all packets have a scheduling delay tolerance of D frames. (See Figure 9.2).

Traffic model correlation (ρ)	Prob. of bit error (BER)				BER % diff. relative to CBR		
	CBR	DAR ($\sigma_X^2 = 2.1$)					
		$D = 0$	$D = 1$	$D = 2$	$D = 0$	$D = 1$	$D = 2$
MAX. 10 CODES PER FRAME							
0	0.027520	0.026366	0.026822	0.026821	-4.2%	-2.5%	-2.5%
0.1	0.027520	0.026366	0.026815	0.026823	-4.2%	-2.6%	-2.5%
0.2	0.027520	0.026366	0.026807	0.026819	-4.2%	-2.6%	-2.5%
0.3	0.027520	0.026366	0.026804	0.026824	-4.2%	-2.6%	-2.5%
0.4	0.027520	0.026366	0.026794	0.026801	-4.2%	-2.6%	-2.6%
0.5	0.027520	0.026366	0.026760	0.026809	-4.2%	-2.8%	-2.6%
0.6	0.027520	0.026366	0.026742	0.026798	-4.2%	-2.8%	-2.6%
0.7	0.027520	0.026366	0.026703	0.026761	-4.2%	-3.0%	-2.8%
0.8	0.027520	0.026366	0.026650	0.026721	-4.2%	-3.2%	-2.9%
0.9	0.027520	0.026366	0.026549	0.026639	-4.2%	-3.5%	-3.2%
MAX. 6 CODES PER FRAME							
0	0.027520	0.024068	0.026516	0.026828	-12.5%	-3.6%	-2.5%
0.1	0.027520	0.024068	0.026379	0.026759	-12.5%	-4.1%	-2.8%
0.2	0.027520	0.024068	0.026217	0.026668	-12.5%	-4.7%	-3.1%
0.3	0.027520	0.024068	0.026067	0.026558	-12.5%	-5.3%	-3.5%
0.4	0.027520	0.024068	0.025892	0.026403	-12.5%	-5.9%	-4.1%
0.5	0.027520	0.024068	0.025694	0.026229	-12.5%	-6.6%	-4.7%
0.6	0.027520	0.024068	0.025479	0.026019	-12.5%	-7.4%	-5.5%
0.7	0.027520	0.024068	0.025233	0.025747	-12.5%	-8.3%	-6.4%
0.8	0.027520	0.024068	0.024946	0.025397	-12.5%	-9.4%	-7.7%
0.9	0.027520	0.024068	0.024600	0.024921	-12.5%	-10.6%	-9.4%

Table B.2: BER with the DAR ($\sigma_X^2 = 2.1$) traffic model and varying levels of traffic stream correlation. **Each cell contains 4 MT's** that use a fixed spreading factor of 16 and MT's move randomly within their own cell. The BTS limits the maximum number of codes transmitted per frame and all packets have a scheduling delay tolerance of D frames. (See Figure 9.3).

Traffic model correlation (ρ)	Prob. of bit error (BER)				BER % diff. relative to CBR		
	CBR	DAR ($\sigma_X^2 = 2.1$)					
		$D = 0$	$D = 1$	$D = 2$	$D = 0$	$D = 1$	$D = 2$
MAX. 10 CODES PER FRAME							
0	0.000005	0.000012	0.000012	0.000012	126.1%	119.4%	125.8%
0.1	0.000005	0.000012	0.000012	0.000012	126.1%	127.3%	122.1%
0.2	0.000005	0.000012	0.000013	0.000012	126.1%	128.6%	122.2%
0.3	0.000005	0.000012	0.000012	0.000012	126.1%	126.1%	124.3%
0.4	0.000005	0.000012	0.000012	0.000012	126.1%	125.7%	120.1%
0.5	0.000005	0.000012	0.000012	0.000012	126.1%	127.4%	123.0%
0.6	0.000005	0.000012	0.000013	0.000013	126.1%	128.7%	128.6%
0.7	0.000005	0.000012	0.000012	0.000012	126.1%	118.4%	124.5%
0.8	0.000005	0.000012	0.000012	0.000012	126.1%	125.7%	125.7%
0.9	0.000005	0.000012	0.000012	0.000012	126.1%	120.9%	126.9%
MAX. 6 CODES PER FRAME							
0	0.000005	0.000010	0.000010	0.000010	74.9%	80.8%	78.7%
0.1	0.000005	0.000010	0.000009	0.000010	74.9%	73.3%	80.2%
0.2	0.000005	0.000010	0.000009	0.000010	74.9%	73.6%	82.3%
0.3	0.000005	0.000010	0.000010	0.000010	74.9%	83.2%	81.6%
0.4	0.000005	0.000010	0.000010	0.000010	74.9%	77.7%	78.9%
0.5	0.000005	0.000010	0.000010	0.000009	74.9%	76.1%	72.7%
0.6	0.000005	0.000010	0.000010	0.000010	74.9%	82.3%	79.3%
0.7	0.000005	0.000010	0.000010	0.000010	74.9%	79.4%	78.7%
0.8	0.000005	0.000010	0.000010	0.000010	74.9%	74.9%	77.4%
0.9	0.000005	0.000010	0.000010	0.000009	74.9%	76.9%	73.2%

Table B.3: BER for a stationary MT located 0.2 radii from the cell centre with the DAR ($\sigma_X^2 = 2.1$) traffic model and varying levels of traffic stream correlation. **Each cell contains 1 MT** that uses a fixed spreading factor of 16. The BTS limits the maximum number of codes transmitted per frame and all packets have a scheduling delay tolerance of D frames. (See Figure 9.4).

Traffic model correlation (ρ)	Prob. of bit error (BER)				BER % diff. relative to CBR		
	CBR	DAR ($\sigma_X^2 = 2.1$)					
		$D = 0$	$D = 1$	$D = 2$	$D = 0$	$D = 1$	$D = 2$
MAX. 10 CODES PER FRAME							
0	0.000068	0.000113	0.000118	0.000119	66.8%	73.2%	74.7%
0.1	0.000068	0.000113	0.000118	0.000119	66.8%	73.5%	75.0%
0.2	0.000068	0.000113	0.000119	0.000120	66.8%	75.0%	76.0%
0.3	0.000068	0.000113	0.000122	0.000121	66.8%	78.6%	77.5%
0.4	0.000068	0.000113	0.000120	0.000121	66.8%	76.8%	77.9%
0.5	0.000068	0.000113	0.000121	0.000121	66.8%	78.1%	77.8%
0.6	0.000068	0.000113	0.000120	0.000121	66.8%	76.2%	78.3%
0.7	0.000068	0.000113	0.000120	0.000122	66.8%	76.3%	79.5%
0.8	0.000068	0.000113	0.000120	0.000122	66.8%	75.7%	78.8%
0.9	0.000068	0.000113	0.000119	0.000119	66.8%	74.4%	75.6%
MAX. 6 CODES PER FRAME							
0	0.000068	0.000065	0.000079	0.000081	-4.2%	16.0%	18.8%
0.1	0.000068	0.000065	0.000079	0.000081	-4.2%	16.4%	19.3%
0.2	0.000068	0.000065	0.000078	0.000080	-4.2%	14.6%	17.8%
0.3	0.000068	0.000065	0.000077	0.000080	-4.2%	13.5%	17.3%
0.4	0.000068	0.000065	0.000076	0.000080	-4.2%	11.1%	17.5%
0.5	0.000068	0.000065	0.000075	0.000078	-4.2%	9.7%	14.7%
0.6	0.000068	0.000065	0.000074	0.000077	-4.2%	8.7%	13.1%
0.7	0.000068	0.000065	0.000072	0.000076	-4.2%	6.4%	11.1%
0.8	0.000068	0.000065	0.000071	0.000073	-4.2%	4.3%	7.8%
0.9	0.000068	0.000065	0.000069	0.000070	-4.2%	0.7%	3.5%

Table B.4: BER for a stationary MT located 0.2 radii from the cell centre with the DAR ($\sigma_X^2 = 2.1$) traffic model and varying levels of traffic stream correlation. **Each cell contains 4 MT's** that use a fixed spreading factor of 16. The BTS limits the maximum number of codes transmitted per frame and all packets have a scheduling delay tolerance of D frames. (See Figure 9.5).

Bibliography

[1] J. De Vriendt, P. Laine, and C. Lerouge, "Mobile network evolution: a revolution on the move," *IEEE Communications Magazine*, vol. 40, no. 4, pp. 104–111, 2002.

[2] International Telecommunication Union (ITU), "ICT statistics database: mobile cellular, subscribers per 100 people." `http://www.itu.int/ITU-D/icteye/Indicators/Indicators.aspx`, October 2008.

[3] S. Parkvall, E. Englund, M. Lundevall, and J. Torsner, "Evolving 3G mobile systems: broadband and broadcast services in WCDMA," *IEEE Communications Magazine*, vol. 44, no. 2, pp. 68–74, 2006.

[4] L. Waverman, M. Meschi, and M. Fuss, "The impact of telecoms on economic growth in developing countries," *Vodafone Policy Paper Series*, vol. 2, March 2005.

[5] V. H. MacDonald, "The cellular concept," *Bell System Technical Journal*, vol. 58, no. 1, pp. 15–41, 1979.

[6] T. T. Ahonen and J. Barrett, *Services for UMTS: Creating Killer Applications in 3G*. Wiley, 2002.

[7] O. C. Ibe, *Converged Network Architectures: Delivering Voice and Data Over IP, ATM, and Frame Relay*. Wiley, 2001.

[8] K. Tutschku and P. Tran-Gia, "Spatial traffic estimation and characterization for mobile communication network design," *IEEE Journal on Selected Areas in Communications*, vol. 16, no. 5, pp. 804–811, 1998.

[9] K. Tutschku, N. Gerlich, and P. Tran-Gia, "An integrated approach to cellular network planning," in *Proceedings of the 7th International Network Planning Symposium (Networks 96)*, pp. 185–190, 1996.

[10] A. Baier and K. Bandelow, "Traffic engineering and realistic network capacity in cellular radio networks with inhomogeneous traffic distribution," in *IEEE Vehicular Technology Conference, 47th Semiannual*, vol. 2, 1997.

[11] V. Brass and W. F. Fuhrmann, "Traffic engineering experience from operating cellular networks," *IEEE Communications Magazine*, vol. 35, no. 8, pp. 66–71, 1997.

[12] E. Brockmeyer, H. L. Halstrom, and A. Jensen, *The Life and Works of A. K. Erlang.* The Danish Academy of Technical Sciences, 1960.

[13] A. Klemm, C. Lindemann, and M. Lohmann, "Traffic modeling and characterization for UMTS networks," in *IEEE Global Telecommunications Conference (GLOBECOM'01)*, vol. 3, 2001.

[14] T. S. Rappaport, *Wireless Communications: Principles and Practice.* Prentice Hall, 1996.

[15] F. H. P. Fitzek and M. Reisslein, "MPEG-4 and H.263 video traces for network performance evaluation," *IEEE Network*, vol. 15, no. 6, pp. 40–54, 2001.

[16] K. S. Gilhousen, I. M. Jacobs, R. Padovani, A. J. Viterbi, L. A. Weaver Jr., and C. E. Wheatley III, "On the capacity of a cellular CDMA system," *IEEE Transactions on Vehicular Technology*, vol. 40, no. 2, pp. 303–312, 1991.

[17] A. M. Viterbi and A. J. Viterbi, "Erlang capacity of a power controlled CDMA system," *IEEE Journal on Selected Areas in Communications*, vol. 11, no. 6, pp. 892–900, 1993.

[18] Y. Ishikawa and N. Umeda, "Capacity design and performance of call admission control in cellular CDMA systems," *IEEE Journal on Selected Areas in Communications*, vol. 15, no. 8, pp. 1627–1635, 1997.

[19] J. S. Evans and D. Everitt, "Effective bandwidth-based admission control for multiservice CDMA cellular networks," *IEEE Transactions on Vehicular Technology*, vol. 48, no. 1, pp. 36–46, 1999.

[20] D. Ayyagari and A. Ephremides, "Cellular multicode CDMA capacity for integrated (voice and data) services," *IEEE Journal on Selected Areas in Communications*, vol. 17, no. 5, pp. 928–938, 1999.

[21] B. C. Sowden and K. W. Sowerby, "The impact of long-range dependent traffic in a CDMA system supporting real-time services," in *IEEE Global Telecommunications Conference (GLOBECOM'01)*, vol. 6, 2001.

[22] B. C. Sowden and K. W. Sowerby, "Impact of short-term correlated traffic in a 3G system," *IEE Electronics Letters*, vol. 38, no. 17, pp. 995–997, 2002.

[23] B. C. Sowden and K. W. Sowerby, "The impact of traffic type on the propagation dependent performance of a CDMA system," in *IEEE International Conference on Communications (ICC'03)*, vol. 1, 2003.

[24] B. C. Sowden and K. W. Sowerby, "Variable-bit-rate traffic modelling for dimensioning 3G CDMA systems," in *IEEE Vehicular Technology Conference, 57th Semiannual*, vol. 1, 2003.

[25] S. S. Haykin, *Communication Systems*. Wiley, 2001.

[26] W. C. Y. Lee, "Overview of cellular CDMA," *IEEE Transactions on Vehicular Technology*, vol. 40, no. 2, pp. 291–302, 1991.

[27] 3GPP, "Physical layer – general description," TS 25.201 V4.3.0, 3rd Generation Partnership Project (3GPP), 2002.

[28] B. Sklar, "Rayleigh fading channels in mobile digital communication systems – Part I: characterization," *IEEE Communications Magazine*, vol. 35, no. 7, pp. 90–100, 1997.

[29] R. R. Gejji, "Forward-link-power control in CDMA cellular systems," *IEEE Transactions on Vehicular Technology*, vol. 41, no. 4, pp. 532–536, 1992.

[30] M. Pursley, "Performance evaluation for phase-coded spread-spectrum multiple-access communication – Part I: system analysis," *IEEE Transactions on Communications*, vol. 25, no. 8, pp. 795–799, 1977.

[31] V. DaSilva and E. S. Sousa, "Performance of orthogonal CDMA codes for quasi-synchronous communication systems," in *Conference on Universal Personal Communications, 2nd International*, vol. 2, 1993.

[32] J. Lehnert and M. Pursley, "Error probabilities for binary direct-sequence spread-spectrum communications with random signature sequences," *IEEE Transactions on Communications*, vol. 35, no. 1, pp. 87–98, 1987.

[33] E. H. Dinan and B. Jabbari, "Spreading codes for direct sequence CDMA and wideband CDMA cellular networks," *IEEE Communications Magazine*, vol. 36, no. 9, pp. 48–54, 1998.

[34] 3GPP, "Spreading and modulation (FDD)," TS 25.213 V4.4.0, 3rd Generation Partnership Project (3GPP), 2004.

[35] G. D. Durgin and T. S. Rappaport, "Effects of multipath angular spread on the spatial cross-correlation of received voltage envelopes," in *IEEE Vehicular Technology Conference, 49th Semiannual*, vol. 2, 1999.

[36] J. B. Andersen, T. S. Rappaport, and S. Yoshida, "Propagation measurements and models for wireless communications channels," *IEEE Communications Magazine*, vol. 33, no. 1, pp. 42–49, 1995.

[37] J. D. Kraus, *Electromagnetics*, pp. 622–627. McGraw Hill, 1991.

[38] F. Ikegami, S. Yoshida, T. Takeuchi, and M. Umehira, "Propagation factors controlling mean field strength on urban streets," *IEEE Transactions on Antennas and Propagation*, vol. 32, no. 8, pp. 822–829, 1984.

[39] J. Walfisch and H. L. Bertoni, "A theoretical model of UHF propagation in urban environments," *IEEE Transactions on Antennas and Propagation*, vol. 36, no. 12, pp. 1788–1796, 1988.

[40] E. Damosso, "Digital mobile radio towards future generation systems," COST 231 final report, European Commission, 1999.

[41] M. Hata, "Empirical formula for propagation loss in land mobile radio services," *IEEE Transactions on Vehicular Technology*, vol. 29, no. 3, pp. 317–325, 1980.

[42] D. C. Hogg, "Fun with the Friis free-space transmission formula," *IEEE Antennas and Propagation Magazine*, vol. 35, no. 4, pp. 33–35, 1993.

[43] W. C. Y. Lee, *Mobile Communications Design Fundamentals*, p. 65. Howard W. Sams & Co., 1986.

[44] S. Y. Seidel, T. S. Rappaport, S. Jain, M. L. Lord, and R. Singh, "Path loss, scattering and multipath delay statistics in four European cities for digital cellular and microcellular radiotelephone," *IEEE Transactions on Vehicular Technology*, vol. 40, no. 4, pp. 721–730, 1991.

[45] P. E. Mogensen, P. Eggers, C. Jensen, and J. B. Andersen, "Urban area radio propagation measurements at 955 and 1845 MHz for small and micro cells," in *IEEE Global Telecommunications Conference (GLOBECOM'91)*, pp. 1297–1302, 1991.

[46] S. Mockford, A. M. D. Turkmani, and J. D. Parsons, "Local mean signal variability in rural areas at 900 MHz," in *IEEE Vehicular Technology Conference, 40th Semiannual*, pp. 610–615, 1990.

[47] T. S. Rappaport and C. D. McGillem, "UHF fading in factories," *IEEE Journal on Selected Areas in Communications*, vol. 7, no. 1, pp. 40–48, 1989.

[48] S. Y. Seidel and T. S. Rappaport, "914 MHz path loss prediction models for indoor wireless communications in multifloored buildings," *IEEE Transactions on Antennas and Propagation*, vol. 40, no. 2, pp. 207–217, 1992.

[49] R. J. C. Bultitude, "Measurements of wideband propagation characteristics for indoor radio with predictions for digital system performance," in *Proceedings of the Wireless '90 Conference, Calgary, Alberta, Canada*, 1990.

[50] D. C. Cox, R. R. Murray, and A. W. Norris, "800-MHz attenuation measured in and around suburban houses," *AT&T Bell Laboratories Technical Journal*, vol. 63, no. 6, pp. 921–954, 1984.

[51] T. S. Rappaport, S. Y. Seidel, and R. Singh, "900 MHz multipath propagation measurements for U.S. digital cellular radiotelephone," *IEEE Transactions on Vehicular Technology*, vol. 39, no. 2, pp. 132–139, 1990.

[52] D. Cox and R. Leck, "Distributions of multipath delay spread and average excess delay for 910-MHz urban mobile radio paths," *IEEE Transactions on Antennas and Propagation*, vol. 23, no. 2, pp. 206–213, 1975.

[53] R. J. C. Bultitude, G. K. Bedal, C. R. Center, and O. Ottawa, "Propagation characteristics on microcellular urban mobile radiochannels at 910 MHz," *IEEE Journal on Selected Areas in Communications*, vol. 7, no. 1, pp. 31–39, 1989.

[54] S. Y. Seidel, T. S. Rappaport, M. J. Feuerstein, K. L. Blackard, and L. Grindstaff, "The impact of surrounding buildings on propagation for wireless in-building personal communications system design," in *IEEE Vehicular Technology Conference, 42nd Semiannual*, pp. 814–818, 1992.

[55] A. Saleh and R. Valenzuela, "A statistical model for indoor multipath propagation," *IEEE Journal on Selected Areas in Communications*, vol. 5, no. 2, pp. 128–137, 1987.

[56] R. H. Clarke, "A statistical theory of mobile-radio reception," *Bell System Technical Journal*, vol. 47, no. 6, pp. 957–1000, 1968.

[57] H. Hashemi, "The indoor radio propagation channel," *Proceedings of the IEEE*, vol. 81, no. 7, pp. 943–968, 1993.

[58] T. Wiegand, G. J. Sullivan, G. Bjntegaard, and A. Luthra, "Overview of the H.264/AVC video coding standard," *IEEE Transactions on Circuits and Systems for Video Technology*, vol. 13, no. 7, pp. 560–576, 2003.

[59] 3GPP, "Quality of Service (QoS) concept and architecture," TS 23.107 V4.6.0, 3rd Generation Partnership Project (3GPP), 2003.

[60] V. S. Frost and B. Melamed, "Traffic modeling for telecommunications networks," *IEEE Communications Magazine*, vol. 32, no. 3, pp. 70–81, 1994.

[61] A. Adas, "Traffic models in broadband networks," *IEEE Communications Magazine*, vol. 35, no. 7, pp. 82–89, 1997.

[62] E. Anderlind and J. Zander, "A traffic model for non-real-time data users in a wireless radio network," *IEEE Communications Letters*, vol. 1, no. 2, pp. 37–39, 1997.

[63] W. E. Leland, M. S. Taqqu, W. Willinger, and D. V. Wilson, "On the self-similar nature of Ethernet traffic (extended version)," *IEEE/ACM Transactions on Networking*, vol. 2, no. 1, pp. 1–15, 1994.

[64] V. Paxson and S. Floyd, "Wide area traffic: the failure of Poisson modeling," *IEEE/ACM Transactions on Networking*, vol. 3, no. 3, pp. 226–244, 1995.

[65] J. Beran, R. Sherman, M. S. Taqqu, and W. Willinger, "Long-range dependence in variable-bit-rate video traffic," *IEEE Transactions on Communications*, vol. 43, no. 234, pp. 1566–1579, 1995.

[66] P. Z. Peebles, *Probability, Random Variables, and Random Signal Principles*. McGraw-Hill, 1993.

[67] V. B. Iversen, *Teletraffic Engineering Handbook*. International Telecommunication Union (ITU), ITU-D Study Group 2, 2002.

[68] D. P. Heyman, A. Tabatabai, and T. V. Lakshman, "Statistical analysis and simulation study of video teleconference traffic in ATM networks," *IEEE Transactions on Circuits and Systems for Video Technology*, vol. 2, no. 1, pp. 49–59, 1992.

[69] J. Gordon, "Pareto process as a model of self-similar packet traffic," in *IEEE Global Telecommunications Conference (GLOBECOM'95)*, vol. 3, pp. 2232–2236, 1995.

[70] D. Stiliadis and A. Varma, "Latency-rate servers: a general model for analysis of traffic scheduling algorithms," *IEEE/ACM Transactions on Networking*, vol. 6, no. 5, pp. 611–624, 1998.

[71] H. Fattah and C. Leung, "An overview of scheduling algorithms in wireless multimedia networks," *IEEE Wireless Communications*, vol. 9, no. 5, pp. 76–83, 2002.

[72] J. M. Capone and I. Stavrakakis, "Determining the call admission region for real-time heterogeneous applications in wireless TDMA networks," *IEEE Network*, vol. 12, no. 2, pp. 38–47, 1998.

[73] S. S. Panwar, D. Towsley, and J. K. Wolf, "Optimal scheduling policies for a class of queues with customer deadlines to the beginning of service," *Journal of the ACM*, vol. 35, no. 4, pp. 832–844, 1988.

[74] 3GPP, "High Speed Downlink Packet Access (HSDPA); Overall description; Stage 2," TS 25.308 V5.7.0, 3rd Generation Partnership Project (3GPP), 2004.

[75] W. R. Stevens, *TCP/IP Illustrated, Volume 1: The Protocols*. Addison-Wesley, 1993.

[76] H. Suzuki, "A statistical model for urban radio propagation," *IEEE Transactions on Communications*, vol. 25, no. 7, pp. 673–680, 1977.

[77] 3GPP, "User Equipment (UE) radio transmission and reception (FDD)," TS 25.101 V4.13.0, 3rd Generation Partnership Project (3GPP), 2006.

[78] A. A. Abu-Dayya and N. C. Beaulieu, "Outage probabilities in the presence of correlated lognormal interferers," *IEEE Transactions on Vehicular Technology*, vol. 43, no. 1, pp. 164–173, 1994.

[79] E. Perahia, D. C. Cox, and S. Ho, "Shadow fading cross correlation between basestations," in *IEEE Vehicular Technology Conference, 53rd Semiannual*, vol. 1, 2001.

[80] K. S. Butterworth, K. W. Sowerby, and A. G. Williamson, "Base station placement for in-building mobile communication systems to yield high capacity and efficiency," *IEEE Transactions on Communications*, vol. 48, no. 4, pp. 658–669, 2000.

[81] K. S. Butterworth, K. W. Sowerby, and A. G. Williamson, "A 1.8 GHz indoor wideband propagation study at the University of Auckland," School of Engineering report no. 569, the University of Auckland, 1996.

[82] D. Stiliadis and A. Varma, "A general methodology for designing efficient traffic scheduling and shaping algorithms," in *Conference of the IEEE Computer and Communications Societies (INFOCOM'97)*, vol. 1, 1997.

[83] R. B. Cooper, *Introduction to Queueing Theory*. North-Holland, 1981.